Structural and functional aspects of Staphylococcus aureus immune evasion

Yang, Yi

Award date:
2015

Awarding institution:
University of Bath

Structural and functional aspects of *Staphylococcus aureus* immune evasion

Yi Yang

A thesis submitted for the degree of Doctor of Philosophy

University of Bath

Department of Biology & Biochemistry

September 2015

Table of Contents

Acknowledgements:

Firstly, I would like to thank my supervisor Dr Jean van den Elsen for his guidance, encouragement and hospitalities during the course of my PhD.

Thanks to my co-supervisor Dr Stefan Bagby for teaching me cloning skills, Dr Susan Crennell for helping me with my crystallographic attempts, Dr Marta Pereira Morais for training me general laboratory techniques, Dr Abhishek Upadhyay and Dr Mareike Posner for their helps with the protein chromatography system. Thanks also to Dr Marjorie Gibbon and Dr Omar Kassaar who are always friendly and helpful to me. Last but not least, I would like to express my gratitude to all the friends from lab 0.34, socializing with me, making my time in Bath even more enjoyable and memorable.

This work would not be completed without the help from our collaborators. Thanks to Dr Kevin Marchbank for providing us with recombinant FHR-1, Prof Dmitri Svergun and Dr Melissa Graewert for their excellent SAXS analysis, Dr Mervyn Lewis for mass spectrometry analysis. I am grateful to Dr Chris Pudney for teaching me the single molecular FRET technique. My thanks also go to instrumental experts in Dynamic Biosensor for their analysis of binding kinetic and hydrodynamic properties of Sbi.

转眼已是到了毕业的时刻，在此要向一直在全方位支持我的亲爱的爸爸妈妈表示深深的感谢。是你们的鼓励和鞭策使我的能百折不挠的完成这个博士项目。在这个研究中我付出的心血和取得的成绩，应该会让您们感到您们的儿子的成长。同时我也向从小到大，一直在关心我的爷爷，奶奶 和姥姥表示感谢，希望我的表现能让您们感到骄傲。虽然已经仙逝的姥爷不能在这里分享我的喜悦， 但是我知道如果没有童年印象里您在书桌前写作的影响，今天，我可能就不会有这样的成就。我感觉很受宠爱， 从小到大都能感到来自大家庭里的关爱，谢谢大姨夫，大姨，二姨夫，二姨，哥哥 和妹妹，来自你们的关心一直驱动这我的前进。谢谢三姐和二大爷一家。最后，但很重要的，谢谢覃品忆在我博士期间对我的陪伴。

Abstract:

Alternative pathway (AP) activation is under strict control of regulators of complement activation (RCA) to prevent unwanted complement activation and to protect host cells against complement induced damage. In recent years numerous *Staphylococcus aureus* proteins have been discovered that facilitate evasion of the host's innate immune response. Several of these complement inhibitors target the central complement component C3 and act by preventing AP activation. *Staphylococcal* immunoglobulin binding protein (Sbi) is unique among all complement evasion proteins because it triggers AP activation causing local fluid-phase consumption of C3. Previous studies have shown that Sbi is a prominent covalent attachment target for nascent C3b, and in this study we show that C3b predominantly deposits on domain IV of Sbi, thereby extending the C3b serum half-life, and facilitating C3 consumption. Previous studies have also shown that in complex with C3 fragments, Sbi can form a ternary complex with complement factor H (FH), however little is known about the mechanistic aspects of this complex. This study shows that Sbi directly binds to FH and complement factor H-related protein 1 (FHR-1), and in complex with C3 fragments the resulting FH and FHR-1 ternary complexes are significantly stronger in avidity. A strong preference for the formation of a FHR-1 ternary complex was also demonstrated. Using site-directed mutagenesis we have been able to determine the amino acids that are critical for the formation of both ternary complexes and their role in Sbi's complement consumption activity. The FHR-1 ternary complex protects C3b from inactivation, and is essential for the C3 futile consumption. Using *ab initio* structural prediction, single molecule fluorescence resonance energy transfer, and small angle X-ray scattering data, two structural models of these ternary complexes were proposed. In addition we show that the Sbi mediated ternary complexes significantly inhibit the formation of the terminal complement complex (TCC), which will aid the development of new complement inhibitors for treatment of autoimmune diseases.

Abbreviations:

A	Acceptor fluorophore
Ag	Antigen
aHUS	Atypical heamolytic ureamic syndrome
α2M	α2-macroglubulin
AMD	Age-related macular degeneration
ANA	Anaphylatoxin domain
AP	Alternative complement pathway
APS	Ammonium persulphate
ALEX	Alternating laser excitation
CD	Circular dichroism
CR	Complement receptor
CUB	Complement C1r/C1s, UEGF, BMP1 domain
C1NH	C1 inhibitor
C-terminal	Carboxyl-terminus
FHR	Factor H-related protein
Clf	Clumping factor
CP	Complement classical pathway
CP*	Capsular polysaccharide
CWA	Cell wall anchored
D	Donor fluorophore
Da	dalton
DAF	Decay-accelerating factor
DNA	Deoxyribonucleic acid
Eap	Extracellular adherence protein
Ecb	Extracellular complement-binding protein
Efb	Extracellular fibrinogen-binding protein
ELISA	Enzyme-linked immunosorbent assay
Emp	Extracellular matrix-binding protein
E.coli	*Escherichia coli*
EDTA	Ethylenediaminetetraacetic acid
EGTA	Ethyleneglycoltetraacetic acid
ESI	Electrospray ionization

EM	Electron microscopy
Fab	Fragment antigen-binding of immunoglobulin
Fc	Fragment crystallizable of immunoglobulin
FH	Factor H
FHL-1	Factor H-like protein 1
FRET	Förster/Fluororescence resonance energy transfer
GAGs	Glycosaminoglycans
GST	Glutathione-S-transferase
HSS	Human serum standard
HRP	Horseradish peroxidase
IgA	Immunoglobulin A
IgG	Immunoglobulin G
IgM	Immunoglobulin M
IPTG	Isopropyl-1-thio-β-galactopyranoside
K_d	Dissociation constant
kb	kilobase
kDa	Kilo dalton
LNK	Linker domain
LB	Luria-bertani medium
M	Molar
mM	millimolar
µM	micromolar
MAC	Membrane attack complex
MASP	MBL-associated serine protease
MBL	Mannose-binding lection
MCP	Membrane cofactor protein
MES	2-ethanesulfonic acid
MG	Macroglobulin
MS	Mass spectrometry
MSCRAMM	Microbial surface components recognizing adhesive matrix molecules
MSSA	Methicillin sensitive *S. aureus*
MRSA	Methicillin resistant *S. aureus*
MW	Molecular weight
NMR	Nuclear magnetic resonance
NHS	N-hydroxysuccinimide

nM	nanomolar
N-terminal	Amino-terminal
PBS	Phosphate-buffered saline
PCR	Polymerase chain reaction
RCA	Regulator of complement activation
PDB	Protein Data bank
pM	picomolar
PVL	Panton-valentine leuocidin
PSM	Phenol soluble modulin
*R*g	Radius of gyration
SAK	staphylokinase
SAXS	Small angle X-ray scattering
Sbi	*Staphylococcal* binder of IgG
SCIN	*Staphylococcal* complement inhibitor
SCR	Short consensus repeat
SDS-PAGE	Sodium dodecyl sulfate polyacrylamide gel electrophoresis
SpA	*Staphylococcal* Protein A
smFRET	Single molecule FRET
SSL	Staphylococcal superantigen-like protein
TCC	Terminal complement complex
TCR	T cell receptor
TED	Thioester-containing domain
TSST	Toll shock syndrome toxi
Tris	Aminomethane
TEMED	N, N, N,' N'-tetramethylenediamine

Publications:

Published:

1: Maisem Laabei, W. David Jamieson, **Yi Yang**, Jean van den Elsen, A. Toby A. Jenkins. "Investigating the lytic activity and structural properties of *Staphylococcus aureus* phenol soluble modulin (PSM) peptide toxins" Biochimica et Biophysica Acta 1838 (2014) 3153-3161

In preparation:

1: **Yi Yang**, Jean MH van den Elsen. "*Staphylococcus aureus* protein Sbi mediates complement C3 futile consumption by forming a ternary complex with C3 activation fragments and CFHR1 " (manuscript in preparation)

2: **Yi Yang**, Jean MH van den Elsen. " C3b covalent attachment on domain IV of *Staphylococcal* complement modulator Sbi facilitates futile consumption of C3" (manuscript in preparation)

3: Anca MD Catici, Hope E Amos, **Yi Yang**, Stephen A Wells, Jean MH van den Elsen and Christopher R Pudney. "Red Edge Excitation Shift Spectroscopy as a Novel Probe of the Protein Free Energy Landscape; Mechanistic Insight into the Ligand Binding Steps of NF-&[kappa]B Essential Modulator" (manuscript in preparation)

Chapter 1: Introduction

1.1 The Complement System

1.1.1 Activation pathways

As a defense mechanism against constant attacks from invading pathogens, the human body has evolved an elaborate immune system that exerts a continuous surveillance to protect against these pathogens. In one approach, the antibody mediated adaptive immune system can swiftly contain and clear invading bacteria by specific immunoglobulin molecules that can recognize the invader from a previous infection. Alternatively, the unacquainted pathogens are tackled by the humoral component of innate immunity, the complement system.

The complement system comprises over 30 soluble plasma proteins and cell surface receptors (Carroll 2004) that interact with each other via an intricate network of interactions. The soluble fraction of this finely regulated protein network consists of a number of proteases that are themselves activated by proteolytic cleavage. These precursor zymogens are widely distributed throughout body fluids and tissues without adverse effect. However, at sites of infection, they are locally activated and trigger a series of potent inflammatory events. In this thesis over 60 complement components and activation fragments are mentioned. The nomenclature of all the complement component (Kemper *et al.* 2014) was dictated by their respective chronology of discovery. Thus, nine central components are arranged from C1 to C9. Furthermore there are anaphylatoxins such as C3a, C4a and C5a, opsonins such as C3b, iC3b, C3d and C4b; proteases such as factor B, factor D and factor I; regulators such as factor H (FH), factor H related proteins 1-5 (FHR 1-5), C1q, properdin and complement receptor type 1 (CR1); assembled enzymes such as C3 convertase and C5 convertases; and finally receptors such as C3a receptor, C5a receptor and C1q

receptor (Zipfel & Skerka 2009).

Complement activation can be categorized into three pathways (Fig.1.1), based on the triggers of activation. Classical pathway activation is initiated by recognition of antibody-antigen complexes, polymerization of the immunoglobulin molecules (e.g. IgG or IgM) or C-reactive proteins. The Lectin pathway activates in response to mannose-binding proteins (MBL) and ficolins binding to the carbohydrate ligands on the bacteria surfaces. Finally, the alternative pathway activation is initiated by the spontaneous hydrolysis property of complement component C3. Despite differences in initiation stages, all three activation pathways converge at the formation of a C3 convertase the central step of complement activation where the activation signal is amplified, eventually leading to the formation of membrane attack complex (MAC).

The complement system collectively recognizes, opsonizes and eliminates pathogens, apoptotic cell debris and immune complexes within minutes after the encounter (Lambris *et al.* 2008). The activation of complement also elicits profound immunological consequences, bridging the innate immunity and adaptive immunity (Isenman 2012). Complement activation products enhance T cell immunity by promoting T cell proliferation and diminishing T cell apoptosis (Kwan *et al.* 2012), while at the same time sensitizing antigens for B cell recognition, resulting in augmented antibody response and enhanced immunological memory (Walport 2001).

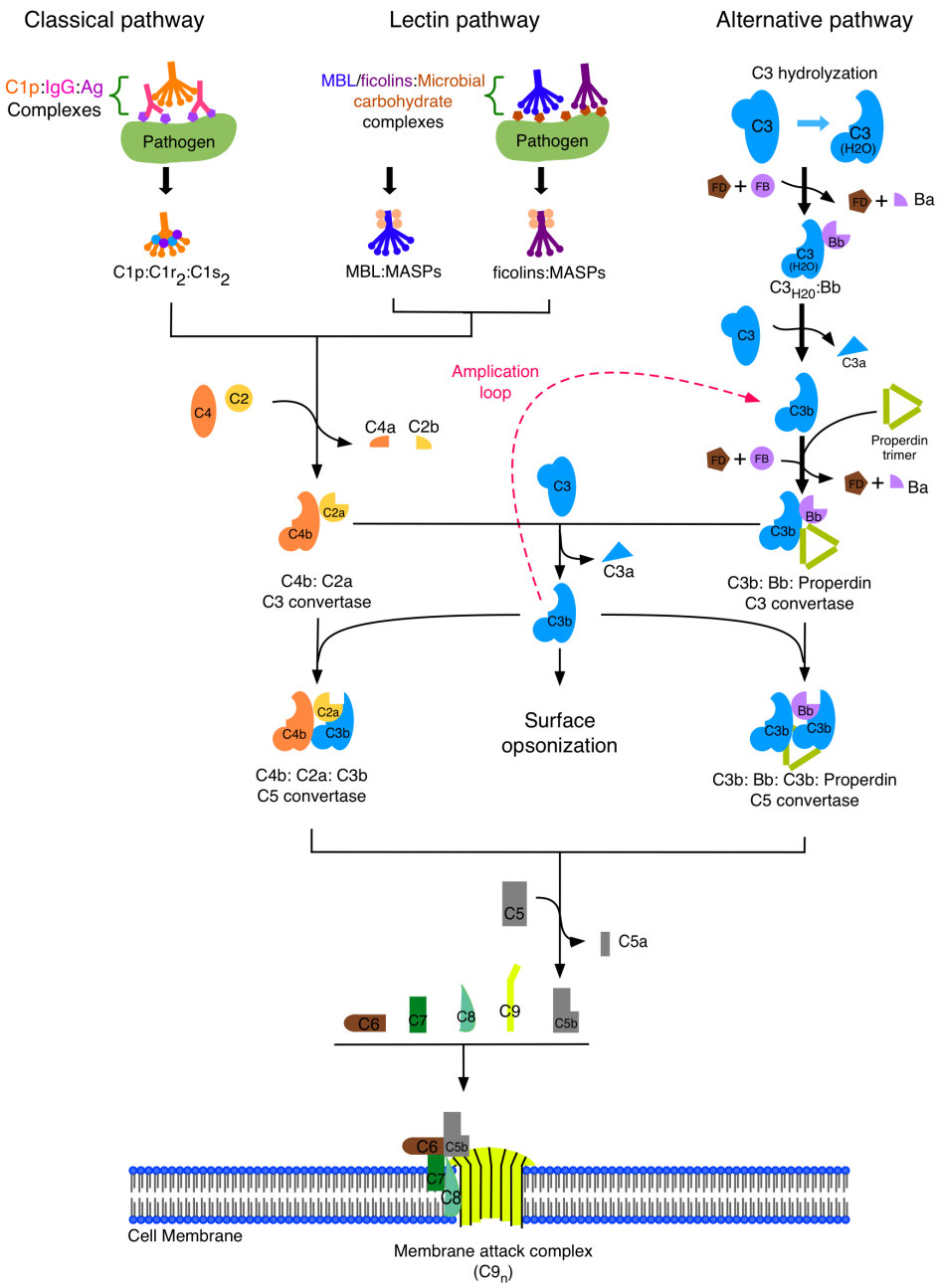

Figure 1.1: Schematic presentation of complement system cascade.

1.1.2 Classical pathway

The initiation of the classical pathway (CP) is triggered by interactions between the first complement component (C1) with antibody-antigen complexes and immune aggregates consisting of immunoglobulins (e.g.IgG1, IgG2, IgG3 or IgM) or C-reactive protein (Fig.1.2.A). Apart from these components of the adaptive

immune system, it is known that activation of the classical pathway can also occur in an immunoglobulin independent manner via direct interaction of C1 with a diverse range of activators, including Gram-positive and Gram-negative bacteria, certain viruses, infected cells, poly-anionic foreign materials and β-amyloid fibrils (Arlaud & Thielens 2001).

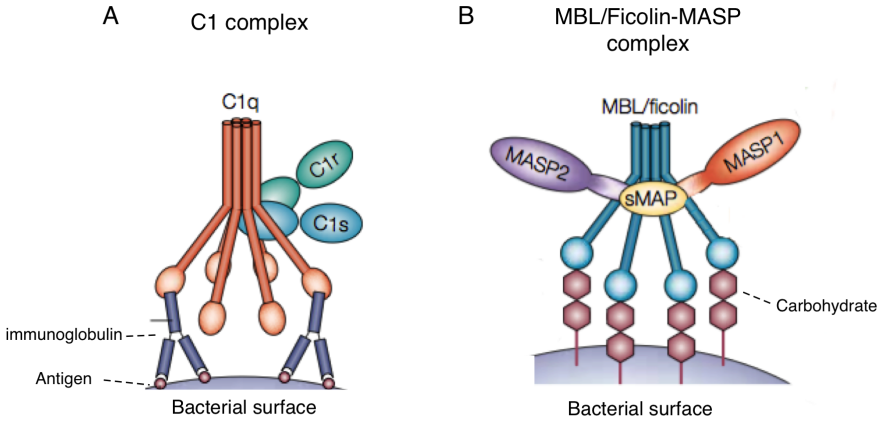

Figure 1.2: Schematic diagrams of the C1 complex and the MBL/Ficolin-MASP complex. Image taken from (Fujita 2002).

This recognition flexibility of the C1 complex can be attributed to its complex molecular design. C1 is composed of a C1q recognition module and two C1r and two C1s molecules forming the protease module, together assembled to form a $C1qr_2s_2$ complex. C1q is a hexameric protein, with each monomer consisting of three chains, with a C-terminal globular domain and a collagen triple helix region at the N-terminus. Consequently, in C1q there are six globular "heads", held together by a "stalk" structure that result from oligomerization of the six N-terminal collagen triplets. C1's recognition capability is located in the six C1q "heads" that bind the fragment-crystallizable (Fc) regions of IgG and IgM. Spontaneous binding of more than one C1q heads is needed to trigger a conformational activation event of the zymogen C1r, where the activated C1r serine protease then cleaves zymogen C1s to its activated serine protease state. The classical pathway proteolytic cascade (Fig.1.1) then proceeds with the cleavage of C4 to anaphylatoxin C4a and opsonin C4b, which opsonize a

pathogen by the activation of a highly reactive thioester in close proximity to the antigenic surface. C4b then binds to zymogen C2, which became cleavable by activated C1s; proteolytic fragment C2b diffuses away, resulting the formation of C4b2a classical pathway C3 convertase. Local C3 molecules are then used as substrate and proteolytically converted to C3a and C3b fragments. The increased local C3b concentration finally leads to the formation of the C4b2a3b classical pathway C5 convertase that activates the C5 molecule, thus initiating the assembly of MAC.

1.1.3 Lectin pathway

In contrast with the classical pathway, antibody recognition is not necessary for activation of the lectin pathway; instead activation is triggered upon recognition of carbohydrates on the surfaces of a broad spectrum of microorganisms. (Fig.1.2.B) Carbohydrates with 3- and 4-hydroxyl groups in the pyranose ring (e.g. mannose and *N*-acetyl-glucosamine (GlcNAc)) are recognized by mannose-binding lectin (MBL), together with ficolins that specifically bind to GlcNAc (Fujita 2002).

MBL and its associated serine proteases MASP1 and MASP2 represent the functional equivalent of C1q in the lectin pathway. They share a similar overall topology with C1q, consisting of a C-terminal carbohydrate binding domain and N-terminal collagen-like domain. The oligomeric state of the native form of MBL varies from a dimer to a hexamer, in contrast with native ficolins which adopt a tetrameric form (Endo *et al*. 2011). MBL and ficolins each individually associate with MASP1, MASP2, and activate MASP2 when bound to microbial carbohydrates. Activated MASP2 then relays the activation signal in a similar fashion to activated C1s during classical pathway activation, eventually leading to the formation of MAC.

1.1.4 Alternative pathway

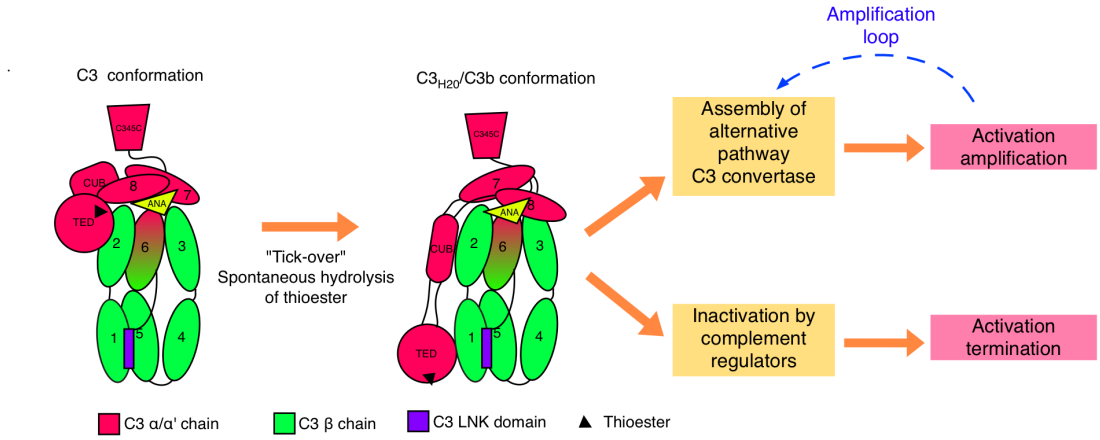

Figure 1.3: Schematic diagram of alternative pathway activation, amplification and regulation.

The alternative pathway (AP) plays a major role in the elimination of invading microorganisms via its signal amplification function (Lachmann & Hughes-Jones 1984) for the other two complement pathways. The first step of alterative pathway activation (Fig.1.3) is the result of a biophysical property of complement component C3. The conformational flexibility of this molecule allows it to undergo spontaneous hydrolysis constantly at a very low rate (0.005% of total C3 per min) (Pangburn *et al*. 1981; Müller-Eberhard 1988), traditionally described as the "tick-over" mechanism (Lachmann 1975). The hydrolysis of the internal thioester located within the thioester domain (TED) of C3 leads to the formation of $C3_{H2O}$ that is trapped in a C3b like conformation. Factor B in the plasma then binds to the newly exposed interaction interface on $C3_{H2O}$ in the presence of Mg^{2+} and becomes a cleavable substrate for factor D. Factor B is cleaved by factor D into two fragments Ba and Bb, the latter remaining associated with $C3_{H2O}$ to form the fluid phase alterative pathway C3 convertase $C3_{H2O}Bb$. The enzymatic complex activates C3 proteolytically, releasing the anaphylatoxin C3a fragment and a metastable C3b molecule, which can become covalently deposited on surrounding self or non-self surfaces (Müller-Eberhard 1966; Dalmasso & Müller-Eberhard 1967). On host cell surfaces, C3 convertase

activity is suppressed by the presence of sialic acid or other polyanionic molecules and complement regulatory proteins. In contrast, on non-self surfaces, uncontrolled C3 convertase activity promotes the positive-feedback amplification loop of C3b amounting to the deposition of large numbers of C3b molecules within a very short period of time. The deposited C3b molecules in turn can function as a new platform for C3 convertase assembly. Stabilization of this alternative pathway C3 convertase complex has a half-life of 90 sec, however the binding of properdin stabilizes the enzyme and extends the half-life by 10-fold (Fishelson & Müller-Eberhard 1982). In the fluid phase, C3b concentrations also increase which in turn can associate with C3bBb to form C3bBbC3b, the alternative pathway C5 convertase, which is analogous to C4b2a3b C5 convertase in the classical pathway.

1.1.5 Membrane attack complex

The terminal or lytic phase of all complement pathways starts with the cleavage of C5 by C5 convertase into C5b and a smaller fragment C5a, a very potent anaphylatoxin that stimulates the chemotaxis of inflammatory cells to the site of complement activation. C5b subsequently binds with C6 to form the C5b6 complex, followed by the association of C7, which results in the formation of the lipophilic C5b67 complex. Additional association of the C5b67 complex with the heterotrimeric C8 protein, forming the C5b678 complex, leads to association with phospholipids and subsequent penetration into the lipid bilayer. The membrane inserted C5b678 then serves as a receptor for C9 and catalyzes its oligomerization, resulting in the formation of a trans-membrane tubular pore called the membrane attack complex (MAC). The oligomerization of ten to seventeen C9 molecules creates a 7-10nm pore that makes the membrane permeable to water and electrolytes, eventually leading to the lysis of cells due to increased osmotic pressure.

In the event of the MAC assembly occuring distal from a membrane or missing the targeted membrane, it binds with clusterin and vitronectin, producing a soluble complex called sMAC or sC5b9. Within both membrane embedded and activated C9, a common neo-epitope on C9 becomes available for antibody recognition. Based on the antibody against this epitope, a commercial enzyme-linked immunosorbent assay (ELISA) was used to quantify activated C9 in serum, therefore leading to the evaluation of residual complement activity of all pathways.

1.2 Complement component C3

C3 belongs to the α2-macroglubulin (α2M) protein family, and has 26-30% sequence identity to complement components C4 and C5, which are also members of this family (Reid & Porter 1981) and are thought to have evolved from C3 via two gene duplication events. α2M family proteins contribute significantly to host innate immunity (Blandin 2004), the proteins of this family normally possess a highly reactive thioester region that, once solvent exposed, can covalently attach to nearby hydroxyl and primary amine groups. Although in C5 it has lost its function during evolution, in C3 and C4 the thioester plays a fundamental role in their immunological function. The substrate specificity and reactivity of the thioester in C3 and C4 have diverged during evolution and whilst in C3 it is able to form both ester and amide linkages with antigenic surfaces (Law & Dodds 1997), humans have two C4 variants (A and B) that preferentially form either amide or ester linkage, respectively (Isenman & Young 1984).

Complement component C3 is considered the central molecule for all complement activation pathways. It circulates in plasma in its immunologically inactive form, with concentrations varying from 1-1.5 mg/ml. However, increased C3 levels are often observed during inflammation and infection. The

majority of C3 in circulation is constantly replenished by hepatocytes (Alper *et al.*, 1969), however under immunological stresses, numerous extra-hepatic cells also produce C3, such as leukocytes, fibroblasts, keratinocytes (Pasch *et al.*, 2000) and endothelial cells (Andoh *et al.*, 1993). Although indisputably the secreted C3 molecules are primarily involved in detecting and removal of pathogens, an increasing amount of evidence indicates that C3 activation fragments are also essential for driving and modulating adaptive T cell immunity. The C3 activation fragments C3a and C3b, generated by T cell itself, are required for the induction of interferon-γ secretion through autocrine binding to their respective receptors, the C3a receptor (C3aR) and C3b receptor (CD46) (Liszewski *et al.*, 2005; Le Friec *et al.*, 2012). This molecular basis correlates with the facts that CD46 deficient patients and C3-deficient patients suffer from recurrent infections and have severely reduced T helper 1 cell mediated responses (Ghannam *et al.*, 2008). It was traditionally accepted that the T cell secreted C3 molecules are cleaved extracellularly via activation of AP (Kemper & Atkinson, 2006). However, it was recently reported that C3 activation could also take place intracellularly through cleavage by the protease cathepsin L (CTSL), providing a new prospective for the role of C3 in maintaining T cell homeostatic survival (Liszewski *et al.*, 2013).

1.2.1 C3 structure

Human C3 is a 185 kDa glycoprotein that encoded by a 41 kb gene, which is situated at the far end of the chromosome 19 long arm. This gene is composed of 41 exons. The primary structure of C3, inferred from its cDNA sequence, consists of 1663 amino acid residues with a 22 amino acid signal peptide. The mRNA of C3 is translated as a single-chain pre-pro-molecule starting with the β chain followed by the α chain. The two chains are joined by a tetra-arginine sequence, which is removed by an enzyme during post-translational modification. As a result, in the correctly folded C3 molecule, α- and β-chains, with molecular weights of 110 and 75 kDa respectively, are linked by disulphide bonds and

non-covalent interactions. After translocation through the endoplasmic reticulum to the Golgi body, three N-linked high-mannose glycans are transferred to both α-and β-chains, at position Asn85 (Zhang *et al.* 2003), Asn939 (Bunkenborg *et al.* 2004) and Asn1617 (Liu *et al.* 2005). The glycan structure (Miki *et al*. 1986; HASE *et al*. 1985) on the α chain mainly contains $Man_8GlcNAc_2$ or $Man_9GlcNAc_2$, whilst in the β chain, the glycan structure consists of $Man_5GlcNAc_2$ or $Man_6GlcNAc_2$. The glycans in C3 represent about 2.3% of its molecular weight.

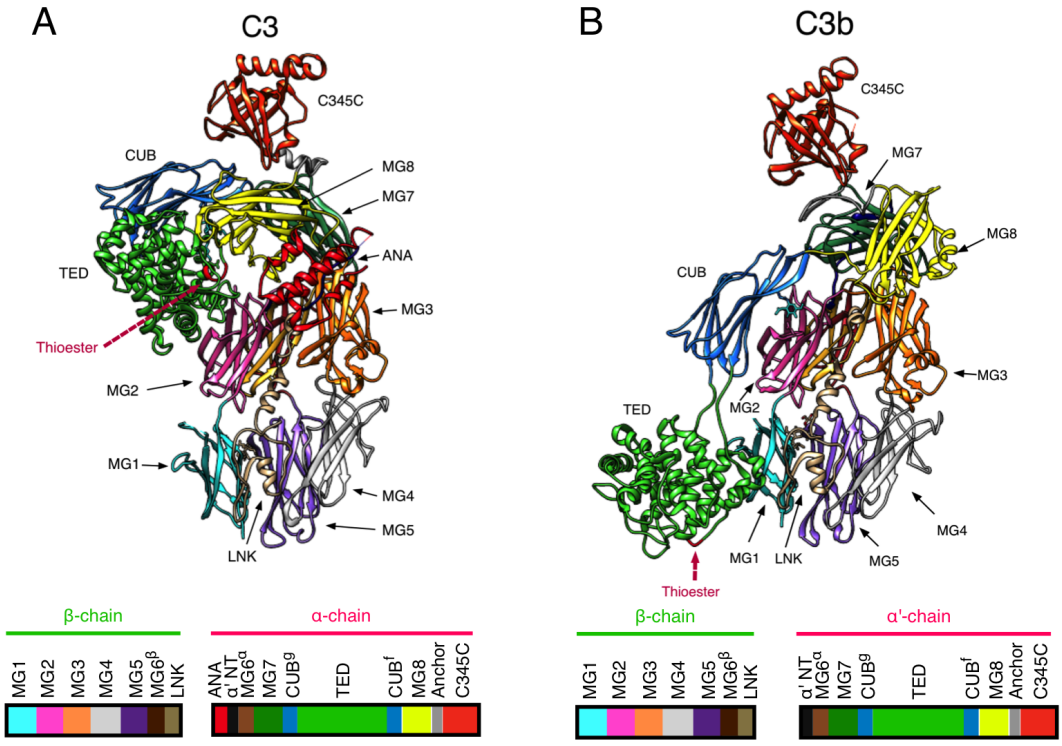

Figure 1.4: Conformation changes of complement component C3. (A) Crystal structure of native human C3. PDB code: 2A73 **(B)** Crystal structure of activated C3 conformation, C3b. PDB code: 2I07. PDB, Protein date bank.

The three-dimensional model of human C3 (Fig.1.4.A) has been determined by X-ray crystallography (Janssen *et al*. 2005), showing that the protein is composed of 13 individual domains. The protein core consists of 8 homologous macroglobulin (MG) domains, surrounded by a thioester-containing (TED)

domain, a C1r/C1s-Uegf-Bmp1 (CUB) domain that links TED to MG domains, and the C345C, LNK and anaphylatoxin domains.

Amino acid residues 1-534 comprise the first five MG domains, which constitute the β-chain of C3. The MG6 domain is composed of residues from the interlaced β- and α-chains, within which residues 535-577 of the β-chain contributes the first half of the domain and α-chain residues 746-806 to the other half. Residues 578-642 form the C-terminal end of the C3 β-chain, called the LNK domain. This domain consists of three helices and an extended β-strand that extends through the ring structure in the core of the C3 structure composed of 8 MG domains. The LNK domain uses three aromatic residues to interact with the nearby MG1 domain.

The α-chain starts with the anaphylatoxin (ANA) domain (residues 650-762). Located next to this domain is a disordered loop with a solvent exposed scissile bond (Arg726-Ser727) that is cleaved by C3 convertases from all complement pathways and results in the release of the C3a fragment from the main body of C3. The CUB-TED domains (residues 911-1331) are straddled between the N-terminal MG6-7 domains and C-terminal MG8-C345C domains. The CUB domain can be divided into the N-terminal CUB^{g} and C-terminal CUB^{f} domains. The TED domain is located between the two CUB domains that resemble two arms holding the TED against the main body of the C3 molecule. The TED domain consists of a solvent facing concave side and a secluded convex face containing the reactive thioester. The MG8 domain that contacts the inward facing thioester region contains a hydrophobic pocket composed of Met1378, Tyr1425 and Tyr1460. Together with Phe1047 from TED domain, this hydrophobic pocket shields the thioester from surrounding water molecules and nucleophiles.

1.2.2 Structure and function of the C3 activation product

The C3 molecules circulating in the plasma constantly undergo "tick-over", monitoring the surrounding environment. A series of protein-protein interaction interfaces, hidden inside the inactive C3 structure conformation contribute to the regulation, communication and modulation, not only of components within the complement system but also the adaptive immune system (Fig.1.5).

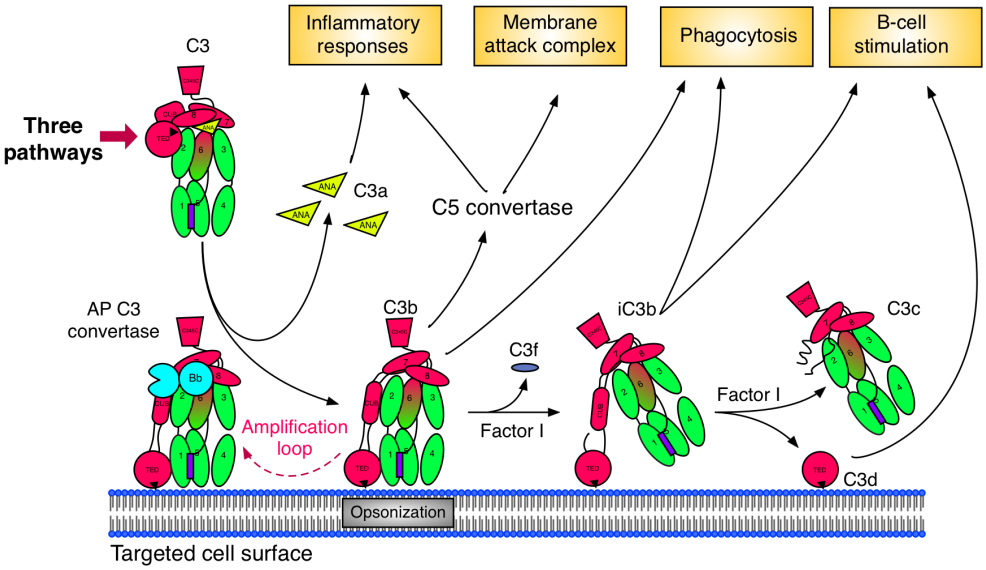

Figure 1.5: Schematic diagram of the conformational changes of C3 and its activation products in the complement cascade. Image adapted from (Gros et al. 2008).

The main activity of C3 is unleashed by the cleavage of C3 convertase, through which the anaphylatoxin fragment C3a is released and the remaining C3 converts into C3b (Fig.1.4.B) followed by a series of dramatic conformational changes. In its C3b conformation it is then recognized by various complement components including factor B, properdin, FH and FHRs, factor H-like protein 1 (FHL-1) and complement receptors (CR). Some of those binding events facilitate the recruitment of additional serum proteases such as factor I and plasmin to further cleave C3b into fragments iC3b and C3dg that display new protein binding interfaces. This final round of cleavage is essential for the communication between complement system and other components of the immune system, as iC3b and C3dg are the ligands for complement receptors CR2, CR3 and CR4,

resulting in B-cell proliferation, nitro oxide synthesis and degranulation and promoting of phagocytosis.

How C3 changes its conformation to accommodate a range of immunological roles is a question that has fascinated "complementologists" and structural biologists for decades. Recent crystal structures of C3 fragments and complexes with their ligands, have been crucial for our understanding of the molecular mechanisms of the function of C3. The most important crystal structures include: native human C3 (Janssen *et al*. 2005), the anaphylatoxin fragment C3a (Huber *et al.* 1980), C3b (Janssen *et al*. 2006), C3c (Janssen *et al.* 2005), C3d (Nagar *et al*. 1998), C3b:factor H SCR-1/4 complex (Wu et al. 2009), C3d:factor H SCR-19/20 complex (Morgan *et al.* 2011), C3d:CR2 SCR-1/2 complex (van den Elsen & Isenman 2011), and the complexes of C3b and C3c with the complement receptor of the immunoglobulin superfamily (CRIg) (Wiesmann *et al*. 2006). Electron-microscopy has become an increasingly powerful technique in recent years, through which structural models of $C3_{H2O}$ (Nishida *et al.* 2006), iC3b (Alcorlo *et al.* 2011) and properdin-C3bBb complex (Alcorlo *et al*. 2013) have been determined.

By comparing crystal structures of C3, C3b and C3c, a putative mechanism of C3 activation has been proposed (Janssen *et al*. 2005). The structural function of ANA is of great interest, given that its removal is a prerequisite for enzymatic C3 activation. It was previously believed that the ANA domain is in direct contact with the TED domain, however, the C3 structure (Fig.1.4.A) shows that the ANA domain plays an indirect structural role and extensively interacts with the MG8 domain on one side and with MG3 on the other side. In this arrangement, the ANA domain may serve to keep the MG8 domain in the correct position for interacting with TED domain. In summary, the removal of ANA and the resulting C3b conformation weakens the interactions between MG8 and TED, therefore allowing the TED domain to swing out from its protective position.

1.3 Complement regulation

It has long been recognized that complement activation is a double-edged sword, as both invading pathogens and host cells are susceptible to lysis mediated by MAC. To make matters even more challenging, the complement system is designed to constantly monitor its surrounding environment, with the compromise that covalent deposition of complement effectors (e.g. C3b and C4b) is largely indiscriminate across different surfaces. Therefore, the advancement of the complement cascade and the activity of its effector molecules have to be tightly controlled at every level by numerous complement regulators and inhibitors (Fig.1.6). These regulators are able to discriminate between self and non-self surfaces, protecting the host cells from complement attack.

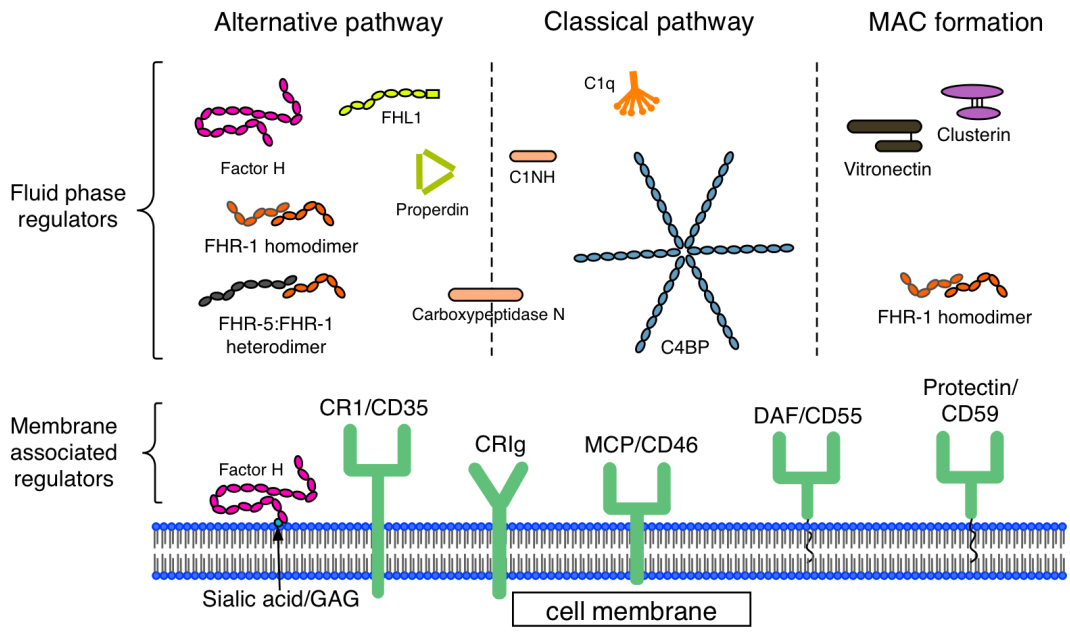

Figure 1.6: Complement regulators in fluid phase and at the cell surface. The function of listed molecules will be explained in section 1.3. Image adapted from (Zipfel & Skerka 2009).

During complement activation the effector molecules are distributed in the fluid phase and on membrane surfaces (Fig.1.6), where complement regulators also coexist in large quantities and great diversity. This results in the strict control of

the severity, propagation and endpoint of the complement attack. In the fluid phase, C1 esterase inhibitor (C1-INH) (Davis *et al.* 2008), a serpin type protease inhibitor regulates the activation of C1q and MBL complexes by binding and irreversibly inhibiting C1r, C1s and MASP-2. sMAP and MAP-1 (Skjoedt *et al.* 2010), the non-proteolytic splice products of the MASP2 and MASP1/3 genes, modulate the lectin pathway activation specifically by competing with MASPs for binding to the MBL and ficolins. In comparison with the regulators for complement pathway initiation, even greater numbers of regulators are dedicated to the regulation of processes downstream of C3 convertase formation.

Factor H and its alternative splicing variant FHL-1 are the two major regulators for AP C3 convertase (C3bBb) activity. C4b-binding protein (C4BP), the regulatory counterpart of the classical pathway, inhibits CP C3 convertase (C4b2a) activity. Their regulatory mechanisms share three common features (Whaley & Ruddy 1976; Pangburn *et al*. 1977; Scharfstein *et al*. 1978; Gigli *et al*. 1979). Firstly, by competing for shared interaction interfaces, they accelerate the dissociation rate (i.e. decay acceleration) of pre-existing C3 convertases. Secondly, they compete with Bb and C2a for the binding of C3b and C4b, thereby averting the formation of fresh C3 convertases. Finally, they function as co-factors for protease factor I, which cleaves C3b and C4b, thus eliminating the platform of new C3 convertase assembly. Noticeably, the regulatory functions of factor H, FHL-1 and C4BP are not limited to the fluid phase, but also extended to human cells surfaces by binding to host-specific surface patterns (such as sialic acid or glycosaminoglycans (GAG)). This contributes significantly to the prevention of self-attack. At the same time, most human cell surfaces are decorated with membrane bound convertase regulators, whose extracellular regulatory domains share high degree of similarity with the fluid phase regulatory proteins. Therefore, membrane bound regulators such as CR1 and decay-accelerating factor (DAF) act as decay accelerators to promote the

dissociation of the C3 convertase. On the other hand, CR1 and membrane cofactor protein (MCP) recruit factor I to inactivate membrane bound C3b.

In contrast with the extremely intricate control of C3 convertase activity, the regulation exerted on C5 activation and MAC formations is relatively straightforward. Only a few regulators targeting C5 have been described. FHR-1 has been reported to inhibit C5 convertase activity by interacting directly with C5 (Heinen *et al.* 2009). CRIg has been shown to inhibit both AP C3 and C5 convertase activities by binding to C3b and causing steric hindrance (Wiesmann *et al*. 2006) for the assembly of both convertases. At the level of MAC, so far only one membrane bound regulator has been described. Protectin (CD59) acts on the C8 to inhibit MAC assembly and formation. Nevertheless, soluble regulators such as vitronectin and clusterin are used to sequester the off-targeted MAC in fluid phase.

In contrast to the down-regulated complement activity on the host cell surface, complement activation is facilitated on the surface of pathogens by complement positive regulators. Properdin is considered to be the only positive regulator of complement activation. It recognizes molecular patterns (e.g. negatively charged molecules) displayed on microbial surfaces and, once bound to surface, promotes AP complement activation by stabilizing AP C3 convertase (C3bBb) (Fearon & Austen 1975; Hourcade 2008). Human plasma contains very low concentrations of properdin (5μg/ml) in the form of oligomeric molecules that comprise two to four monomers (Pangburn 1989c). Each monomer of this 53 kDa glycoprotein consists of seven thrombospondin-like repeat (TSR) domains. More recently, several proteins from the FHR family have also been indicated to positively modulate complement activation, by antagonizing factor H activity. FHR-1 and FHR-5 homo or hetero-dimers (Goicoechea de Jorge *et al*. 2013) as well as FHR-4 (Hebecker & Jozsi 2012) were shown to compete for C3b binding with factor H and thereby to stabilize the AP C3 convertase.

1.4 Complement Factor H and FHR family

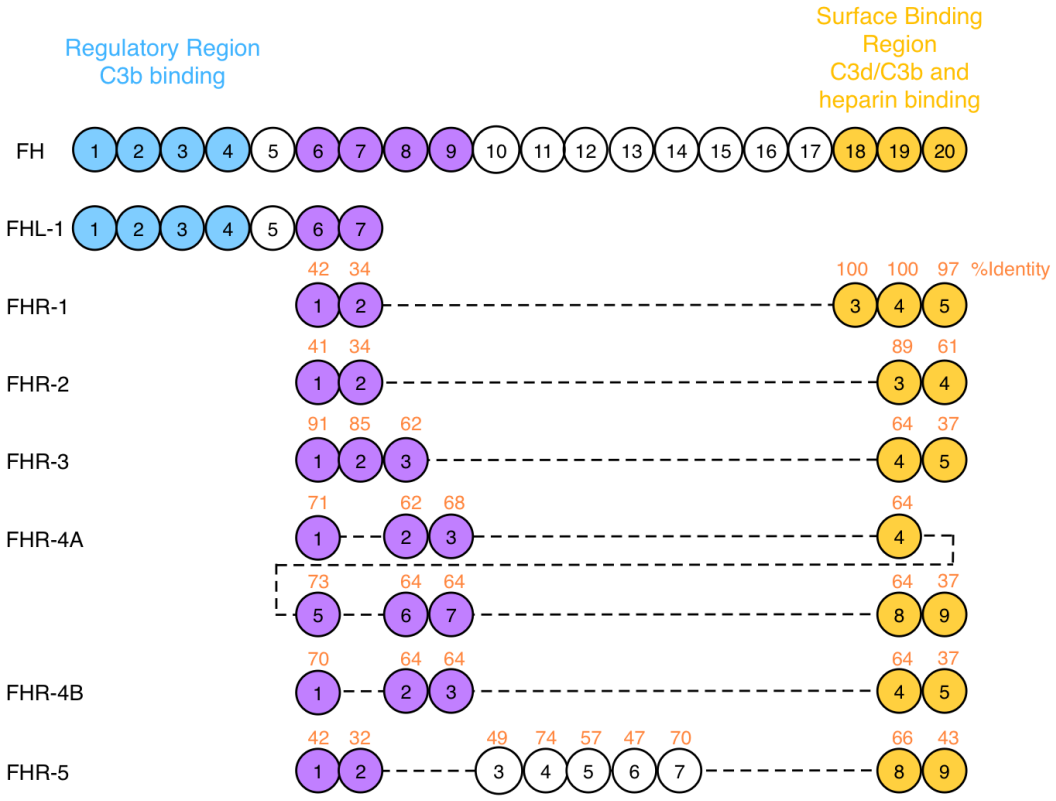

Figure 1.7: A schematic structure of factor H and its family members. The homologous domains are indicated by their vertical position. The percentage of sequence identity between each domain and the equivalent FH domain is presented above as a yellow number.

The factor H family (Fig.1.7) of proteins includes complement factor H, FHL-1 and five FHR proteins. These proteins are highly similar in primary structure but different in size, varying from 4 to 20 short consensus repeats (SCRs, also known as complement control protein (CCP) modules). The intertwined relationships of cooperation and competition within this group of proteins contribute significantly to the elevated complexity of complement regulation. This interconnected relationship is demonstrated again on the genomic level by the tandem arrangement of the factor H gene and five FHR genes in the regulators of complement activation (*RCA*) gene cluster on human chromosome 1q32. These proteins are constitutively synthesized in hepatocytes and secreted into the plasma. Early studies reported that plasma factor H concentrations can vary from 116 to 562 μg/ml, but a more recent study revealed that mean Factor H

concentrations only vary between 2-3μM (233 μg/ml in young adults and 260 μg/ml in older individuals)(Hakobyan *et al*. 2008). The rest of the factor H family exists in much lower concentrations in plasma, FHL-1, FHR-1, are present at concentration of 30-50 μg/ml (Zipfel & Skerka 1999) and 70-100 μg/ml (Skerka & Zipfel 2008), respectively. Precise concentration determination of FHR proteins remains a challenge, largely because these proteins are generally associated with lipoprotein particles, and because of the lack of specific monoclonal antibodies.

1.4.1 Factor H

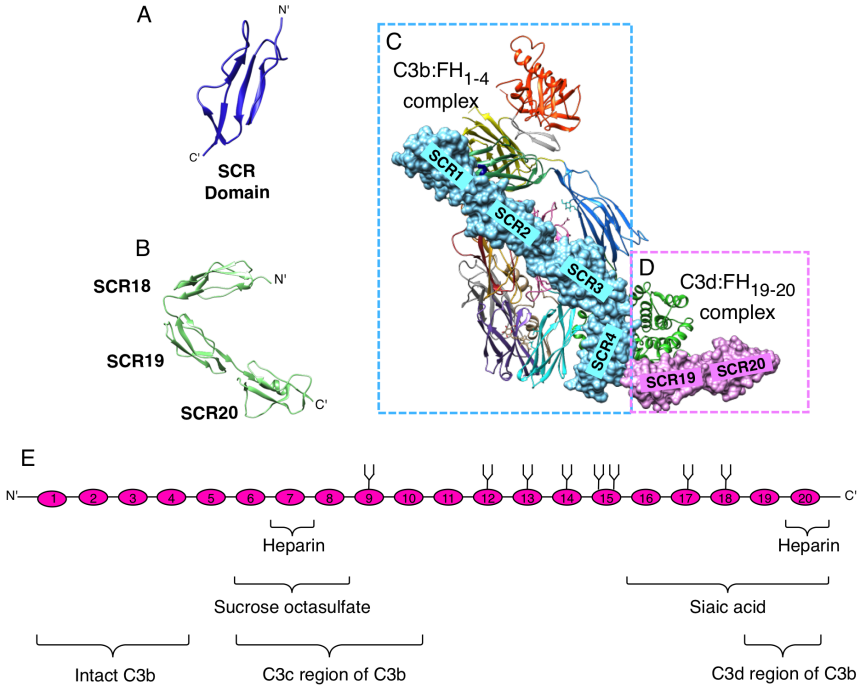

Figure 1.8: Factor H and its interactions with C3 activation fragments. (A) An example of the SCR domain, the structure of FH domain 1. **(B)** Crystal structure of FH domain 18-20. (PDB code: 3SW0). The crystal structures (C-D) shows that FH binds at two locations of C3b. **(C)** Crystal structure of C3b:FH_{1-4} complex. (PDB code: 2WII) The binding of FH_{1-4} accelerates C3 convertase dissociation, mediates Factor I cleavage. **(D)** Crystal structure of C3d:FH_{19-20} complex (PDB code: 3OXU). **(E)** Mapping of binding sites on the 20 SCR domains for FH ligands: Heparin; Sucrose octasulfate; Sialic acid, C3b binding. Eight glycosylation sites are labeled using black forks.

Factor H is a 150 kDa multi-modular multi-functional glycoprotein (Fig.1.8.E) composed of 20 SCR domains. Its two major functional sites are located at either end of its sequence. Four N-terminal SCR domains (SCRs 1-4) enforce AP C3

convertase regulation, by binding to C3b (Fig.1.8.C), accelerating the dissociation of C3 convertase and facilitating factor I cleavage of C3b. The C-terminal SCR domains (SCRs 18-20, Fig.1.8.B), on the other hand, contribute to surface binding and contain the ligand-binding sites for C3b, C3d, heparin, sialylated glycans and cell surface glycosaminoglycans. Their concerted activities are essential for the effectiveness and directionality of factor H mediated complement regulation. Crystal structures (Fig.1.8.C and D) (Morgan *et al*. 2011; Wu *et al*. 2009) have demonstrated that the N- and C-terminal domains of factor H target two different interaction interfaces on C3b , suggesting that factor H could bind to these two sites simultaneously . Furthermore, a recent crystal structure (Blaum *et al.* 2014) of the SCR 19-20 domains in complex with C3d and an analogue of a glycosaminoglycan provides a detailed explanation for the positive cooperativity (Meri & Pangburn 1990) between SCR 19-20 C3d and heparin binding sites.

In addition to the two most validated ligand-binding sites, further binding sites for C3b and heparin have been found distributed across the molecule. Factor H appears to possess a third C3b binding site, initially suggested to be situated near SCR 6-10 (Sharma & Pangburn 1996), later pinpointed to SCR 6-8 (Schmidt *et al*. 2008). Due the weak and transient binding properties, further studies are required to validate and explain the biological significance of this site. Heparin binding is also mediated by multiple binding sites, apart from the C-terminal binding site, factor H SCR 6-10 domains were determined to have heparin binding ability (Sharma & Pangburn 1996). Crystallographic studies (Prosser *et al*. 2007) have indicated that SCR-6 and the linker region between SCR-7 and SCR-8 may possess heparin binding sites. The multiple contact pattern of factor H is a explanation of the 'back-folded' conformation(DiScipio 1992) of fluid phase factor H and implicates the possibility of a conformational transition between the compact fluid phase and the extended surface bound conformation.

1.4.2 Complement factor H like protein 1

FHL-1 is a 42 kDa glycoprotein produced by alternative splicing of factor H gene. It is composed of seven N-terminal domains of factor H (Fig.1.7), with four extra amino acids at the C-terminal end. This truncated form of factor H possesses C3b binding and C3 convertase regulatory functions and in addition binds to heparin via its C-terminal SCR 7 domain. Despite its similarity with factor H, FHL-1 also functions as a matrix protein component which mediates cell adhesion (Hellwage *et al*. 1997), possibly partially explaining the differences in expression pattern compared with factor H. While the majority of the cell lines constitutionally express both FHL-1 and FH, MRC-5 lung fibroblasts only express FHL-1 mRNA. The presence of cytokines, inflammatory mediators and anti-inflammatory agents further diversifies the expression pattern of FH and FHL-1 (Friese *et al*. 1999).

1.4.3 Complement factor H related protein

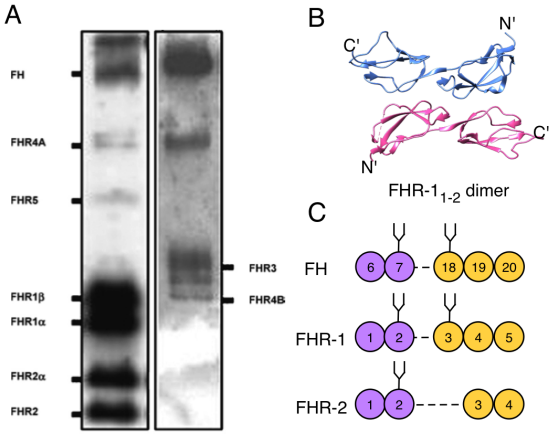

Figure 1.9: Biochemical properties of FHR proteins. (A) Western blot analysis of proteins from the FH family. Due to high sequence similarity, FHR proteins cross react with polyclonal anti-FH serum. (Skerka & Zipfel 2008) **(B)** Crystal structure of FHR1$_{1-2}$. Two chains of FHR1$_{1-2}$ form a head-to-tail dimer. The two chains are colored separately. (PDB code: 3ZD2)**(C)** Schematic domain structure of FHR-1 and FHR-2. The glycosylation sites are indicated by black forks.

The five FHR proteins (FHR 1-5) are encoded by five separate genes that are situated immediately next to the factor H gene. Like factor H, they are modular glycoproteins constituted of multiple SCR domains, varying in number from 4 to 9 (Fig.1.7). All FHR SCR domains share sequence identity (between 40 and 100%) with their corresponding factor H SCR domains, indicating the potential for

differential functions and protein-binding properties. Some signature factor H activities are conversed. For instance, FHR-1, FHR-3, FHR-4 and FHR-5 all bind to C3b; FHR-1, FHR-3 and FHR-5 bind to heparin, although only FHR-5 shows very weak factor I cofactor activity (Mölkänen *et al*. 2002; McRae *et al*. 2005). Novel functions are also emerging, and the first two N-terminal SCR domains (Fig.1.9.B) of FHR-1, FHR-2 and FHR-5 have now been shown to mediate the formation of homo- and heterodimers between FHR-1, FHR-2 and FHR-5 (Goicoechea de Jorge *et al*. 2013). These FHR dimers show elevated affinity to tissue deposited complement effectors, and compete with factor H binding, causing local relaxation of complement regulation. Another novel biochemical property of FHR proteins is the existence of differentially glycosylated forms (Fig.1.9.A and C). FHR-1 can be singly or doubly glycosylated (Skerka *et al*. 1991), while FHR-2 contains only one flexibly glycosylated site (Skerka *et al*. 1992). Additionally, nearly all FHR proteins are able to associate with lipoprotein particles, apart from FHR-3 (Skerka & Zipfel 2008). The most structurally characterized protein among FHR protein family is FHR-1. Within the 5 SCR domains, the crystal structure of first two was solved showing a head-to-tail dimer (Fig.1.9.B) (Goicoechea de Jorge *et al*. 2013), the rest of the SCR domains are believed structurally identical to the FH_{18-20} (Fig.1.8.B) due to the 98% sequence identity (Skerka *et al*. 2013).

FHR protein deletions and variations have been associated with susceptibility to numerous diseases. Individuals with FHR-1/3 deletion copy number polymorphism are associated with reduced risk of IgA nephropathy (Gharavi *et al*. 2011), age-related macular degeneration (Hughes *et al*. 2006) and systemic lupus erythematosus (Zhao *et al*. 2011). Duplication in FHR-5 copy number is strongly linked with familial C3 glomerulopathy (Gale *et al*. 2010). A recent report also revealed a link between the reduced copy number of FHR-1 and the presence of FH auto-antibody, which contributes strongly to the pathological mechanism of atypical hemolytic uremic syndrome (aHUS) (Moore *et al*. 2010).

These studies show that disruption of the delicately balanced interaction network between factor H and FHR proteins could have disastrous consequences.

1.4.4 Factor H family protein and immune evasion protein interactions

As the major down-regulator for AP activity on host cell surfaces, factor H is also frequently hijacked by microbial immune evasion proteins to aid microbes in the evading complement attack. *Streptococcus pyogenes* M protein was the first protein to be associated with factor H binding activity (Horstmann *et al*. 1988), and its role in the evasion of complement-mediated opsonophagocytosis.

There are two main microbial binding regions on factor H. One is located within SCRs 6-7, which is mainly exploited by group A *Streptococci pyogenes* and *Candida albicans* to recruit functional active factor H. C-terminal SCRs 19-20 contain a favorable binding site for *Neisseria gonorrhoeae* complement evasion proteins Por1A, Por1B (Ram *et al*. 1998) and OspE (Hellwage *et al*. 2001; Alitalo *et al.* 2004) from *Borrelia burgdorferi*, both of which have convergently evolved to target this site to mimic the glycosaminoglycan binding on FH. In fact, this site is universally targeted by a range of pathological bacterial strains (Meri *et al*. 2013). The overlapping of the heparin binding sites and evasion protein binding sites prompted the hypothesis that the surface bound factor H has to be correctly positioned in order to achieve maximum activity. This assumption is confirmed by the observation that *B.burgdorferi* produces two evasion proteins targeting different factor H heparin binding sites: CRASP1 (Kraiczy *et al*. 2004) which binds to the SCR-7 and OspE (Hellwage *et al*. 2001), which binds to the SCR 19-20. The heparin binding sites are highly conserved within the factor H family; therefore in addition to acquisition of factor H, homologous FHL-1 and FHR 1-5 proteins are also targeted.

In contrast to the similarity in surface acquisition of factor H by microbes, the

routes to acquire fluid phase factor H demonstrate greater diversity. Shiga toxin (Stx2) of enterohemorrhagic *Escherichia coli* recruits fluid phase factor H by binding to SCR 6-8 and 18-20 (Orth *et al*. 2009). At the same time FHL-1 and FHR-1 (Poolpol *et al*. 2014) are also sequestered. *Staphylococcal* binder of IgG (Sbi),excreted by *Staphylococcus aureus* was reported to form a tripartite complex with factor H SCR 18-20 in combination with complement C3 degradation isoforms(Haupt *et al*. 2008), but the biological significance remains to be investigated. In this study, the complement modulatory mechanism of Sbi will be explored in detail.

1.5 *Staphylococcus aureus*

1.5.1 General features

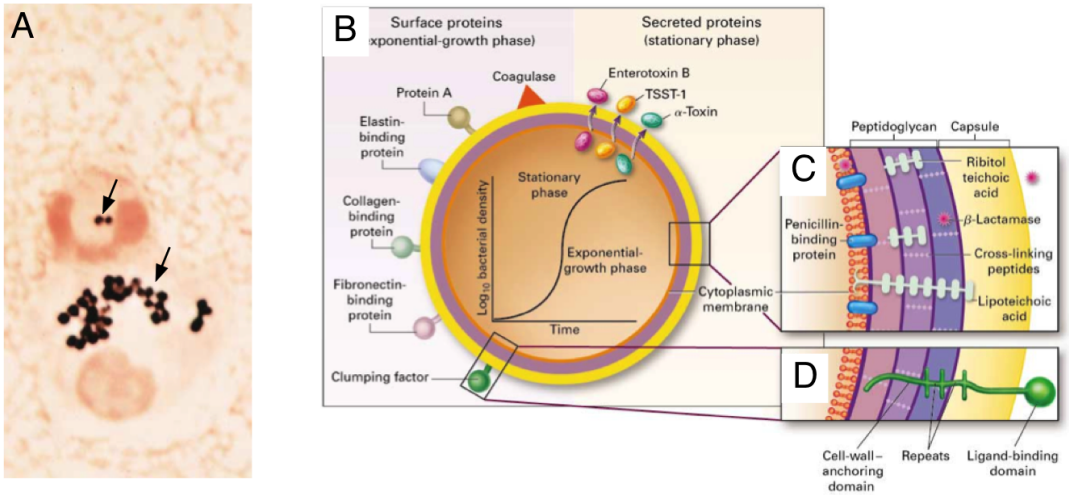

Figure 1.10: General features of *S.aureus.* (A) *Staphylococci* (black arrow pointed) with polymorphonuclear Leukocytes (Gram's stain, X1000) **(B)** Cellular structure of S.aureus. Image taken from (Lowy 1998).

The gram-positive bacterium *Staphylococcus aureus* (*S. aureus*) is a major opportunistic human pathogen. It was first discovered in 1880 by Sir Alexander Ogston in Aberdeen, Scotland and was found within the pus of an acute abscess (Ogston 1882). Under bacterial taxonomy, it is classified as a member of genus *Staphylococcus* within the family of *Micrococcaceae*. The name "*aureus*" was derived from the appearances of its golden colonies (*aureus* means golden in

Latin) when cultured on sheep blood agar. Under the microscope (Fig.1.10.A), it forms gram-positive cocci in clusters and the individual bacterium with a spherical shape has a size of approximately 1 μm in diameter.

1.5.2 The genome

The majority of the genetic material of *S. aureus* is stored in a circular chromosome assisted with additional prophages, plasmids and transposons (Lowy 1998). The genome of *S. aureus* was sequenced in 2001, revealing the size of the genome to be 2.8 Mb with a low GC content of 33%. About 85% of the genomic DNA constitutes approximately 2600 open reading frames (Hiramatsu 2001). Lateral gene transfer processes provide great dynamic for the genetic content, which agrees with the observation that most antibiotic resistance genes and virulence factor gene are carried by mobile elements such as plasmids and unique pathogenicity islands.

1.5.3 Cell wall structure

The exterior structural features and chemical characteristics have been demonstrated as indispensable for the virulence of *S. aureus*. The bacteria cell (Fig.1.10.B) is protected by an inner layer cell wall and an exterior capsule structure. *Staphylococcal* cell wall is composed of primarily peptidoglycan (50% by weight), ribitol teichoic acid and lipoteichoic acid. Together with structural peptides, they form a densely cross-linked matrix that covers the cell membrane, and provides a foundation for cell wall anchored proteins. Immunologically, the peptidoglycan shows endotoxin-like activity, stimulates the release of cytokines by macrophages, promotes platelet aggregation (Lowy 1998) and activates the complement system through both CP and AP (Verbrugh 1979).

Most *staphylococci* produce extracellular capsular polysaccharides (CP*), the variations in synthetic pathways provide observable morphological differences

between different strains of *S. aureus*. Further studies based on reactivity to monospecific rabbit and mouse antisera identified 11 types of CP* serotypes, within which types 5 and 8 account for 75% of human *S. aureus* isolates (O'Riordan & Lee 2004). Encapsulation has been associated strongly with increased virulence of the bacteria, protecting the bacteria from opsonization and phagocytosis. In the presence of the capsule layer, deposited C3b is found mostly on cell wall, buried under the capsule layer and therefore unable to promote efficient phagocytosis. Only antibody mediated complement activation can efficiently opsonize throughout the capsule layer (Verbrugh *et al*. 1982).

Many *Staphylococcal* proteins are located on the surface of the bacteria, embedded in the cell wall through the peptidoglycan. Although these proteins demonstrate great structural diversity, they share common characteristics as cell wall anchored (CWA) proteins. The protein architecture starts with a N-terminal signal peptide that directs proteins to be translocated through the secretory apparatus in the membrane, followed by functional domains. The C-terminal part of CWA protein typically contains a cell wall-spanning domain and a characteristic sorting signal which facilitates their covalent anchorage to peptidoglycan (Foster *et al*. 2014). Most of the *staphylococcal* CWA proteins are essential for invasion and survival of the bacteria. Iron-regulated surface determinant extracts heme groups from hemoglobin and transports them across the cell membrane into the cytoplasm (Pilpa *et al*. 2009; Grigg *et al*. 2010). *Staphylococcal* Protein A (SpA) binds to the Fc fragment of the IgG that inhibits CP complement activation, and it also acts as a superantigen for B-lymphocytes and disrupts the adaptive immune system. Furthermore, apart from those interfering with the immune system, the most abundant group of CWA proteins is the matrix molecule adhesion (MSCRAMM) family proteins, which demonstrate essential roles in the colonization, dissemination and pathogenesis stages of bacterial advance. Recently, more and more CWA proteins are being associated with previously un-annotated functions, which elicit the idea that

CWA proteins carry redundant functions to provide advantages for bacteria under constantly changing physiological condition.

1.5.4 Colonization

S. aureus is a common human commensal, it colonizes approximately 30 to 50 percent of healthy adults and about 20 percent of the human population becomes permanently and persistently colonized (Kluytmans *et al*. 1997). It is most commonly found colonized in the moist squamous epithelium of the anterior nares, but also colonizes the mucous membrane of the pharynx, vagina and axillae (Peacock *et al*. 2001; Lowy 1998). The colonized bacteria normally persist unnoticed by the host, reaching a state of mutual acceptance and tolerance. But upon disintegration of this balanced condition, the previously localized and non-invasive commensal bacteria can quickly disseminate and spread throughout the body. *S. aureus* infection can result in a wide range of diseases. The detailed mechanism leading to *S. auerus* infection is still largely unknown but traditionally *S. aureus* was described as an opportunistic pathogen, which preys on individuals with compromised immune systems or having undergone major surgery. Therefore the deteriorated host immune system and the breached epithelial barrier could partially account for the invasion of *S. aureus*. However, the capability of *S. aureus* to cause disease in hosts without obvious predisposing conditions is getting increasingly recognized (van Belkum & Melles 2009).

1.5.5 *Staphylococcal* infection disease

The persistent carriers of *S. aureus* are at higher risk of infection when immune-compromized, the colonized nasal epithelium provides a reservoir of bacteria from which subsequent infections can develop (Wenzel & Perl 1995). Mild skin infections, including impetigo, folliculitis and furunculosis, are the

common symptoms of *S.aureus* infections (Darmstadt & Lane 1994), which are usually self-limiting or can be easily treated with topical applications. However, if left untreated, bacteria could enter the blood stream through the damaged skin and mucosal tissue, leading to more serious and even life-threatening conditions.

Once the circulation system becomes bacteraemic, the previously localized infection is able to spread to other tissues. *S. aureus* is known to spread to joints, bones and kidneys and lungs. However the most vulnerable tissue is the heart (Fowler *et al*. 2005). Endocarditis is the infection of cardiac valves, whereby *S. aureus* can adhere to and establish thrombi on healthy or damaged valves. The heart valves are a susceptible location for *S. aureus* infection, since they lack a separate blood supply, therefore they cannot directly be reached by neutrophils. Clinical complications of endocarditis include stroke and cardiac arrest and the mortality rate is over 50% (Lowy 1998).

Toxic shock syndrome (TSS) is another complication caused by *S. aureus* infection. *S. aureus* secretes pyrogenic-toxin superantigens (Fraser *et al*. 2000). These superantigens bind directly to the major histocompatibility complex (MHC) class II molecule on the antigen-presenting cell and the T cell receptor (TCR) on the T cells. This leads to extensive T-cell proliferation and substantial cytokine release, which in turn causes severe tissue damages and eventually leads to TSS. As the consequence of this cytokine spike, patients experience a rash, high fever and hypotension. If these conditions remain unalleviated, the symptoms can rapidly escalate to capillary leak, coma, multi-organ failure and eventually death (Lowy 1998).

1.5.6 *Staphylococcal* transmission

Transmission of *S. aureus* occurs in both the hospital environment and within the community. Individuals with family members or close contacts who are infected

or those living in crowded residences are subjected to a high risk of community acquired *S. aureus* infections. However, the nosocomial infections are acquired through three common routes: skin-to-skin contact, compromise of the skin barrier and sharing contaminated equipment. Nevertheless, it is now clear that a patient's own endogenous reservoir is the most prevalent origin for nosocomial *S. aureus* infection (Eiff *et al.* 2001). Nasal carriage increases the risk for auto-infection by the factor of three (Wertheim *et al.* 2004).

1.5.7 History of MRSA

Over the last hundred years, evolving in parallel with the episodic discoveries of new antibiotics, *S. aureus* has earned a reputation for being versatile under the selective pressures from antibiotics. Until the discovery of penicillin, *S. aureus* infection was extremely lethal and the mortality rate was as high as 80% (Skinner 1941). In 1940, penicillin was introduced to treat *S. aureus* infection. It functions as an inhibitor of the penicillin binding proteins (PBP), which catalyze the cross-linking reaction of peptidoglycan during cell wall biosynthesis; the inhibition directly causes the lysis of bacteria. However, only two years after clinical usage, the first *S. aureus* strains resistant to this antibiotic were isolated (Chambers 2001). The resistance was established by acquisition of a plasmid that encoded penicillinase, catalyzing the hydrolysis of penicillin. By 1960, approximately 80% of all *S. aureus* strains had become resistant to penicillin. In response to rising penicillin resistance, in 1961, a penicillinase-resistant penicillin derivative called methicillin was introduced to treat *S. aureus* infection. However only after a year, *S. aureus* developed resistance to this antibiotic and was later named methicillin resistant *S. aureus* (MRSA). The methicillin resistance (mec) is attained by the acquisition of the *mecA* gene that is located on a mobile island designated the *staphylococcal* cassette chromosome mec (SCCmec) (Katayama *et al*. 2000). The *mecA* gene encodes an unique PBP, PBP2a, which demonstrates low affinity for all β-lactam antibiotics (e.g. penicillin and

methicillin) (Hartman & Tomasz 1984). Therefore even if other types of PBPs are totally inhibited, the PBP2a can still mediate normal cell wall biosynthesis.

Taking advantage of the resistance to the β-lactam antibiotic family, by the 1980s MRSA had become prevalent in the nosocomial setting, where bacteria can constantly replicate under fresh antibiotic selection pressures. Unfortunately MRSA has conquered nearly all antibiotics discovered since 1940, and so MRSA is now a term often associated with strains that carry multiple antibiotic resistances. According to MRSA statistics between 2009 and 2013 (Public Health England 2014). In England, Wales and North Ireland, over 80% of MRSA isolates are resistant to ciprofloxacin, over 60% of the isolates show resistance to erythromycin and below 20% of all isolates are resistant to fusidic acid, gentamicin, mupirocin and rifampicin. Only vancomycin, tigecycline, linezolid and daptomycin show minimal resistant isolate counts and serve as the last resort for MRSA treatment. However this last line of defense is being constantly challenged, as MRSA isolates that are resistant to these antibiotics are sporadically being reported globally.

Until the mid-1990s, MRSA infections were mostly confined within hospitals, targeting immune compromised patients. However, since the arrival of the new millennium, MRSA transmission has demonstrated a new trend. Increasing MRSA outbreaks in the community setting were reported (Chambers 2001), which lead to the isolation of a distinct strain of MRSA, community acquired MRSA (CA-MRAS). CA-MRSA demonstrates high virulence and fitness (Voyich *et al*. 2005), as it not only can spread continuously in immune-compromised population but also cause disease in healthy individuals. According to genomic and biochemical analysis, most CA-MRSA possess the *LukF* gene encoding the panton-valentine leuocidin (PVL) toxin and produce increased amounts of phenol-soluble modulins (PSMs) peptides, both toxins contribute immensely to the neutrophil killing. CA-MRSA has also shown increased expression level of

alpha-toxin, which induces lysis of human macrophages and erythrocytes. Therefore, in contrast to most hospital acquired MRSA (HA-MRSA) and methicillin sensitive *staphylococcus aureus* (MSSA), CA-MRSA demonstrates enhanced ability to resist and evade immunological effector cells. However, this aggressive behavior also brings detrimental side effects, CA-MRSA is usually sensitive to most antibiotics other than the β-lactam family (Otto 2013) and usually a lower concentration of the antibiotic is required to sufficiently contain the infection (Cheung *et al*. 2011). Type IV and V SCCmer mobile elements are the universal genetic characteristics of CA-MRSA (Daum *et al.* 2002), these shorter methicillin resistant determinant elements could be attributed to the relaxed antibiotic resistance, therefore causing less fitness burden (Lee *et al.* 2007) which is the prerequisite condition for increased CA-MRSA virulence.

Since 2005, in England, Wales and Northern Ireland, due to elevated hospital hygiene standards and tightened monitoring measures, both MRSA related infections and deaths are in a steadily decline. Nevertheless, the sporadic appearances of the multi-drug resistant MRSA strains and the intermittent outbreaks of the CA-MRSA remind us the challenges we are facing from this constantly evolving pathogen.

1.6 *S. aureus* proteins for invasion attachment and immune evasion

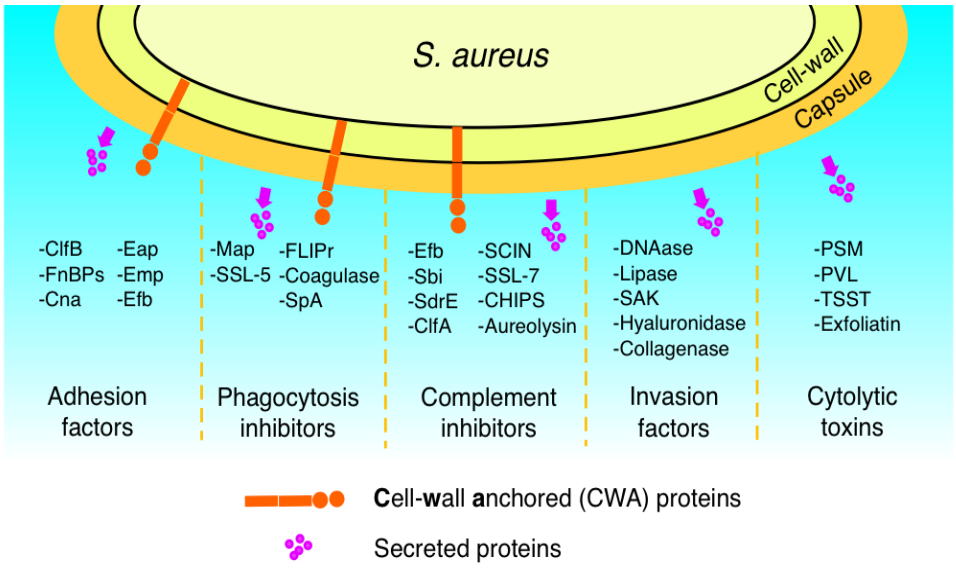

Figure 1.11: *S.aureus* expresses cell wall anchored and secreted immune evasion factors. These factors are responsible for the resistance against the complement system and phagocytosis, targeted host cell adhesion, efficient tissue invasion and direct damage on host cells. The inhibitors of complement and phagocytosis not only suppress the innate immune response, but also dampen the development of adaptive immunity. Adhesion, invasion and cytolytic factors are part of an invaluable arsenal, by which *S.aureus* thrives inside the host system. The selected molecules are described in detail in section 1.6, the full name is given in abbreviation section.

As a commensal bacterium, millions of years of coexistence and coevolution with humans has created the *S. aureus* of today, a versatile pathogen that is capable of both persistent colonization and opportunistic invasion. As introduced in Section 1.5.3, CWA proteins and secreted proteins contribute immensely to various steps of *staphylococcal* infection. Virulence factors produced by *S. aureus* are summarized in Fig.1.11 and can be roughly categorized into proteins attenuating complement activation (complement inhibitors) and phagocytosis (phagocytosis inhibitors), proteins mediating host environment adhesion (adhesion factors), proteases that degrade extracellular matrix (invasion factors) and leukocyte lytic proteins (cytolytic toxin).

1.6.1 *S. aureus* complement evasion

The complement system functions partially as an early warning system for the host against colonizing and invading pathogens; it coordinates concerted bactericidal attacks involving both innate and adaptive immune system components. During the course of evolution, *S. aureus* has adapted numerous physical and biochemical mechanisms to avoid detection by the complement system. Firstly, the encapsulated exterior is extremely futile for complement deposition and amplification. Secondly, underneath the capsule layer, the cell wall of the *S. aureus* is embedded with a large spectrum of CWA proteins that deteriorate complement activity. Finally, to actively inhibit complement activation in close vicinity, *S. aureus* expresses and secretes an arsenal of immune evasion proteins that block complement cascades.

As introduced earlier (Section 1.1.1), specific protein-protein interactions and sequential proteolytic cleavages are essential for complement activation and regulation. This provides numerous stages of intervention that can be exploited by *staphylococcal* immune evasion proteins to efficiently debilitate this carefully regulated protein interaction network. *Staphylococcal* complement inhibition strategies can be roughly categorized into three distinct mechanisms. Firstly *S. aureus* secretes small fluid phase proteins to the surrounding environment where they directly interfere with complement activation at almost every level. Secondly, *S. aureus* expresses CWA proteins that are able to recruit host complement regulators onto the bacterial surface, avoiding complement attack by imitating the host cell surface. Thirdly, *S. aureus* produces proteases that specifically degrade complement component C3.

Given that all complement pathways converge on the proteolytic activation of C3 by C3 convertase, to exert most effective inhibition on complement activation, most secreted *staphylococcal* immune evasion proteins are designed to attenuate

C3 convertase activity.

Staphylococcal extracellular fibrinogen binding (Efb) protein consists of two functional domains. The N-terminal domain (Efb-N) mediates fibrinogen binding, resulting in inhibition of platelet activation (Palma *et al*. 2001). The C-terminal domain (Efb-C) inhibits the activation of both CP and AP (Lee *et al*. 2004) through strong interactions (Hammel *et al.* 2007b) with C3d containing C3 activation products (e.g. C3b, iC3b and C3d). The strong binding (K_d of 0.8 nM) alters the C3b native conformation, causing impaired binding of factor B, thereby allosterically preventing the assembly of AP C3 convertase (Chen *et al*. 2010). Furthermore, the binding of C3 could also render the Efb:C3 complex an unsuitable substrate for CP C3 convertase, causing inhibited CP activation. Not only does it interrupt complement activation, the Efb-C binding to the C3d concave surface also physically blocks CR2 binding, by which the effect of complement mediated B cell activation is severely disrupted.

In 2007, a homolog of Efb-C, (Efb homologous protein) Ehp or the extracellular complement binding protein (Ecb) was identified (Hammel *et al*. 2007a). In contrast to Efb, Ehp is a slightly shorter (105 aa) secreted protein, sharing 44% identity with Efb-C, binding to the C3d part of C3 molecule in similar fashion to Efb-C. Therefore, Ehp largely demonstrates similar complement inhibition and B-cell activation inhibition properties. However in a recent study, Ehp has been shown to form a tripartite complex with C3b and factor H, which contributes to the bacterial survival *in vitro* (Amdahl *et al*. 2013).

In addition to complement inhibition by direct binding to C3, *Staphylococcal* complement inhibitor, SCIN, a 9.8 kDa secreted protein, blocks both AP and CP activation by trapping AP and CP C3 convertases in an enzymatically defunct dimeric state (Rooijakkers *et al.* 2005a). Although the trapped C3 convertase dimers are not able to accept new C3 substrate or to form subsequent C5

convertase, the SCIN mediated complexes demonstrate extremely long half-lives comparing with physiological AP C3 convertase. This property allows crystallographic studies of the SCIN stabilized C3 convertase complex (Rooijakkers *et al*. 2009), which provided molecular details on both the SCIN inhibition mechanism and the AP C3 convertase architecture.

To counteract the already deposited complement effector molecules (e.g. C3b and C4b), *S. aureus* acquires host complement regulatory proteins through numerous membrane anchored CWA proteins on its surface. Serine-aspartate acid repeat protein (SdrE) was first hypothesized as an adhesive molecules (Corrigan *et al.* 2009). However, recent functional investigations demonstrated that SdrE not only acquires serum factor H (Sharp *et al.* 2012) but also C4BP (Hair *et al.* 2013). The presence of surface bound factor H and C4BP inhibits C3 convertases activity, but they have to work with protease factor I to cleave C3b or C4b into their inactivated forms. *S. aureus* expresses Clumping factor A (ClfA) on the cell surface to recruit active factor I, leading to increased local concentration of factor I by which C3b and C4b inactivation can be accelerated.

The severity and efficiency of the complement attack is directly related to the local C3 level. To diminish the high concentration of local C3 with low bacterial burden, *S. aureus* has learned to kidnap host proteolytic pathways, among which the plasminogen activation pathway is frequently exploited. *S. aureus* secretes staphylokinase (SAK) that proteolytically activates the zymogen plasminogen to plasmin (Mölkänen *et al*. 2002). Subsequently, activated plasmin in the fluid phase can cleave C3 into its activation products (Gorham *et al.* 2014; Barthel *et al.* 2012). Numerous *staphylococcal* immune evasion proteins (e.g. Efb and Sbi) have been described that accelerate this process by mediating plasminogen and C3 binding, leading to consumption of local C3, but they do not directly trigger plasminogen activation (Koch *et al*. 2012). SAK activated plasmin also contributes significantly to the removal of bacterial surface opsonin by

proteolytically degradation of C3b and IgG molecules (Rooijakkers, *et al.* 2005b). So far, *staphylococcal* zinc-dependent protease aureolysin is the only protease that has been shown to directly degrade C3 molecules. It cleaves C3 near the C3 convertase cleavage site, producing C3a and C3b. C3b is then subsequently degraded by factor H and factor I (Laarman et al. 2011).

It is evident that *S. aureus* is equipped with a bounteous arsenal of immune evasion proteins to avoid complement attack, and the central complement component C3 is heavily targeted. This reflects the complicated and ever-changing relationship between the host and invading bacteria. By combining factors such as the expression level, cellular location, inter-molecular synergy and expression timing of these immune evasion proteins, a variety of complement evasion tactics can be employed to suit different stages of *S. aureus* infection.

1.7 *Staphylococcal* binder of immunoglobulin (Sbi)

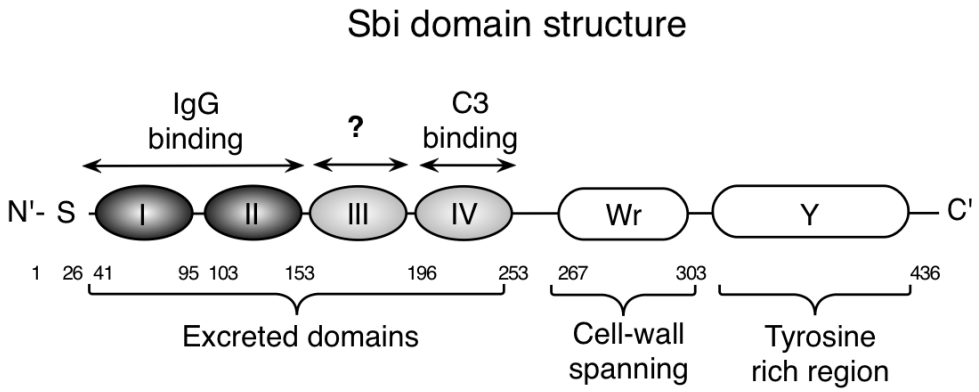

Figure 1.12: Domain structure of full length Sbi. (Burman *et al.* 2008) The predicted cell wall-spanning proline-repeat region (Wr) (Zhang *et al.* 1998). C-terminal tyrosine-rich region (Y), which has been implicated in IgG-mediated signal transduction. (Zhang *et al.* 2000).

Staphylococcal binder of immunoglobulin (Sbi) is the second IgG binding protein identified from *S. aureus* (Zhang *et al*. 1998). It was discovered in a shotgun phage display experiment utilizing *S. aureus* strain 8325-4 chromosomal DNA, but later shown to be expressed in numerous clinical strains of *S. aureus* (Jones *et al*. 2008). The Sbi gene encodes a protein of 436 amino acids. Structural and

bioinformatical analyses revealed that it comprise four N-terminal functional domains (Fig.1.12), a proline rich domain and a tyrosine rich domain, but without the typical Gram-positive cell wall anchoring sequence LPXTG (Burman *et al*. 2008).

Most of the immune-modulating activities of Sbi are located at the N-terminal end of the molecule. The IgG binding domains I-II share high sequence identity with the IgG binding domain of SpA, however they bind to the Fc region of the IgG molecule in a unique way that causes the formation of cross-linked insoluble IgG immune-complexes (Atkins *et al*. 2008). In contrast to the clear functional annotation of domain I-II (Sbi-I-II), Sbi domain III-IV (Sbi-III-IV) has been associated with a range of activities. Initially, the phage display experiments demonstrated that peptides from domain IV (Sbi-IV) bind to β_2-glycoprotein I (β_2-GPI), a protein involved in blood coagulation (Zhang *et al*. 1999). However, in subsequent pull-down studies using recombinant proteins, domain IV was associated with C3 fragments binding activity. When domain III-IV was used, it was found to bind to C3 fragments together with factor H to form a tripartite complex (Burman *et al*. 2008; Haupt *et al*. 2008). The crystal structure (Clark *et al*. 2011)of Sbi-IV in complex with C3d shows that Sbi-IV binds to the concave surface of C3d, sharing the interaction interface with Efb-C and Ehp. In addition, Sbi-IV also binds to the convex surface of the C3d fragment, providing an unprecedented alternative binding mode. Although the binding strength on the convex side has been shown to be extremely weak (Upadhyay *et al*. 2008), interaction interface analysis and *in silico* binding simulation studies support this binding mode being physiologically genuine (Gorham *et al*. 2014).

Among *staphylococcal* C3d binding proteins, Sbi demonstrates the weakest binding strength. However, the complement modulation function of Sbi is the most intriguing. By binding to C3, Sbi-IV alone inhibits the alternative pathway activation in a dose dependent manner. Like Efb-C and Ehp, Sbi-IV antagonizes

C3d binding to CR2, inhibiting B cell activation. Together with domain III, Sbi-III-IV inhibits all complement pathways by inducing the futile consumption of C3 through AP activation. It was hypothesized that Sbi triggers C3 activation distally and limits the deposition of the metastable C3b molecule to nearby IgG and Sbi itself, through which it safely depletes local C3 and protects *S. aureus* from opsonization. Noticeably, during this process, Sbi itself becomes deposited with C3 fragments, however the functional roles of Sbi-C3b adducts still remain to be elucidated (Burman *et al.* 2008). Finally, as mentioned earlier, Sbi-III-IV facilitates the plasmin-mediated degradation of C3 (Koch *et al.* 2012).

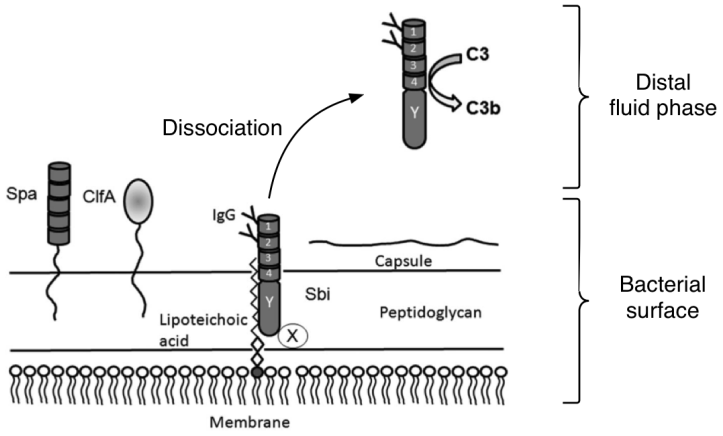

Figure 1.13: Putative model of Sbi cellular localization. Sbi is tethered on the *S.aureus* surface through interactions with lipoteichoic acid and a putative second membrane component X. The IgG binding domain I and II are biologically active even associated with cell membrane. On the contrary, Sbi-III-IV becomes activated after dissociation. The dissociation mechanism remains to be investigated. CWA proteins Spa and ClfA are also shown on the image. Image taken from (Smith et al. 2012).

Given the counter-intuitive role of Sbi as a C3 activator, its cellular location, expression pattern and immune evasion mechanism are scrutinized in detail in order to make sense of how this protein is utilized to consume C3 without causing damage to the bacteria. Sbi gene deletion severely compromises the survival rate of *S. aureus* Newman strain in a whole-blood based survival assay. The deletion of Sbi has a slightly weaker impact on the survival rate reduction compared with the deletions of other well-known *staphylococcal* immune

evasion factors (e.g. SpA, ClfA and Isd). Therefore, Sbi is an immune evasion factor that contributes to the avoidance of opsonophagocytosis. Moreover, the secreted Sbi containing N-terminal domains III and IV is the minimal requirement for Sbi mediated protection (Smith *et al*. 2011).

The sophisticated domain arrangement confers upon Sbi a unique flexibility in cellular location. It can be secreted abundantly to the surrounding environment (Zhang *et al.* 1999; Burman *et al.* 2008). It is also found tethered on the cell wall using C-terminal proline rich and tyrosine rich domains through lipoteichoic acid (LTA), in this way (Fig.1.13), the N-terminal domains of Sbi-III-IV are buried by the capsule layer, with only Sbi-I-II in contact with ambient environment. Although, the molecular detail about the release of the cell wall bound Sbi is still unknown, but it has been shown that both cell wall bound and secreted forms of Sbi contribute to immune evasion by the bacterium (Smith *et al*. 2012).

The expression of Sbi is strictly regulated by at least three independent regulatory mechanisms. The presence of IgG in the surrounding environment induces Sbi expression (Zhang *et al*. 2000), but both accessory gene regulator (agr) and small pathogenicity island rNAs D (SprD) are the negative regulators of Sbi expression (Chabelskaya *et al.* 2010). Both regulatory elements have been shown to contribute significantly to the virulence of *S.aureus* in animal models.

1.8 Aims:

Among the four Sbi N-terminal domains, Sbi domain III and IV have been shown to be the minimal domain requirement to trigger futile consumption of C3. Based on the Sbi-III-IV construct, a systematic site-directed mutagenesis study will be performed, and the resulting Sbi mutants will be examined for their C3 consumption activity. Using the functionally defective mutants of Sbi, a series of comparative structural and functional experiments will be performed to discover

the underlying molecular characteristics. The design of the experiment will be based on the proposed working mechanisms of Sbi.

It was previously proposed that the Sbi-C3b covalent adduct could be a crucial component of the Sbi triggered C3 consumption mechanism, however experimental evidence supporting this view is still scarce. To carry out in-depth studies of the Sbi-C3b adduct, initially a protocol of *in vitro* reconstitution of Sbi-C3b will be developed. Then, the C3b covalent attachment sites on Sbi-III-IV will be investigated by site-directed mutagenesis, C3b deposition assays, and mass spectrometry. Results will be cross-examined with the convex surface binding mode of the Sbi-IV:C3d complex, and eventually a mechanism of Sbi-C3b adduct formation will be proposed. Complement assays will be performed on the purified Sbi-C3b adduct in order to investigate the potential complement modulatory function of the Sbi-C3b adduct.

This study establishes a functional connection between Sbi triggered C3 consumption and Sbi:C3:FHR-1 ternary complex formation. The structural basis of Sbi:C3d:FHR-1 will be investigated using I-TASSER protein structure prediction methods, single molecular fluorescence resonance energy transfer (smFRET), and small angle X-ray scattering (SAXS). A putative structural model of Sbi-III-IV:C3d:FHR-1 will be proposed.

The results are expected to increase our understanding of infection and immunity and provide insight into the mechanisms deployed by *S.aureus* to achieve host immune evasion. An advanced understanding of the immune evasion mechanism is advantageous not only for the development of antibacterial strategies but also for development of therapeutic products for complement related human conditions.

Chapter 2: Materials and Methods

2.1 Plasmids, cell strains and media

2.1.1 DNA plasmids for use as PCR templates

pQE30$^{Sbi\text{-}III\text{-}IV}$

The DNA sequence of Sbi N-terminal domain III-IV (150-266 aa) was cloned into pQE30 vector by Dr Elizabeth Clark. This vector contains an ampicillin resistance gene and the inserted sequence is under control of the T5 promoter. The expressed Sbi-III-IV protein contains a N-terminal 6×His tag. (Appendix Fig.9.1.1.1)

pQE30$^{Sbi\text{-}III\text{-}IV\text{-}cys}$

A derivative construct of pQE30$^{Sbi\text{-}III\text{-}IV}$ made by Dr Sylvain Royer. A C-terminal cysteine residue was inserted for the convenience of sulfhydryl-specific labeling investigations. (Appendix Fig.9.1.1.2)

pET15b-C3d^{17A}

Prof David E. Isenman (University of Toronto) kindly provided the expression vector for human complement component C3 fragment C3d. The DNA sequence of the C3d fragment (D^{996}-R^{1303}) was cloned into pET15b. A single point mutation, C1010A, was inserted to prevent the formation of inter-molecular disulfide bond. This vector contains an ampicillin resistance gene and the expression of the inserted gene is under control of a T7 promoter. During cloning, the N-terminal His-tag sequence was deleted to produce tag-free C3d^{17A} protein. (Appendix Fig.9.1.1.3)

pMA-T-C3a

The codon optimized C3a gene suited for *Escherichia coli* (*E.coli*) expression was

commercially synthesized by the GeneArt service provided by Invitrogen. According to the protein sequence of human complement component C3 (Swissprot accession No.P01024.3), the coding region from amino acid 672 to 749 was inserted into the pMA-T vector carrying an ampicillin resistance gene. (Appendix Fig.9.1.1.4 and Fig.9.11)

2.1.2. Expression plasmids

pQE30

This plasmid contains a non-cleavable N-terminal 6×His-tag and an ampicillin resistance gene. The expression is under control of a T5 promoter. (Appendix Fig.9.1)

pET28a

This plasmid contains a N-terminal thrombin cleavable 6×His-tag, a T7 tag and a C-terminal 6×His-tag, a kanamycin resistance gene and is under the control of a T7 promoter. (Appendix Fig.9.3)

pGEX-htb

This plasmid is a derivative vector of pProex-htb (Appendix Fig.9.2), which contains a TEV protease cleavable N-terminal GST-tag, an ampicillin resistance gene and is under the control of a tac promoter.

2.1.3 Cell strains

The *E.coli* strain DH5α (NEB) chemically competent cells were used for molecular cloning experiments in this study. For mutagenesis experiments, *E.coli* strains XL-Gold Ultra and XL-Blue (Agilent) chemically competent cells were used. *E.coli* strains. BL21 (DE3) (BIOLINE) and Origami (DE3) (Agilent) chemically competent cells were used for protein expression.

2.1.4 Microbial media

E.coli cells were cultured in autoclave sterilized *luria-bertani* broth (LB, 1% tryptone, 0.5% yeast extract, 1% NaCl) liquid medium or LB-agar (LB medium supplemented with 2% agar). Antibiotic stock solutions (100 mg/ml ampicillin or 50 mg/ml kanamycin) were added to the medium at a dilution of 1 in 1000 prior to the culturing of cells. The LB-agar was allowed to cool down to near body temperature before the antibiotic was added and the medium was poured into 90mm Petri dishes. The LB agar plates were sealed and stored in a 4°C cold room.

E.coli cells after transformation were recovered in super optimal medium (SOC, 2% tryptone, yeast extract 0.5%, 10 mM NaCl, 2.5 mM KCl, 10 mM $MgCl_2$ and 20 mM glucose).

LB 5052 auto-induction medium was used to express proteins that were cloned into pET vectors where protein expression is controlled by T7 promoter. 5052 stock solution (25% glycerol, 2.5% glucose and 10% lactose) was added to the LB medium using a dilution factor of 1 in 50 prior to the up-scaled secondary cell culture.

2.2 Cloning and Site-directed mutagenesis

2.2.1 General molecular cloning methods

Phusion High-Fidelity DNA polymerase (ThermoFisher) was used to amplify DNA fragments for subsequent cloning procedures. PCR reactions were carried out using an MJ Research PTC-200 thermocycler. The final volume for each reaction was maintained between 20-25 µl, by making aliquots from a master mix. Lyophilized synthesized DNA was resuspended with water to a final concentration of 100 ng/µl; another 1:50 dilution with sterile water was made

for the usage as DNA template. Mini-prep purified plasmids being used as template DNA were diluted 1:20 in sterile water. After the PCR products were digested by restriction enzymes, purified and ligated with linearized plasmid, the insert-containing plasmids were transformed into competent cells. Individual clones were then screened for the correct insert by OneTaq polymerase (NEB) colony PCR.

Phusion High-Fidelity DNA polymerase was used to amplify all DNA fragments for standard cloning experiments described in this study. The recipe for a typical reaction master mix is shown in table 2.1, the corresponding temperature cycle program is in table2.2.

Table 2.1: Phusion DNA polymerase PCR reaction mix

Volume(μl)	**Component**
10	5×Phusion HF Buffer
1	10 mM dNTPs
1	Forward Primer (25 μM working stock)
1	Reverse Primer (25 μM working stock)
1	Template DNA
0.5	Phusion DNA Polymerase (2 U/μl)
40.5	Autoclaved Water

Table 2.2: Phusion DNA polymerase PCR program

Step	**Temperature**	**Duration**
1. Initial denaturation	98°C	30 sec
2. Denaturation	98°C	10 sec
3. Annealing	72°C	30 sec
4. Elongation	72°C	1 min
	Go to step 2 for 35 cycles	
5. Final elongation	72°C	10 min
6. End	4°C	-

OneTaq polymerase was used to screen transformed cells for the plasmid containing the DNA insert of interest. For each clone, small amount of cells were transferred to the PCR tube using a sterile pipette tip. A prolonged initial heat lysis step was added to ensure complete cell lysis by which the DNA template

becomes accessible to the polymerase. Table 2.3 shows a recipe for a typical reaction, Table 2.4 shows the corresponding temperature cycle program.

Table 2.3: OneTaq DNA polymerase PCR reaction mix

Master mix (8×25µl reactions)	**Component**
1µl	OneTaq polymerase
8µl	Forward Primer
8µl	Reverse Primer
40µl	Standard Reaction Buffer×5
4µl	10 mM dNTP
139µl	Sterile Water

Table 2.4: OneTaq DNA polymerase PCR program

Step	**Temperature**	**Duration**
1. Initial denaturation	95°C	5 min
2. Denaturation	95°C	30 sec
3. Annealing	55°C	30 sec
4. Elongation	68°C	1 min
	Go to step 2 for 35 cycles	
5. Final elongation	68°C	10 min
6. End	4°C	-

2.2.2 Site-directed Mutagenesis methods

In this study, mutations were inserted by mutagenic PCR reactions utilizing synthesized DNA primers incorporating the altered genetic code. For each mutagenesis experiment, a 50 µl PCR master mix (Table 2.5) was set up and then divided into five 10 µl aliquots, through which five different extension temperatures (72°C, 72.5°C, 73.3°C, 74.3°C and 75°C) were tested for the optimal amplification conditions. A typical mutagenic PCR program is shown in Table 2.6. During the extension step, different temperatures are achieved by creating a temperature gradient using a thermocycler.

After amplification, the PCR products were analyzed on a 1% agarose gel to evaluate the result of the mutagenesis reaction. The successfully amplified plasmids were then digested by methylation sensitive DpnI fast digest

(ThermoFisher) restriction enzyme for 30min at 37°C. The Pfu DNA polymerase that was utilized in the PCR reaction yields mutated, unmethylated double stranded circular plasmids, which were incompatible as substrates for the DpnI restriction enzyme and thus survive the digestion. The mutated plasmids were then purified from the digestion mixture by MiniElute PCR reaction clean-up kit (Qiagen). 5µl of the purified mutant plasmids were added to 10 µl of XL-Gold ultra-competent cells. After transformation, several successful colonies were selected and cultured in 15 ml of LB broth at 37°C overnight. Cells were then recovered by centrifugation (8000*g*, 10 min) and resuspended in 1 ml of water, from which plasmids were then extracted using GeneJet miniprep kit and stored at -20°C. The purified plasmid was sequenced to confirm the success of the mutagenesis experiment. For double, triple and quadruple mutants, the mutations were inserted step-wise based on verified mutated plasmid.

Table 2.5: Pfu DNA polymerase mutagenic PCR reaction mix

Volume (µl)	**Component**
10	10×*Pfu* Buffer with $MgSO_4$
1	10mM dNTPs
1	Forward Primer (125 ng/µl)
1	Reverse Primer (125 ng/µl)
1	Template DNA (2 ng/µl)
1	*Pfu* DNA Polymerase (2 U/µl)
40	Autoclaved Water

Table 2.6: Pfu DNA polymerase mutagenic PCR program

Step	**Temperature**	**Duration**
1. Initial denaturation	95°C	1 min
2. Denaturation	95°C	30 sec
3. Annealing	60°C	30 sec
4. Elongation	72-75°C	8 min
	Go to step 2 for 17 cycles	
5. Final elongation	72-75°C	15 min
6. End	4°C	-

2.2.3 DNA analysis and purification

DNA electrophoresis

Agarose gels (30 ml or 50 ml) were made by dissolving 1% (w/v) agarose in 1×TAE buffer (40 mM Tris-acetate, 1 mM EDTA, pH 8.0) and a 1:20000 dilution of a 10 mg/ml ethidium bromide solution was added for visualization of DNA. 5 µl of the PCR product was added to 1 µl of 6×DNA loading buffer (0.25% (w/v) bromphenol blue, 0.25% xylene cyanol FF, 30%(v/v) glycerol in sterile water) and electrophoresed using horizontal flatbed chambers (BioRad) at a constant current of 80 mA. For DNA size estimation, the DNA ladders (NEB) shown in Fig.2.1 were utilized. Gels were imaged using a Chemidoc-it^2 UV transilluminator (UVP).

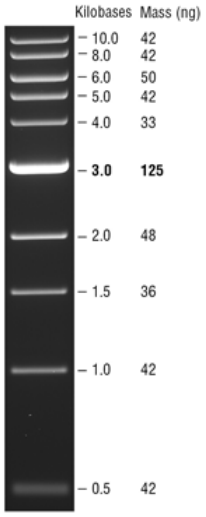

Figure 2.1: Markers used for DNA fragment size estimation. NEB 1Kb DNA ladder

DNA purification

A MinElute PCR purification kit (Qiagen) was used to purify nucleic acid samples (e.g. PCR products and single restriction enzyme digested DNA) through which protein contaminants in the sample were removed and DNA was eluted with 10 µl of sterile water. In cases where PCR reactions amplified more than one band, the whole PCR reaction mixture was electrophoresed, and the desired band was excised for DNA extraction. In this study, the double restriction enzyme digested DNA insert and plasmid pending ligation reaction were always purified by electrophoresis and then extracted from the gel. QIAquick gel extraction kit

(Qiagen) was used in all gel extraction procedures. The resulting purified DNA was eluted with 50 µl of sterile water.

2.2.4 Insertion of DNA fragments into plasmids

PCR products and vectors were sequentially digested with restriction endonucleases according to the manufacturers instruction. After the first digestion cycle, the DNA fragment was purified with MiniElute PCR purification kit. After the second restriction digest, the DNA fragment was electrophoresed and extracted from the gel using a QIAquick gel extraction kit. Restrictive enzyme digestion details of DNA fragments are summarized in Table 2.7. Before the stick-end ligation reaction, concentrations of all double digested DNA fragments were measured. Ligation reactions were set-up according to equation 2.1. Two insert:vector ratios (3:1 and 1:1) were normally tested for successful ligation conditions, at least 100 ng of DNA was added for each reaction. The ligation reaction was catalyzed by T4 DNA ligase at room temperature for 1 hour, a typical T4 ligation reaction set-up is shown in Table 2.8.

Table 2.7: DNA insert

PCR products	Plasmid	Restriction Enzymes
C3a	pGEX-htb	BamHI/HindIII
Sbi-III-IV	pET28a	BamHI/HindIII

$$\frac{ng\ of\ vector \times size\ of\ insert\ (Kb)}{size\ of\ vector\ (Kb)} \times \frac{insert}{vector}\ molar\ ratio = ng\ of\ insert \quad \text{[Equation 2.1]}$$

Table 2.8: Typical recipe for DNA ligation reaction

Volume (µl)	**Component**
X_V	Vector
X_I	Insert
1.5	10×T4 Ligase Buffer
0.75	T4 DNA Ligase
To final volume 15µl	Sterile Water

2.2.5 Transformation of *E.coli* cells

To insert the plasmid into cloning cell lines, 3-5 µl of the ligation mixture or mutated plasmid were added to 10 µl of chilled cells on ice and left for 30 min. The cells were heat-shocked at 42°C for 45 sec and returned to ice for 5 min. 200 µl of SOC medium was added to the cells which were then incubated at 37°C, shaking at 220 rpm for 2 hours. 100 µl of the transformation mixture was spread onto an LB plate containing the appropriate antibiotic.

When mini-prepped plasmid was used for transformation into expression cell lines, 1 µl of plasmid was added to 10 µl of chemically competent cells. The rest of the procedure was performed as described above. Heat-shock duration may vary depending on the cell strains; so corresponding adjustments were made according to the manufacturer's instructions.

2.2.6 DNA sequencing of plasmids

Table 2.9: DNA sequencing primer selections

Vector Name	Sequencing primer
pQE30	T5 promoter forward primer
pGEX-htb	pBAD reverse primer
pET28a	T7 promoter forward primer

SourceBioscience provided DNA sequencing services for all experiments carried on in this study. The sequencing primer was chosen based on the plasmid. Table 2.9 summarizes the sequence primer selection for different plasmids.

2.3 Protein and Immunochemistry techniques

2.3.1 SDS-PAGE and Gradient gel

In this study sodium dodecyl sulphate polyacrylamide gel electrophoresis (SDS-PAGE) was done using the Novex Mini gel system (Invitrogen) using 4% polyacrylamide stacking gels (Table 8.2) and 8%, 12% 15% polyacrylamide resolving gels (Table 8.1), 4-20% gradient gel (Table 8.3) was made by a

gradient maker and used in some circumstances. Protein samples to be analyzed were mixed with 2×loading buffer and boiled for 10 min. Reducing and non-reducing loading buffers (Table 8.4) were prepared to suit the requirements of different experiments. Generally 5-15 µl samples (approximately less than 25 µg of protein) were loaded in each lane, electrophoresed in 1×Tri-Glycine running buffer (Table 8.5), using a constant current setting of 60-80 mA until the bromophenol blue dye ran off the gel. Gels were extracted from the cassette then subjected to downstream immunoblotting or protein extraction procedures, however most commonly gels were stained with Coomassie Blue (Table 8.6) for 1 hour after being heated in a microwave for 40 sec. Gels were then de-stained (Table 8.7) and dried in cellophane membrane (Invitrogen). Pierce Unstained Protein MW Marker (Invitrogen), Pierce Prestained Protein MW Marker (Invitrogen) and Amersham Rainbow Marker (GE Healthcare) (Fig2.2) were used to estimate the size of proteins.

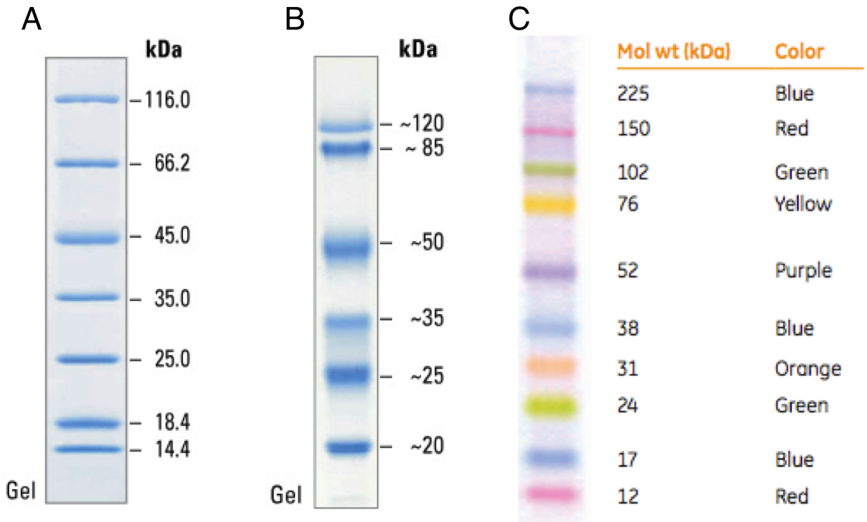

Figure 2.2: Protein markers for protein size estimation. (A) Pierce Unstained Protein MW Marker **(B)** Pierce Prestained Protein MW Marker **(C)** Amersham Rainbow Marker. 5 µl marker was loaded on the gel. Images taken from manufactures website.

2.3.2 Protein expression

The general technique for recombinant protein expression is described in later

sections. After an expression vector was transformed into an *E.coli* strain, a single colony was picked and grown at 37°C overnight in a 15 ml of LB medium with addition of the appropriate antibiotic. The overnight primary culture was then used to inoculate a scaled-up secondary LB culture (500-1000 ml) with appropriate antibiotic added. Cells were grown in a temperature-controlled incubator with shaking at 180 rpm. The expression of protein was generally induced during the exponential phase of bacterial growth (OD_{600}≥0.7) by adding isopropyl thiogalactoside (IPTG) to the culture. IPTG concentration, expression temperature and duration of expression were factors requiring unique optimization for specific expression constructs. Table 2.10 summarizes the expression conditions for proteins included in this study.

Table 2.10: Summary of protein expression conditions

	Constructs	E.coli strain	Antibiotic Marker	OD_{600nm} of induction	Temperature of Induction	Duration of induction	IPTG concentration
A	pQE30-Sbi-III-IV WT, Mutants, Cys	BL21(DE3)	Ampicillin	0.6-0.8	37°C	3hours	0.5mM
B	pET28-Sbi-III-IV (N & C terminal His tag)	BL21(DE3)	Kanamycin	0.6-0.8	37°C	3hours	0.5mM
D	pGEX-C3a	Origami (DE3)	Ampicillin and Tetracycline	1.0-1.2	12°C	Overnight (16 hours)	0.05mM
H	pET15b-C3d^{C17A}	BL21(DE3)	Ampicillin	Auto-induction	25°C	Overnight (16 hours)	

2.3.3 Harvest & Lysis of cells

E.coli cells were harvested by centrifugation (8000 *g,* 25 min, 4°C). Cell pellets were suspended in 20 ml of protein dependent buffer. The resuspended cells were sonicated (Branson digital sonicator) on ice for 6 cycles of an 80% amplitude burst for a total of 10 sec; each cycle was separated by 10 min interval to prevent over-heating of the sample. The resulting extract was clarified by centrifugation (60,000 *g*, 30 min, 4°C).

2.3.4 ÄKTA purification

The supernatant was collected and purified through affinity chromatography. Typically, the supernatant sample was loaded on a pre-packed chromatography column (GE healthcare) using a ÄKTA purifier 10 Chromatography unit (GE healthcare). The loaded column was washed with starting buffer and the bound protein was eluted with a 0-100% gradient of elution buffer. Common chromatographic buffers used in Chapter 3 and 4 are listed in Table 2.11.

Table 2.11 Summary of chromatographic buffers

Buffer:	Composition
Section 3.2.1.1	
Coupling buffer	0.2 M $NaHCO_3$, 0.5 M NaCl, pH 8.3
Buffer-1A	0.5 M ethanolamine, 0.5 M NaCl pH 8.3
Buffer-1B	0.1 M sodium acetate, 0.5 M NaCl, pH 4.0
Storage buffer	0.05 M Na_2HPO_4, 0.1% NaN_3, pH 7.0
Elution buffer	100 mM glycine pH 2.7
Section 3.2.1.2	
Buffer-2A	50 mM Tris pH 8.5
Buffer-2B	50 mM Tris, 500 mM NaCl, pH 8.5
Buffer-3A	50mM Tris pH7.5
Buffer-3B	50mM Tris, 500mM NaCl, pH7.5
Section 3.2.2.1	
Buffer-QA	20 mM Tris-HCL, pH 7.5
Buffer-QB	20 mM Tri-HCL, 500 mM NaCl, pH 7.5
Buffer-SA	50 mM MES, 50 mM NaCl pH 5.2
Buffer-SB	50 mM MES, 500 mM NaCl pH 5.2
Section 3.2.3.2	
GST elution buffer	10 mM reduced glutathione, 50 mM Tris, pH 8.0
Cleavage buffer	50 mM Tris pH 7.5, 1 mM EDTA, 30 mM reduced glutathione and 3 mM oxidized glutathione
Section 3.2.4.2	
MES-1A buffer	50 mM MES, pH 5.5
MES-1B buffer	50 mM MES, 500 mM NaCl pH 5.5
MES-2A buffer	50 mM MES, pH 5.0
MES-2B buffer	50 mM MES, 500 mM NaCl, pH 5.0
Section 4.2.1	
His-A	50 mM Tris, 300 mM NaCl and 20 mM Imidazole, pH 7.4
His-B	50 mM Tris, 300 mM NaCl and 500 mM Imidazole, pH 7.4

2.3.5 Buffer exchange

Three buffer exchanging methods were used in the study. When using Vivaspin centrifugal concentrators to enrich purified protein, a series of dilutions and enrichment cycles were repeated utilizing the replacement buffer, until an equivalent of 625× dilution (4 cycles of 5× dilution) of the original buffer was achieved. Alternatively, protein samples were also buffer exchanged by PD-10 gravitational desalting column. Essentially, to a PD-10 column that had been pre-equilibrated with 25 ml of replacement buffer, 2.5 ml of protein sample was added. After the protein sample was totally absorbed, 3.5 ml of replacement buffer was added to elute 3.5 ml of protein solution in desired buffer.

Finally, for small volumes and concentrated protein samples, Protein Desalting Spinning Columns (7 kDa cut-off, Thermo Scientific) were used. Briefly, the spin column was first equilibrated with replacement buffer through 3 wash cycles (400 µl each time). The column was centrifuged at 1500 *g* for 1 min to remove excess liquid. After placing in a new collection tube, 30-120 µl of protein sample was spotted on the center of the dry resin bed, after which the column was spun at 1500 *g* for 2 min to recover the buffer exchanged protein sample.

2.3.6 Concentrator and Concentration measurement

Vivaspin centrifugal concentrators were used to concentrate protein samples; samples were spun at 3500 *g* until concentrated to the desired concentration. The protein concentrations were determined by measuring absorbance at 280 nm using a NanoVue spectrophotometer (GE Healthcare).

2.3.7 Antibodies & antisera

The following primary antibodies were used in this study: rabbit anti-Sbi serum, polyclonal goat anti-C3 (CompTech), polyclonal rabbit anti-C3d (Dako), polyclonal rabbit anti-C3a (CompTech), polyclonal goat anti-factor-B

(CompTech), polyclonal goat anti-factor-H (MerckMillipore), monoclonal biotinylated anti-factor-H OX-24 (Catalog number: MA5-17735, Thermo Scientific) and monoclonal horseradish peroxidase (HRP) conjugated anti-penta-histidine (SigmaAldrich). The following horseradish peroxidase (HRP) conjugated secondary antibodies were used in this study: anti-rabbit IgG (Thermo Scientific), anti-Goat IgG (SigmaAldrich), and Streptavidin-HRP conjugate (GE healthcare).

2.3.8 Western blot analysis

Table 2.12: Summary of antibody dilution

Antigen	Clonality	Primary antibody Dilution	Anti-Goat Secondary antibody Dilution	Anti-Rabbit Secondary antibody Dilution
Sbi	Polyclonal	1.5/5000	-	15/5000
C3	Polyclonal	1/10000	1.5/50000	-
C3a	Polyclonal	1/20000		15/5000
C3d	Monoclonal	1.5/5000	-	15/5000
Factor B	Polyclonal	1/10000	1.5/50000	-
Factor H	Polyclonal	6/5000	1.5/50000	-
6×Histidine tag	Monoclonal	1/20000	-	-
Biotin	Streptavidin-HRP	1/20000	-	-

After protein samples had been separated by SDS-PAGE electrophoresis, SDS-PAGE gel and methanol-activated polyvinylidene fluoride (PVDF) membrane were soaked for 15 min in Pierce Fast semi-dry transfer buffer (Thermo Scientific). Immunoblotting was performed using pierce G2 semi-dry fast blotter (Thermo Scientific). Blotting was performed at a constant 25 V for 15 min. The

blocking, washing and antibody detection steps were carried out on a SNAP i.d 2.0 western blotting system (Millipore) according to the manufacturer's instructions. Briefly, the membrane was blocked with blocking buffer (PBS supplemented with 0.3% skimmed milk, 0.1% Tween 20) at room temperature followed by incubation with the appropriate primary antibody (Antibody dependent dilution in blocking buffer) for 15 min at room temperature. The membrane was extensively washed with PBST and incubated with corresponding horseradish peroxidase (HRP)-conjugated secondary antibody (antibody dependent dilution in blocking buffer) for 15 min at room temperature. After the final extensive washing step, the antibody recognized proteins were detected using Pierce ECL western blotting substrate (Thermo Scientific) and then exposed to light sensitive film before being developed in a developer. Table 2.12 summarizes antibody dilutions for western blot analysis.

2.4 Sera and complement protein

2.4.1 Sera

Complement-active lyophilized human serum standard (HSS) was purchased from Euro-diagnostica, Sweden. Citrated human plasma was purchased from TCS bioscience, UK and stored at -80°C. Factor B, factor D, factor H, factor I and factor P depleted sera were purchased from CompTech, USA.

2.4.2 complement proteins

Human factor B, factor D, factor H, factor I and factor P were purchased from CompTech (Tyler Texas, USA). Recombinant FHR-1 (rFHR-1) was provided by Dr Kevin Marchbank (The Medical School, Newcastle University, UK). All other proteins used in this study were either purified or recombinantly produced in house, if not mentioned otherwise.

Chapter 3: Optimized expression and purification of complement components

3.1 Introduction

Purified complement components are essential for the biochemical and structural characterizations of the Sbi-C3b adduct and Sbi ligand-binding properties. Given that substantial amounts of these proteins were needed in this study, the majority of the complement components were prepared in house. Since complement is a well-established field, the purification protocols for majority of the complement components have been published before (Morgan 2000). However, considerable modifications were made to tailor these protocols for our chromatography system. Attempts were made to establish a protocol of immune-affinity purification of human FH and FHR-1. Complement component C3 was purified largely based on the work described by (Alsenz *et al*. 1992). In comparison to the intact complement components, the smaller C3 fragments, C3a and C3d, were cloned, expressed and purified using *E.coli* recombinant protein technique. The purification protocols presented in this chapter contributed immensely to the mechanistic studies of Sbi.

3.2 Results

3.2.1 Purification of FH and FHR-1 from human serum

3.2.1.1 Making the anti-FH/FHR-1 antibody column

The goat anti-FH/FHR-1 anti-serum was acquired from Merck Millipore. 100 µl of the goat serum was diluted to 1 ml with PBS buffer and loaded on a gravity column packed with 500 µl of protein G Sepharose resin (SigmaAldrich). The flow-through fraction was reloaded twice for maximum capture of the antibody. After intensive washing (10 column volumes of PBS), the bound goat IgG molecules were eluted with elution buffer (the compositions of buffers used in

this chapter are detailed in Table 2.11). The eluted protein was then collected in a tube pre-loaded with 2 ml of 1 M sodium phosphate pH 7.2 buffer. The purified goat IgG protein was confirmed by SDS-PAGE analysis, concentrated using a Vivaspin 10 kDa cut-off spin concentrator. The concentrated IgG sample was then buffer exchanged to coupling buffer with a PD-10 column (GE healthcare).

Next, purified goat IgG molecules were covalently coupled to a 1 ml Hitrap NHS-activated column (GE healthcare) through surface lysine residues. The coupling process was performed based on the manufacturer's instructions. Briefly, after preparing the column with 6 column volumes of ice-cold 1 mM HCl solution, 1 ml of 1.2 mg/ml goat IgG in coupling buffer was injected onto the column. The sealed column was kept at 25°C for 30 min for the coupling process. After the coupling reaction, the column was washed repetitively by 6 column volumes of Buffer-1A and-1B. Samples of IgG before coupling and after coupling were analyzed by SDS-PAGE to evaluate the efficiency of the coupling process. The IgG coupled column was stored in storage buffer.

As shown by Fig.3.1.A, the IgG fraction of anti-FH/FHR-1 goat serum was successfully purified using protein G affinity chromatography. Under reducing conditions, the purified goat IgG proteins demonstrate a band slightly higher than the 45 kDa MW marker and another band slightly higher than the 25 kDa MW marker. These two bands match with the estimated masses of IgG heavy chain (50 kDa) and light chain (25 kDa). As described above, the IgG sample was coupled onto the NHS-activated Sepharose column based on the manufacture's instruction, but by comparing the SDS-PAGE profile of protein sample before and after the coupling (Fig.3.1.B), it is clear that a considerable proportion of the IgG molecule was not coupled on the column. Therefore, using the un-coupled IgG sample multiple NHS-activated columns were coupled, and connected together for elevated binding capacity during affinity purification of FH and FHR-1.

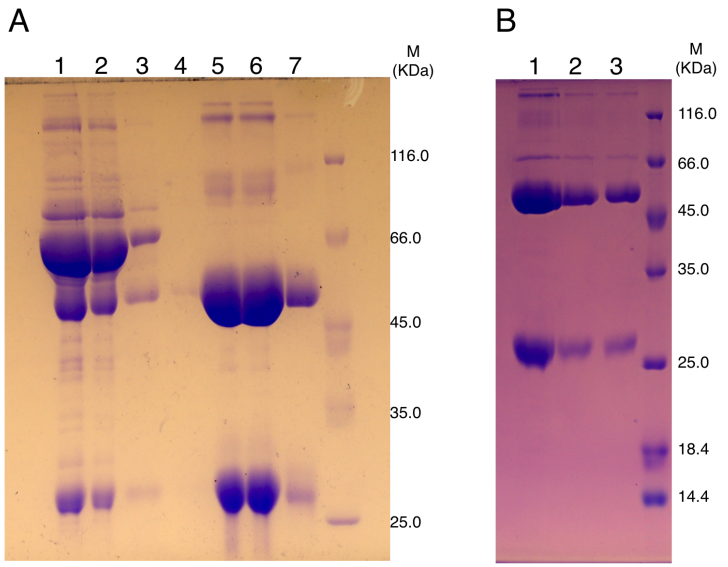

Figure 3.1: Generation of anti-FH/FHR-1 antibody column. (A) SDS-PAGE analysis summarizing protein G affinity purification of IgG from goat anti-FH/CFHR1 serum. Lanes: 1 Goat serum before purification, 2 Goat serum after purification, 3 Wash I, 4 Wash II, 5 Elution I, 6 Elution II, 7 Goat IgG positive control. **(B)** SDS-PAGE evaluation of goat IgG coupling to NHS-activated column. Lanes: 1, IgG before coupling reaction, 2 Flow through fraction 1, 3 Flow through fraction 2.

3.2.1.2 Purification of FH and FHR-1

FH and FHR-1 were prepared from citrated human plasma (TCS bioscience), using a newly developed affinity purification protocol. Firstly the citrated plasma was allowed to clot by adding $CaCl_2$ to final concentration of 15 mM. After one hour's incubation at 37°C, the clot was removed by centrifugation (5000 *g*) for 20 min. EDTA stock was added to the serum to a final concentration of 25 mM to prevent unwanted complement activation. 5 ml filtered EDTA-serum was then loaded on two 1 ml anti-FH/FHR-1 IgG coupled Sepharose columns (anti-FH/FHR-1 column) using a ÄKTA purifier. During loading of the serum, flow-rate was set for 0.4 ml/min, the slow flow-rate enhances the capture of FH and FHR-1 from serum. After loading, the flow-rate was raised to 1 ml/min, the column was washed by 10 ml of PBS buffer and the bound protein was eluted with an 8 ml wash of elution buffer. 100 µl of 1 M Tris pH 8.0 buffer was added to

each fraction collecting tubes beforehand. Therefore the pH environment of the eluted protein was neutralized immediately after the elution step. According to the chromatogram, elution fractions were collected, concentrated and analyzed by SDS-PAGE.

As the antibody column was coupled with polyclonal anti-FH antibodies, not only FH and FHR-1 will be enriched from serum, but also FHL-1 and other FHR proteins. Thus, the sample was then subjected to anion exchange chromatography. Under anion exchange conditions, at a given pH the net positively charged protein surface will bind to the anionic column matrix, the retained proteins are then sequentially eluted with a gradient of increasing positive ion concentration in the elution buffer. Firstly, the protein sample was buffer exchanged to Buffer-2A using PD10 column. Then the sample was loaded on a 1 ml Q Sepharose HP column, with the flow rate set for 1 ml/min. After loading, the column was washed by 8 column volume of Buffer-2A, the bound protein was subsequently eluted by a 50 column volume 0-100% gradient of Buffer-2B. Each peak was analyzed by SDS-PAGE to identify FH or FHR-1 containing fractions.

At the final polishing step, FH or FHR-1 containing fractions were subjected to heparin affinity chromatography separately. Protein fractions were firstly buffer exchanged to Buffer-3A, subsequently loaded on 1ml HiTrap Heparin High Performance column using the ÄKTA purifier. The bound protein was washed by 8 column volumes of Buffer-3A, and eluted with a 25 column volume 0-100% gradient of Buffer-3B. Elution fractions were then examined for the presence of purified FH or FHR-1 protein.

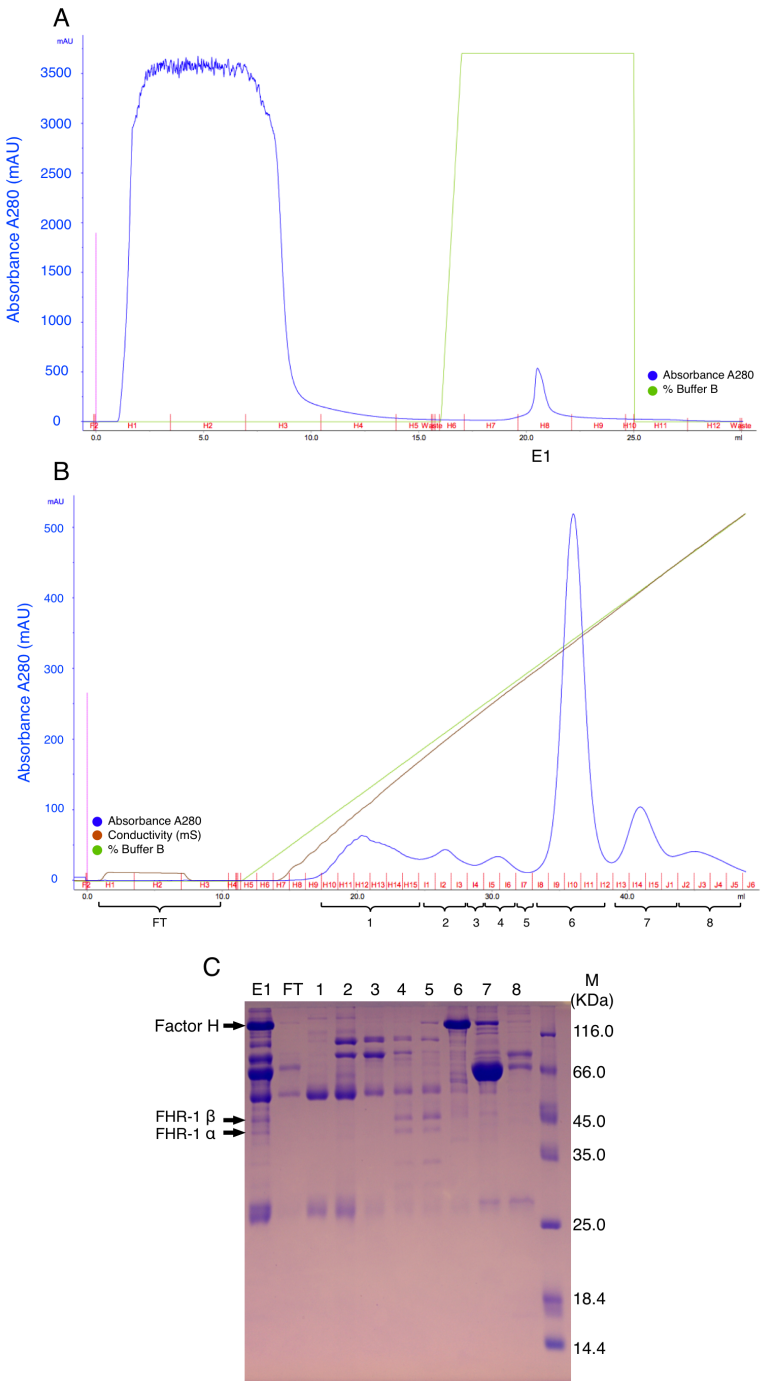

Figure 3.2: Purification of FH and FHR-1 from human serum (A) Chromatogram of affinity purification using anti-FH/FHR-1 antibody column. Elution fraction "E1" was collected and prepared for secondary purification. **(B)** Chromatogram for the secondary anion exchange chromatography. The immune-affinity purified protein sample was separated again according to their charge at pH8.5. Elution fractions of different peaks were mixed and concentrated as indicated. **(C)** SDS-PAGE analysis of the affinity and anion exchange purification fractions. Labeled chromatographic sections were examined for their protein composition. Putative bands of FH and FHR1 were pointed using black arrows.

Utilizing the anti-FH/FHR-1 antibody column, affinity chromatography was performed to purify FH and FHR-1 from human serum. Fig.3.2.A shows that after passing through EDTA-serum, proteins were retained on the anti-FH/FHR-1 column. Using 100 mM glycine pH 2.7 as eluting buffer, the immune complexes were successfully dissociated, resulting in a 500 mAU elution peak. The

SDS-PAGE analysis (Fig.3.2.C) of this elution peak shows that although it contains putative protein bands corresponding to FH and FHR-1, this fraction was also heavily contaminated by other serum proteins. Therefore, a secondary anion exchange purification was carried out to not only remove serum protein contamination but also separate FH and FHR-1 from each other.

The anion exchange separation of the immune-affinity purified fraction yielded six peaks, as shown by Fig.3.2.B, the corresponding fractions of each peak were mixed and concentrated as indicated by curly bracket. The SDS-PAGE analysis (Fig.3.2.C) shows that FH and FHR-1 were successfully retained on the column, and sufficient separation was achieved by anion exchange chromatography. The majority of the FHR-1 protein was eluted as the third peak, using NaCl concentration with an equivalent conductivity reading of 15 mS. Immediately following this peak, FH elution was identified as the fourth peak on this chromatogram. The elution was achieved by the NaCl concentration with equivalent conductivity reading of 18 mS. Although successful separation of FH and FHR-1 was achieved by this procedure, based on the SDS-PAGE profile (Fig.3.2.C, Lane 4 and 6), the estimated FHR-1 purity was only about 20%, and for FH was about 60%.

Therefore, a final polishing step was designed relying on the heparin binding property of FH and FHR-1 proteins. FH and FHR-1 containing fractions were desalted and buffer exchanged, the resulting samples were then loaded on a 1ml Hitrap Heparin HP column separately. The bound proteins were eluted by a prolonged NaCl gradient.

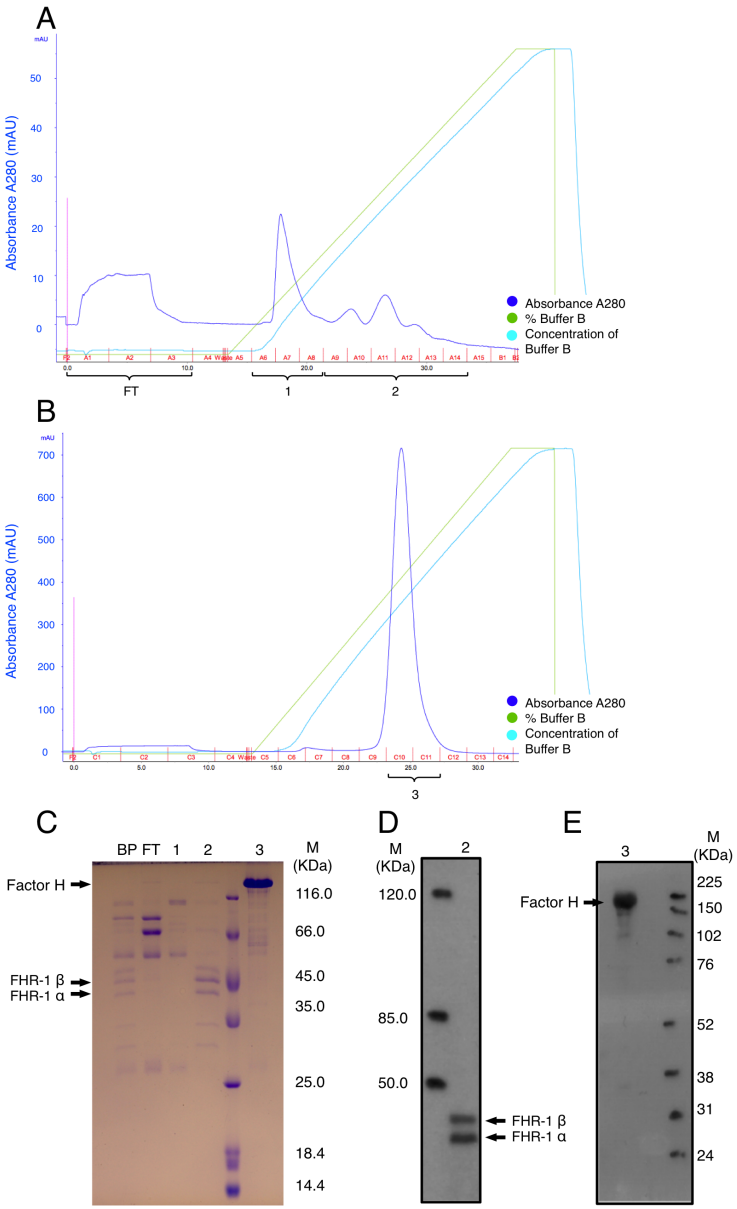

Figure 3.3: Heparin affinity purification of FH and FHR-1 proteins (A) Heparin affinity chromatography of FHR-1 containing fraction. Fractions confined by the curly bracket were mixed, concentrated and analyzed by SDS-PAGE electrophoresis. **(B)** Heparin affinity chromatography of FH containing fraction. Fractions confined by the curly bracket were mixed, concentrated and analyzed by SDS-PAGE electrophoresis. **(C)** SDS-PAGE analysis of heparin affinity purification of FHR-1 and FH. According to figure A and B, labeled elution fractions were examined for their protein composition. "BP" is an abbreviation of before purification. **(D-E)** Anti-FH Western blots of purified FHR-1 and FH. Labeled elution fractions were examined.

Heparin affinity polishing step of FHR-1

As shown in Fig.3.3.A, a considerable amount of serum protein contamination was removed during the loading stage. In the following elution process, one major peak was observed by elevating the NaCl concentration to 175 mM, and a subsequent increase of the NaCl concentration yielded a series of smaller peaks. As indicated by the curly bracket in Fig.3.3.A, fractions were mixed, concentrated and subjected to SDS-PAGE analysis. Fig.3.3.C demonstrates that while the

majority of the serum protein contaminations were found in the flow-through fraction and peak fraction 1, putative FHR1 was eluted at the later stage of the purification and located in peak fraction 2. The series of small peaks may be the result of FHR1 in different dimerization states (Section 1.4.3). Estimated from the gel, FHR1 purity in peak fraction 2 was about 60%. The purity and identity of purified FHR1 were verified by the polyclonal anti-FH Western blot (Fig.3.3.D).

Heparin affinity polishing step of FH

Heparin affinity chromatography strategy was also used to polish the FH containing secondary purification fraction. As shown in Fig.3.3.B, one major peak in the middle of the elution process was observed. SDS-PAGE analysis of the peak fraction 3 demonstrated a band corresponding to the size of FH. Estimated from the gel, the purity of putative FH protein is approaching 90%. The purity and identity of purified factor H were verified by the polyclonal anti-FH Western blot (Fig.3.3.E).

3.2.2 Preparation of C3 and its activation fragments

3.2.2.1 Purification of Human C3

Human C3 was purified from EDTA treated human serum based essentially on previous published method (Alsenz *et al*. 1992) with considerable modifications (Fig.3.4). PEG 4000 was added to 10 ml of freshly prepared human serum to the final weight/volume ratio of 4%. The mixture was stirred for 30 min at 4 °C, and then was clarified by centrifugation (10,000 *g*, 30 min, 4°C). The PEG concentration of the supernatant was then adjusted to 16%, after another round of the stirring and centrifugation, the final C3 containing pellet was resuspended with 20 ml of Buffer-QA . 10 ml of the filtered suspension sample was loaded on

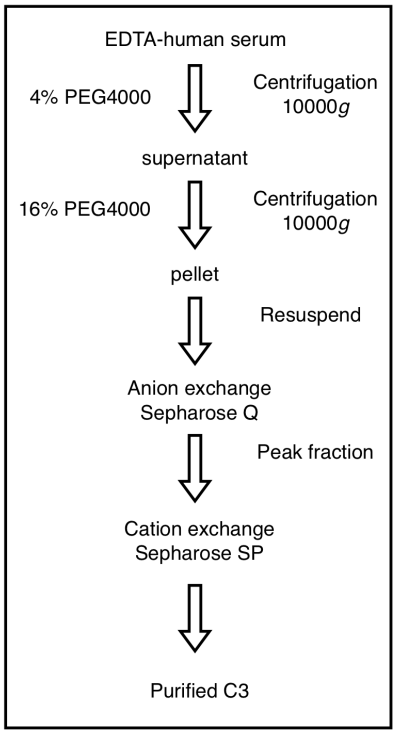

Figure 3.4: Summary of C3 purification

a 5 ml Q-Sepharose fast flow anion exchange column (Amersham Biosciences, GE healthcare, Uppsala. Sweden) using a ÄKTA purifier. After washing the column with 75 ml of Buffer-QA, the NaCl concentration was increased to 150 mM by elevating the Buffer-QB concentration to 30%. After an additional 50 ml washing step, bound C3 molecules were eluted by raising the NaCl concentration to 265 mM (53% Buffer-QB). The 53% Buffer-QB elution step was held for 5 column volumes (total of 25 ml) to completely elute the targeted protein and to avoid contamination with unwanted proteins. The C3 fractions, roughly 25 ml, were then pooled and concentrated to 5 ml.

To perform the subsequent cation exchange chromatography, the concentrated C3 fractions were buffer exchanged to Buffer-SA. 10 ml buffer exchanged C3 sample was then loaded on a 1 ml SP-Sepharose High Performance column. After washing the column with Buffer-SA to remove unbound proteins, a washing step (15 column volumes) with 45% Buffer-SB was used to elute the loosely bound protein contaminations. Then in the following step, purified C3 was eluted by increasing the Buffer-SB percentage from 45% to 100% over 20 column volumes.

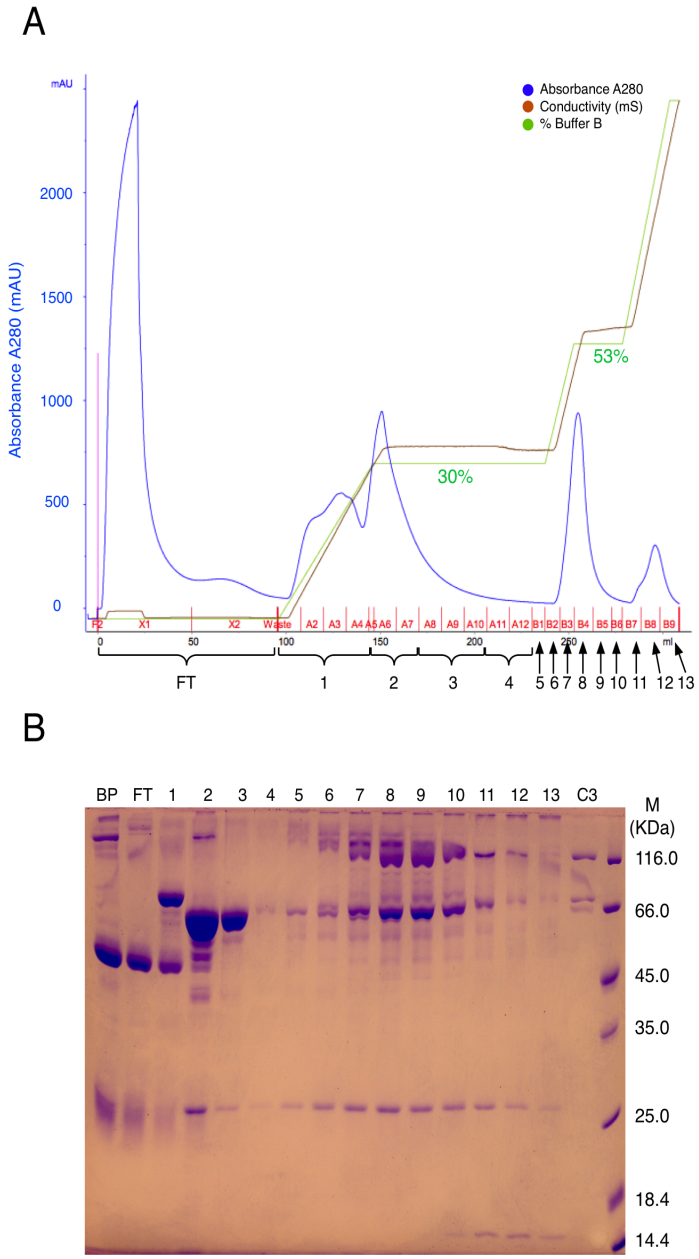

Figure 3.5: Primary purification of C3. (A) Anion exchange chromatography of enriched C3 sample. After the initial loading stage, the elution process was divided into three stages. Firstly, Buffer B concentration was elevated to 30%, after intensive wash, Buffer B concentration was increased to 53%, after which a major peak was produced. The buffer concentration was then elevated to 100% in a sharp gradient. Fractions for analysis were indicated using curly brackets and arrows. **(B)** SDS-PAGE analysis of anion exchange chromatography purification of C3. The fractions labeled in chromatogram A were analyzed. "BP" is an abbreviation of before purification. "C3" sample contain purified C3 as positive control. C3 α-chain: 120 kDa, C3 β-chain: 70 kDa.

A protocol for purifying functional active C3 using an inexpensive chromatographic set-up from EDTA human serum has been described. Fig.3.5.A

shows that an optimized step-wise elution strategy was used to maximize the purity of C3 containing fractions. In the first stage of elution, the Buffer-QB concentration was increased to 30% and held at this concentration for 15 column volumes. The SDS-PAGE analysis (Fig.3.5.B) of elution fractions 1-4 shows that during this prolonged elution step, a major serum protein contamination (approximately 66 kDa) was completely eluted. At the second stage of elution, the column was washed by 53% of Buffer-QB for 5 column volumes. A sharp Buffer-QB gradient was utilized to elute proteins as a single major peak. SDS-PAGE analysis of peak fractions 5-10 demonstrates that the major constituents of this peak were complement C3 and a 25 kDa serum protein. In the final elution step, Buffer-QB concentration was adjusted to 100% within 5 column volumes, which elutes the proteins as a slightly skewed peak. The SDS-PAGE analysis of the corresponding peak fractions (11-13) shows that this peak consists of nearly equal proportion of complement C3, serum protein 1 (25 kDa) and serum protein 2 (15 kDa). Given that this peak proportionally contains much more unwanted protein contamination than C3, this peak was not included in the subsequent secondary purification process.

To further increase the purity of C3, the C3 containing fractions from the primary purification (Fig.3.5.A fraction 5-10) were concentrated, buffer exchanged, and separated by cation exchange chromatography. In the secondary purification a slightly easier step-wise elution strategy was utilized to achieve maximal separation of C3 from unwanted serum proteins. It is clear from the chromatogram (Fig.3.6.A) that during the loading stage a reasonable amount of protein was removed. In the first stage of the elution the Buffer-SB concentration was elevated to 45% and held at this concentration for 15 column volumes. During this stage the absorbance at 280 nm suggested that a considerable amount of less charged serum proteins were eluted. The prolonged 45% Buffer-SB washing ensures that unwanted proteins were completely removed before the next elution step. In the second elution step, Buffer-SB concentration

was increased to 100% in 20 column volumes, during this step a symmetrical elution peak was observed. SDS-PAGE analysis (Fig.3.6.B) of the peak fractions suggests that the main constituent of this peak is complement C3. Based on the SDS-PAGE profile of secondary purification C3 fractions, the purest fractions were pooled, concentrated and buffer exchanged to PBS for further usage. Following this protocol, normally 3 mg of C3 molecule can be purified from 5 ml EDTA normal human serum.

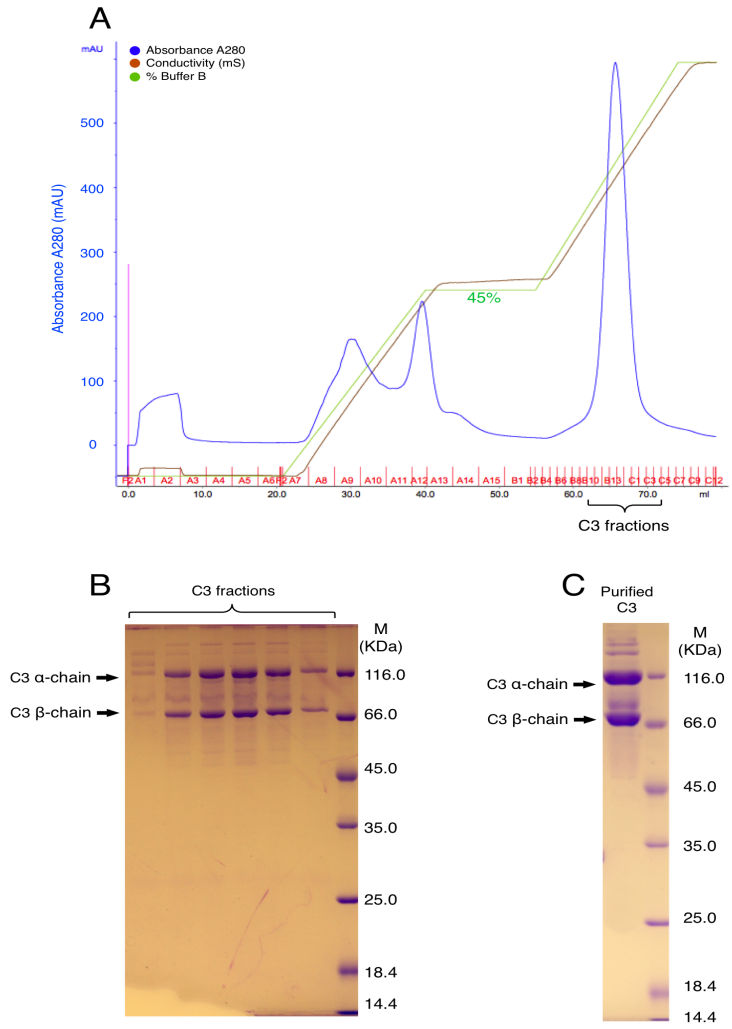

Figure 3.6: Secondary Purification of C3. (A) Secondary cation exchange chromatography purification of C3. C3 containing fractions from primary purification were separated again using cation exchange chromatography at pH5.5. Fractions to be analyzed were indicated using a curly bracket. **(B)** SDS-PAGE analysis of selected cation exchange fractions. The analyzed fractions represent the elution peak of C3 molecule, C3 α-chain (120 kDa) and β-chain (70 kDa) were the two major protein bands on this gel. **(C)** SDS-PAGE profile of purified C3 molecule.

3.2.2.2 Purification of C3b

During the preparation of the Sbi-C3b adduct through the reconstituted AP pathway, a large amount of free C3b molecules was produced. As shown in Fig.5.3.4.A, after Ni^{2+} affinity purification, free C3b molecules were separated from His-tagged molecules and collected in the flow-through fraction. Given that other AP components could also exist in the flow-through fraction, an extra anion exchange chromatography step was utilized to polish the purity of the C3b sample. The C3b-containing flow-through fraction was firstly buffer exchanged to Buffer-QA. 10 ml of diluted C3b was then loaded on a 1 ml Q-Sepharose High Performance anion exchange column using a ÄKTA purifier. After washing the column with 10 ml of Buffer-QA, the bound proteins were eluted by a 40 column volume gradient of Buffer-QB. Chromatographic peaks were analyzed by SDS-PAGE to identify the C3b containing elution fractions.

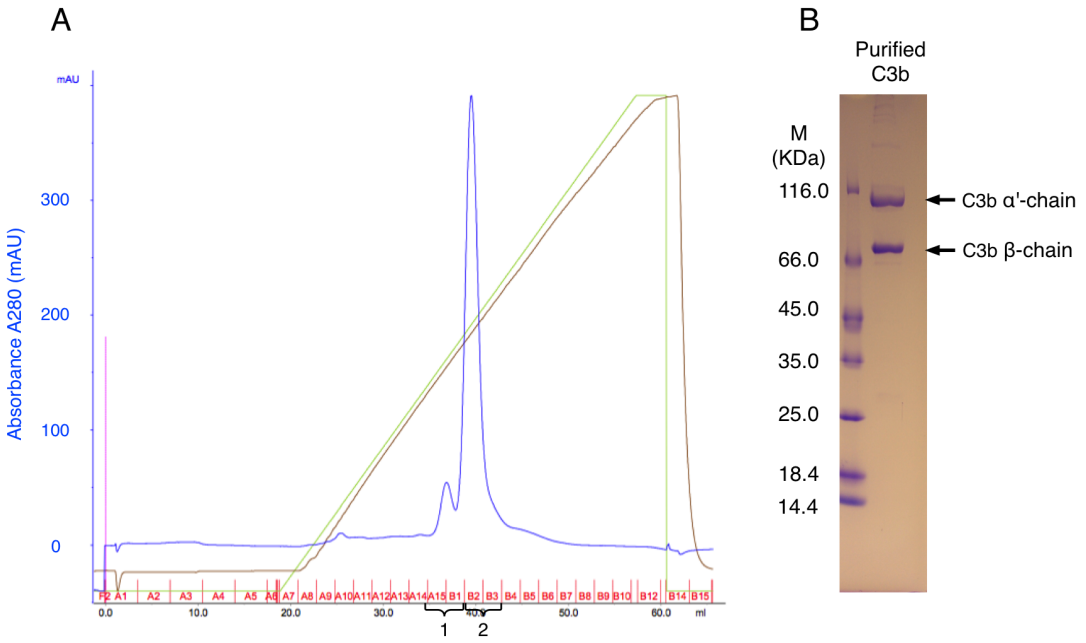

Figure 3.7: Polishing of C3b molecule. (A) Anion exchange chromatography of C3b. C3b molecules were eluted as the major peak, labeled using curly bracket as "2". (B) SDS-PAGE profile of purified C3b.

The chromatogram (Fig.3.7.A) shows continuous low UV 280nm absorbance until the middle of the elution stage, two peaks were observed indicated by the curly bracket on the chromatogram as peak fraction 1 and 2. The SDS-PAGE

analysis of the peak fraction 2 demonstrates the present of purified C3b molecule.

3.2.3 Cloning, Expression and purification of C3a

3.2.3.1 C3a Cloning

The codon optimized C3a gene suited for *E.coli* expression was commercially synthesized by the GeneArt service provided by Invitrogen. According to the sequence of human complement component C3 (Swissprot accession No.P01024.2), the coding region from amino acid 672 to 749 was inserted in the pMA-T vector carrying ampicillin resistance. The coding sequence was amplified by PCR using the pMA-T-C3a vector as a template (Primers, forward 5'- CTC GGATCCATGAGCGTTCAG-3', reverse 5'- GCTCCAGGTACCCCCGGG-3'). PCR reactions were carried out using the recipe and program given in Section 2.2.1.

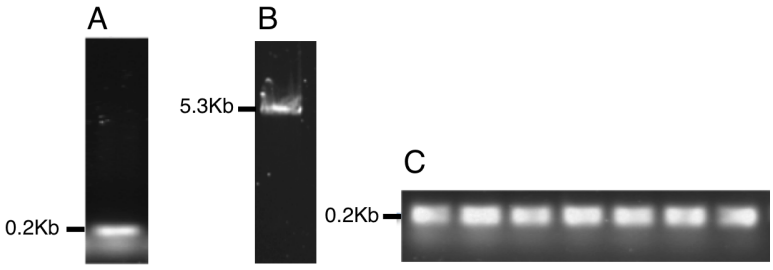

Figure 3.8: Cloning of C3a gene. (A) BamHI and KpnI double digested C3a PCR product. (B) BamHI and KpnI double digested pGEX-htb vector. (C) After ligation, Colony PCR for 0.2Kb C3a DNA insert.

The resulting PCR (Fig.3.8.A) products were sequentially digested by restriction enzymes BamHI and KpnI. The digested C3a coding DNA fragment was purified using a gel extraction kit (QIAGEN) and ligated with double digested GST-tag fusion vector pGEX-htb (Fig.3.8.B). Colony PCR (Fig.3.8.C) was performed to screen for a positive clone, and the sequence of the positive clone was confirmed by DNA sequencing (Appendix 9.1.1.5).

3.2.3.2 GST-C3a purification and cleavage

The *E.coli* Origami (DE3) strain was used for GST-C3a fusion protein expression. Bacteria containing the pGEX-htb^{C3a} plasmid (Appendix Fig.9.1.1.5) were grown overnight in LB medium supplemented with 100 µg/ml ampicillin and 20 µg/ml tetracycline at 37℃. The 15 ml primary culture was incubated with 1 L LB medium containing 100 µg/ml ampicillin and 20 µg/ml tetracycline. Cells were grown at 37°C with shaking at 180 rpm. The expression of the GST-C3a fusion protein was induced during the exponential growth phase (OD_{600}=0.8-1.0) by adding 0.05 mM isopropyl thiogalactoside (IPTG) to the culture at 12℃. *E.coli* cells were collected by centrifugation (8000 *g*, 20 min) 16 hours after induction. The cell pellet was suspended in 20 ml of PBS buffer supplemented with EDTA free protease inhibitor cocktail (Roche). Lysis of the cells was performed as described in 2.3.3. The supernatant sample was then loaded on a 5 ml GSTrap column (GE healthcare) using an ÄKTA purifier with a flow rate of 1 ml/min. The loaded column was washed with 6 column volumes of PBS buffer and the bound GST-C3a fusion protein was eluted with GST elution buffer. Prior to the cleavage, GST-C3a protein was concentrated using a 10 kDa cut-off spin-concentrator and buffer exchanged into cleavage buffer. The C3a protein was cleaved from the GST-C3a fusion protein with AcTEV protease (Invitrogen). 20 U of AcTEV protease was added to 2.5 ml of GST-C3a fusion protein sample (10 mg/ml) and the cleavage reaction was carried out at 4℃ for 48 hours.

GST-C3a fusion protein was solubilized in PBS buffer and purified using glutathione affinity chromatography (Fig.3.9.A). Analyzing the purification fraction by SDS-PAGE and coomassie staining revealed that at least 70% of protein purified was GST rather that the GST-C3a fusion protein (Fig.3.9.B, lane 1 and 2). The yield of GST-C3a was about 5 mg fusion protein per liter of LB medium. GST-C3a fusion protein was digested by AcTEV protease to produce GST and C3a proteins. The progress of the digestion was evaluated by SDS-PAGE

(Fig.3.9.B), totally digested protein sample was then subjected to cation exchange chromatography.

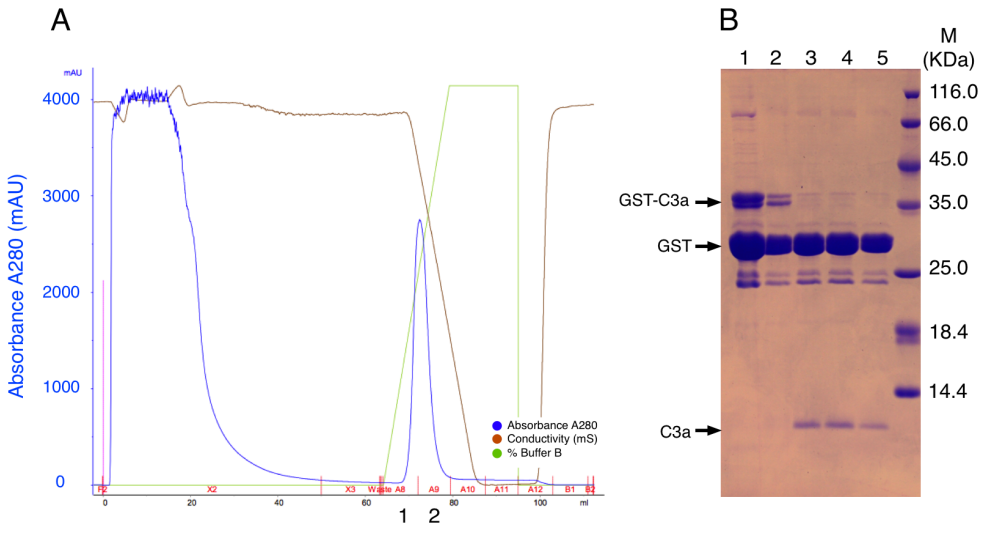

Figure 3.9: Purification of GST-C3a fusion protein. (A) Glutathione affinity chromatography purification of GST-C3a protein, elution fraction 1 and 2 were analyzed by SDS-PAGE. **(B)** SDS-PAGE analysis of GST-C3a purification and AcTEV digestion of GST-C3a. Lane: 1, elution fraction 1; 2, elution fraction 2; 3-5 GST-C3a digestion samples.

3.2.3.3 C3a tag removal

Removal of the GST tag was achieved by cation exchange chromatography utilizing a 1 ml SP sepharose High Performance column on a ÄKTA purifier (GE Healthcare). The column was initially equilibrated with 10 column volumes of Buffer-3A, then 2.5 ml of the cleaved protein mixture was subsequently loaded on the column with a flow rate of 0.5 ml/min. The loading step was followed by a 10 column-volume washing step. Next the bound C3a molecule was eluted by a gradient of Buffer-3B. Finally, the purity of the purified C3a was accessed on a 15% Tris-Glycine SDS-PAGE gel, the purest fractions were mixed and concentrated. Fig.3.10.A shows that the majority of the protein (GST tag) was not retained by the column. Elution fractions 1 and 2 were analyzed by SDS-PAGE (Fig.3.10.B). Approximately 0.5mg of C3a protein was produced from 1 liter of LB medium.

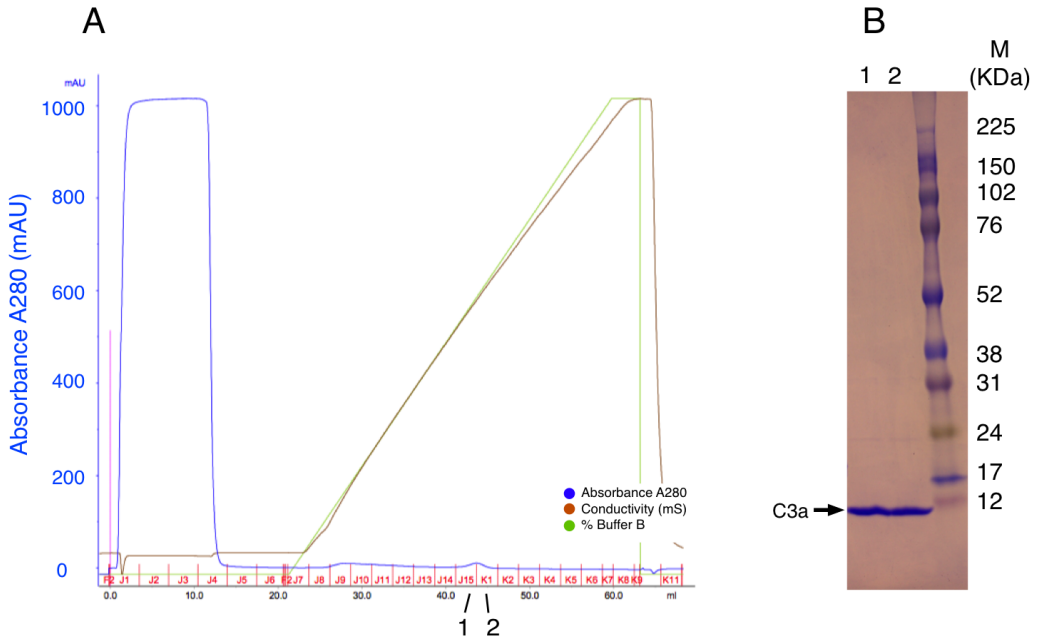

Figure 3.10: GST tag removal. (A) Cation chromatography purification was performed to purify recombinant C3a protein. Elution fractions 1 and 2 were collected, concentrated and analyzed by SDS-PAGE. **(B)** SDS-PAGE profile of concentrated elution fraction 1 & 2.

3.2.4 Expression & purification of C3d

3.2.4.1 Expression of C3d^{17A}

In the pET15b-C3d^{17A} expression vector (Section 2.1.1 and Appendix 9.1.1.3), the N-terminal 6×Histidine tag was deleted for the expression of the untagged C3d molecule. The *E.coli* BL21 (DE3) strain was used for protein expression, a freshly transformed bacterial colony was incubated in LB medium with 100 µg/ml ampicillin and grown overnight at 37℃. 15 ml of the overnight primary culture was incubated with 1 L LB-5052 medium. Recombinant protein expression was induced by the bacterial consumption of lactose for 20h at 25℃. The cell pellet was harvested by centrifugation (8000 *g*, 20 min) from 1 L culture medium and re-suspended in 40 ml of MES-1A buffer and lysed as described above (2.3.3). The cell lysate was centrifuged at 60,000 *g* for 30 min at 4℃. The bacterial culture after induction, the supernatant and insoluble protein fractions were

analyzed by SDS-PAGE (Fig.3.11.B).

3.2.4.2 Purification of C3d

Primary purification

$C3d^{17A}$ protein was purified from the soluble fraction by a two-step cation exchange chromatography method using SP Sepharose column on a ÄKTA purifier (GE Healthcare). After the lysate was clarified, the supernatant was equally split (roughly 20 ml for each sample) and applied on a SP-Sepharose Fast Flow 5 ml column sequentially with a flow rate of 1 ml/min. Before the elution step, the non-specifically bound proteins were removed by washing the column with 10 column volumes of MES-1A buffer. The elution of bound proteins was achieved by washing with gradient of MES-1B buffer, the recombinant $C3d^{17A}$ protein was eluted by ion strength corresponded to an electrical conductivity of 20 mS/cm. After the first purification step, the peak fractions and column flow through were examined by SDS-PAGE gel (Fig.3.11.B).

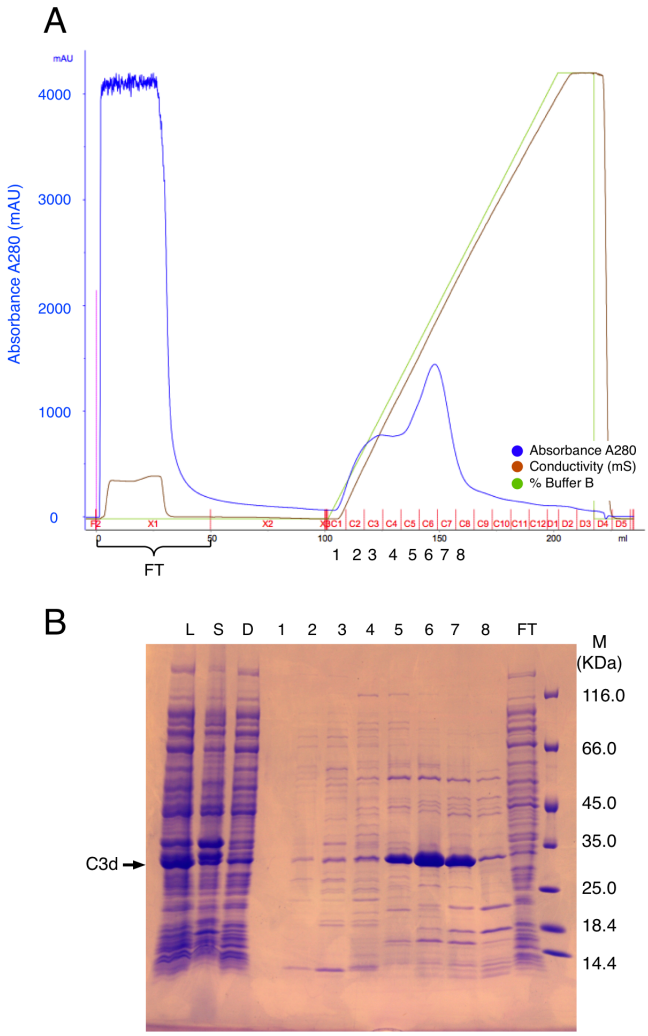

Figure 3.11: Primary purification of C3d (A) Cation exchange chromatography purification of C3d. Flow-through (FT) fraction and 8 elution fractions (1-8) were collected and analyzed by SDS-PAGE. **(B)** SDS-PAGE analysis of C3d expression and primary purification. Samples analyzed: whole cell lysate (L), soluble fraction (S), cell debris (D), elution fractions 1-8, and purification flow-through (FT).

Secondary purification of C3d

The confirmed $C3d^{17A}$ peak fractions were mixed and concentrated using a Vivaspin 10 kDa cut-off spin concentrator and desalted with a PD-10 column (GE healthcare) with the sample eluted in MES-2A buffer complemented with 0.25% of NaCl. The secondary purification involved a 1ml SP Sepharose HP column on a ÄKTA purifier. After loading and extensive washing, the bound $C3d^{17A}$ protein was eluted by a gradient of MES-2B buffer. The purity of the purified $C3d^{17A}$ was accessed by SDS-PAGE gel, and the purest fractions were concentrated and buffer exchanged for future usage.

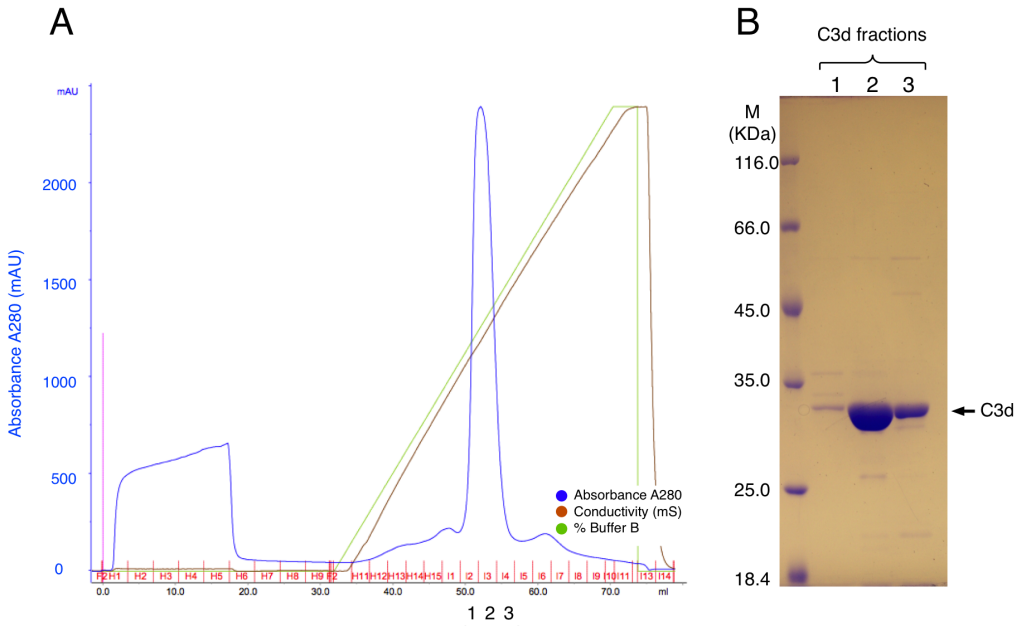

Figure 3.12: Secondary purification of C3d. (A) Secondary cation exchange chromatography purification of C3d. The peak fractions of primary purification were separated again in pH5.0. Peak fractions 1-3 were collected and analyzed. **(B)** SDS-PAGE analysis of the secondary purification of C3d. Three peak fractions indicated in A were analyzed.

The chromatogram for the secondary purification is shown in Fig.3.12.A. The bound proteins were eluted by a prolonged gradient of MES-2B buffer by which proteins emerged as distinct peaks. The C3d peak was eluted in the middle of the Buffer-2B gradient; peak fractions were collected and examined by SDS-PAGE (Fig.3.12.B). Utilizing these strategies C3d with over 90% purity was produced; normally 6 mg of recombinant C3d protein was purified from 1 L of the LB-auto-induction medium.

3.3 Discussion and further improvements

3.3.1 FH/FHR-1 purification

As described in this section protocols have been established for the purification of FHR-1 and FH. Immune-affinity purification protocols for FH have been described elsewhere, in some cases monoclonal antibodies were used to target specifically particular disease-associated isoforms of FH (Alsenz *et al*. 1985). A relatively decent yield of FH can be derived from serum, as the normal serum concentration of FH is 500 μg/ml. However, the estimated serum concentration of FHR-1 is only 70 μg/ml, this poses a great challenge for the efficiency of the current purification protocol. The protocols described in this study deliberately exploit the cross-reactivity of polyclonal anti-FH antibody in order to enrich FH and FHR-1 at the same time. Following this three-step protocol described in Section 3.2.2, FH and FHR-1 were successfully separated, 90% purity was achieved for FH, but only 60% purity was achieved for FHR-1. Heterogeneous natural dimerization states are the major handicap to further increasing the purity of FHR-1. As introduced in Section 1.4.3, FHR-1 forms homodimers and heterodimers with itself and FHR-2 and FHR-5 in the serum. These dimerization states of FHR-1 are held together by strong hydrophobic interactions(Goicoechea de Jorge *et al*. 2013). Therefore it is unlikely that these FHR-1 dimers will disassemble and only FHR-1 monomer will be purified under conventional chromatographical conditions. The dimerization states of FHR-1 were vividly demonstrated by the series of small peaks observed during heparin chromatograph polishing step (Fig.3.3.A curly bracket 2), according to the previously published study(Goicoechea de Jorge *et al*. 2013), these series of peaks represent different dimerization states of FHR-1. However, as indicated by the 280nm absorbance reading (Fig.3.3.A), the protein content of individual peak was extremely low, therefore all these peaks are mixed and concentrated for the sake of FHR-1 recovery percentage. As shown by Fig.3.3.C lane 2, despite the

majority of this sample being made up by FHR-1, there are two protein bands between 35 kDa and 25 kDa molecular weight markers that could represent two differently glycosylated FHR-2. Despite the contamination from other FHR protein, the purified FHR-1 sample is free from FH contamination (Fig.3.3.D); therefore it is usable in the *in vitro* assays.

There are several attempts that could be made in the future to increase the yield and purity of the serum derived FHR-1. Firstly, during the capturing step, a FHR-1 monoclonal antibody coupled column could be used. In current protocol, although FHR-1 was captured, the huge concentration excess of FH often saturates all the antibody binding-sites, therefore the initial enrichment of FHR-1 was frequently inefficient. Secondly, the heparin chromatograph polishing could be performed again. But instead of mixing all the peaks, individual peaks should be analyzed for the presence of FHR-1 homo-dimer. Based on an efficiently enriched FHR-1 sample, a sufficient amount of pure FHR-1 sample could be derived from an individual heparin-polished peak (Goicoechea de Jorge *et al*. 2013).

3.3.2 GST-C3a production

The codon optimized C3a gene has been cloned into pGEX-htb expression vector. The expression of GST-C3a fusion protein is under the control of a Trc-promoter; analyzing the purified GST-C3a protein fraction by SDS-PAGE revealed that only 30% of the recombinantly expressed protein is GST-C3a fusion protein whilst 70% is the GST protein tag. Given that the DNA sequencing of the plasmid revealed the gene has been correctly cloned into the vector, the possibility of production of GST due to cloning problems is ruled out. Plasmid contamination may be another explanation for the co-expression. However, the 4 DNA sequence verified clones screened for GST-C3a expression all showed similar

co-expression behavior, therefore it is unlikely that the co-expression was caused by plasmid contamination. A literature search revealed that the GST tagged expression of numerous proteins that are low in solubility or prone to misfolding, showed similar co-expression behavior (Harper & Speicher 2010). Therefore, the co-expression of GST and GST-C3a protein could be a result of differences in mRNA stability or translation stall at where two proteins fuse. The richness of C3a in disulfide bonds (three pairs) could be the cause of the huge protein property discrepancies, compared with GST. Fine-tuning the expression condition of GST-C3a revealed that lowering the IPTG concentration to as low as 0.05 mM increases the yield of GST-C3a gradually, suggesting that the expression strength of GST-C3a needs to be maintained at a relatively low level. Otherwise only the GST tag will be the dominant over-expression product. Currently, 0.5 mg of C3a can be produced per liter of culture. To improve the yield of this protein, vectors with molecular chaperone fusion tag can be screened as well as the vectors adopting tunable promoter.

Chapter 4: Mechanistic study of Sbi triggered C3 futile consumption

4.1 Introduction:

Sbi was first described as a modulator of complement activity in 2008 (Burman *et al*. 2008), when it was demonstrated that Sbi domain III-IV induces fluid phase futile consumption of C3. In the same paper, it was also demonstrated that Sbi triggered C3 consumption is compatible with the addition of EGTA. This observation indicated that the nature of Sbi triggered C3 consumption is the exploitation of complement alternative pathway. Based on these results, it was proposed that Sbi-III-IV binds to the intact C3 in serum, this binding then induces C3 to adopt a conformation that is primed for factor B binding through which the regulation of complement is subverted. This controlled depletion of C3 is in turn advantageous toward the survival of invading pathogen.

Later the same year, (Haupt *et al*. 2008) reported a new molecular characteristic of Sbi-III-IV, that it can bind C3d-containing C3 isoforms in combination with complement regulatory protein factor H to form tripartite complexes. The authors suggest that in combination with C3 activation fragments, Sbi could bind to factor H in a more stable form as tripartite complexes, thereby increasing the amount of host inhibitory regulator at the site of infection, consequently protecting the pathogen from complement attack and improving bacterial survival rate.

In the context of these two previous works, the first aim of this thesis is to elucidate the detailed molecular mechanism by which Sbi triggers C3 consumption. In this study, Sbi-III-IV was subjected to a systematic mutagenesis procedure to generate mutant proteins with defective functionality. By designing various comparative studies utilizing mutant and wild type proteins, we hope a credible mechanism of Sbi triggered C3 consumption can be proposed.

To guide the design of experiments, based on fundamental understanding of alternative pathway activation and regulation, three hypotheses were proposed to explore the role of Sbi-III-IV in the activation of C3.

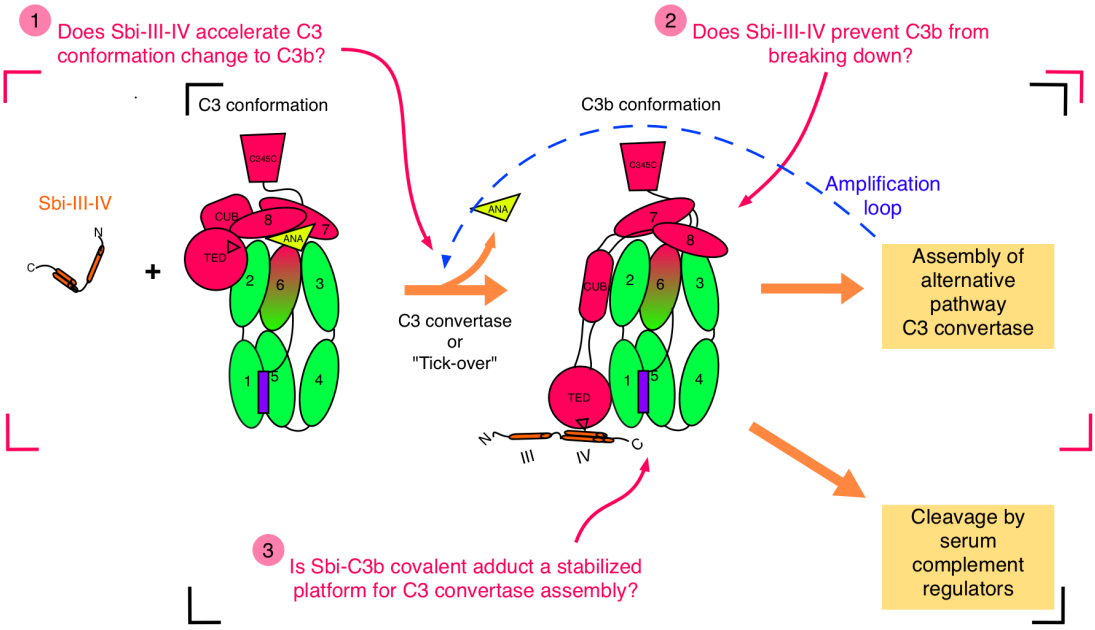

Figure 4.1.1: Hypotheses for Sbi-III-IV triggered C3 consumption. The diagram confined by **black edges** summarizes the structural conversion of C3 to the C3b conformation. C3 molecules undergo conformation change to the C3b conformation via the C3 convertase cleavage and "tick-over" mechanism. The stabilized C3b molecule is able to form a new alternative pathway C3 convertase, therefore causes positive feedback for the activation of C3 (blue dashed line), leading to the local activation of C3 molecule. However, in most cases, C3b molecules are immediately recognized and broken down by complement regulators, by which the activation of complement alternative pathway is constantly under strict control. In the presence of Sb-III-IV (diagram confined by **red edges**), the assembly of C3 convertase and depletion of local C3 molecule are strongly promoted. This phenomenon leads us to the following three hypotheses: **(1)** Sbi-III-IV binding to C3 molecule could accelerate the structure conversion from C3 to C3b. Increased local C3b concentration could in turn overwhelm the complement regulation. **(2)** Sbi-III-IV could increase the half-life of C3b molecule. **(3)** Sbi-III-IV is known to form a covalent adduct with the C3b molecule, this unique species of C3b may be more resistant toward serum C3b degrading enzymes.

4.1.1. Hypotheses for Sbi triggered C3 activation

The current model of AP activation describes the "tick-over" of C3 as the source of the initial C3b-like species. Relying on the intrinsic structural flexibility of C3, the "tick-over" process happens constantly in serum, providing potential new platforms for the assembly of initial fluid phase AP C3 convertase. This process normally occurs at a very low rate reaching an equilibrium status with the serum complement regulatory activity. Previous binding studies suggested that apart from the TED domain part of C3 molecule, Sb-III-IV also demonstrates weak interaction with the C3a fragment (Burman *et al*. 2008). Other than the most well-known function as an anaphylatoxin, C3a also functions as a crucial structural component within the C3 molecule. The cleavage of C3a triggers a series of structural rearrangements, resulting in the formation of C3b conformation. Therefore, the first hypothesis states that by interacting with these two regions of the C3 molecule, Sbi-III-IV could accelerate C3 conversion to C3b conformation in a mechanism that based on protein interactions. The resulting increase in local C3b concentration in turn overwhelms the regulation of AP activation.

It is evident that modulation of the nascent C3b stability is the essence of multiple complement activation regulatory mechanisms. AP activation is inhibited if the C3b molecule is swiftly degraded. On the contrary, a long-lived C3b molecule could develop into nascent AP C3 convertase leading to complement AP activation. As introduced in Section 1.3, the stability of the nascent C3b molecule is mainly dependent on three factors: the local concentration of complement regulators (e.g. factor H, factor I), the presence of complement positive regulators (e.g. properdin), and the biochemical characteristics of the surface where C3b molecule is deposited.

Hypothesis 2 proposes that in addition to binding of C3/C3b, Sbi-III-IV binds to other serum proteins simultaneously, thereby recruiting complement regulator

antagonists and AP C3 convertase stabilizers, leading to consumption of C3. In addition, under the same consideration of C3b stability, an alternative hypothesis (hypothesis 3) was also investigated. In this hypothesis, we proposed that the covalent adduct formed between Sbi-III-IV and C3b is essential for the C3 consumption process. Sbi-C3b covalent adducts could became less accessible for complement regulator binding. Therefore, the Sbi-C3b adduct helps to overcome the regulation of AP, leading to the consumption of C3.

4.2 Materials & Methods

4.2.1 Expression and Purification of Sbi-III-IV

The expression vectors of $pQE30^{Sbi\text{-}III\text{-}IV}$ WT or mutant were transformed into the *E.coli* strain BL21 (DE3). In each case, a single colony was picked and grown at 37°C overnight in 15 ml of LB medium containing ampicillin (100 µg/ml). The overnight primary culture was then used to inoculate 500 ml of LB medium containing ampicillin. Cells were grown at 37°C with shaking at 180 rpm. The expression of Sbi-III-IV protein was induced during the exponential phase of bacterial growth (OD_{600}=0.7) by adding isopropyl thiogalactoside (IPTG) to a final concentration of 0.5 mM in the culture. The *E.coli* cells were collected by centrifugation, 3 hours post-induction. Cell pellets were suspended in 20 ml of HisA buffer (Table 2.11) supplemented with EDTA free protease inhibitor cocktail mini tablets (Roche). The resuspended cells were lysed by sonification. The resulting lysate was clarified by centrifugation (60,000 g, 30 min, 4°C).

The supernatant was collected and purified through metal affinity chromatography, typically 15 ml of supernatant sample was loaded on a 1 ml HisTrap column (GE healthcare) using an ÄKTA purifier. The loaded column was washed with 15 column volumes of HisA buffer and the bound Sbi-III-IV protein was eluted with a 0-100% gradient of HisB (Table 2.11) buffer over 12 column

volumes. Based on the chromatogram, the Sbi-III-IV containing fractions were collected accordingly and evaluated by SDS-PAGE analysis. The purest fractions were then selected, pooled, concentrated and finally buffer exchanged using a PD10 column into phosphate buffer saline (PBS) buffer according to the manufacturer's instructions.

For assays requiring high protein purity, Sbi containing fractions from the primary purification were collected, concentrated and buffer exchanged back to HisA buffer. The prepared sample was loaded on a 1ml Histrap HP column for secondary purification. The bound proteins were eluted with an extended HisB gradient (20 column volumes). Based on the chromatogram the peak fractions were collected and analyzed by SDS-PAGE. The purest fractions were then mixed, concentrated and buffer exchanged into PBS buffer. Protein concentrations (Section 2.3.6) were determined using a NanoVue (GE life Science).

4.2.2. Complement activation in serum

One vial of complement active lyophilized human serum standard (HSS) was dissolved in 100 µl pre-chilled sterile water to 2×HSS. For a typical Sbi serum incubation experiment, 10 µl of 2×HSS was mixed with equal volume of Sbi solution in a PCR tube. After thorough mixing, the mixture was incubated in a thermocycler at 37°C for 30min. Treated serum samples were collected regularly (e.g., 5, 10, 15 and 30 min), normally 1 µl of treated serum was retrieved and added to 20 µl of 1×SDS loading buffer. To collect treated serum samples for ELISA analysis or other experiments, at least 2.5 µl of treated serum sample was retrieved and immediately frozen on dry ice, unless the treated serum samples were subjected to downstream measurement immediately.

Factor B, factor D, factor H, factor I and factor P depleted sera were also used to

perform incubation experiments with Sbi. For a typical Sbi depleted sera incubation experiment, equal volumes of depleted serum and Sbi solution were mixed at a final volume of at least 10 µl, 1 µl of $MgCl_2$-PBS stock solution was also added to adjust the final $MgCl_2$ concentration to 0.5 mM. Sample collection procedure and storage methods were as described above.

4.2.3. Complement assay

In this study, residual serum complement activity was determined using a Wieslab complement system assay kit (Euro Diagnostica) that measures the formation of terminal pathway component C5b-9 by an ELISA approach. Using ELISA strips coated separately with activators for the classical, MBL and alternative pathways, residual complement activities are determined correspondingly. Residual complement activity of Sbi treated serum was normally determined by both classical and alternative pathway assays.

Briefly, to determine residual classical pathway activity, Sbi was incubated with 2× HSS as described in section 4.2.2. Typically, 2.5 µl of treated serum was immediately added to 250 µl of classical pathway diluent. After all serum samples had been prepared, 100 µl of diluted serum was transferred into each well. Each sample was measured in duplicate together with positive and negative controls and buffer blank samples. The loaded plate was incubated at 37°C for 1 hour. After incubation, the plate was washed 3 times with 300 µl of washing solution; 100 µl of antibody alkaline phosphatase conjugate was added. After 30 min of incubation at room temperature, and a further washing step, 100 µl of n-nitrophenyl phosphate substrate solution was added. After 30 min, the absorbance of the wells was read using a plate reader at Abs_{405nm}. Absorbance values were converted to percentage of residual complement pathway activity following manufacturer's instructions.

A similar protocol was used to determine alternative pathway residual activity, with minor changes. Essentially, to prepare the ELISA sample, 15 µl of treated serum sample was retrieved and mixed with 240 µl alternative pathway diluent. 100 µl of diluted sample was then transferred to LPS coated wells.

4.2.4. Sbi-III-IV mutagenesis

Systematic mutagenesis studies were carried out on Sbi-III-IV. Based on a previously cloned pQE30$^{Sbi\text{-}III\text{-}IV}$ construct, the mutagenesis protocol described in 2.2.2 was used to generate Sbi-III-IV single mutants. Customized primers (Table 4.2.1 & 4.2.2) were obtained from Invitrogen (Life Technologies). pQE30$^{Sbi\text{-}III\text{-}IV}$ plasmid, the template DNA, was purified from a 10 ml overnight *E.coli* XL-Gold cell culture using GeneJet plasmid miniprep kit (Invitrogen, Life Technologies). Concentration of the purified plasmid was measured by NanoVue spectrophotometer.

Table 4.2.1: Mutagenic PCR primers. Mutations are highlighted in red.

Mutation	Primer (5'-3')
N191A	**F:**gctaactcaaaattacctaaagatttacgcgataaa**gct**aaccgctttgtagaaaaag
	R:ctttttctacaaagcggtt**agc**tttatcgcgtaaatctttaggtaattttgagttagc
N192A	**F:**gctaactcaaaattacctaaagatttacgcgataaaaat**gcc**cgctttgtagaaaaagttt
	R:aaacttttttctacaaagcg**ggc**atttttatcgcgtaaatctttaggtaattttgagttagc
D208N	**F:**gtttcaattgaaaaagcaatcgttcgtcat**aat**gagcgtgtgaaatc
	R:gatttcacacgctc**att**atgacgaacgattgctttttcaattgaaac
S213A	**F:**gtcatgatgagcgtgtgaaa**gca**gcaaatgatgcaatct
	R:agattgcatcatttgc**tgc**tttcacacgctcatcatgac
R231A	**F:**atgaaaaagattcaattgaaaacaga**gct**ttagcacaacgtgaagttaacaaag
	R:ctttgttaacttcacgttgtgctaa**agc**tctgttttcaattgaatctttttcat

Table 4.2.2: mutagenic PCR primers. Mutations are highlighted in red.

Mutation	Primer (5'-3')
N156A	**F:** ccatcacggatccgaacgtcaaaatattgaa**gct**gcggataaagcaatt
	R:aattgctttatccgc**agc**ttcaatattttgacgttcggatccgtgatgg
K159A	**F:**tccgaacgtcaaaatattgaaaatgcggat**gca**gcaattaaagatttccaag
	R:cttggaaatctttaattgc**tgc**atccgcattttcaatattttgacgttcgga
K162A	**F:**caaaatattgaaaatgcggataaagcaatt**gca**gatttccaagataacaaagcacc
	R:ggtgctttgttatcttggaaatc**tgc**aattgctttatccgcattttcaatattttg
K168A	**F:**cggataaagcaattaaagatttccaagataac**gca**gcaccacacgataaatca
	R:tgatttatcgtgtgg**tgc**tgcgttatcttggaaatctttaattgctttatccg
P170A	**F:**tttccaagataacaaagca**gca**cacgataaatcagcagc
	R:gctgctgatttatcgtg**tgc**tgctttgttatcttggaaa
D172A	**F:**caagataacaaagcaccacac**gcc**aaatcagcagcatatgaagcta
	R:tagcttcatatgctgctgattt**ggc**gtgtggtgctttgttatcttg
K173A	**F:**aagataacaaagcaccacacgat**gca**tcagcagcatatgaagctaac
	R:gttagcttcatatgctgctga**tgc**atcgtgtggtgctttgttatctt
S174A	**F:**gcttcatatgctgct**gct**ttggcgtgtggtgcttt
	R:aaagcaccacacgccaa**agc**agcagcatatgaagc
S199A	**F:**ataaccgctttgtagaaaaagtt**gca**attgaaaaagcaatcgttcgt
	R:acgaacgattgctttttcaat**tgc**aacttttctacaaagcggttat
K212A	**F:**gttcgtcatgatgagcgtgtg**gca**tcagcaaatgatgcaatctc
	R:gagattgcatcatttgctga**tgc**cacacgctcatcatgacgaac
S226A	**F:**tgcaatctcaaaattaaatgaaaaagat**gca**attgaaaacagacgtttagcac
	R:gtgctaaacgtctgttttcaat**tgc**atctttttcatttaattttgagattgca
Y177F	**F:**caccacacgataaatcagcagca**ttt**gaagctaactca
	R:tgagttagcttc**aaa**tgctgctgatttatcgtgtggtg
N180A	**F:**cgataaatcagcagcatatgaagct**gcc**tcaaaattacctaaagatttacgc
	R:gcgtaaatctttaggtaattttga**ggc**agcttcatatgctgctgatttatcg
K182A	**F:**atcagcagcatatgaagctaactca**gca**ttacctaaagatttacgcgataaa
	R:tttatcgcgtaaatctttaggtaa**tgc**tgagttagcttcatatgctgctgat
K185A	**F:**cagcagcatatgaagctaactcaaaattacct**gca**gatttacgcgataaaaa
	R:tttttatcgcgtaaatc**tgc**aggtaattttgagttagcttcatatgctgctg
R188A	**F:**gcatatgaagctaactcaaaattacctaaagattta**gcc**gataaaaataaccgcttt
	R:aaagcggttatttttatc**ggc**taaatctttaggtaattttgagttagcttcatatgc
K190A	**F:**ctcaaaattacctaaagatttacgcgat**gca**aataaccgctttgtagaaaaagtttca
	R:tgaaacttttctacaaagcggttatt**tgc**atcgcgtaaatctttaggtaattttgag

4.2.5 Sbi-III-IV mutant serum activation assay

Sbi-III-IV treatment of HSS was performed as described in section 4.2.2. For each Sbi mutant, treated serum samples at 5, 10, 15 and 30 min were collected. The resulting Sbi-C3b adduct formation and C3 activation were detected by both polyclonal anti-Sbi and anti-C3d Western blots (Section 2.3.8).

4.2.6 *In vitro* Sbi-$C3_{H2O}$ adduct formation

1.5 mg/ml of purified C3 molecule (3.3.1) was incubated with 10 μM of Sbi-III-IV WT or K173A respectively. The incubation mix was collected at 2 hour intervals for 16 hours. SDS-PAGE and anti-Sbi Western blot analyses were performed to detect the formation of Sbi-$C3_{(H2O)}$ adduct.

4.2.7 Circular Dichroism spectroscopy

The secondary structure compositions of Sbi-III-IV WT, K173A and S199A were analyzed by circular dichroism (CD) using a Chirascan spectrometer (Applied Photophysics). For CD measurement, Sbi-III-IV proteins were purified twice as described in section 4.2.1 for maximal purity. The purest fractions were mixed, concentrated and buffer exchanged to phosphate buffer (10 mM Na_3PO_4 pH 7.4). The CD experiments were carried out using a 0.3 mm cuvette. Concentrations of the protein sample were screened to determine an optimal value where the high tension voltage reading was less than 700 V. Eventually, the CD spectra of Sbi WT and mutants were acquired at concentrations between 2.45 and 3.50 μM (0.035-0.0508 mg/ml). For each Sbi-III-IV protein, ten replicate CD spectra between 190 and 280 nm (1 nm increments) were acquired. The corresponding CD spectrum of phosphate buffer was also acquired. To present the CD data, the resulting scans were averaged, smoothed, and the buffer signal was subtracted. Finally, the measurements were converted to mean residual ellipticity (θ). The averaged CD spectra of Sbi-III-IV were deconvoluted using CDNN software, written by Dr. Gerald Böhm. This program compares the acquired CD spectrum with a range of reference spectra of known protein structure, which yields an

approximation of the secondary structure composition of the query protein.

4.2.8. Preparation of Sbi-III-IV-cys K173A, S199A R231A mutants

Single amino acid substitution mutation K173A, S199A and R231A mutations were inserted into pQE30$^{\text{Sbi-III-IV-cys}}$ construct individually. Apart from the changes in PCR template, the rest of the mutagenesis procedures were identical to that described in Section 4.2.4 and the primer information was provided in table 4.2.1 and 4.2.2. Methods described in Section 4.2.1 were used to express and purify Sbi-III-IV-cys WT, K173A, S199A and R231A proteins.

4.2.9 SwitchSENSE hydrodynamic diameter and kinetic measurements

A SwitchSENSE DRX 2400 instrument (Dynamic Biosensors) was used to characterize the binding kinetics and protein size changes based on SwitchSENSE technology (Langer *et al.* 2013; Knezevic *et al.* 2012).

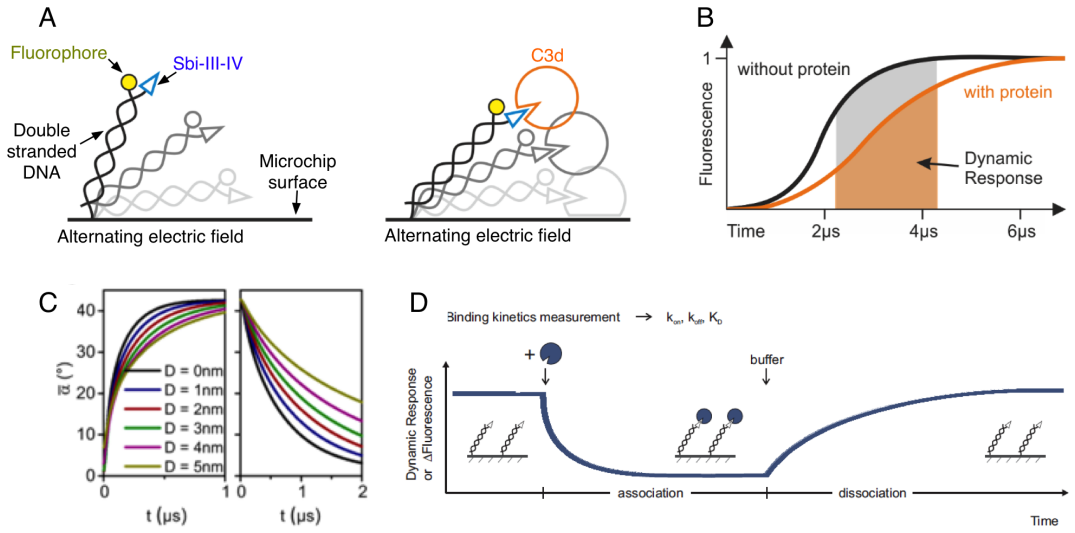

Figure 4.2.1: Principle of SwitchSENSE technology (A) Immobilization of protein and the electrically switchable nanolevers **(B)** Increasing in protein size reduces dynamic response **(C)** Dynamic response changes during increasing hydrodynamic diameter **(D)** Dynamic response changes over a protein binding event. Figures adapted from Dynamic Biosensor website www.dynamic-biosensors.com.

Purified Sbi-III-IV-cys WT, S199A, K173A, R231A and their ligand C3d were sent to Dynamic Biosensor's protein analyzing facility (Germany) for binding kinetic and hydrodynamic diameter analysis. Given the novelty of this technique, a brief introduction of the technique is given below. To perform the measurement, using the free thiol group in the cysteine residue (Section 9.1.1.2), these four types of Sbi-III-IV were covalently linked with a 48 bp sense single strand DNA fragment. By complementary binding to a fluorophore labeled anti-sense DNA strand that had been pre-coated on the surface of a gold-microchip, the protein analyte was immobilized. (Fig.4.2.1.A) A high frequency alternating electric field was then applied to the microchip to switch the double stranded DNA lever between "standing" and "lying" states. The kinetics of this movement were followed by a single photon counter, which measures the quenching of the fluorophore down to a resolution of nano-seconds. The switching dynamics of the DNA-protein complexes gradually slow down with increasing protein (or protein complex) size (Fig.4.2.1.B). In the case of a protein binding event (Fig.4.2.1.D), based on the real-time measurements of the switching dynamics in a range of ligand concentrations, binding rate constants (k_{ON} and k_{OFF}) and dissociation constants (K_d) can be analyzed. Alternatively, under saturated binding conditions, the switching dynamic of the protein (or protein complex) can be compared with the switching dynamic standards of proteins with known size (Fig.4.2.1.C), by which the size of the immobilized protein (or protein complex) can be determined.

For determination of Sbi-III-IV:C3d binding kinetic parameters, 130 nM, 100 nM, 70 nM and 40 nM of C3d were applied sequentially onto the Sbi-III-IV immobilized microchip. All Sbi:C3d complexes' hydrodynamic diameters were estimated at a C3d concentration of 130 nM.

4.2.10 Sbi-III-IV-cys biotinylation

To prepare Sbi-III-IV-cys protein samples for labeling, 10 mM β-mercaptoethanol

was added to reduce the cysteine residue at the C-terminus of the protein. After 1 hour incubation at room temperature, the protein sample was buffer exchanged to the appropriate labeling buffer and the labeling reagent was added immediately. Protein samples were labeled with two types of biotin label to satisfy the requirements of different experiments.

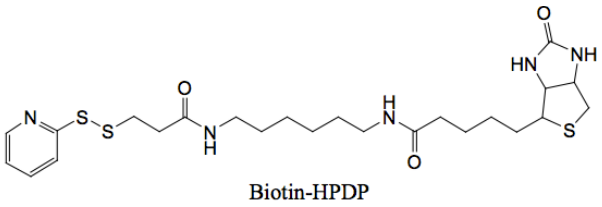

Figure 4.2.2: EZ-link HPDP biotin

EZ-link N-[6-(Biotinamido) hexyl]-3'-(2'-pyridyldithio)Propionamide (HPDP) biotin label (Thermo Scientific) was used to label proteins that required biotin tag removal afterward. After protein samples were reduced, they were buffer exchanged into reaction buffer (PBS containing 2 mM EDTA). 4 mM HPDP-biotin stock dissolved with dimethylformamide was added to the buffer exchanged protein sample to a final concentration of 0.4 mM. The labeling reaction took place at room temperature for 2 hours. Afterwards, the labeled protein samples were concentrated and buffer exchanged back to PBS buffer, stored at -80°C pending usage.

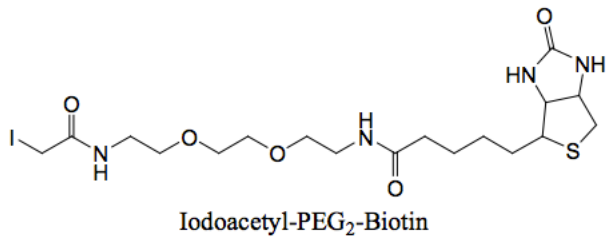

Figure 4.2.3: Iodoacetyl-PEG2-biotin

Non-cleavable and reduction resistance iodoacetyl-PEG2-biotin tag (Thermo Scientific) was also utilized to label protein samples. After reduction of protein samples, they were buffer exchanged into reaction buffer (50 mM Tris-HCl, 5 mM

EDTA pH 8.0). 4 mM iodo-PEG2-biotin stock dissolved in reaction buffer was added to a final concentration of 200 µM. The labeling reaction was kept in the dark for 90 min at room temperature, then the labeled protein samples were concentrated and buffer exchanged to PBS buffer, stored at -80°C pending usage.

4.2.11. Pull-down experiment

HPDP biotin labeled Sbi-III-IV WT and mutants (K173A, S199A and R231A) were immobilized on 100 µl of neutravidin agarose beads. The loaded beads were then washed extensively with PBS buffer by which excess non-immobilized proteins were removed. After washing with PBS, 2 ml of human serum (TCS bioscience) supplemented with 20 mM EDTA was incubated with Sbi loaded neutravidin agarose beads for 30 min with rotation. The incubated agarose beads were then recovered by centrifugation (1000 *g*) and washed extensively with PBS with 0.1% tween20 (PBST) buffer to reduce non-specific binding. The binding of serum proteins to bait proteins Sbi-III-IV WT, K173A, S199A and R231A was analyzed using SDS-PAGE and stained with Coomassie blue R-250, utilizing uncharged neutravidin agarose beads as negative control.

4.2.12. In-gel Trypsin digestion

For protein identification, protein bands of interest were excised from the SDS-PAGE gel. An in-gel tryptic digestion kit (Thermo Scientific) was used to prepare trypsinized protein fragments according to the manufacturer's instruction. Briefly, the excised gel slices (2×2 mm) were repetitively washed with de-stain buffer (25 mM NH_4HCO_3, 50% acetonitrile) until the gel slices became transparent. Gel slices were then reduced by adding 30 µl of reducing buffer (50 mM TCEP in de-stain buffer), after which an alkylation step was performed by adding 30 µl of alkylation buffer (100 mM Iodoacetamide and 25

mM NH_4HCO_3) and incubated for 1 hour in the dark. After re-equilibration with de-stain buffer, 100% acetonitrile (50 µl) was added to shrink the gel slice, until the gel slice became white in color and decreased in size. The excess acetonitrile was then removed and allowed to thoroughly evaporate (15 min, room temperature). Finally, 35 µl of 100 ng of trypsin in digestion buffer (25 mM NH_4HCO_3) was used to swell the air-dried gel slice. The digestion reaction took place at 30°C overnight with shaking; afterward the digestion mixture was removed and placed in a clean tube ready for mass spectrometry analysis.

4.2.13 Mass spectrometry protein identification

After in-gel protein digestion, the resulting peptide samples were sent to Chemical Characterization and Analysis facility (CCAF, University of Bath) where Electrospray ionization (ESI)-quadrupole (Q)-Time of Flight (TOF) mass spectrometry (MS) analysis was performed. Briefly, between 0.1-0.5 µl of peptide sample was spotted on C8 or C18 column integrated HPLC-Chip, after separation (Buffer A: 0.1% Formic acid; Buffer B: 0.1% Formic acid and 90% Acetonitrile; Flow rate: 0.6 µl/min) the resulting peptides were ionized by HPLC-Chip Cube MS interface (Agilent), and subsequently analyzed by 6520 series Accurate-Mass Quadrupole Time of Flight mass spectrometer (Agilent). Utilizing the peptide fragment pattern generated, SwissProt searches were carried out using Mascot program to discover the identity of the protein.

4.2.14. BLItz ternary complex reconstruction

In vitro reconstruction of Sbi:C3d:FH and Sbi:C3d:FHR-1 ternary complexes were performed using bio-layer interferometry on a BLItz system (Fortebio) following manufacturer's instruction. Briefly, a Ni-NTA coated biosensor tip was hydrated for 30 min in assay buffer (PBS). His-tag protein (Sbi-III-IV) was loaded on the biosensor tip for 120 sec with orbital shacking at 2200 rpm. The loaded sensor

tip was soaked in PBS for 30 sec with shaking until a stable base line was established. An association curve was acquired by exposing the loaded sensor tip to 2 µl of secondary complex component (e.g. 2 µM of C3d) for 120 sec with shaking at 2200 rpm. After the assembly of the dimeric complex on the biosensor surface, the biosensor tip was immediately exposed to 2 µl of the tertiary complex component (e.g. 6 µM of factor H) for 180 sec with shaking at 2200 rpm. The formation of the tripartite complex was revealed as a further association event. Finally the biosensor tip was soaked in PBS buffer for 120 sec, during which the dissociation curve of the tripartite complexes was recorded.

4.2.15 Ternary complex reconstruction ELISA

Table 4.2.4: Reconstituted ternary complex formation. Purified C3, C3b, C3d, FH and FHR-1 were used in this study.

Ternary complex components		
Sbi-III-IV 1 µg/well	C3 (0.11 µM) C3b (0.11 µM) C3d (0.28 µM)	FH (0-500 nM) FHR-1 (0-400 nM)

Sbi-III-IV mediates binding of factor H or FHR-1 in combination with C3 isoforms (C3, C3b and C3d), resulting in the formation of the ternary complexes. An ELISA based binding assay was designed to measure Sbi-III-IV mediated tripartite complex formation. Typically 1 µg/well of Sbi-III-IV WT or mutants were coated on a Nunc MaxiSorp flat-bottom 96 well polystryrene plate in a predetermined pattern using sodium carbonate buffer pH 9.5. Coating of the plate took place overnight at 4°C. Once the coating buffer was removed the plate was then blocked with 300 µl/well of PBST supplemented with 5% skimmed milk for 1 hour and washed once with 300 µl/well of PBST. The complex components were then added to the well in PBST-1.25% milk and left for 1 hour. The plate was then thoroughly washed with PBST (4 times with 5 min intervals) before

applying polyclonal goat anti-FH antibody (recognizing both human factor H and FHR-1) diluted in PBST-1.25% milk (1:4000 dilution) for 1 hour at room temperature. Again the plate was thoroughly washed before the addition of the secondary anti-goat IgG antiserum (1:18,000 dilution) for 1 hour at room temperature. After the final wash cycle, 100 µl/well of the 1-step Ultra TMB ELISA substrate solution was added. 20 min later the absorbance of the wells was read using a plate reader at Abs_{650nm}.

4.2.16. FH/FHR-1 Competition assay

Based on the existing ELISA assay for tripartite complex formation, considerable modifications were made, by which the competitive relationship between FH and FHR-1 for binding of C3 isoforms was elucidated. Firstly 1 µg/well of Sbi-III-IV WT were coated on a Nunc MaxiSorp plate in a predetermined pattern using sodium carbonate buffer pH 9.5. After coating at 4°C overnight, the plate was emptied. Then, PBS supplemented with 2% BSA was added (300 µl/well) to each wells to block the uncoated surface for 1 hour at 37°C and then washed with PBS buffer. The complex components (FH, FHR-1 and C3 isoforms; in PBS-2% BSA) were then added in such a way that a decreasing FHR-1:FH molar ratio (from 4 to 0) was created within each column of the ELISA plate. At the same time C3 isoforms' concentration remained the same as an invariable. After 1 hour incubation at room temperature, the plate was thoroughly washed with PBS before monoclonal anti-FH antibody OX-24 (biotinylated, ThermoPierce) diluted with PBS-2% BSA (1 in 2000) was added for 1 hour. OX-24 binds to a FH specific epitope on SCR domain 5. Following a thorough wash of the plate, Streptavidin-HRP conjugate solution (1 in 5000 dilution with PBS-2% BSA, GE Healthcare) was utilized to bind the biotinylated primary antibody for 1 hour at room temperature. Finally after final washing steps, 1-step Ultra TMB ELISA substrate solution was added, 20 min later the absorbance of the wells was read using a plate reader at Abs_{650nm}.

4.2.17. $C3_{H2O}$ preparation

C3 with hydrolyzed thioester was prepared by supplementing purified C3 solution (2 mg/ml, PBS) with 50 mM methylamine. The hydrolysis reaction was kept in a 37°C water bath for 2 hours.

4.2.18. $C3_{H2O}$ cleavage assay

$C3_{H2O}$ (400 μg/ml) was incubated with factor H (160 μg/ml), rFHR-1 (50 μg/ml) and factor I (4 μg/ml). Incubation reactions were divided into two groups according to whether Sbi-III-IV WT (80 μg/ml) or K173A (80 μg/ml) was added, the final reaction volume was adjusted to 12 μl. Cleavage reactions were kept at 37°C using a thermocycler, samples (2 μl) were retrieved regularly and mixed with reducing SDS sample buffer, boiled at 96°C for 10 min, then separated by SDS-PAGE electrophoresis.

4.2.19. Double depletion serum validation

Firstly, EDTA-serum pull-down experiment was performed using factor H depleted serum (1 ml) with neutravidin resin immobilized Sbi-III-IV^{WT}, based on Section 4.2.15. Secondly, serum albumin and IgG were depleted from the factor H depleted serum (10 μl) using Pierce Top2 abundant protein depletion spin column (Thermo Scientific), and concentrated to 20 μl by Vivaspin 500 (3 kDa cut-off) centrifugal concentrator. 5 μl of the sample was then separated by SDS-PAGE. Both pull-down sample and triple depleted serum were analyzed by anti-Fh/FHR-1 Western blot.

4.2.20. Double depleted serum recovery experiment

PBS buffer, Sbi-III-IV WT or K173A mutants were incubated with double depleted serum supplemented with rFHR-1 or factor H or both. In each reaction, the final concentration of the double depleted serum was diluted to 40%, with

other assay components. All protein components of this assay were buffer exchanged to PBS buffer to avoid fluctuation of salt concentration. To reconstitute the double depleted serum, 2 µl of factor H (1 mg/ml) and 1 µl of rFHR-1 (0.25 mg/ml) were added to 4 µl of serum. When added together a 1:1 molar ratio of factor H and rFHR-1 was achieved. After incubation at 37°C for 1 hour in the thermocycler, C3 consumption was evaluated by anti-C3a and anti-C3 Western blot (Section 2.3.8). Reaction compositions are shown in Table 4.2.5.

Table 4.2.5: Recipes of double depleted serum recovery experiments

Group	Double depleted sera	Sbi-III-IV WT	Sbi-III-IV K173A	Factor H (1mg/ml)	rFHR-1 (0.25mg/ml)	5mM $MgCl_2$	PBS
Serum only	4	-	-	-	-	1	5
	4	1	-	-	-	1	4
	4	-	1	-	-	1	4
FHR-1	4	-	-	-	1	1	4
	4	1	-	-	1	1	3
	4	-	1	-	1	1	3
FH	4	-	-	2	-	1	3
	4	1	-	2	-	1	2
	4	-	1	2	-	1	2
FHR-1/ FH	4	-	-	2	1	1	2
	4	1	-	2	1	1	1
	4	-	1	2	1	1	1

All volume in µl

4.3 Results

Sbi N-terminal domain III-IV inhibits all complement pathways by mediating futile consumption of C3. Previous studies indicated that the consumption process involves manipulation of the alternative pathway to achieve local depletion of C3 molecules. However, the molecular details remain elusive (Burman *et al*. 2008). In this section, the biochemical changes during Sbi induced consumption of C3 were characterized.

4.3.1 Expression and purification of Sbi-III-IV

The gene fragment encoding Sbi-III-IV in pQE30 vector was transformed and expressed in *E.coli* BL21 (DE3) strain as a N-terminal 6×His tagged protein. As described in Section 4.2.1, protein expression was induced by IPTG, cells were solubilized and proteins were purified by two-step Ni^{2+} affinity chromatography and analyzed on SDS-PAGE. Fig.4.3.1.A & B shows the primary purification elution profile and the corresponding SDS-PAGE gel. The gel shows Sbi-III-IV was successfully over-expressed and solubilized in His-A buffer, the purified recombinant Sbi-III-IV demonstrates expected molecular weight of 14.9 kDa. Limited endogenous *E.coli* protein contaminations were detected in the first two fractions of the Sbi peak.

Sbi fractions to be further purified were mixed and buffer exchanged to His-A buffer. The secondary purification using 1 ml Histrap HP column with prolonged elution volume aims to produce high purity Sbi-III-IV for subsequent functional and structural assays. Fig.4.3.1.C & D shows the elution profile and SDS-PAGE gel of the secondary purification, based on the purity of Sbi-III-IV fractions 4-7 were collected for further usage.

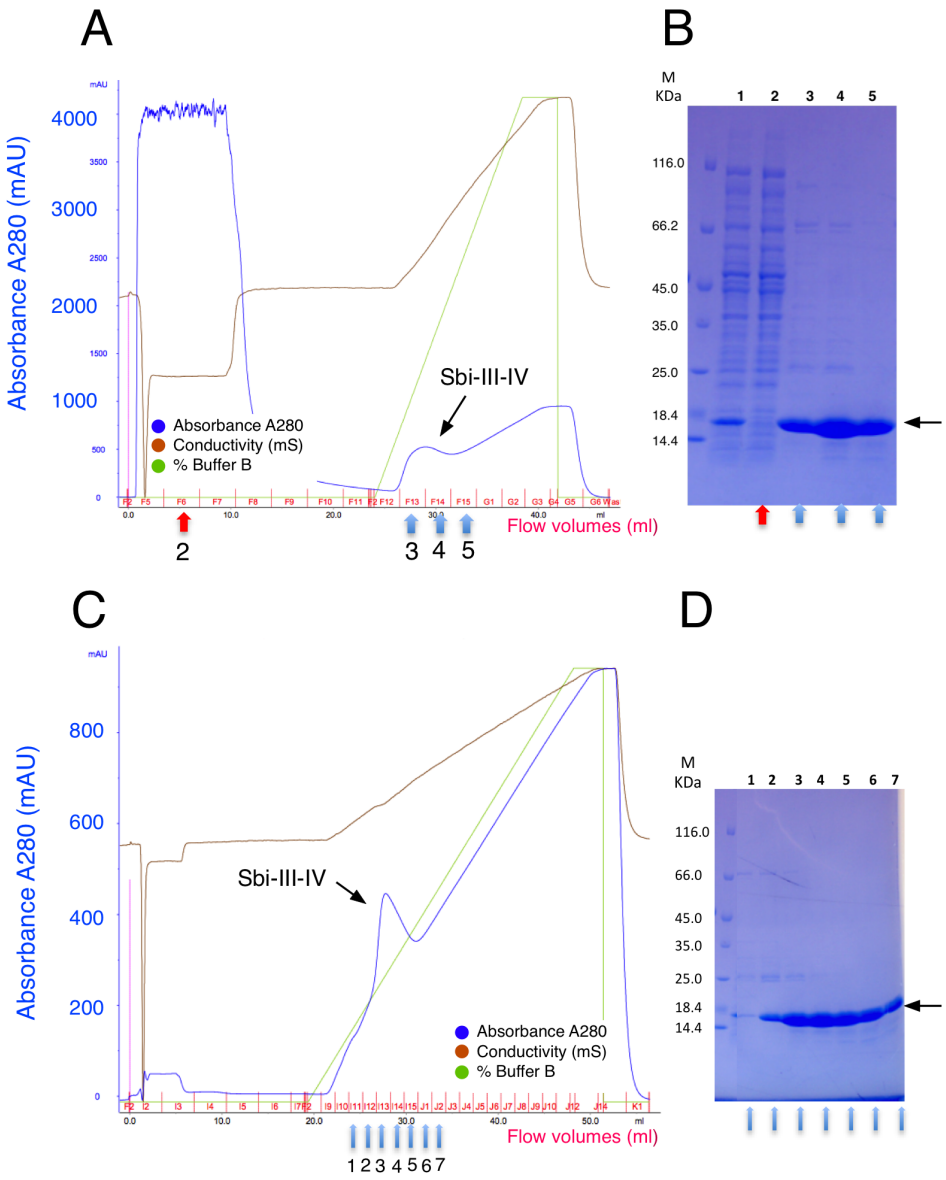

Figure 4.3.1: Two-step Ni^{2+} affinity chromatography and SDS-PAGE profiles of Sbi-III-IV purification. **(A)** Chromatogram of primary purification, volume (ml) and fractions are shown on X-axis. **(B)** Coomassie stained gel of Sbi-III-IV primary purification, Lane *1* soluble fraction before purification, *2* purification flow-through, *3-5* purified fractions. Sbi-III-IV (black arrow), with an expected size of 14.9 kDa is located between 18.4 kDa and 14.4 kDa molecular weight markers. Lane 3 and 4 demonstrate that two thirds of the purified Sbi is slightly contaminated. **(C)** Chromatogram of secondary purification. **(D)** The purity of Sbi-III-IV containing fractions are verified by SDS-PAGE and Coomassies blue staining. Lanes 1-7 represent the corresponding fractions on the chromatogram indicated by blue arrows. Fractions 4-7 show the minimum level of contamination and were mixed for future usage.

4.3.2 Sbi induces futile consumption of C3

To investigate the molecular detail of the complement consumption induced by Sbi, Sbi-III-IV treated human serum standard (HSS) samples (Section 4.2.2) were analyzed by immuno-blotting with various polyclonal antibodies to monitor the deposition of activated C3, formation of Sbi-C3b adducts, cleavage of factor B and release of C3a. Proteolytic activation of C3 releases anaphylatoxin C3a and produces metastable C3b molecules that subsequently become covalently deposited on surrounding protein targets among which Sbi-III-IV itself has been shown as a primary transacylation target (Burman *et al*. 2008). To assemble the AP C3 convertase, the $C3_{H2O}$ bound factor B molecule is cleaved by factor D to larger enzymatic fragment Bb and smaller fragment Ba. The cleavage process occurs simultaneously with the activation of AP, therefore it makes an ideal marker for AP activation detection. HSS incubation with Sbi-III-IV (10 μM) at 37°C for 30 min demonstrated that 5 min lagging-time was required before the initiation of C3 activation. Once activated, the C3b molecules deposit on surrounding serum proteins, causing the formation of high molecular weight C3b covalent adduct species (Fig.4.3.2.A). The activation of C3 was also captured by polyclonal anti-C3a immuno-blotting. As shown in Fig.4.3.2.D, over time the C3a epitope disappears from the intact C3 α-chain (120 kDa) and reappears in the form of free C3a molecules (9 kDa). Synchronized factor B activation was also detected, which suggests that AP C3 convertase is involved in the C3 consumption process (Fig.4.3.2.C). Finally, the polyclonal anti-Sbi Western blotting demonstrated that a small fraction of free Sbi-III-IV molecule increases in their molecular weight significantly during the C3 activation process, by forming covalent adducts with C3d containing C3 isoforms (e.g. C3b and iC3b). The C3b component within the Sbi-C3b adduct (approximately 140 kDa) is subject to proteolytic cleavage by serum proteases, thereby gradually being converted to a smaller Sbi-iC3b adduct (120 kDa). (Fig.4.3.2.B)

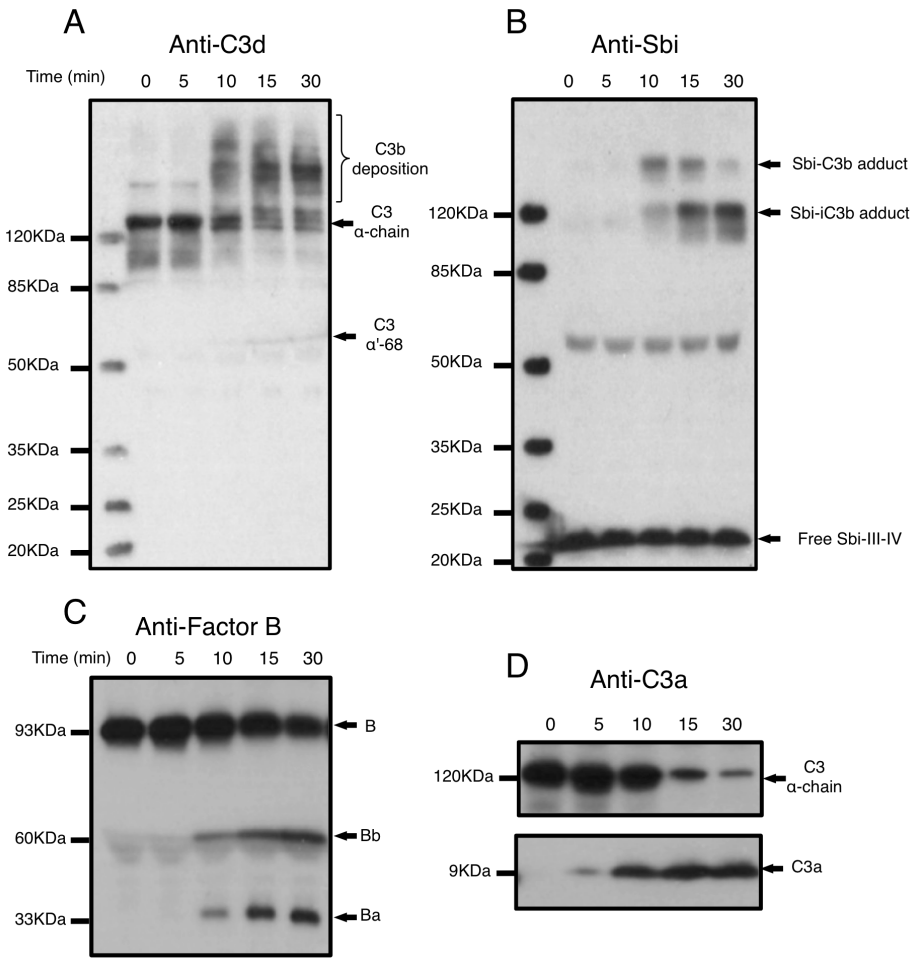

Figure 4.3.2: Sbi-III-IV induces C3 futile consumption. Immunoblots of Sbi treated serum detected by polyclonal anti-C3d (A), anti-Sbi (B), anti-Factor B (C) and anti-C3a (D). **(A)** C3 activation and deposition in serum after incubation with 10 μM Sbi-III-IV for 30 min. **(B)** Detection of Sbi-C3b adduct formation and free Sbi-III-IV used in the incubation reaction. **(C)** Detection of factor B cleavage products in serum. **(D)** Synchronized disappearance of intact C3 α-chain and the release of anaphylatoxin C3a during Sbi-III-IV mediated C3 futile consumption.

4.3.3 Sbi triggers C3 consumption via alternative pathway

The activation of different complement activation pathways has been shown to be highly dependent on divalent ions. Classical and lectin pathway activations are mediated by calcium ions, and magnesium ions play essential roles in alternative pathway activation. Using this property, ion chelation by EDTA is used to inhibit all complement pathways; on the contrary the classical and lectin pathways can be selectively inhibited by adding preferential calcium ion ion-chelating reagent, EGTA. Previous studies indicated that in the presence of

EDTA, Sbi triggered C3 consumption was inhibited. However, with the addition of EGTA-Mg^{2+}, Sbi-III-IV was still able to trigger C3 consumption. These results implied that the Sbi triggered C3 consumption process is in essence the activation of the complement system, perhaps by hijacking solely the alternative pathway. To verify this hypothesis, human sera with depleted alternative pathway components (e.g. factor I, factor H, factor P, factor D and factor B) were incubated with Sbi-III-IV. C3 consumption and Sbi-C3b adduct formations were then analyzed by Western blots (Fig.4.3.3.A & B). Given that only serum components required for the alternative pathway were depleted, the depleted sera should still demonstrate normal CP activity; therefore the CP activity of all depleted sera were determined (Fig.4.3.3.C) and compared with HSS.

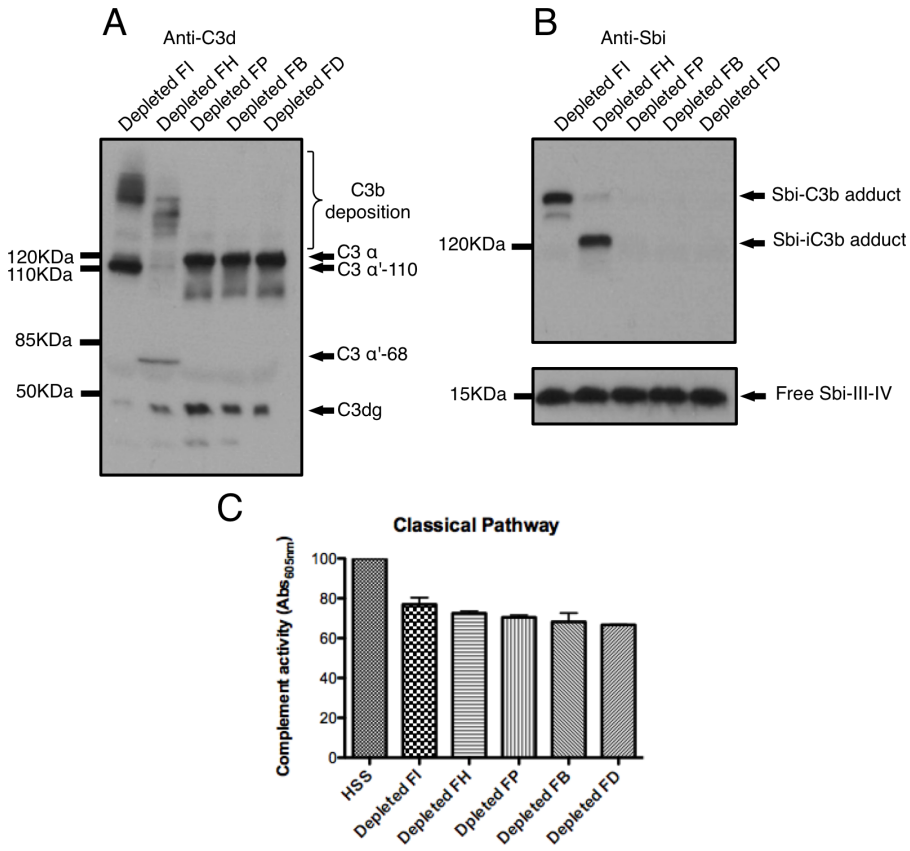

Figure 4.3.3: Alternative pathway components are essential for the Sbi triggered C3 consumption. (A) Anti-C3d Western blot detects Sbi triggered C3 activation in human sera depleted of complement factor I, factor H, factor P, factor B and factor D. **(B)** Anti-Sbi Western blot detects the formation of Sbi-C3b covalent adduct. **(C)** Measurement of classical pathway complement activity using HSS and depleted sera. FI for factor I, FH for Factor H, FP for properdin, FB for factor B and FD for factor D.

With the complement regulators factor I and H depleted, incubation of the depleted sera with Sbi-III-IV results in the spontaneous activation of C3. Fig.4.3.3.A shows that C3 consumption in factor H depleted serum shares a similar Western blot profile with consumption of C3 in normal serum. As shown in Fig.4.3.2.A, missing of C3 α-120 kDa chain, C3b deposition and the appearance of iC3b α'-68 chain all signify the consumption of C3. However, when using factor I depleted serum, due to the absence of protease factor I, C3b molecules accumulate in the solution and presence as the C3b α'-110 chain in the Western blot (Fig.4.3.3.A). The deposited C3b molecules are also free from proteolytic cleavage and therefore appear as the very high molecular weight covalent adduct species. With the absence of essential alternative pathway components (e.g. properdin, factor B and factor D), Sbi-III-IV is unable to trigger C3 consumption. After prolonged incubation, the majority of the C3 remains as the unreacted form of 120 kDa C3 α-chain. Although factor H is regarded as the cofactor for factor I mediated C3b cleavage, our results show that in the absence of factor H, C3b molecules in the serum are also subjected to proteolytic processing, which could be a result of the presence of other factor I cofactors (e.g. C4BP and sCR1) in the serum.

The same C3 consumption pattern was reproduced when the samples were analyzed by anti-Sbi polyclonal antisera. Sbi adduct formations were observed only after incubation with factor H and I depleted sera (Fig 4.3.3.B). Without factor I cleavage, intact Sbi-C3b adduct was observed (approximately 140 kDa). However, in factor H depleted serum, the majority of the Sbi-C3b adduct was converted to the Sbi-iC3b adduct (120 kDa). Finally, all depleted sera possess roughly 70% classical pathway activity comparing with positive control HSS (Fig.4.3.3.C). The discrepancies could be the results of differences in C3 and C5 concentration, since sera were acquired from different sources. Nevertheless, the results show all depleted sera demonstrate normal C3 activity.

4.3.4 Sbi triggered C3 consumption can also be captured by CP ELISA assay

As Sbi is an activator of AP, an AP inhibition experiment might not be an ideal way to characterize the speed of the C3 futile consumption process. Here, the Sbi mediated inhibition of AP and CP were compared.

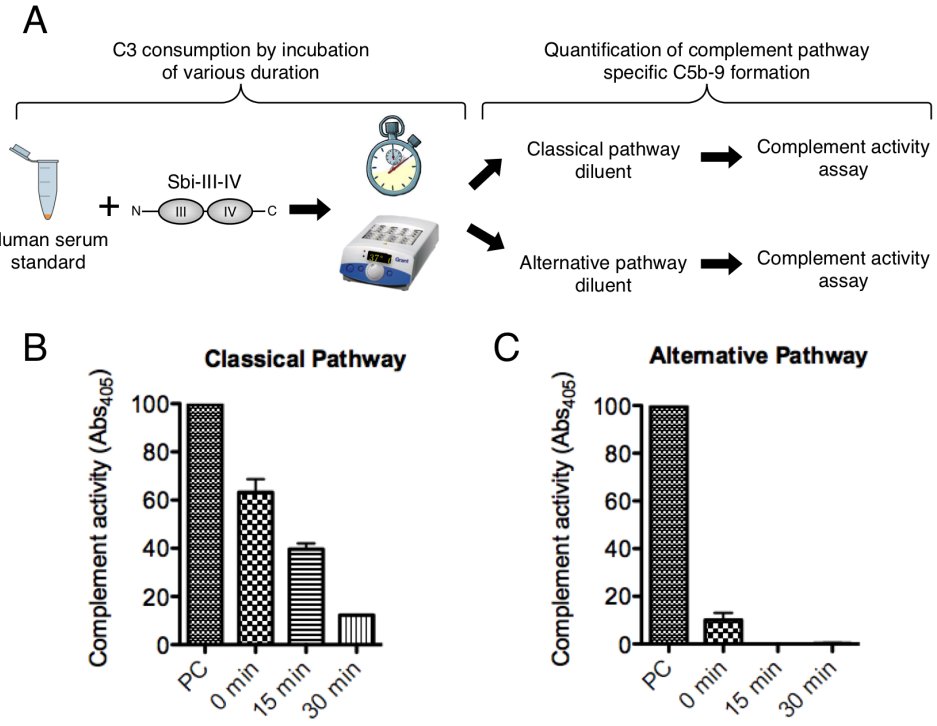

Figure 4.3.4: Pre-incubation dependent Sbi-III-IV inhibitions of classical and alternative pathway activities. **(A)** Schematic diagram of the experiment design, HSS was first pre-incubated with Sbi-III-IV at 37°C for different length of time (0, 15 and 30 min). Two sets of treated sample were collected; their residual classical or alternative pathway activities were then measured. **(B)** Residual classical and **(C)** alternative pathway complement activities of Sbi-III-IV treated sera samples. Percentage activity was calculated using absorbance readings at 405 nm with the equation *activity =[(sample-negative control)/positive control (PC)]×100*. Each condition was assayed in duplicate and the error bars represent the upper and lower result. PC is a abbreviation of positive control.

As shown in Fig.4.3.2.A, after the initial lag time, the C3 consumption process occurs at a steady pace. To quantify the speed of C3 consumption, HSS was incubated with Sbi-III-IV (Fig.4.3.4.A), samples were taken at various time points and the residual AP and CP activities were determined separately (Section 4.2.3). Fig.4.3.4.B shows that without pre-incubation, the presence of 10 μM Sbi-III-IV inhibits CP activity to 60%. After 15 min of incubation the residual CP activity

was reduced to 40% and finally after another 15 min incubation only 12% residual CP activity was detected. In contrast to the time dependent steadily decline in CP activities, the inhibition of AP activity (Fig.4.3.4.C) hardly shows any correlation with incubation duration. At 0min, the residual AP activity was reduced to 10%, after 15min incubation the AP activity was reduced to minimum. The reason for the pre-incubation independent inhibition of AP activity is that after the samples were collected, they were incubated for an extra hour in AP diluent on the ELISA plate, during which Sbi-III-IV could still trigger the consumption of C3. Therefore, determination of residual CP activity offers a more subjective measurement of C3 consumption process.

The results of the CP inhibition experiment suggest that the complete inhibition of CP activity by Sbi-III-IV is the result of two separate mechanisms. One inhibition mechanism is independent from incubation, likely to be a result of protein-protein interactions. The secondary mechanism is dependent on the length of incubation, which agrees with the gradual C3 consumption Western blotting profile shown in Fig.4.3.2.A. Thus, binding of Sbi-III-IV to CP component and futile C3 consumption together contribute to the effective inhibition of CP activity.

4.3.5 Sbi-III-IV interferes with AP driven C5b-9 formation

The results presented here expose another molecular feature of the Sbi mediated C3 futile consumption process. To measure AP activity, a Wieslab ELISA plate was coated with AP activator lipopolysaccharide (LPS) that triggers the activation of C3, leading to the formation of quantifiable C5b-9 membrane attack complex. However, when Sbi-III-IV was added, severe inhibition of C5b-9 formation was observed which contradicts with the C3 activating function of Sbi. (Fig.4.3.4.C,0min). In contrast to the effective inhibition of AP C5b-9 formation (Fig.4.3.4.C,0min), Sbi-III-IV is less potent in the inhibition of C5b-9 formation from CP. (Fig.4.3.4.B,0min)

In conclusion, Sbi-III-IV mediates C3 futile consumption exclusively via the alternative pathway, and the C3 futile consumption differs from AP activation as the terminal pathway is strongly inhibited.

4.3.6 Sbi-III-IV mutagenesis studies

4.3.6.1 Creation of Sbi-III-IV mutants

It was demonstrated previously that the Sbi N-terminal domains III and IV are the minimal domain requirement for Sbi induced C3 consumption (Burman *et al*. 2008). Whilst Sbi domain IV was characterized as a three-helix bundle C3/C3d binding domain (Upadhyay *et al*. 2008; Clark *et al*. 2011), very little is known about the structural and functional aspects of Sbi domain III. Given that Sbi domain III was reported as intrinsically unfolded (Upadhyay *et al*. 2008) we adopted a systematic mutagenesis approach aiming to elucidate the function of Sbi domain III by biochemical assays. At the same time, based on information from a previous publication (Clark *et al*. 2011), selected residues on Sbi domain IV were also mutated. The impacts on activity of Sbi-III-IV were then evaluated by C3 activation assay.

Aiming to generate a systematic Sbi domain III-IV mutant library, site-directed mutagenesis primers were designed to mutate Sbi domain III residues by following three criteria (Fig.4.3.5.A). Firstly, Sbi is known to form covalent adducts with metastable C3b molecules, and hydroxyl group containing amino acids (serine (S), threonine (T) and tyrosine (Y)) are the primary target for C3b deposition. At the same time the hydroxyl side chain could also contribute immensely to protein-protein interactions and protein tertiary structure. Therefore, hydroxyl group containing residues were also included in this mutagenesis study. Secondly, similar to hydroxyl side chain residues, amino acids with amine containing side chains could also take significant structural functions. Thus, arginine (R), asparagine (N) and lysine (K) residues in Sbi

domain III were substituted with alanine residue respectively. Finally, analysis of the Sbi primary sequence revealed that domain III contains a large number of lysine residues existing in combination with adjacent aspartate (D) residues, forming acid-base residue pairs ("DK" pair). Therefore the lysine residues participating in the "DK" pairs were included in the mutagenesis study. Overall, 38% of domain III residues were studied in this systematic mutagenesis experiment (Fig.4.3.5.B).

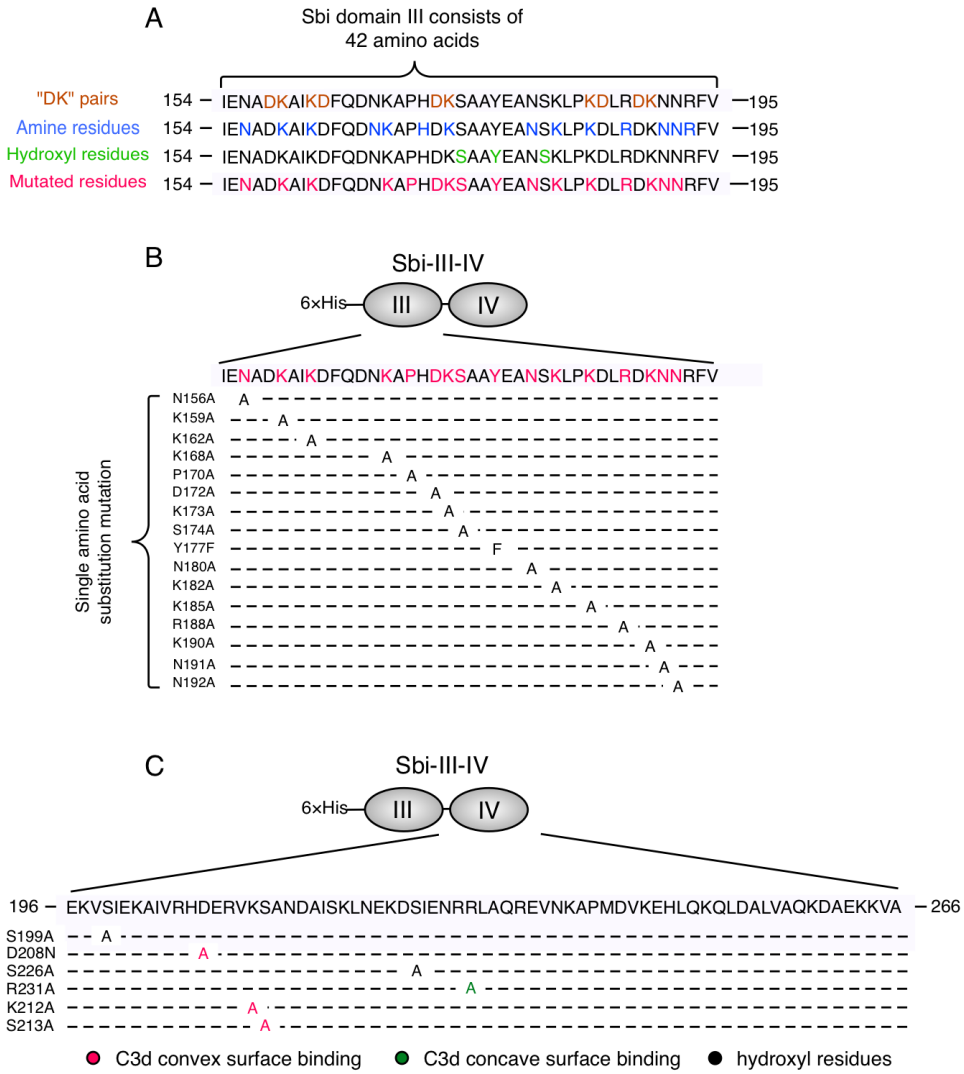

Figure 4.3.5: Schematic diagrams summarizing the systematic mutagenesis experiment of Sbi-III-IV. (A) Color coded Sbi domain III primary sequences. Within domain III five "DK" pairs are identified, labeled in orange. Amine containing residues are labeled in blue; hydroxyl-containing residues are labeled in green. Red-color labeled residues represent the residues involved in the mutagenesis study. **(B)** An overview of the single amino acid substitution mutant distribution across the Sbi domain III. **(C)** Selection and distribution of Sbi domain IV mutants.

In contrast to the large-scale systematic mutagenesis study on domain III, the mutagenesis study on domain IV was much more concise and pinpointed (Fig.4.3.5.C). Using previous structural data of Sbi domain IV interacting with C3d, key interaction residues were mutated to alanine. R231 is essential for the Sbi domain IV to bind to the concave surface of the C3d fragment (Upadhyay *et al*. 2008). D208, K212 and S213 are the key residues mediating Sbi domain IV interaction with the convex surface of C3d (Clark *et al*. 2011). In addition, serine 199 and 226 were also mutated. S199 is located in the junction between domain III and domain IV, S226 is located in the loop connecting domain IV helix I and II. These two serine residues were selected for the identification of the potential C3b deposition site.

All single amino acid substitutions mentioned in Fig.4.3.5 were created using a PCR based site-directed mutagenesis method (Section 4.2.4). During each PCR reaction, mutation incorporated PCR primers were used to amplify the entire $pQE30^{Sbi\text{-}III\text{-}IV}$ construct, producing the $pQE30^{Sbi\text{-}III\text{-}IV}$ mutant plasmid. To maximize the chance of incorporation, for every mutation, PCR reactions were conducted at five different extension temperatures. The outcome of each PCR reaction was then accessed by agarose gel electrophoresis. Fig.4.3.6 shows the PCR amplification results for the incorporation of every Sbi single amino acid substitution mutation. For every mutation, at least two PCR reactions demonstrated significant PCR amplification products at the expected size. Although the majority of the mutation incorporation occurs in all extension temperatures, some mutations prefer relatively lower PCR extension temperature. The incorporation of mutation was verified by DNA sequencing (Appendix 9.1.2.1).

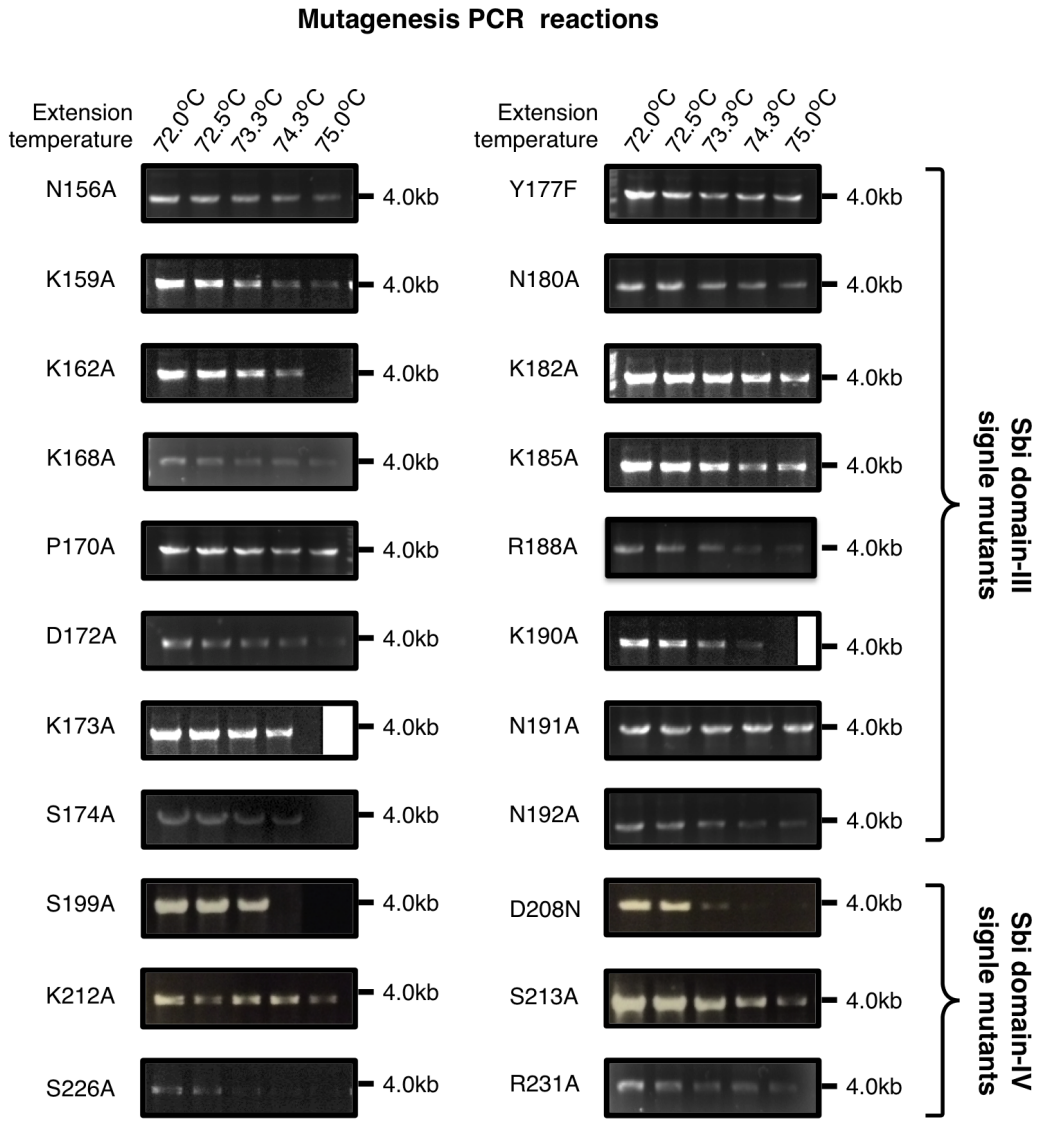

Figure 4.3.6: Agarose gel analysis of mutation incorporated pQE30$^{Sbi\text{-}III\text{-}IV}$ vectors. All mutations were based on the pQE30$^{Sbi\text{-}III\text{-}IV}$ construct. Using site-directed mutagenesis, single amino acid substitutions were inserted at the selected amino acid position. Mutagenic PCR reactions were carried out at five extension temperatures (72°C, 72.5°C, 73.3°C, 74.3°C and 75°C). The outcomes of mutation insertion and PCR amplification were represented as the intensity of the DNA band at 4.0 kb.

After the successful incorporation of a single mutation into the pQE30$^{Sbi\text{-}III\text{-}IV}$ plasmid, the mutated plasmids were purified and transformed into *E.coli* strain BL21 (DE30). Given that all Sbi-III-IV mutants are single amino acid substitution mutants, the expression and purification protocol used for all the mutants was identical to the protocol used for Sbi-III-IV wild type protein (Section 4.2.1).

After IPTG-induced over-expression, *E.coli* cells were lysed; the mutant proteins were then purified from the soluble fraction of the cells using Ni^{2+} affinity chromatography. Under the same purification parameters, the majority of Sbi-III-IV mutants demonstrated a similar chromatogram to that shown in Fig.4.3.7.A**.** After the initial loading and washing of the 1 ml Histrap FF column, the His-tagged protein was eluted with a 12 column-volume gradient of 0 to 100% HisB buffer. At the early stage of the elution, a 280 nm absorption peak was observed and normally consisted of three peak fractions (Fig.4.3.7.A Black arrow). The peak fractions for each Sbi-III-IV mutant were collected. The purity of the purified protein was then accessed by SDS-PAGE electrophoresis analysis (Fig.4.3.8 and 4.3.9). Although the majority of the Sbi-III-IV mutants reach a consensus in their chromatographic profile, the Sbi-III-IV^{Y177F} mutant demonstrated an abnormal chromatographic profile (Fig.4.3.7.B). On the chromatogram, no significant protein peak was detected, but the putative peak fractions (Fig.4.3.7.B Black arrow) were collected and analyzed by SDS-PAGE (Fig.4.3.8).

Fig.4.3.8 and Fig.4.3.9 demonstrate that the peak fractions of every Sbi-III-IV mutant purification contain purified Sbi-III-IV mutant protein of the expected size (14.9 kDa). Although some of the peak fractions were slightly contaminated by *E.coli* endogenous proteins, every Sbi mutant contained at least one peak-fraction, which was free from contamination (Fig.4.3.8 and 4.3.9 black arrow). The corresponding fraction was then used for subsequent Sbi-III-IV functional characterizations.

Although the Sbi-III-IV^{Y177F} mutant failed to produce an elution peak in its chromatogram (Fig.4.3.7.B), the SDS-PAGE analysis of the putative peak fractions detected the presence of purified Sbi-III-IV^{Y177F} protein in the fractions. Therefore the absence of the 280 nm absorption peak is a result of poor 280 nm absorption property of the Y177F mutation. By mutating the only 280 nm

absorptive residue (tyrosine 177 to a phenylalanine), the Y177A mutant of Sbi-III-IV has become nearly transparent to 280 nm UV light.

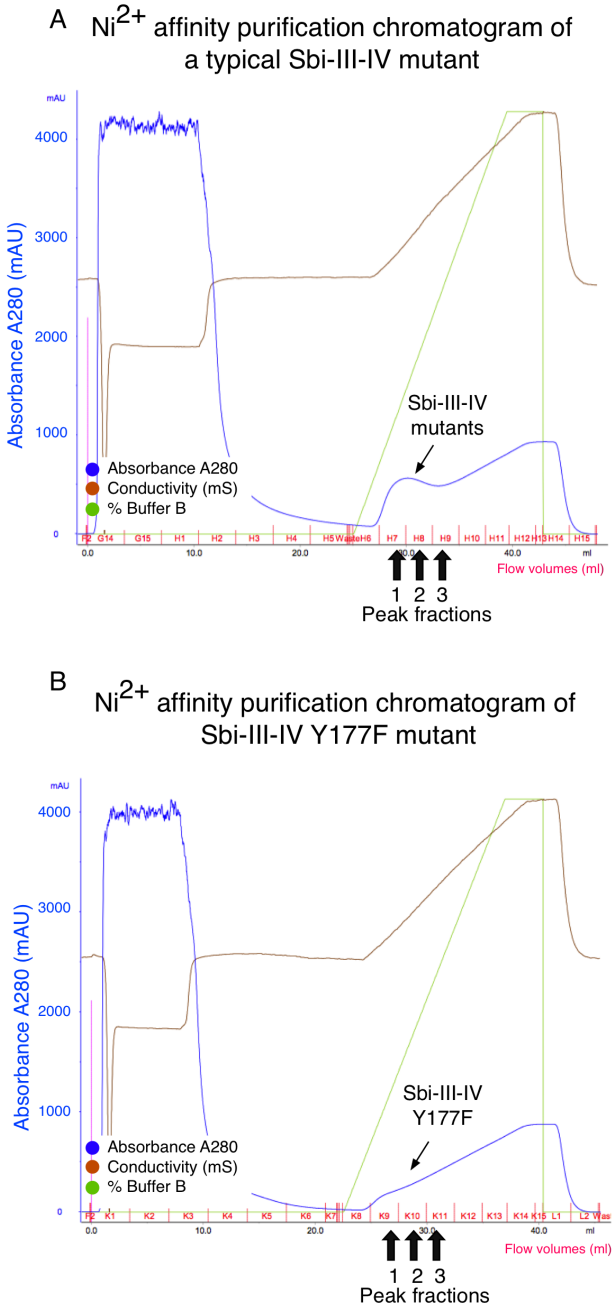

Figure 4.3.7: Chromatograms of Sbi-III-IV mutant protein purifications. (A) A typical Ni^{2+} affinity purification chromatogram for a Sbi-III-IV mutant. Due to the same purification method being used for all Sbi mutants, the majority of the Sbi-III-IV single amino acid mutant proteins demonstrate similar chromatograms. Peak fractions (1, 2 and 3, indicated by black arrow) from every purification procedures were collected. The purity of the purified protein was then examined by SDS-PAGE analysis. (**B**) An abnormal purification chromatogram of Sbi-III-IV Y177F mutant. No significant protein peak was observed. However, three predicted peak fractions (1, 2 and 3) were taken for SDS-PAGE analysis.

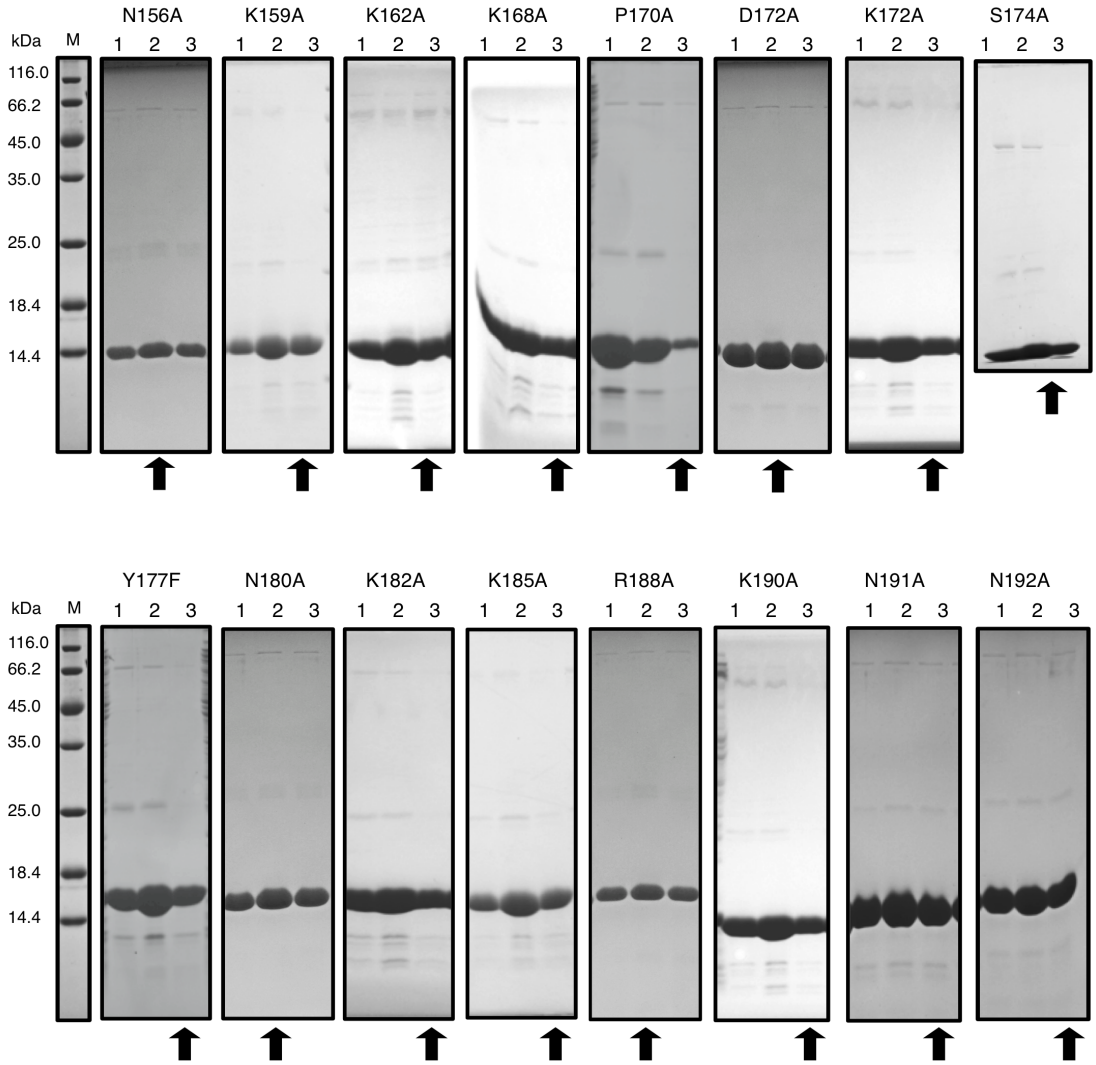

Figure 4.3.8: SDS-PAGE profiles of purified Sbi-III-IV domain III single amino acid substitution mutants. Each mutant was purified by Ni^{2+} affinity chromatography with 1 ml Histrap FF column. Three peak fractions (1, 2 and 3) were analyzed by SDS-PAGE and shown as a single gel segment. All Sbi-III-IV mutants display the expected size of 14.9 kDa, located between 18 kDa and 14.4 kDa molecular weight marker. According to the gel, normally the 3rd fraction of every purification reaction is the purest. The fractions taken for subsequent studies are indicated by a black arrow.

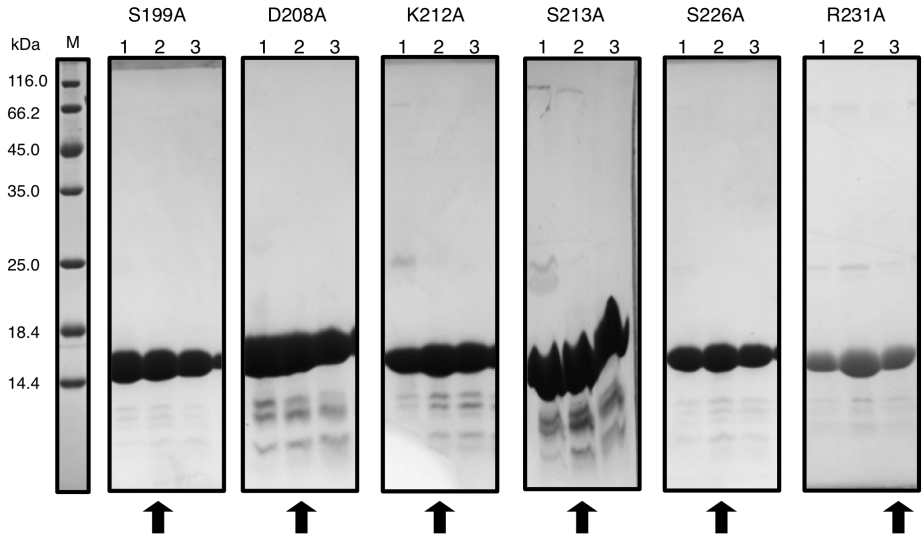

Figure 4.3.9: SDS-PAGE profiles of purified Sbi-III-IV domain IV single amino acid substitution mutants. Each mutant was purified by Ni^{2+} affinity chromatography with a 1 ml Histrap FF column. Three peak fractions (1, 2 and 3) were analyzed by SDS-PAGE and shown as a single gel segment. All Sbi-III-IV mutants display expected size of 14.9 kDa, located between 18 kDa and 14.4 kDa molecular weight marker. According to the gel, the most pure fractions were taken for subsequent studies, indicated by a black arrow.

4.3.6.2 Sbi-III-IV mutants serum activation assay

This study utilized a library of Sbi-III-IV mutants to evaluate the functional impacts of these substitutions. Sbi-III-IV mutants were incubated with the HSS (Section 4.2.2), the C3 consumption process was then followed by anti-C3d and anti-Sbi Western blots (Section 4.2.5), over a 30 min period (Fig.4.3.10). It was demonstrated in Section 4.3.2 that the formation of Sbi-C3b adduct and the consumption of C3 α-chain are two indications of Sbi's C3 consumption process. As demonstrated by Fig.4.3.11 and 4.3.12, the systematic screening of Sbi-III-IV single mutants shows that majority of the Sbi-III-IV single mutants is still able to induce time-dependent consumption of C3 α-chain and to form Sbi-C3b adduct. However, several Sbi-III-IV mutants with aberrant phenotypes (highlighted in red, Fig.4.3.11 and 4.3.12) were also identified.

R231 in domain IV had previously been implicated as a crucial residue that mediates Sbi binding on the C3d concave surface. As expected, the activity screens demonstrate that the mutation of this residue causes a significant

decrease in Sbi's activity. At very high concentration, 30 min incubation was needed to initiate the activation of C3 (Fig.4.3.11). Based on the anti-Sbi Western blot (Fig.4.3.12), R231A also demonstrated decreased adduct formation level, which could be a result of the reduced C3 avidity.

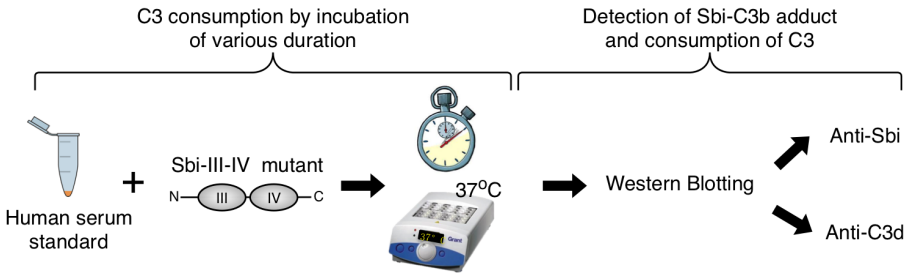

Figure 4.3.10: Functional screen of Sbi-III-IV mutants. The C3 consumption activity of Sbi-III-IV mutants and truncation variants was assayed individually. Treated serum samples were collected in various time points and analyzed by both anti-Sbi and anti-C3d Western blots.

According to the anti-C3d Western blot screening (Fig.4.3.11), the substitution of lysine 173 in the middle of the Sbi domain III to alanine (K173A) produces the most dramatic decrease in Sbi's activity, since no C3 consumption was observed during the 30 min incubation period. The corresponding anti-Sbi Western blot shows this mutant lacks the ability to form Sbi-C3b adducts. Serine 199 (S199) is located at the N-terminal end of Sbi domain IV in the junction region between domain III and IV. The substitution of S199 also causes significant reduction in C3 consumption activity, and shows a 15 min lag-time on C3 activation.

Three mutations (D208N, K212A, S213A) were designed to evaluate the role of Sbi domain IV convex surface binding in the C3 consumption process. All three Sbi-III-IV mutants demonstrate comparable C3 consumption activity to the Sbi-III-IV wild type. However, the mutation of a nearby amino acid residue serine 226 (S226) produces the most unexpected C3 consumption profiles. The anti-C3d Western blot demonstrates that S226A is an activator of C3, and at very high concentration no significant delay in C3 activation was detected. But, uniquely, this mutant shows no detectable Sbi-C3b formation. These observations suggest that S226 could be a covalent attachment site of C3b. This

possibility will be explored in detail in chapter 5.

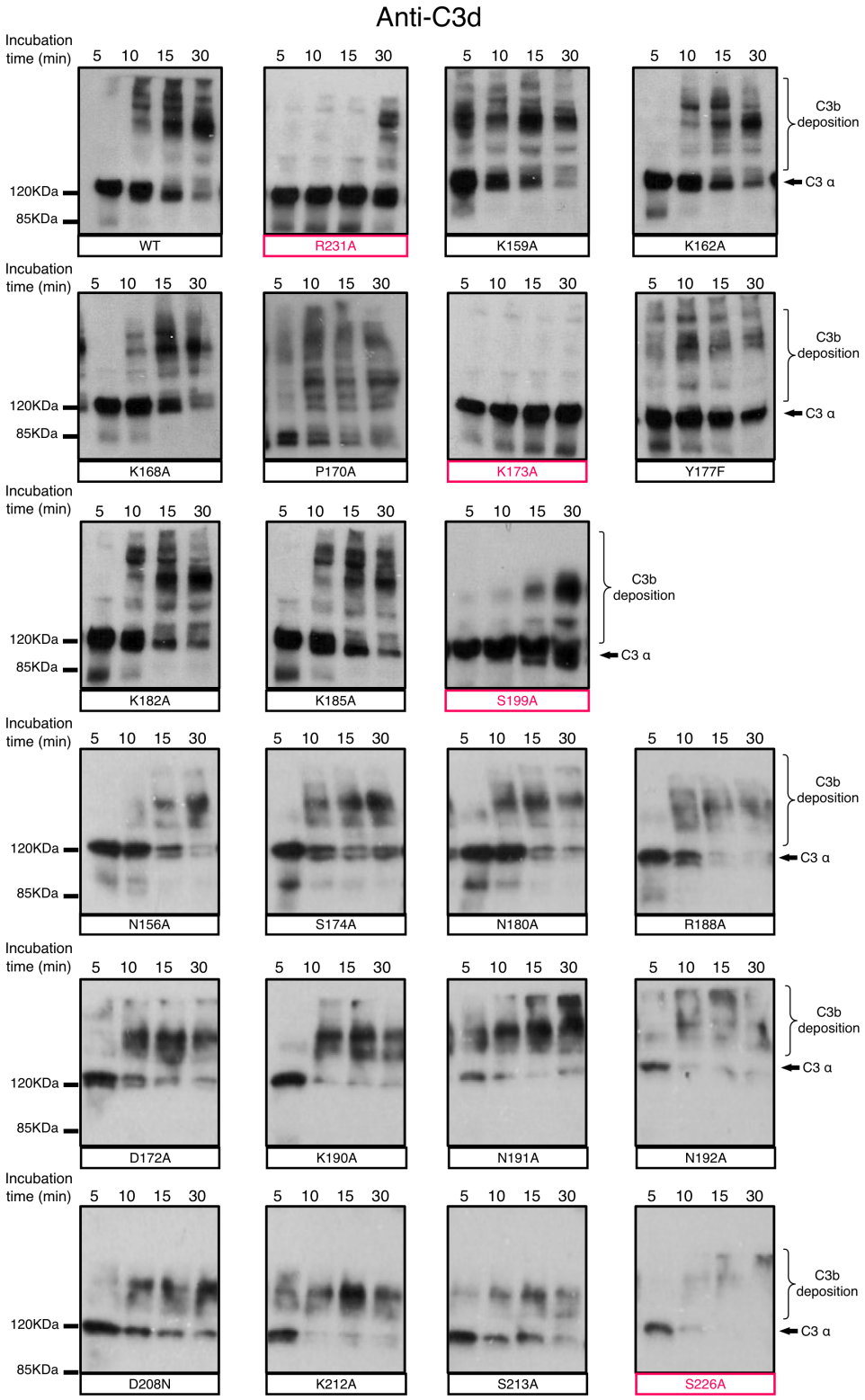

Figure 4.3.11: Anti-C3d western blots of Sbi single mutant treated serum. The Sbi mutants K173A, S199A, R231A and S226A were highlighted in red.

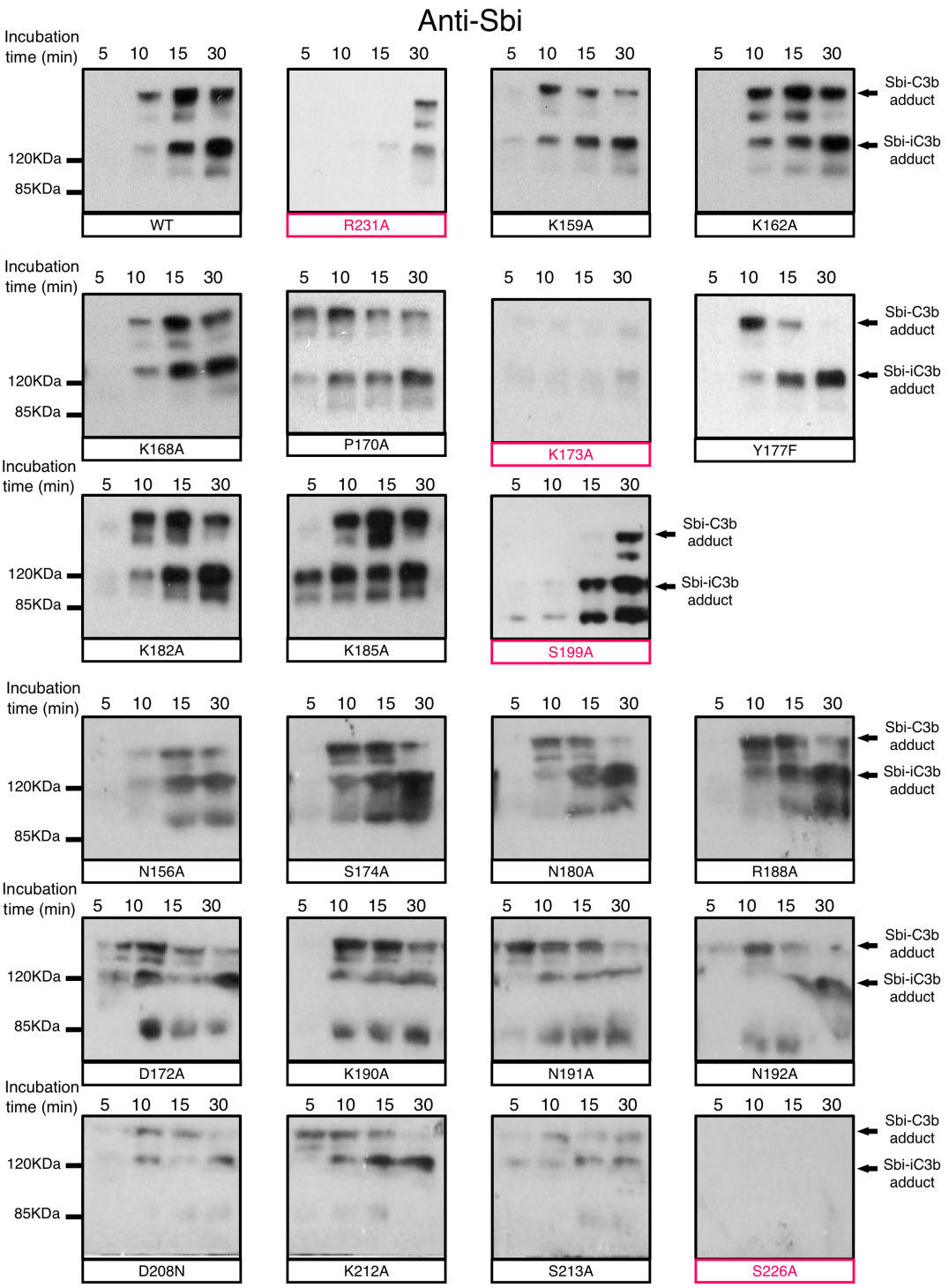

Figure 4.3.12: Anti-Sbi western blots of Sbi single mutant treated serum. The Sbi mutants K173A, S199A, R231A and S226A were highlighted in red.

4.3.7 Role of Sbi-III-IV in C3 consumption

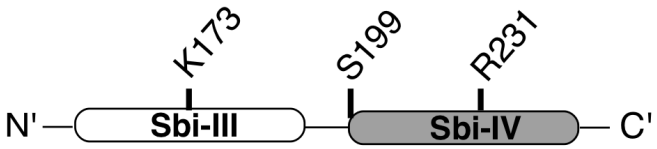

Figure 4.3.13: Location of Sbi defective mutations

In this study, via systematic mutagenesis and ensuing functional defect screening, amino acid residues that contribute significantly to Sbi induced C3 consumption were located, among which three Sbi-III-IV mutation representatives were selected and utilized in a series of subsequent comparative studies aiming to challenge different hypotheses about Sbi triggered C3 consumption mechanisms. As shown in Fig.4.3.13, the three chosen mutations were evenly distributed along Sbi-III-IV molecule. K173A is located in the middle of domain III, S199A is found in the junction region and the R231A mutation is located in domain IV. Among these three mutations, only the negative impact of R231A is explicable with previous data. The reasons of the compromised C3 consumption activities caused by K173A and S199A mutations remain to be investigated. In the following sections the structural aspects of the Sbi-III-IV mutants will be investigated first, then functional assays will be performed.

4.3.8 Structural analyses of Sbi-III-IV defective mutants

4.3.8.1 CD spectrometry studies of Sbi-III-IV WT and mutants

It is generally accepted that the structure of a protein is closely linked with its function and the primary sequence of a protein is essential for the folding of a protein to its correct secondary structure. It is evident in our Sbi-III-IV mutant functional screen (Section 4.3.6.1) that the substitution of charged side-chain amino acid residues with alanine can greatly affect the activity of Sbi-III-IV. Therefore, it is reasonable to speculate that these substitution mutations are

structurally different from the wild type Sbi-III-IV and the resulting structural defects could be the underlying reason for their impaired activity.

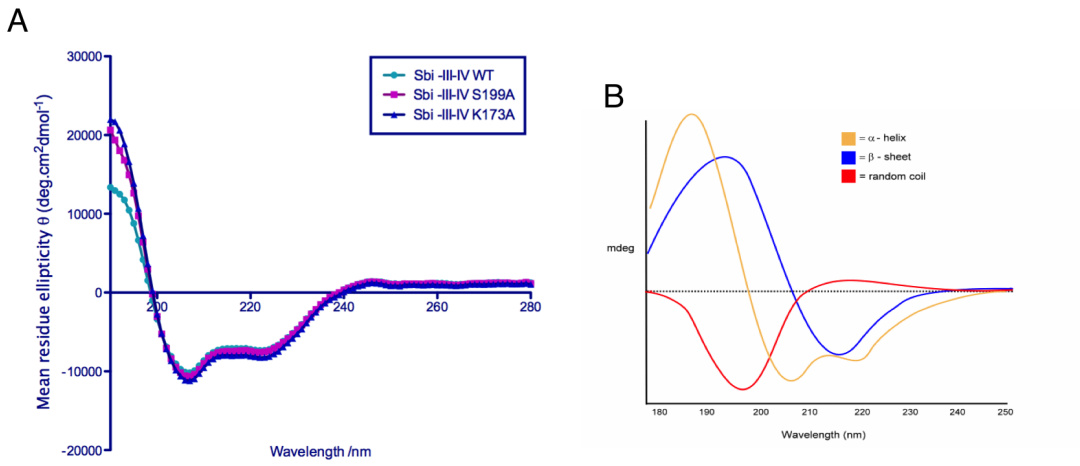

C

Structural composition (190-260nm)	WT	K173A	S199A
Helix	27.40%	32.00%	30.30%
Antiparallel	19.10%	12.20%	14.49%
Parallel	8.80%	7.90%	8.30%
Beta-Turn	18.80%	17.70%	18.10%
Random Coil	30.40%	28.00%	28.90%
Total sum	104.50%	97.90%	100.00%

Figure 4.3.14: Circular dichroism (CD) analysis of Sbi-III-IV WT and mutants. (A) CD spectra of Sbi-III-IV WT, S199A and K173A, with background absorbance subtracted and expressed in mean residue ellipticity θ. The positive peak at 190 nm and negative peaks at 205 and 215 nm are indicative of alpha-helicity. A decreased 200 nm reading is indicative of increased random coil content. **(B)** Idealized CD spectra of defined protein secondary structure. The spectrum of α-Helix in yellow shows two negative peaks at 222 nm and 208 nm and a positive one at 190 nm. The spectrum of β-sheet in blue demonstrates a negative peak at 219 nm and a positive one at 196 nm. The spectrum of random coil in red has a positive band at 212 nm and a negative one around 195 nm. **(C)** Secondary structure composition estimation by CDNN.

In this study, Sbi-III-IV WT, S199A and K173A were analyzed by circular dichorism (CD) spectroscopy to estimate their secondary structure content. As described in Section 4.2.1, different Sb-III-IV proteins were expressed and purified twice with Ni^{2+} affinity chromatography, finally buffer exchanged into 10 mM sodium phosphate buffer pH 7.4 before CD analysis. To improve the signal to noise ratio, for each Sbi-III-IV protein ten repetitive CD spectra between

190 and 280 nm were acquired (Appendix 9.4.1), and then averaged to one representative spectrum. Compared with the characteristic CD spectra of different secondary structures (Fig.4.3.14.B), the CD spectra of all three types of Sbi-III-IV (Fig.4.3.14.A) resemble the CD spectrum of protein composed mainly of α-helix secondary structure. Overlay of all three representative spectra shows that there are no significant CD differences between 200 nm to 280 nm of the spectrum. However, between 190 nm and 200 nm of the spectrum, the CD reading of Sbi-III-IV mutants (K173A and S199A) are noticeably higher than the WT CD reading. By deconvoluting the representative spectra using CDNN software (Section 4.2.7), the secondary structure composition of different types of Sbi-III-IV was interpreted. Fig.4.3.14.C shows that all three types of Sbi-III-IV demonstrate comparable secondary structure compositions with limited differences. The two types of Sbi-III-IV mutants show subtly increased α-helix content. The WT protein contains the highest percentage of random coil secondary structure.

4.3.8.2 Analysis of Sbi-III-IV and Sbi:C3d hydrodynamic diameter

In addition to the traditional structural analysis like CD spectroscopy, Sbi-III-IV WT and mutants were also analyzed by switchSENSE technology, which determines the hydrodynamic diameter of a protein or a protein complex. In this study, the hydrodynamic diameter of Sbi-III-IV WT and its mutants were measured and the hydrodynamic diameters of their C3d bound forms were also determined. The experiments were performed as described in Section 4.2.9.

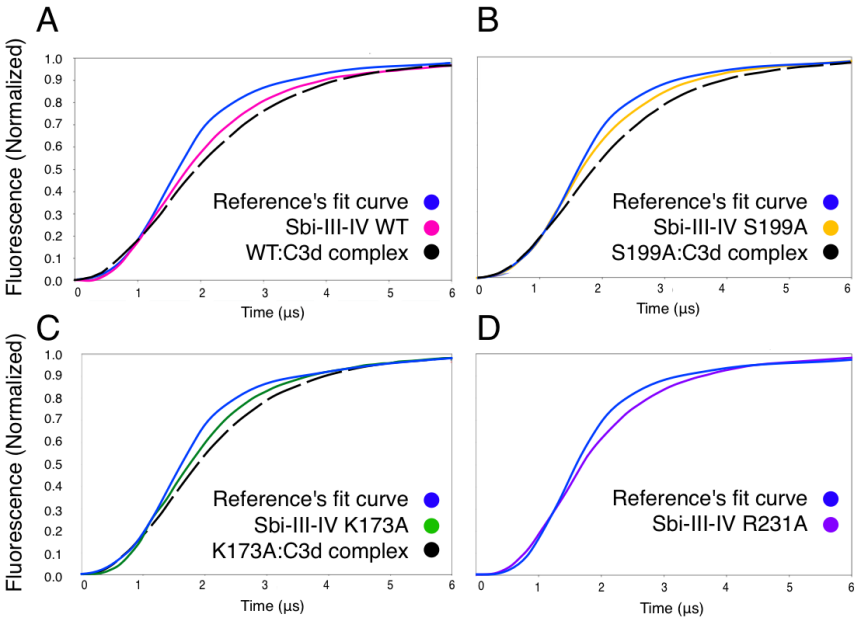

E

	Hydrodynamic diameter (nm) of Sbi-III-IV	Hydrodynamic diameter (nm) of Sbi:C3d complex
WT	4.3±0.1	6.6±0.2
S199A	4.3±0.3	6.3±0.6
K173A	3.8±0.3	5.0±0.3
R231A	4.7±0.3	No binding

Figure 4.3.15: Hydrodynamic diameter measurements of various types of Sbi-III-IV and their C3d bound complex forms. (A) Time resolved normalized fluorescence of a 48 bp Cy3-labeled DNA reference (blue), after immobilization of Sbi-III-IV WT (pink) and addition of C3d (black dash line). **(B)** Time resolved normalized fluorescence of DNA reference (blue), after immobilization of Sbi-III-IV S199A mutant (yellow) and addition of C3d (black dash line). **(C)** Time resolved normalized fluorescence of DNA reference (blue), after immobilization of Sbi-III-IV K173A mutant (green) and addition of C3d (black dash line). **(D)** Time resolved normalized fluorescence of DNA reference (blue), after immobilization of Sbi-III-IV R231A mutant (purple). **(E)** Table summarizes the hydrodynamic diameters of various types of Sbi-III-IV and their C3d bound form.

Hydrodynamic diameter analysis (Fig.4.3.15.E) shows that among unliganded Sbi-III-IV variants, the K173A mutant adopts the most compact conformation (3.8 nm), R231A exhibits most extended conformation (4.7 nm) and WT and S199A share a similar hydrodynamic diameter (4.3 nm). When bound with C3d, the K173A complex is the most compact (5 nm). WT and S199A complexes show similar hydrodynamic diameters, 6.6 nm and 6.3 nm respectively. Because the Sbi-III-IV R231A mutant does not bind C3d, no R231A:C3b complex diameter

data could be acquired. These results demonstrate that the Sbi-III-IV variants with opposed functional characteristics also show discrepancies structurally. To be specific, the unliganded Sbi-III-IV WT is 0.5 nm larger than the K173A mutant, and in the C3d bound form the WT complex is 1.6 nm larger than the K173A complex. The differences in diameter are augmented by the binding of C3d, assuming that in both types of complexes C3d contributes equally to the overall diameter, Sbi-III-IV WT must be able to switch into an extended conformation that consumes more space and the K173A mutant fails to reach this extended conformation.

4.3.9 Functional analyses of Sbi-III-IV WT and mutants

4.3.9.1 C3d binding kinetics of Sbi-III-IV WT and mutants

Comparison of the Sbi-III-IV WT and R231A's C3 consumption profiles indicates that the ability to trigger C3 consumption is related to the binding strength between Sbi-III-IV and C3. Although K173 and S199 were not indicated as C3d binding residues by previous crystallography studies, they could lead to unexpected structural defects that in turn effect C3 binding. Therefore, in this study the binding affinities between four types of Sbi-III-IV (WT, S199A, K173A and R231A) and C3d were determined by "SwitchSENSE" real time binding kinetic analysis. The C3 proteolytic fragment C3d was used as the ligand due to its smaller size and the close mimicry of C3-Sbi interaction interface. To measure the binding kinetics, the upward dynamic responses of immobilized Sbi-DNA conjugate were monitored at four C3d concentrations (40 nM, 70 nM, 100 nM and 130 nM) in real time (Fig. 3.3.16.A-G)**.** A decrease in the upward dynamic response signifies the binding of C3d to Sbi, an increase in the upward dynamic response represents the dissociation of Sbi:C3d complex. As summarized in Fig.3.3.16.H, for each complex three parameters were acquired, dissociation constant (K_d), "on-rate" (k_{on}) and "off-rate" (k_{off}).

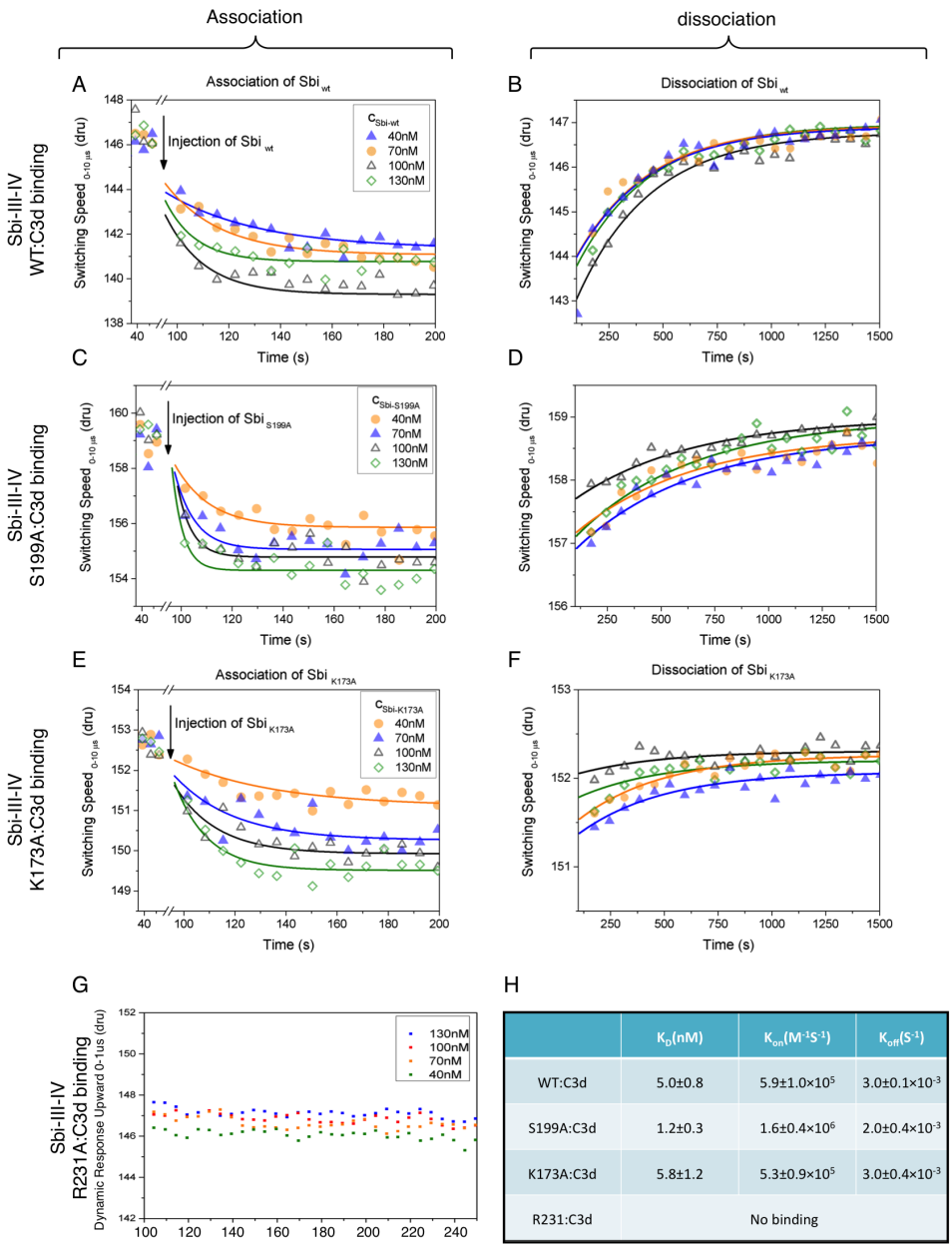

H

	K_D(nM)	K_{on}($M^{-1}S^{-1}$)	K_{off}(S^{-1})
WT:C3d	5.0±0.8	$5.9±1.0\times10^{5}$	$3.0±0.1\times10^{-3}$
S199A:C3d	1.2±0.3	$1.6±0.4\times10^{6}$	$2.0±0.4\times10^{-3}$
K173A:C3d	5.8±1.2	$5.3±0.9\times10^{5}$	$3.0±0.4\times10^{-3}$
R231:C3d	No binding		

Figure 4.3.16: SwitchSENSE binding kinetic measurements of C3d fragment binding to various types of Sbi-III-IV. (A-B) Time resolved dynamic response of immobilized Sbi-III-IV WT during C3d association and dissociation. **(C-D)** Time resolved dynamic response of immobilized Sbi-III-IV S199A during C3d association and dissociation. **(E-F)** Time resolved dynamic response of immbolized Sbi-III-IV K173A during C3d association and dissociation. **(G)** Time resolved dynamic response of immobilized Sbi-III-IV R231A during C3d association **(H)** Table summarizes the three binding kinetic measurements (i.e. dissociation constant (K_d), "on-rate"(k_{on}) and "off-rate"(k_{off})) for every type of Sbi-III-IV:C3d interaction. Upward dynamic response readings were recorded every 5 s. The association and dissociation curves were determined by global fitting and used to calculate the kinetic parameters.

This binding kinetic analysis (Fig.4.3.16) agrees with previous data that the R231A mutation significantly impairs C3d binding. In this study, no measurable

binding was observed between Sbi-III-IV R231A and C3d. Apart from the mutation on domain IV, the rest of the function-compromising mutations do not have a negative impact on the C3d binding property. Sbi-III-IV WT and K173A share a set of nearly identical binding constants to C3d. S199A demonstrates an unexpected increased binding affinity to C3d, the "on-rate" of S199A to C3d is almost three times higher than the corresponding WT "on-rate". Therefore, the C3 binding strength does affect Sbi-III-IV's ability to consume C3 but it does not proportionally correlate with Sbi's power to trigger C3 consumption. As described by this study, Sbi-III-IV mutants with higher, lower and the same C3d binding strength as WT all demonstrate severe functional defects. Consequently, additional factors must also play a role facilitating Sbi-III-IV to consume C3 in serum.

The kinetic parameters of Sbi-III-IV binding to C3d had been determined in two previous reports (Burman *et al.*, 2008; Upadhyay *et al.*, 2008). The K_d measured by surface plasmon resonance (SPR) is 1.4 μM, which is significantly higher than 0.17 μM that was determined using isothermal titration calorimetry (ITC). In this study, the WT Sbi-III-IV:C3d affinity (5.0 nM) measured by SwitchSENSE is one order of magnitude lower than the previously reported values. The similar discrepancy was observed previously in a study of antibody antigen interaction using both SwitchSENSE and SPR (Villa 2012). This could be attributed to two reasons, 1) the higher detection sensitivity of the switchSENSE method and 2) the superimposed surface effects of SPR due to the requirement to chemically couple one of the binding partners to the biosensor surface.

4.3.9.2 Do defective Sbi-III-IV mutants show a lack of adduct formation?

As was revealed in our functional screening, the Sbi-III-IV^{K173A} mutant shows no C3 activation nor Sbi-C3b adduct formation. One possible explanation for this is that the substitution of a lysine residue for an alanine residue eliminates this

location as a potential C3b deposition site. Hypothesis three (Section 4.1) proposes that the formation of the Sbi-C3b adduct is the central step of C3 consumption. Therefore, whether the K173A mutant could still form the Sbi-C3b adduct was examined.

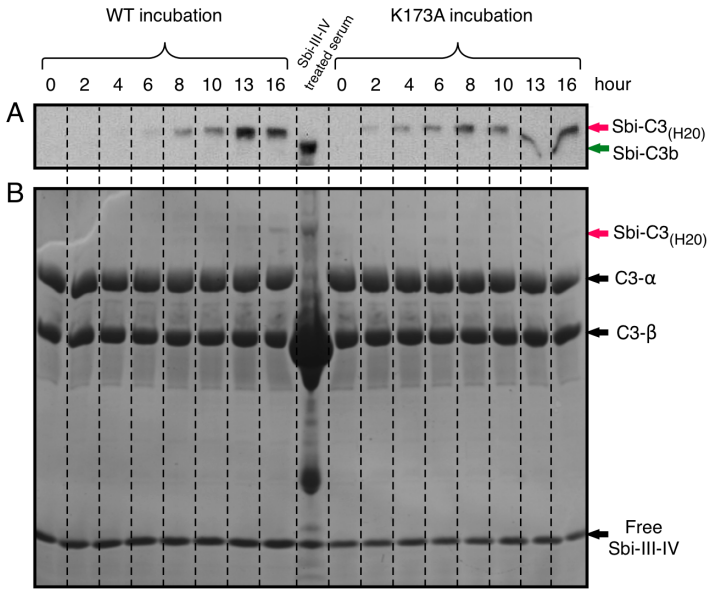

Figure 4.3.17: ***In vitro*** **Sbi-C3 adduct formation assay. (A)** Anti-Sbi western blot analysis. **(B)** SDS-PAGE 4-20% gradient gel analysis. 1.5 mg/ml of purified C3 molecule was incubated with 10 µM of Sbi-III-IV WT or K173A respectively. Each condition was incubated at 37°C for a total of 16 hours; samples were collected every 2-hour. Sbi-$C3_{(H2O)}$ adduct is indicated by pink arrow, Sbi-C3b adduct is indicated by green arrow. C3 α and β chains and free Sbi-III-IV molecules are indicated by black arrow. Individual incubation conditions were separated by black dashed lines.

Based on the C3 "tick-over" mechanism, formation of the Sbi-$C3_{(H2O)}$ adduct was expected after prolonged incubation between C3 and Sbi-III-IV. Fig.4.3.17.B shows the SDS-PAGE analysis of the incubation samples, which were also probed by anti-Sbi Western blot shown in Fig.4.3.17.A. Although the formation of the Sbi-$C3_{(H2O)}$ adduct was not readily observable on the SDS-PAGE gel, the Western blot analysis shows that both types of Sbi-III-IV are able to form covalent adducts with $C3_{(H2O)}$. The Sbi^{WT}-$C3_{(H2O)}$ adduct becomes detectable after 6 hours of incubation, but interestingly the Sbi^{K173A} -$C3_{(H2O)}$ adduct is detectable from hour 2 of incubation. Since in the Sbi-$C3_{(H2O)}$ covalent adduct the C3a fragment is not proteolytically removed, it is slightly larger than the Sbi-C3b adduct formed in the serum.

4.3.9.3 Do Sbi mutants affect the binding of other serum proteins?

To search for the serum components that are essential for Sbi induced C3 consumption, comparative serum pull-down experiments (Fig.4.3.18) were performed using C-terminal biotinylated Sbi-III-IV WT, K173A, S199A and R231A as bait proteins. A SDS-PAGE analysis of serum proteins that were retained on neutravidin agarose beads charged with Sbi-III-IV^{WT} and mutants is shown in Fig.4.3.19.A.

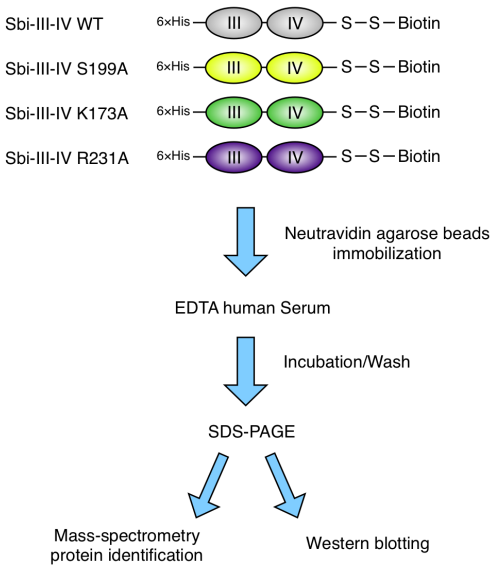

Figure 4.3.18: Serum pull-down experiment using biotin labeled Sbi-III-IVs. Different types of biotin labeled Sbi-III-IV were immobilized on neutravidin agarose beads. The pull-down was performed in human serum supplemented with 10mM EDTA. After incubation and intensive washing of the neutravidin beads, pull-down samples were then subjected to analysis including SDS-PAGE, MS protein identification and western blotting.

Comparing Sbi-III-IV^{WT} and mutant SDS-PAGE profiles, significant band intensity variations are observed at molecular weight of 150 kDa, 120 kDa and 45 kDa. Protein bands labeled *a, b* and *c* on Fig.4.3.19.A were identified respectively as complement factor H, complement C3 alpha chain and FHR-1 by NanoLC coupled ESI-TOF mass spectrometry. In addition, the identical samples were analyzed by Western blotting (Fig.4.3.19.B-C) to further evaluate the interaction profiles of Sbi-III-IV mutants. Having demonstrated the variation in C3 consumption activity between Sbi-III-IV WT and mutants, the analysis of interaction profiles appears to show that functionally intact Sbi-III-IV WT interacts strongly with factor H and FHR-1, while functionally compromised Sbi-III-IV S199A and R231A mutants demonstrate weaker interaction patterns and the functionally null Sbi-III-IV K173A mutant shows the weakest interaction strength. It was

previously demonstrated that Sbi-III-IV binds C3 isoforms in combination with FH to form a ternary complex, but the pull-down result presented here suggests that FHR-1 also could be a constituent of the ternary complex. It is surprising to discover that the R231A pull-down sample demonstrated comparable C3 binding level as other types of Sbi-III-IV (Fig.4.3.19.C). This suggests that the binding of FH and FHR-1 could enhance C3 binding.

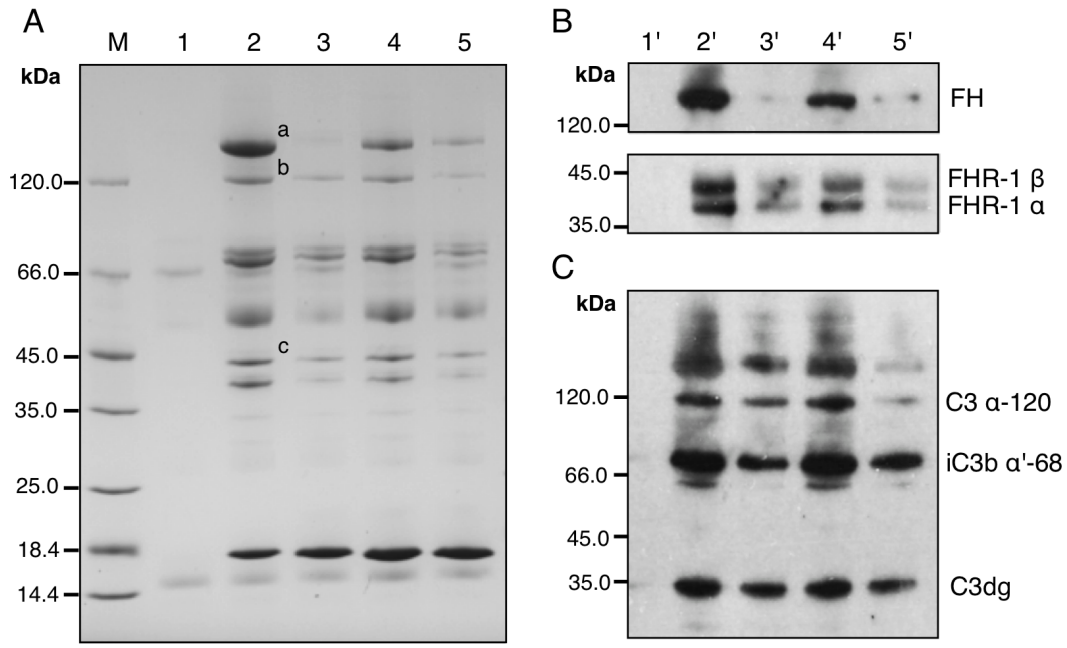

Figure 4.3.19: SDS-PAGE and Western blot analysis of Sbi-III-IV serum pull down sample. Numbers are designated to different samples. 1 Neutravidin beads control, 2 WT pull-down, 3 K173A pull-down, 4 S199A pull-down, 5 R231A pull-down. Samples were first analyzed by SDS-PAGE **(A)**, polyclonal anti-factor H Western blot **(B),** and polyclonal anti-C3d Western blot **(C)**. Protein bands showing intensity variation across different Sbi-III-IV pull-down samples are labeled *a*, *b* and *c*.

4.3.9.4 Mutation's effect on complement activation

Sbi-III-IV WT and mutants in this assay were adjusted to 10 μM. The sample collection procedure is summarized by Fig.4.3.4.A. The treated serum samples at different time points were added to either CP or AP assay diluent, their residual complement activities were measured by assessing C5b-9 formation using the Welisa lab complement activity kit (Section 4.2.3).

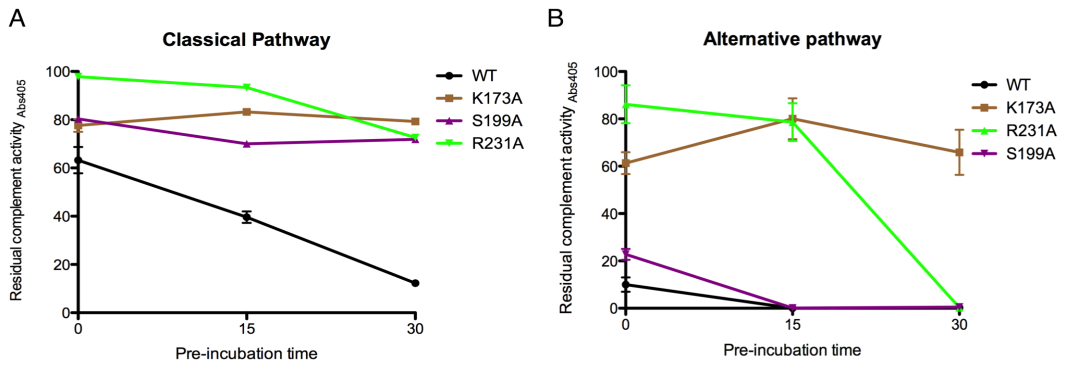

Figure 4.3.20: Classical and alternative pathway residual activities of Sbi-III-IV mutant-treated human serum. HSS was incubated with Sbi-III-IV WT, K173A, S199A and R231A. For each incubation reaction, treated serum samples were collected at three time points 0, 15 and 30 min. Their residual classical **(A)** or alternative **(B)** pathway residual complement activities were then determined. Percentage activity was calculated using an absorbance reading at 405 nm with the equation *activity =[(sample-negative control)/positive control]×100*. Each condition was assayed in duplicate and the error bars represent the upper and lower result.

Residual CP activity measurements (Fig.4.3.20.A) agree with the results of Western blot based Sbi-III-IV activity screens. Sbi-III-IV WT inhibits CP activity in a timely manner, but all three mutants' inhibition activities were greatly compromised. The residual CP activities of K173A at all three time-points fluctuate around 80%. Similar results were observed for the S199A mutant. Similarly to the anti-C3d Western blot (Fig.4.3.11), with the addition of R231A, a weak time dependent inhibition of CP activity was observed, the residual CP activity drops from 98% to 92% then to 72%. Another intriguing observation was that without pre-incubation (0 min), only the C3 binding mutant R231A shows almost no inhibition (residual activity of 98%).

In contrast to the CP measurements, AP measurements (Fig.4.3.20.B) do not totally correlate with the results from Western blot based C3 activation assay. As mentioned earlier, Sbi-III-IV^{WT} inhibition of AP activity does not show any correlation with pre-incubation time. Without incubation, WT protein can reduce the residual AP activity to 10%, with incubation no measurable residual AP

activity was detected at all. The inhibition provided by K173A also shows no dependency on pre-incubation time. The residual AP activity remains above 60% after 30 min inhibition. Measurements of AP inhibition from R231A mutant shows the most interesting results, after 15 min pre-incubation only limited inhibition was measured, but with an additional 15 min incubation, complete inhibition of AP activity was observed.

4.3.10 Reconstructions of Sbi mediated ternary complexes

Having demonstrated that Sbi mutants show differences in their ability to form ternary complexes in serum, further *in vitro* analyses were carried out to investigate the extent to which mutated side chains contribute to the formation of the stabilized ternary complexes.

4.3.10.1 Reconstruction of FH containing ternary complex by BLItz

Sbi-III-IV WT, K173A and S199A constructs were immobilized on Ni-NTA biosensors and subjected to BioLayer Interferometry (BLI) measurements. Complex formation was followed in real time by step-wise addition of C3d and FH as analytes. All three Sbi-III-IV constructs were successfully immobilized and excess Sbi molecules were removed by an immediate washing step (Fig.4.3.21.A). Upon addition of C3d, the formation of Sbi:C3d complexes was detected in all three Sbi constructs as an increase in BLI signal. Upon addition of the FH, a significant secondary binding event was observed based on Sbi-III-IV^{WT}:C3d complex, followed by rapid dissociation of the ternary complexes in PBS buffer. In contrast, no strong FH association was detected based on the S199A:C3d or K173A:C3d complexes, slow Sbi:C3d complex dissociation starts immediately after the addition of FH and protein complexes dissociate considerably in PBS buffer washing step. Similar binding characteristics were observed when ternary complexes were reconstituted using C3 as an intermediate analyte. Ni-NTA

immobilized Sbi-III-IV WT and K173A constructs showed similar level of C3 binding (Fig.4.3.21.B). However, upon addition of FH, only the Sbi-III-IV^{WT}:C3 complex forms ternary complexes with FH in comparison with the impaired association of K173A mediated complex.

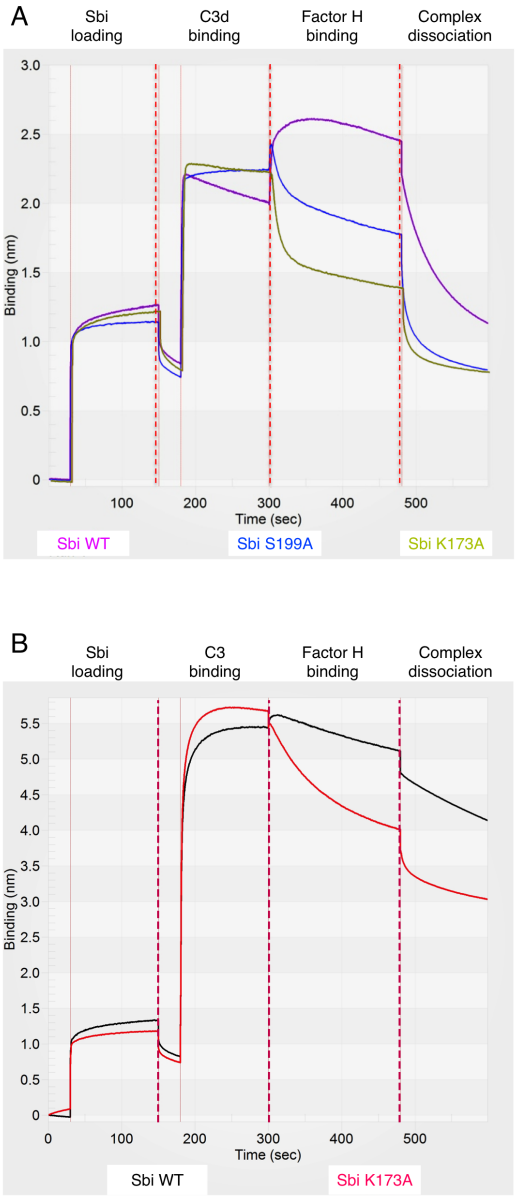

Figure 4.3.21: Analyzing Sbi:C3d:FH ternary complex formation by biolayer interferometry. (A) Sbi-III-IV WT, S199A and K173A were immobilized and C3d and factor H were applied in fluid phase sequentially. The Ni-NTA surface was loaded with saturated amount of all three types of Sbi-III-IV. After the application of C3d, similar binding level was observed. Upon application of factor H a secondary binding event was detected based on Sbi WT:C3d complex. No significant secondary factor H binding event was detected in S199A and K173A mutants. **(B)** Sbi-III-IV WT and K173A were immobilized and C3 and factor H were applied in fluid phase sequentially. An additional secondary binding event was detected based on Sbi WT:C3 complex, but not when C3 was bound with Sbi K173A. Due to the large size of C3 molecule, a large binding signal was produced.

4.3.10.2 ELISA reconstruction of ternary complexes

To analyze the formation of ternary complexes, an ELISA approach was developed and utilized to assay dose-dependent factor H and FHR-1 binding (Section 4.2.15). Sbi-III-IV WT, K173A and R231A were immobilized; C3 and its

activation fragments C3b and C3d were added, followed by the addition of increasing amount of purified FH or FHR-1. After washing, the amount of the ternary complex formation was quantified using a polyclonal anti-factor H antiserum.

Sbi-III-IV^{WT} binds FH in combination with intact C3 and its activation products (C3b and C3d) (Fig.4.3.22.A). The highest affinity is achieved when C3 (K_d=6.8 nM) and C3d (K_d=15.1 nM) were used as secondary ligands, the binding levels reach saturation after factor H concentration of 120 nM. However, in combination with C3b (K_d=181.0 nM), a higher concentration of factor H (250 nM) was needed to reach binding saturation. Compared with WT, the K173A mutant (Fig.4.3.22.B) shows impaired FH binding. Weak concentration dependent FH binding was observed in combination with C3 or C3d, however in combination with C3b no FH binding was detected. When Sbi-III-IV^{R231A} was coated (Fig.4.3.22.C), FH binding was reduced to a minimal level independent of the type of C3 isoforms.

Sbi-III-IV^{WT} also binds FHR-1 in combination with C3 isoforms. Using C3 (K_d=3.5 nM) and C3d (K_d=1.6 nM) as secondary ligand a similar saturated binding level (25 nM) was observed. However, higher concentration (≈100 nM) of FHR-1 was needed to reach saturated binding level in combination with C3b (K_d=10.0 nM) (Fig.4.3.22.D). Similar to FH binding profile, K173A mutant shows impaired FHR-1 binding kinetic and binding level. Again, in combination with C3b, no concentration dependent FHR-1 binding was detected. The assembly of FHR-1 ternary complex is most affected by the C3 binding mutant R231A. Regardless of the C3 isoform, no increasing trend of FHR-1 binding was detected.

The Sbi-III-IV^{WT} ternary complex binding kinetics suggest that independent of the type of C3 isoforms, Sbi-III-IV^{WT} preferentially recruits FHR-1 over FH. In combination with C3, C3d and C3b, 2-, 9- and 18-fold decreases in K_d were

observed for FHR-1 containing ternary complexes.

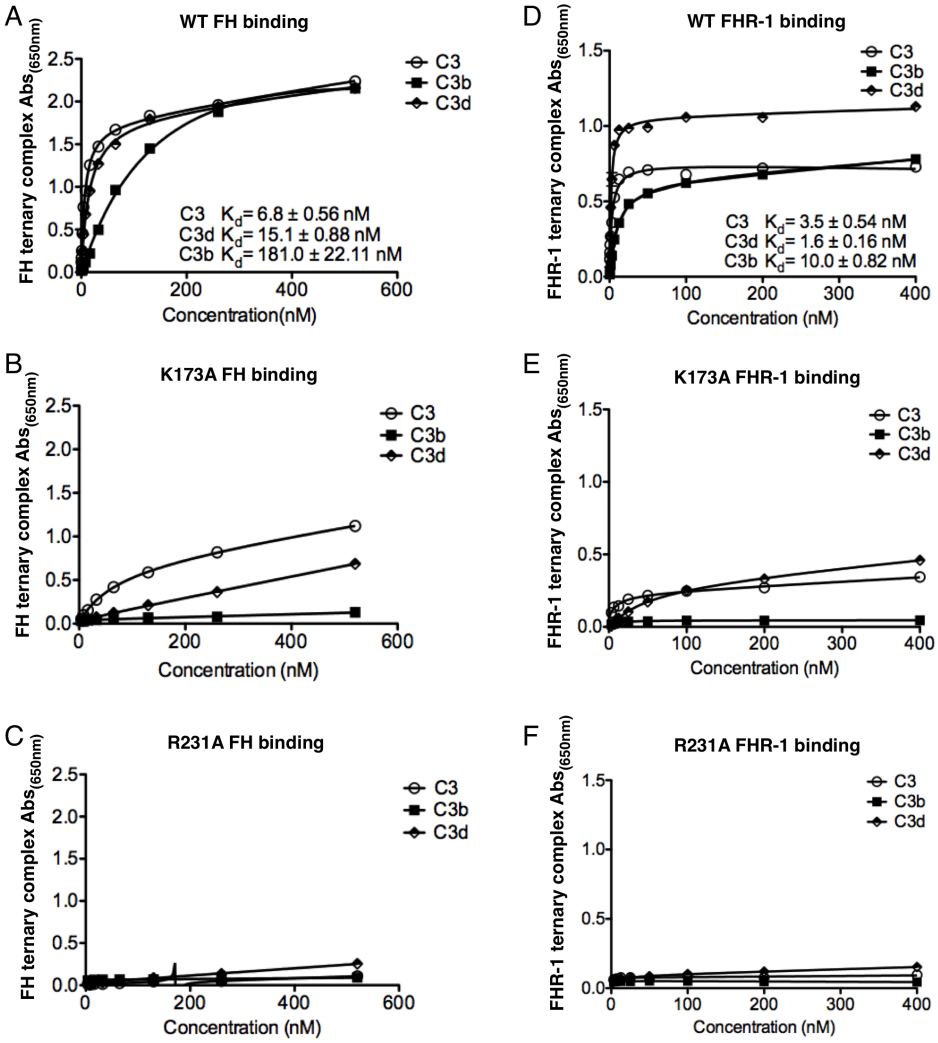

Figure 4.3.22: ***In vitro*** **factor H and CFHR1 ternary complex formation is affected by C3 isoforms and mutations in Sbi-III-IV. (A-C)** Sbi-III-IV WT, K173A and R231A were immobilized and for each type of Sbi the concentration dependent binding of factor H (0-500 nM) in combination with C3 (0.11 µM), C3b (0.11 µM) and C3d (0.28 µM) was measured by polyclonal Factor H antiserum. **(D-E)** Sbi-III-IV WT, K173A and R231A were immobilized and for each type of Sbi the concentration dependent binding of CFHR1 (0-400 nM) in combination with C3, C3b and C3d was measured by polyclonal factor H antiserum. Measurements were done in duplicate. The K_d values were determined from the fitted curve using GraphPad Prism.

Due to the poor FH binding profiles, the accuracy of estimated K_d for K173A and R231A is not satisfactory; therefore these values are not provided. More sensitive methods might be used in the further for the determination of these values. Slightly contradictory to the pull-down results (Fig.4.3.18), which suggest

that K173A mutant is more impaired than the R231A mutant, in this section, the ELISA reconstruction of ternary complexes shows the opposite. This could be a consequence of the differences in the serum C3 concentration (5.4-8 μM) and the experimental C3 concentration (0.11 μM). In serum, R231A might still able to bind C3, this binding then enhanced by the binding of FH/FHR-1.

4.3.10.3 Binary binding of Sbi-III-IV to FH or FHR-1

Previously, Sbi had been described to only bind FH in combination with C3d containing C3 isoforms (Haupt *et al*. 2008). Given the discovery of the previously uncharacterized FHR-1 ternary complex in this study, the possibility of the direct binding of Sbi-III-IV to FH or FHR-1 was examined.

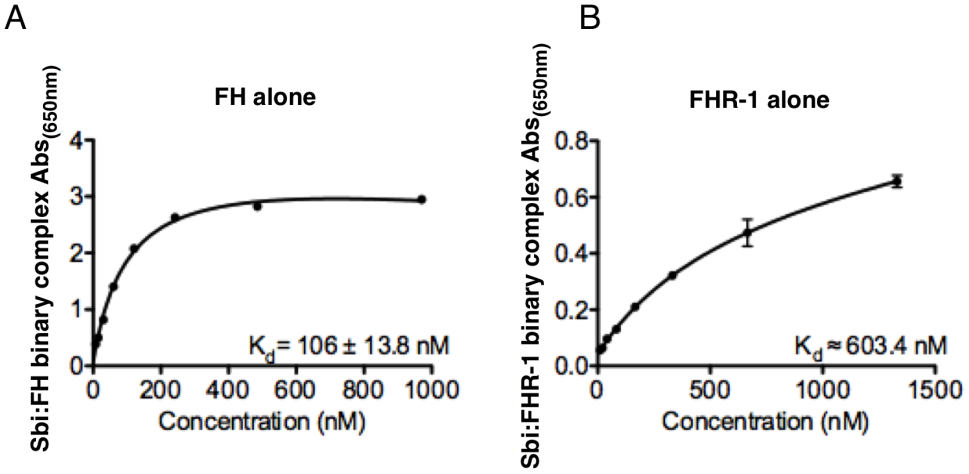

Figure 4.3.23: Sbi-III-IV^{WT} forms binary complex with factor H and FHR-1. (A) Sbi-III-IV^{WT} was immobilized and the concentration dependent binding of factor H (0-1000 nM) was measured by polyclonal Factor H antiserum. **(B)** Sbi-III-IV^{WT} was immobilized and the concentration dependent binding of FHR-1 (0-1500 nM) was measured by polyclonal factor H antiserum. Measurements were done in duplicate. The K_d values were determined from the fitted curve using GraphPad Prism.

Based on Section 4.2.15, Sbi-III-IV^{WT} was coated on ELISA plate, and then the concentration dependent binding of FH or FHR-1 was determined. Surprisingly, the binding experiments (Fig.4.3.23) indicated Sbi-III-IV^{WT} could bind directly to both FH and FHR-1. Compared with the K_d of ternary complex formation (Section 4.3.16), both binary complexes (Sbi:FH K_d=106.0 nM and Sbi:FHR-1 K_d≈603.0 nM) are considerably weaker in avidity. Noticeably, the FH binary interaction with

Sbi-III-IV^{WT} is stronger than the FH binding to Sbi:C3b complex. This suggests a possibility that Sbi-III-IV discourages the binding of FH to C3b, which antagonizes the factor I mediated C3b degradation.

4.3.11 Factor H and FHR-1 compete for C3 isoforms binding in combination with Sbi-III-IV^{WT}

An ELISA procedure (Section 4.2.16) was developed to determine whether FH and FHR-1 compete for the formation of Sbi-III-IV^{WT} mediated ternary complexes.

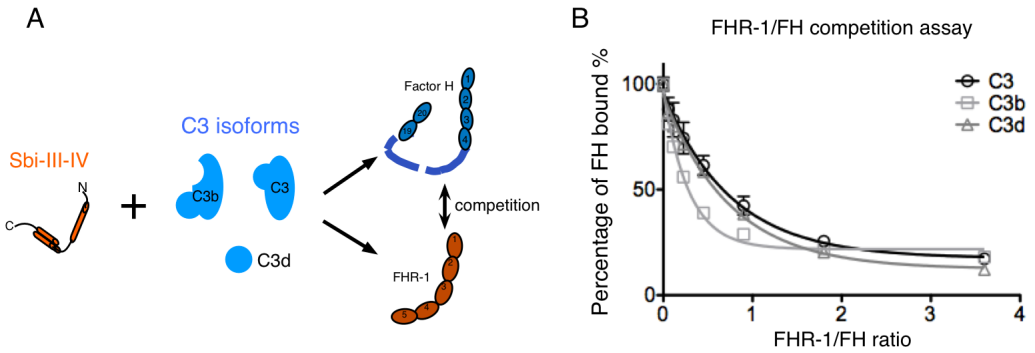

Figure 4.3.24: FH and FHR-1 compete for the formation of ternary complex with C3 isoforms and Sbi-III-IV. (A) Proposed competitive binding mechanism between factor H and FHR-1. **(B)** The formation of factor H ternary complex is inhibited by the increasing amount of FHR-1. ELISA wells were coated with 1 µg of Sbi-III-IV, as secondary ligand 0.4 µM of C3, 0.14 µM of C3b and 0.3 µM of C3d were added respectively, finally 0.014 µM of factor H was incubated with increasing amount of purified FHR-1 (0-0.055 µM). Measurements were done in duplicate.

Sbi-III-IV^{WT} was coated on the ELISA plate then a constant concentration of factor H and three C3 isoforms (C3, C3b and C3d) were added together with increasing amounts of FHR-1, the factor H binding was detected by the monoclonal antibody OX-24. This assay (Fig.4.3.24) demonstrated that the formation of Sbi:C3 isoforms: FH ternary complexes were inhibited in a dose-dependent fashion by increasing concentration of purified FHR-1. The inhibition effects are common over different C3 activation fragments, but when C3b is used the most pronounced effect is observed. At equal FH and FHR-1 molar ratio, regardless of the type of C3 isoforms, less than 50% of ternary

complexes are FH bound, which suggests preferential binding of FHR-1. Interestingly, at the physiological FHR-1:FH molar ratio of 0.5:1 (Skerka *et al*. 2013), FH binding was reduced by 40% (secondary ligand: C3 or C3d) or by 60% (Secondary ligand: C3b).

4.3.12 Functional role of FHR-1 containing ternary complex

4.3.12.1 Sbi mediated ternary complexes are protective for C3b conformation

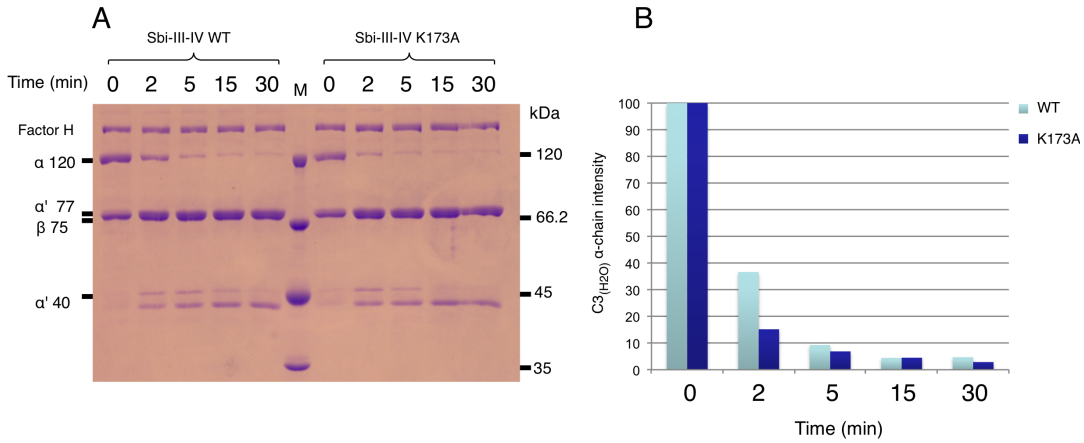

Figure 4.3.25: Sbi mediated ternary complexes extend C3b conformation half-life. (A) *In vitro* cleavage of $C3_{H2O}$, $C3_{H2O}$ (2.2 µM) was incubated with either Sbi-III-IV WT (5 µM) or K173A (5 µM) mutant together with factor H (1.2 µM), FHR-1 (1.2 µM) and Factor I (4 ng/µl) at 37 °C, the cleavage process was analyzed at different time points by SDS-PAGE. (B) A gel densitometric analysis of C3 α chain degradation in the present of different Sbi-III-IV.

Because of the competitive nature between the FH and FHR-1 containing ternary complexes, this competition could affect the *in vitro* factor I cleavage rate of C3b conformations such as $C3_{H2O}$. As the vital component of the initial AP C3 convertase, the longevity of $C3_{H2O}$ is one of the determinants of AP pathway activation. The assay components (Section 4.2.18) were mixed with either Sbi-III-IV^{WT} or Sbi-III-IV^{K173A} at 37°C. This assay (Fig.4.3.25) demonstrated that in the presence of Sbi-III-IV^{WT} the cleavage rate of $C3_{H2O}$ was reduced, after 2 min of cleavage reaction an extra 20% of residual $C3_{H2O}$ α-chain was observed. Due to the similar molecular weight of $C3_{H2O}$ α'-chain (77 kDa) and $C3_{H2O}$ β-chain (75 kDa), these two chains appear as a single band in SDS-PAGE analysis (Fig.4.3.25.A), slightly higher than the 66.2 kDa molecular weight marker.

4.3.12.2 FHR-1 containing complex is essential for Sbi induced C3 consumption.

Having established that Sbi-III-IV's C3 consumption activity is related to the formation of Sbi:C3:FH and Sbi:C3:FHR-1 ternary complexes, further experiments were required to determine individual roles of those complexes in the mechanism of C3 consumption. During the course of the research, it was observed that Sbi-III-IV failed to trigger C3 consumption in FH reconstituted FH depleted serum, therefore it was suspected that the immune-affinity depletion method used during the manufacturing process could deplete both FH and FHR-1 molecules, due to high degree of protein identity shared between two molecules.

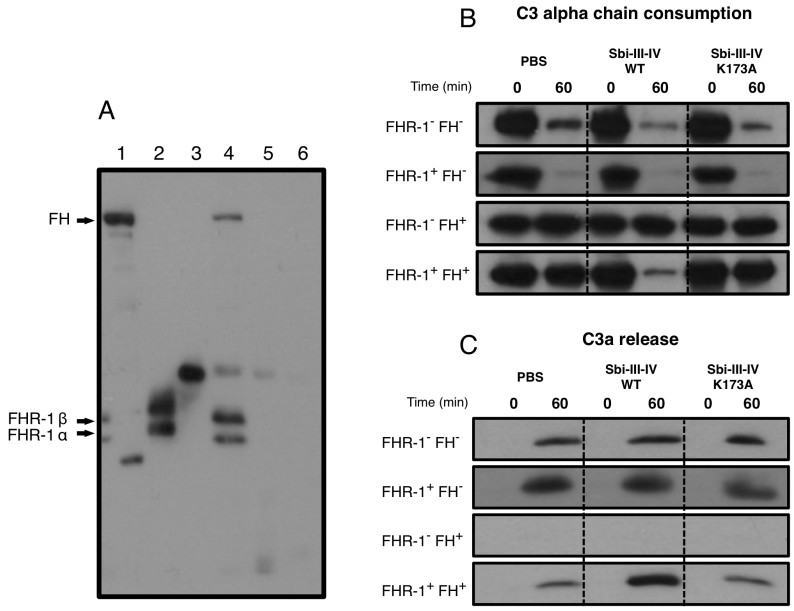

Figure 4.3.26: rFHR-1 plays decisive role in Sbi triggered C3 consumption. (A) Polyclonal anti-Factor western blot, 1 Purified factor H, 2 FHR-1, 3 Neutravidin resin pull-down control, 4 Normal human serum Sbi-III-IV pull-down, 5 Factor H depleted serum Sbi-III-IV pull-down and 6 Albumin/IgG depleted Factor H depleted serum. **(B)** Detection of C3 α-chain variation using anti-C3a antibody. C3 activation was induced by the addition of PBS, WT and K173A Sbi-III-IV in step-wisely reconstituted factor H and FHR-1 double depleted sera. **(C)** Detection of C3a release. One representative experiment from a total of three repeats was presented.

To test this theory, Sbi-III-IV affinity pull-down experiments were performed using factor H depleted serum (Section 4.2.19), Fig.4.3.26.A lane 5 shows that neither factor H nor FHR-1 were retained on Sbi-III-IV immobilized neutravidin resin, whereas the formation of Sbi:C3 complex was observed (Appendix Fig.9.7). To complement the pull-down result, an excess amount of HSA/IgG double depleted factor H depleted serum sample was also analyzed (Fig.4.3.26.A lane 6). Based on the results of both analyses, we concluded that the factor H depleted serum is in fact FH/FHR-1 double depleted serum.

The double depleted serum offers a unique opportunity to study the individual function of those two types of tripartite complexes in relation to the C3 consumption activity of Sbi molecule (Section 4.2.20). PBS-Mg^{2+} buffer, Sbi-III-IV WT or K173A mutant were incubated with the double depleted serum supplemented with FHR-1 or FH or both, C3 consumption was detected by monitoring C3 α-chain (Fig.4.3.26.B) and release of anaphylatoxin C3a (Fig.4.3.26.C). Incubation of double depleted serum with PBS-Mg^{2+}, Sbi-III-IV^{WT} or K173A results in depletion of the intact C3 molecule, and similar results were also observed when FHR-1 supplemented double depleted serum was used. However, when incubations were performed using factor H supplemented double depleted serum, C3 levels were maintained over one hour incubation period in all three conditions. Finally, the double depleted serum was reconstituted by addition of an equal molar ratio of FHR-1 and factor H. Under this condition, very limited amount of C3 consumption and C3a release were detected in the present of PBS-Mg^{2+} buffer or K173A mutant, but with the addition of Sbi-III-IV^{WT} significant C3 consumption was achieved. These results suggest that fluid phase complement regulator FH prevents spontaneous complement activation. The sequestering of factor H in the form of Sbi:C3:FH tripartite complexes is insufficient to suppress complement regulation, however with the co-existence of the Sbi:C3:FHR-1 complex, complement regulations are subverted.

4.4. Discussion

In this chapter, the expression and purification protocols for Sbi-III-IV WT and mutants were presented. We showed that Sbi exploits complement AP to deplete intact C3 molecules in serum. Interestingly, the activation of AP is controlled to prevent the activation of C5. The mutagenesis studies of Sbi-III-IV successfully pinpointed the residues affecting Sbi's activity. Analyses of the mutants suggest that the impaired FHR-1 ternary complex formation could be the reason for their defective phenotypes.

4.4.1 Analysis of Sbi-III-IV triggered C3 futile consumption

At the beginning of this chapter, results for expression and purification of Sbi-III-IV^{WT} protein were presented. High purity Sbi-III-IV^{WT} molecule was prepared for downstream assays. By analyzing the Sbi-III-IV^{WT} treated HSS sample, it was demonstrated that Sbi-III-IV^{WT} triggered C3 consumption process is a time dependent phenomenon. The activation of C3 coincides with formation of the Sbi-C3b adduct, proteolytic activation of factor B and release of C3a. A 5 min lag time was observed, until the explosive activation of C3 molecule, this suggests that even in the presence of excessive amounts of Sbi-III-IV (10 μM), C3 consumption does not occur immediately, implying that a time-dependent process in the serum could be an essential part of the Sbi triggered C3 consumption mechanism. It is known that the spontaneous hydrolysis of C3 molecule, the "tick-over" of C3, takes places at a slow but steadily rate, approximately 0.005%/min (Pangburn *et al*. 1981). This process could account for the lag time observed, as a putative threshold of protected $C3_{H2O}$ molecules has to be reached in order to overwhelm regulation of AP activation.

It has been shown before that futile C3 consumption by Sbi involves activation of AP. By analyzing the outcome of Sbi induced C3 consumption in AP component

depleted sera, we concluded that all AP essential components (factor B, D and P) are irreplaceable. This suggests that apart from the initiation step, the downstream activation cascade is probably shared between C3 futile consumption and AP. However, incubation with depleted sera did offer several interesting observations. Firstly, although factor H is described as the co-factor for factor I that facilitates the cleavage of C3b molecule, using FH depleted serum after 30 min incubation no residual C3b α'-chain was detected (Fig.4.3.3.A). Secondly, after incubation with factor B, D and P depleted sera, no C3 activation was detected, but degradations of intact C3 α-chain were observed (Fig.4.3.3.A). This agrees with the report that accredited Sbi-III-IV with the activity of recruiting C3/C3b cleaving proprotease plasminogen (Koch *et al*. 2012).

4.4.2 Functional screens of Sbi-III-IV mutants provide molecular insights into C3 futile consumption

In this study, systematic mutagenesis was performed in combination with structural and functional analyses to unravel the molecular details of Sbi induced complement consumption. A Western blot approach was designed to perform the primary functional screening of Sbi mutation library. This method was employed because it can directly report molecular weight changes of the C3 and Sbi-III-IV molecules during the C3 consumption process. However, it is not a quantitative assay, thus it can only serve as an estimation method for the amount and the speed of C3 consumption. Despite the limitations of this method, the results clearly demonstrated that the mutations, K173A, S199A and R231A greatly reduced the amount of Sbi-C3b adduct formation and the speed of C3 consumption.

To determine the underlying molecular explanations for these defective mutants and to challenge the hypothesis of the C3 futile consumption mechanism, a range of comparative assays were designed and performed using the selected mutants.

In many aspects, these mutants behave in very similar ways to the WT protein. Both WT and K173A offer covalent deposition sites for $C3_{(H20)}$ molecule, and CD spectra reveal limited secondary structural differences. In terms of C3d binding affinity, WT and K173A demonstrate comparable binding affinity, the S199A mutation increases the binding affinity, and the R231A mutation abolishes C3d binding completely as previously reported. The measurement of hydrodynamic diameter suggests that the K173A mutant is more compact in length compared to WT and other Sbi mutant proteins, offering the first clue for its defective phenotype.

Comparative pull-down experiments were also conducted to study the potential differences in Sbi mediated protein complex formation in serum. Previously a pull-down experiment demonstrated that Sbi interacts with various C3 isoforms, during which Sbi-III-IV was immobilized through its lysine residues on a NHS-column, and then serum components retained on the charged column were analyzed. However as shown in Section 4.3.6.2, the lysine 173 has a significant functional impact, therefore to preserve this residue, in this study, a specially engineered C-terminal cysteine residue was used to immobilize various Sbi-III-IV constructs on the solid phase. The new pull-down experiment revealed that Sbi-III-IV WT binds to C3, FH and FHR-1. But WT, R231A, S199A and K173A mutants of Sbi-III-IV demonstrate increasingly weak binding to FH and FHR-1, while C3 binding level remains less affected. In comparison, no binding of properdin was detected, which is considered the most established up-regulator of complement activation (Hourcade 2006), and previously shown as an essential component of C3 futile consumption (Fig.4.3.3). We proposed that Sbi forms ternary complexes in combination with C3 isoforms and FH/FHR-1, impaired ternary complex formation could lead to the defective complement consumption activity.

The Sbi mutant library functional screening (Section 4.3.6.2) also indicated a putative C3b deposition residue, S226. As this residues does not fit with the previous beliefs regarding to the C3b deposition site on Sbi (Burman *et al*. 2008), in chapter 4 not only the authenticity of the covalent attachment site will be verified but also the Sbi-C3b adduct formation mechanism as a whole will be securitized.

4.4.3 Ternary complexes

In this study the results confirm the previous findings (Haupt *et al*. 2008) of stepwise ternary complex formation between Sbi-III-IV, FH and various C3 isoforms. In the same study it was also shown that all TED domain containing fragments of C3 are eligible constituents for ternary complex formation, and the minimal binding domains of FH were located to domain 19-20, despite domain 15-20 demonstrated enhanced binding level. However, the new data provided in this thesis lead to the development of an additional scenario that Sbi-III-IV could also bind FHR-1 in combination with various C3 isoforms. As mentioned in the introduction in Section 1.4.4, the domain 18-20 of FH is almost identical in primary sequence to the domain 3-5 of FHR-1. Therefore, it is possible for FHR-1 to substitute for FH as an alternative tertiary ligand of the ternary complex, which explains the observation in the pull-down study (Section 4.3.9.3).

The formation of Sbi:C3 isoform:FHR-1 ternary complexes were subsequently verified by an ELISA approach. It was noticed that, for Sbi-III-IV^{WT}, when C3b was used as secondary ligand, higher concentrations of FH or FHR-1 were needed to reach binding saturation, which could be related to the poor binding strength between Sbi-III-IV and C3b (Burman *et al*. 2008). Moreover the ability to assemble FH or FHR-1 containing ternary complexes were compared between the WT and mutant Sbi-III-IV. It was found that the mutations (K173A and R231A) inserted in Sbi-III-IV impair the formation of both types of ternary

complexes, regardless of the type of C3 isoforms used.

Primary sequence mapping of identified mutants reveals further insights into Sbi-III-IV mediated ternary complex assembly. R231 is located within Sbi-IV, (Upadhyay *et al*. 2008) reported that the alanine substitution mutation of this residue abolishes C3d concave surface binding, therefore this C3 binding property is essential for ternary complex formation. K173 is located in the middle of Sbi-III, the mutation of this residue severely impairs the Sbi's ability to assemble the ternary complex. Thereby for the first time a defined functional role of Sbi domain III is discovered. Finally, within Sbi-III-IV S199 is located between Sbi-III and Sbi-IV, the functional significance of this residue suggests that ternary complex formation requires synergy from both Sbi-III and Sbi-IV. Previously, Sbi-IV homologue *staphylococcal* proteins Ecb and Efb were reported that are able to form ternary complex with FH in combination with C3b (Amdahl *et al*. 2013). However, unlike Sbi, Ecb and Efb do not contain any Sbi-III like domains, therefore this suggests that the Sbi-III domain is a unique molecular adaption specialized in mediating ternary complex formation.

In order to deepen the understanding concerning the impact of ternary complexes on complement activation and regulation, using the present structural biology data, models of ternary complexes are extrapolated and presented in Fig.4.4.1. Initially, based on crystal structures of Sbi-IV:C3d complex (Clark *et al*. 2011) and FH_{19-20}:C3d complex (Morgan *et al*. 2011), a putative structural model of ternary complex Sbi-IV:C3d:FH_{19-20} was constructed (Fig.4.4.1.A). Subsequently, the FH_{19-20} component of this model was replaced by the crystal structure of FH domain 18-20 (Morgan *et al*. 2012)(Fig.3.4.1.B). The location of Sbi-III is at the N-terminal end of Sbi-IV, therefore based on this model the putative binding sites of Sbi-III could be on both FH domain 18 and 19. The putative ternary complex models of Sbi, FH_{18-20} in combination of C3 or C3b are also constructed (Fig.4.4.1.C and D). Although in the modeling process FH_{18-20} is utilized, given the high sequence identity between FH_{18-20} and $FHR\text{-}1_{3-5}$, it is

reasonable to assume they share an identical 3D structure. In fact apart from a loop region in FH domain 20 and FHR-1 domain 5, the crystal structures of FHR-1_{4-5} and FH_{19-20} are largely superimposable(Bhattacharjee *et al*. 2015).

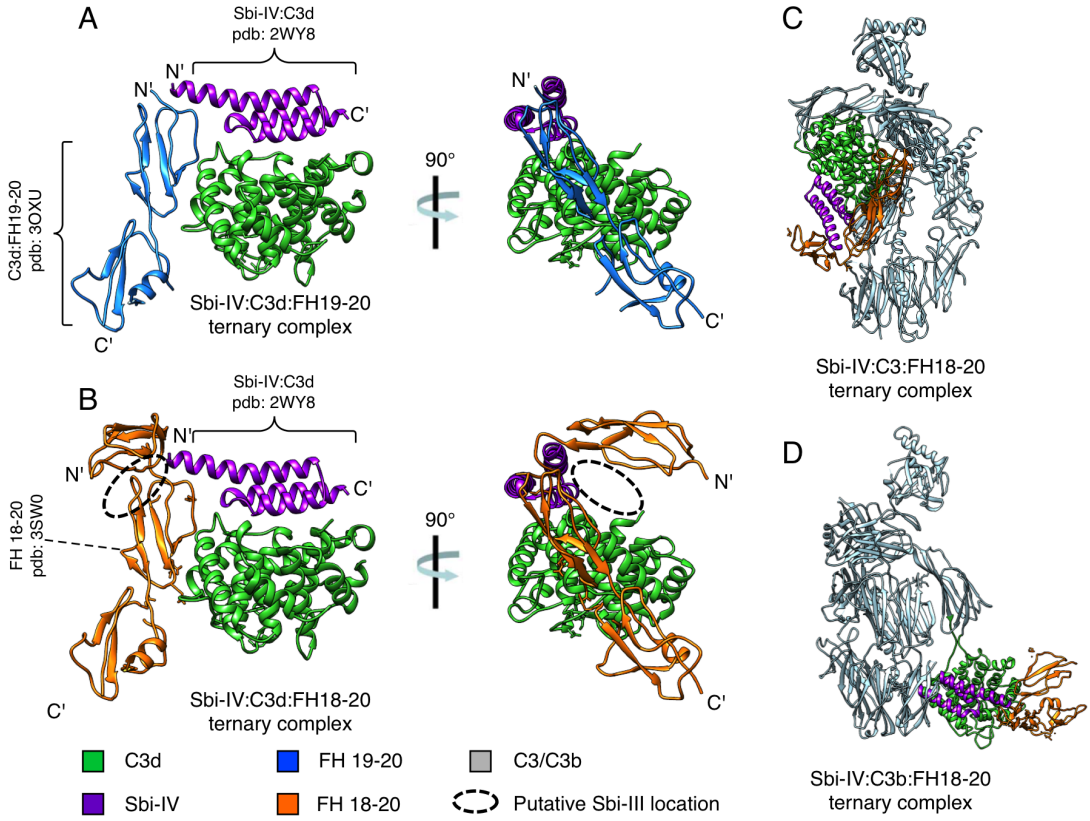

Figure 4.4.1: Structural models of ternary complex. (A) Putative structural model of Sbi-IV:C3d:FH19-20 ternary complex. **(B)** Putative structural model of Sbi-IV:C3d:FH18-20 ternary complex.**(C)** Putative structural model of Sbi-IV:C3:FH18-20 ternary complex.**(D)** Putative structural model of Sbi-IV:C3b:FH18-20 ternary complex. Putative Sbi-III location is indicated by the black dashed oval. Protein data bank association code: 2WY8 (Sbi:C3d), 3OXU(FH19-20:C3d), 3SWO (FH 18-20), 2A73 (C3),2I07(C3b) .

In the pull down study we found Sbi preferentially favours the formation of a FHR-1 ternary complex over a FH-containing complex, this suspicion was subsequently confirmed by the ELISA measurement. However, given the high sequence identity between FH_{18-20} and FHR-1_{3-5}, the binding selectivity is very hard to explain. We propose an explanation based on the observation that the FHR-5 that forms the correct dimeric state binds to renal-bound mouse C3 significantly better than FHR-5 dimerization mutant (Goicoechea de Jorge *et al*.

2013). A similar scenario could apply to the formation of Sbi:C3:FHR-1 tripartite complex. The preferential binding might not be a result of ligand selectivity of Sbi but due to the physiological dimerization state of FHR-1. Differential glycosylation of FHR-1 could also be a likely cause as discussed in Section 5.5.4.

4.4.4 Binary complexes

In contradiction to previous findings (Haupt *et al*. 2008) that C3 isoform binding is a essential step for Sbi to bind FH, in this study, it was shown that Sbi-III-IV could directly bind to FH or FHR-1 in a concentration dependent manner. As shown in Section 4.3.10, it was determined that when bound to C3 isoforms, Sbi-III-IV demonstrates significantly increased binding affinities to both FH and FHR-1. Although the structural basis of this change in binding kinetic properties is elusive, it seems that binding of C3 isoform is a prerequisite step for Sbi-III-IV to achieve high affinity FH/FHR-1 binding.

4.4.5 Functional significance of Sbi containing ternary complexes

Here, for the first time a functional connection between ternary complex formation and C3 consumption is established. It has been shown in previous publications (Goicoechea de Jorge *et al*. 2013) that FHR-1 acts as an antagonist of FH to deregulate complement activation, and the deregulatory activity is further enhanced by the formation of homo/heterodimers of FHR-1 with either itself or other FHRs (FHR-2 & 5). The proposed complement deregulation mechanism is that FHR-1 competes with FH for C3b binding, which results in protection of C3b against FH mediated FI cleavage.

It was discovered that within the ternary complexes, Sbi-III-IV mediates the competitive binding between FH and FHR-1 to various C3 isoforms (e.g. C3, C3b

and C3d). Without Sbi-III-IV, a 28 times molar excess of FHR-1 is needed to replace 60% of C3b bound FH (Goicoechea de Jorge *et al*. 2013), but in the presence of Sbi-III-IV at equal molar ratio (FH:FHR-1=1:1) a similar reduction in FH binding is achieved regardless of the type of C3 isoforms. This demonstrates again that Sbi preferentially utilizes FHR-1 to form ternary complexes, which fits with the observation that the Sbi mediated FHR-1 binding is 2,9 and 18 fold lower in K_d than the corresponding FH binding profiles (Section 4.3.10). At the same time, the positive relationship between ternary complex formation and protection of $C3_{H20}$ against FI cleavage was also demonstrated (Section 4.3.12.1).

One unique experiment presented in this study involves the application of FH/FHR-1 double depleted serum. The serum was purchased from Comptech,USA as FH single depleted serum, however during downstream usages, suspicions were raised that the serum could be FH/FHR-1 double depleted. The pull-down experiment shown in Fig.4.3.26.A confirmed this suspicion. The verification of FH/FHR-1 double-depleted status is advantageous for this study. As shown in Fig.4.3.26.B & C, the individual and combined effects of FH and FHR-1 containing ternary complexes were examined, the results indicated that only the FHR-1 containing ternary complex is required for Sbi triggered C3 consumption.

4.4.6 Complement inhibitory activities of Sbi-III-IV

The mutagenesis studies of Sbi-III-IV created several Sbi-III-IV mutants with specific defective phenotypes. S199A and K173A demonstrate impaired ability to form ternary complexes, but have normal C3 binding activity. In comparison, R231A lacks both abilities. As shown in Section 4.3.9.4, the AP and CP inhibition profiles of these mutants vary considerably. In the following discussion section, the putative molecular mechanisms are proposed.

4.4.6.1 CP complement assay demonstrates inhibition caused by C3:Sbi-III-IV binding

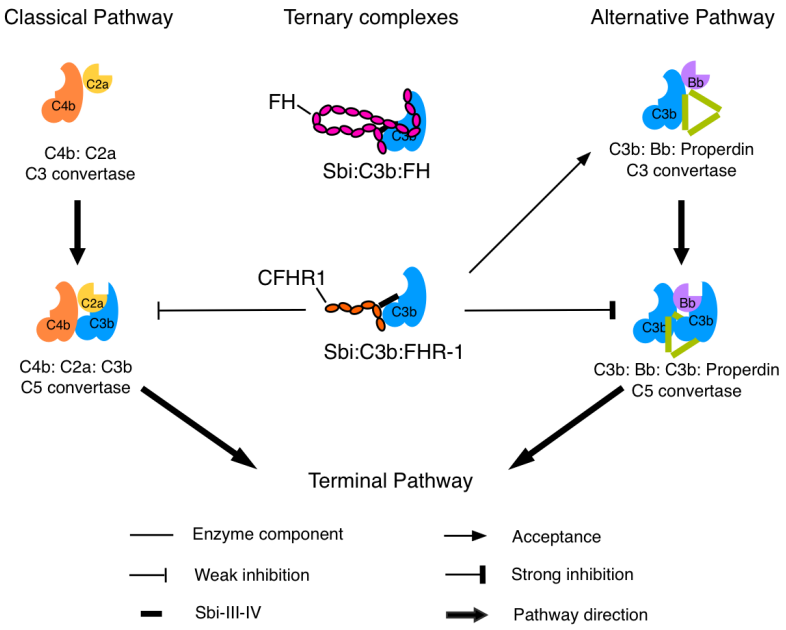

Figure 4.4.2: Schematic diagram summarizing the C3/C5 convertase inhibition caused by ternary complex.

As shown by Fig.4.3.20, the degree of CP activity inhibition is proportional to the pre-incubation time. But at the same time, without any pre-incubation, CP activities were differentially suppressed by the presence of Sbi-III-IV mutants. Because Sbi triggered C3 consumption does not take place under CP experimental conditions without pre-incubation, the CP measurement demonstrates the extent of Sbi mediated inhibition that is not a consequence of C3 consumption. The percentages of inhibition caused by Sbi-III-IV mutants with different molecular features demonstrate that the molecular basis consists of both C3 binding and ternary complex formation. At 0 min (Fig.4.3.20.A), R231A (no C3 binding, no ternary complex) demonstrates no CP inhibition. K173A and S199A (impaired ternary complex formation) demonstrate 20% reduction in CP activity. Finally, WT protein shows a 40% inhibition in CP activity. As shown in Fig.4.4.2, apart from using C3 as substrate, CP only uses C3b as the component of C5 convertase. Therefore, by direct interactions and formation of ternary

complexes, Sbi-III-IV could either make C3 a less useable substrate or make C3b an impaired CP C5 convertase component. It is shown in Fig.4.4.1.C, that the C3 structure is compatible with the formation of ternary complexes, but Fig.4.4.1.D shows a steric clash between C3b MG1 domain and Sbi-IV, this steric clash was shown to inhibit AP C3 convertase (Chen *et al*. 2010), thus I proposed that this steric clash could also responsible for the jeopardized CP C5 convertase activity. The binary binding between Sbi-III-IV and C3b is weak and unstable (Burman *et al*. 2008), but the ternary complex stabilizes this interaction, therefore K173A and S199A mutants are less potent as inhibitors of CP activity than the WT protein.

4.4.6.2 Sbi ternary complexes' impact on AP C3/C5 convertases .

So far Sbi-III-IV has been firmly established as an activator of AP, therefore any inhibition of AP residual activity without pre-incubation (Fig.4.3.20.B) seems rather counter-intuitive. Given that the assay plate surface has already been universally coated with AP pathway complement activators, the presence of C3 activator Sbi-III-IV should not cause inhibition to a great extent. But the opposite was observed. At 0 min Sbi-III-IV WT inhibits AP activity by 90%. To explain these results a new hypothesis is proposed where the Sbi-III-IV weakly inhibits AP C3 convertase activity, but heavily inhibits AP C5 convertase activity. The C3 convertase inhibition is shared among numerous *Staphylococcal* C3 binding proteins (Chen *et al*. 2010), which bind a common binding surface on the C3b TED domain but vary in their binding strength, Sbi has the weakest affinity to C3b, this expands the modest inhibition of AP C3 convertase.

The severe AP C5 convertase inhibition is rather hard to explain, as AP C5 convertase comprises two C3b molecules. One possibility is that Sbi-III-IV simultaneously binding on two C3b molecules jeopardizes the C5 convertase activity; another possibility is that the inhibition is a result of FH/FHR-1

recruitment via formation of ternary complexes. These two possibilities are evaluated by analyzing C5 convertase inhibition activities of *staphylococcal* C3 binding proteins, including Efb-C, Ecb and Sbi-IV. These three proteins target the same surface on TED domain, potentially causing inhibition of both AP C3 and C5 convertases. Among these proteins, Efb-C demonstrates the strongest C3b affinity, although it completely inhibits AP C3 convertase, it only mildly inhibits AP C5 convertase activity by 30% (Jongerius *et al*. 2007). In contrast to Efb, Ecb demonstrates similar C3b affinity and similar C3 convertase inhibition, but it is a better C5 convertase inhibitor (70% reduction). This enhancement could be the consequence of the recent discovery that Ecb forms tighter ternary complexes with C3b and FH than Efb-C (Amdahl *et al*. 2013). Since Sbi has a weaker binding strength than Efb and Ecb to C3b, it is not likely that the significant inhibition on AP C5 convertase caused by Sbi is due to binary Sbi:C3b interaction. Considering with the example of Ecb, I conclude that Sbi-III-IV's C5 convertase inhibition activity is largely due to the formation of ternary complexes. This conclusion correlates well with the K173A AP inhibition profile, which only shows a 30% reduction in AP activity.

According to the above discussion sections, Fig.4.4.2 was constructed that summarizes the current theories about the relationships between ternary complexes and inhibition on CP/AP activity. Given that Sbi-III-IV is able to bind FH or FHR-1 in combination with various C3 isoforms, therefore in the presence of Sbi-III-IV the majority of the C3 substrate presented to C3 convertase is in the form of two types of ternary complexes (Sbi:C3:FH or Sbi:C3:FHR-1). After the intra-complex conversion to C3b, the C3b embedded in the FHR-1-containing complex is protected from proteolytic inactivation, but the C3b embedded in FH containing complex undergoes immediate FI mediated cleavage. Thus it is unlikely to participate in the modulation of C3/C5 convertase activity. Consequently, by forming the Sbi:C3:FHR-1 ternary complex, Sbi slightly inhibits CP C5 convertase, but strongly inhibits AP C5 convertase. The bound FHR-1

could be responsible for the inhibition of C5 convertase, as demonstrated by (Heinen *et al*. 2009) that FHR-1 inhibits C5 activation in a dose-dependent manner.

4.4.7 Hypothesis evaluation

In the beginning of this chapter, three hypotheses were proposed regarding the complement modulatory function of Sbi-III-IV. The experimental evidence presented in this chapter strongly supports hypothesis 2, that Sbi-III-IV prevents C3b from breaking down. Hypothesis 1, that Sbi-III-IV accelerates C3 conformational change to C3b is opposed by the observations of the activation lagging time and K173A mutant demonstrating a comparable $C3_{H20}$ deposition speed (Section 4.3.10).

In terms of hypothesis 3, the C3 consumption profile of Sbi-III-IV S226A mutant suggests that at very high Sbi concentration (60 μM), the formation of Sbi-C3b adduct might not be necessary for C3 consumption to initiate and proceed. Further studies using purified Sbi-C3b adduct or at a physiologically relevant Sbi concentration are required to reveal the full extent of Sbi-C3b adducts complement modulatory potential. The functional and structural aspects of Sbi-C3b adducts are explored further in Chapter 5.

Chapter 5: Functional and molecular characterization of Sbi-C3b adduct

5.1 Introduction:

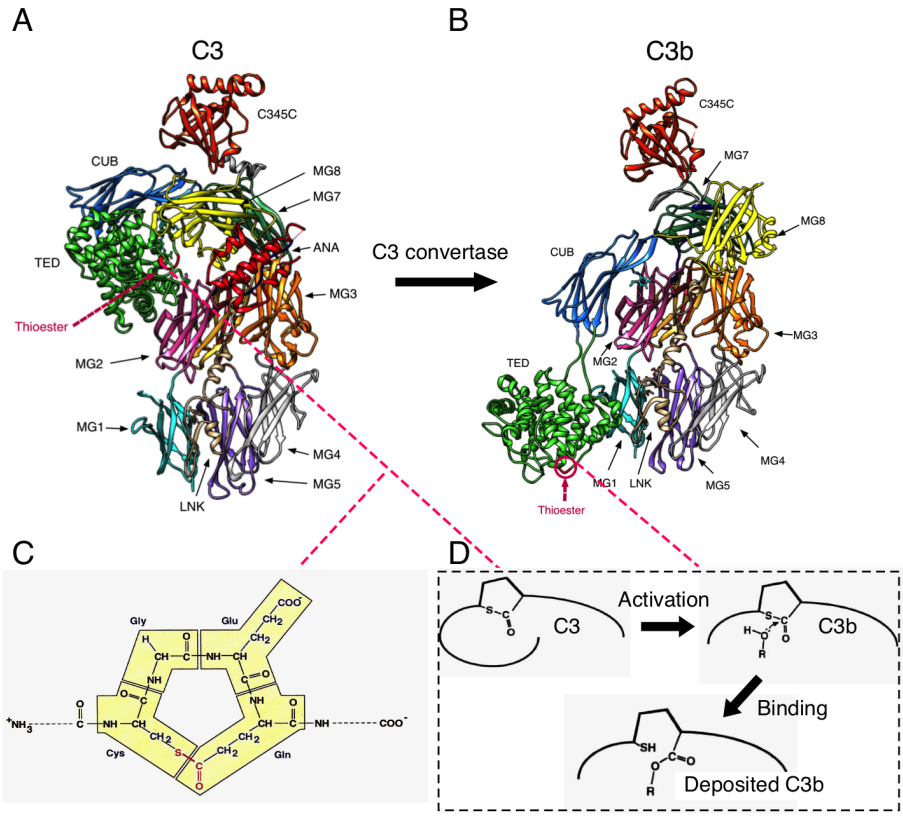

Figure 5.1.1: C3 thioester. (A) Domain structure of C3 **(B)** Domain structure of C3b **(C)** Thiolactone ring composed of -Cys-Gly-Glu-Gln-. The polypeptide backbone is in black. The side-chains are in blue, and the thioester in red. **(D)** Simplified covalent binding mechanism of C3. C-D taken from (Law & Dodds 1997).

Covalent deposition was one of the first molecular features discovered about the complement component C3 molecule. Following the proteolytic activation of C3, the nascent C3b molecule utilizes its internal thioester motif to covalently target hydroxyl and amine chemical groups in the surrounding environment (Law & Dodds 1997). Based on early biochemical experiments, the primary structure and covalent attachment mechanism of the thioester motif were established, however the complete working mechanism was not fully revealed until the publication of the C3 and C3b crystal structures (Janssen *et al*. 2005; Janssen *et al*.

2006). The C3 thioester motif consists of four residues, -Cys-Gly-Glu-Gln- (Nonaka *et al*. 1985; de Bruijn & Fey 1985), forming a thiolactone ring structure, in the immunological inert C3 molecule. This motif is facing inward and the thioester bond is protected by a hydrophobic pocket formed by the MG7 and MG8 domains of C3 (Fig.5.1.1.A). However in the C3b molecule (Fig.5.1.1.B), the dramatic conformational changes expose this motif to the surrounding environment. Catalyzed by a nearby histidine residue (H^{1106}), the exposed thioester bond is highly susceptible to nucleophilic attacks from hydroxyl or amine groups, resulting in the formation of ester or amide linkages (Fig.5.1.1.D). The thioester motif is highly conserved within the macroglobulin protein family including C3 and C4 molecules from various animal species (Blandin 2004). However, the subtle amino acid differences within these molecules diversify the kinetic properties and covalent linkage preference of their embedded thioester motif. It is known that human C3 thioester prefers to form ester linkages over amide linkages (Law *et al*. 1979).

The C3b deposition process plays a crucial role in fighting infections, as the C3b molecules deposited on the pathogen surface signal a range of innate and adaptive immune responses. In addition to the immunological signaling functions, as part of the complement activation cascade, the deposited C3b molecule is also involved in determining the fate of the complement activation cascade. It has become increasingly clear that the proteolytic stability of the surface deposited C3b molecule is the key property utilized by the complement system to differentiate self and non-self surfaces (Morgan *et al*. 2011; Kajander *et al*. 2011). Targeted by serum complement regulators, C3b molecules are degraded rapidly to iC3b and C3d on self-surface, but when deposited on a non-self surface, the half-life of deposited C3b can be dramatically prolonged at most 10-fold (Meri & Pangburn 1990), which increases the probability of complement activation and amplification on the particular surface.

The current theory for the molecular basis of this mechanism is that the chemical property of a particular biological surface could either attract or repel the recruitment of C3b binding complement regulators (e.g. FH). In addition to the detailed characterization of the biological surface (e.g. host cell membrane), which actively down-regulates surface complement activity, various biological surfaces have also been shown to be able to extend the half-life of the C3b molecule, thereby facilitating complement activation. Long-chain polysaccharides (Pangburn 1989a; Meri & Pangburn 1990) as the main component of bacterial cell walls were demonstrated to be able to extend the half-life of the deposited C3b molecule. Meanwhile, it was also shown that forming adducts with serum proteins can be a mechanism for increasing C3b serum half-life (Pangburn 1989b). Given the almost non-discriminative nature of the C3 thioester reactivity, C3b can be covalently attached on almost any kind of biological target. However, C3b preference for deposition targets is documented. Complement component C3b, C4b are heavily targeted by nascent C3b molecules (Jelezarova & Lutz 1999), but IgG is accredited as the most prominent C3b deposition target in the serum. Several in-depth investigations on IgG-C3b adduct formation revealed that C3b can weakly interact non-covalently with IgG molecule (Kulics *et al*. 1983) and serine-132 on the IgG surface is responsible for the majority of C3b deposition (Vidarte *et al*. 2001; Shohet *et al*. 1993). More importantly, a concentration dependent relationship was demonstrated between purified IgG-C3b adduct and the extent of AP C3 consumption (Fries *et al*. 1984); thereby suggesting that the C3b adduct can function both as facilitator and initiator of C3 activation through complement AP.

Normally C3b deposition on bacterial proteins is considered a form of antigen-opsonin interaction, however in this study, the complement modulatory function of Sbi prompts us to re-evaluate the purpose and the ramifications of Sbi-C3b adduct formation. Although in chapter 4, it was demonstrated that Sbi:C3:FHR-1 ternary complexes play an irreplaceable role in the mechanism of

C3 futile consumption, the complement modulating impact of Sbi-C3b adducts should not be underestimated or ignored. Thus, in this chapter, I aim to establish protocols for the production of Sbi-C3b adducts, to identify the C3b deposition site/s on Sbi-III-IV, and finally to elucidate the potential complement modulatory function of Sbi-C3b adduct.

5.2 Materials & Methods:

5.2.1 Sbi-III-IV recloning into pET28a vector

Using pQE30$^{Sbi\text{-}III\text{-}IV}$ plasmid as the PCR template, a gene fragment corresponding to Sbi domain III and IV (from I^{154} to V^{266}) was amplified by PCR reaction using primers (Forward: 5'- CGCGGATCC ATTGAAAATGCGGATAAAGCAATTAAAGATTT C-3' Reverse: 5'- CCCAAGCTTCGCCACTTTCTTTTCAGCATCTTTTTG-3'). The PCR product flanked by BamHI and HindIII restriction sites was then double digested, purified and ligated with double digested pET28a plasmid. After transformation of the ligation mixture into *E.coli* DH5α cell line, colony PCR was performed to screen for insert containing clones. The integrity of the DNA insert was further verified by DNA sequencing. Sequence verified pET28a$^{Sbi\text{-}III\text{-}IV}$ vectors were transformed into *E.coli* BL21(DE3). Following the standard expression protocol their expression profiles were analyzed by SDS-PAGE. Finally, for experiment described in Section 5.2.2 one pET28a$^{Sbi\text{-}III\text{-}IV}$ clone was selected for large-scale production of Sbi-III-IV^{28a} following the method described in Section 2.3.2.

5.2.2 Large-scale preparation & labeling of Sbi-C3b adduct

Alternative pathway activation was reconstituted *in vitro* to achieve large-scale production of the Sbi-C3b adduct. For a typical reaction 300 µg of purified C3, 50 µg of Sbi-III-IV^{28a}, 6 µg of factor B, 50 ng of factor D and 25 ng of factor P were mixed to final volume of 120 µl. All components were buffer exchanged into PBS pH7.2 buffer in advance. The reaction was kept at 37°C for 1 hour.

In order to produce biotinylated Sbi-C3b, in addition to the components described above, 200 μM of iodoacetyl-PEG2-Biotin (Fig.3.2.2) was also added. A lightly alkine pH environment maintained by PBS buffer pH 8.2 was used to ensure the labeling of nascent Sbi-C3b.

5.2.3 Sbi-C3b adduct purification

Purification of Sbi-C3b adducts was achieved by using a spin-column loaded with metal affinity chromatography resin. Following *in vitro* Sbi-C3b adduct formation described by Section 5.2.2, the reaction mixture was loaded on 300 μl of Ni^{2+} sepharose resin, washed intensively with HisA buffer and high-salt stringent washing buffer (50 mM Tris-HCl, 1 M NaCl and pH 7.5) and finally eluted with 300 μl of HisB buffer. Mild centrifugation speed (1000 *g*) was used in all buffer exchange and washing steps to avoid damage to the spin-column. Protein samples were collected during each step of the preparation of biotinlyated Sbi-C3b adducts. Afterwards protein samples were analyzed by SDS-PAGE, anti-Biotin and anti-Sbi Western blots.

5.2.4 Hydroxylamine sensitivity assay

Two-dimensional SDS-PAGE analysis (reducing condition, 8% or 12% acrylamide gel in both dimensions), after the Sbi treated human serum was separated by the 1st dimension gel, the protein containing gel strip was excised and soaked in 1 M hydroxylamine solution (pH 10) for 1 hour at 37°C. Then the gel strip was recharged with 1× SDS loading buffer, rotated 90 degree and loaded on a 2nd dimension gel. An anti-Sbi Western blot was then used to study the location of Sbi-C3b, Sbi-iC3b adducts and the potentially dissociated Sbi-III-IV molecule. anti-C3d Western blot was also carried out to confirm the effectiveness of hydroxylamine treatment.

An alternative version of the 2D gel based hydroxylamine sensitivity assay was designed based on purified Sbi-C3b adduct. After separating the purified Sbi-C3b adduct using a 12% acrylamide gel, guided by pre-stained protein molecular weight markers, the gel segment located above 120 kDa was excised and treated with hydroxylamine solution (pH 10) for 1 hour at 37°C. After treatment, the gel segment was re-charged with SDS sample buffer and loaded on a 15% acrylamide 2nd dimension gel. The location of Sbi was then revealed by polyclonal anti-Sbi Western blot.

5.2.5 Sbi-III-IV mutagenesis:

Mutagenic PCR reactions were carried out based on the protocol presented in Section 2.2.2. A list of mutagenic PCR primers is presented in following tables.

Table 5.2.1: Mutagenic PCR primers. Mutations are highlighted in red.

Template (pre-existing mutations in pQE30$^{Sbi\text{-}III\text{-}IV}$)	Inserting mutation	Primer (5'-3')
D172A	K168A	F: gataaagcaattaaagatttccaagataac**gca**gcaccacacgccaaatc R: gatttggcgtgtggtgc**tgc**gttatcttggaaatctttaattgctttatc
D172A K168A	K162A	F: aaaatattgaaaatgcggataaagcaatt**gca**gatttccaagataacgcagcac R: gtgctgcgttatcttggaaatc**tgc**aattgctttatccgcattttcaatatttt
D172A K168A K162A	K159A	F: ccgaacgtcaaaatattgaaaatgcggat**gca**gcaattgcagatttccaa R: ttggaaatctgcaattgc**tgc**atccgcattttcaatattttgacgttcgg
S174A	S181A	F: agcagcagcatatgaagctaac**gca**aaattacctaaagatttacg R: cgtaaatctttaggtaattt**tgc**gttagcttcatatgctgctgct
S174A S181A	Y177F	F: cacgccaaagcagcagca**ttt**gaagctaacgcaaa R: Tttgcgttagcttc**aaa**tgctgctgctttggcgtg
No	K212A S213A	F: cgttcgtcatgatgagcgtgtggca**gcagca**aatgatgcaatctcaaaa R: ttttgagattgcatcatttgc**tgctgc**cacacgctcatcatgacgaacg
K212A S213A	S219A K220A	F:cgtgtggcagcagcaaatgatgcaatc**gcagca**ttaaatgaaaaagattcaattgaaaac R: gttttcaattgaatctttttcatttaa**tgctgc**gattgcatcatttgctgctgccacacg

Table 5.2.2: Mutagenic PCR primers. Mutations are highlighted in red.

Template (pre-existing mutations in pQE30$^{Sbi\text{-}III\text{-}IV}$)	Inserting mutation	Primer (5'-3')
no	K259A	F: acaattagacgcattagtagctcaa**gca**gatgctgaaaagaaagtggc R: gccactttcttttcagcatc**tgc**ttgagctactaatgcgtctaattgt
K259A	K250A	F: tatggatgtaaaagagcatttacag**gca**caattagacgcattagtagctcaa R: ttgagctactaatgcgtctaattg**tgc**ctgtaaatgctcttttacatccata
K259A K250A	K245A	F: gaagttaacaaagcacctatggatgta**gca**gagcatttacaggcacaa R: ttgtgcctgtaaatgctc**tgc**tacatccataggtgctttgttaacttc
K259A K250A	K263A K264A	F: gcattagtagctcaagcagatgctgaa**gcggca**gtggcgtaatgaaagcttaattag R: ctaattaagctttcattacgccac**tgccgc**ttcagcatctgcttgagctactaatgc
KSSK (K212A S213 S219A K220A)	K259A	F: acaattagacgcattagtagctcaa**gca**gatgctgaaaagaaagtggc R: gccactttcttttcagcatc**tgc**ttgagctactaatgcgtctaattgt
KSSK K259A	K250A	F: tatggatgtaaaagagcatttacag**gca**caattagacgcattagtagctcaa R: ttgagctactaatgcgtctaattg**tgc**ctgtaaatgctcttttacatccata
KSSK K259A K250A	K245A	F: gaagttaacaaagcacctatggatgta**gca**gagcatttacaggcacaa R: ttgtgcctgtaaatgctc**tgc**tacatccataggtgctttgttaacttc
KSSK K259A K250A K245A	K263A K264A	F: gcattagtagctcaagcagatgctgaa**gcggca**gtggcgtaatgaaagcttaattag R: ctaattaagctttcattacgccac**tgccgc**ttcagcatctgcttgagctactaatgc

5.2.6 Sbi-III-IV purification:

In this chapter, Sbi-III-IV^{pQE30} mutant proteins were expressed and purified based on the method described in Section 3.2.1.

5.2.7 Adduct formation assay using factor I depleted serum

For a typical factor I depleted sera incubation experiment, equal volume of Factor I depleted serum and Sbi solution (40 µM) were mixed to a final volume of 10 µl, 1 µl of $MgCl_2$-PBS stock solution was also added to adjust the final $MgCl_2$ concentration to 0.5 mM. After thorough mixing, the mixture was incubated in a thermocycler at 37°C for 30 min. At the end of the incubation, 1µl of treated

serum was retrieved and added to 20 µl of 1×SDS loading buffer. Normally, 10 µl of sample was analyzed by SDS-PAGE and subsequently anti-Sbi Western blot.

5.2.8 In solution trypsin digest and peptide purification

To 100 µl of 1 mg/ml of Sbi-C3b adduct, the trichloroacetic acid (TCA) solution precipitation procedure was carried out according to Section 5.2.9. 30 µl of reducing and denaturation buffer (50 mM Tris pH 7.4, 6 M guanidine HCl, and 5 mM DTT) was added to dissolve the precipitated protein pellet, and boiled for 15 min. Next, 270 µl of 50 mM ammonium carbonate buffer pH8.0 was added to dilute the guanidine HCl concentration to 0.6 M. For each digestion reaction, 3 µg of Trypsin Gold protease (Promega) was added, and left in a 37°C incubator with shaking (200 rpm) for at least 20 hours.

Following the digestion reaction, 10 µg of soybean trypsin inhibitor was added; the trypic peptide digest was then mixed with 100 µl of pre-washed neutravidin resin in 50 mM ammonium bicarbonate. After 15 min incubation, the bound neutravidin agarose beads were pelleted by centrifugation (1000 *g*) and washed extensively with PBS buffer and with sterile water. To elute the bound peptides from the neutravidin resin, 200 µl of elution buffer (8 M guanidine HCl pH 1.0) was added, after 5 min of room temperature incubation. Neutravidin agarose was pelleted, and peptide-containing supernatant was collected. Finally to remove guanidine HCl from mass spectrometry (MS) samples, the eluted peptides was desalted using C18 MS sample cleanup column as described in Section 5.2.10.

5.2.9 TCA precipitation

100% (w/v) TCA was made by adding 5 g TCA to 3.5 ml of sterile water, the solution was stored at room temperature. To precipitate proteins, 1 volume of

TCA stock was added to 4 volume of protein solution. The precipitation reaction was held for 10 min on ice, and then the precipitated protein was pelleted by centrifugation at (13000 *g*). Supernatant was removed and discarded; the pellet was then washed with several cycles of ice-cold acetone solution (200 µl per cycle). Finally the protein pellet was dried at 95°C for 5 min.

5.2.10 C18 peptide clean-up

To prepare protein or peptide samples for mass spectrometry analysis, Pierce C18 Spin Columns (Thermo Scientific) were used to desalt and concentrate samples at once. Briefly, 2 cycles of 200 µl of 50% (v/v%) methanol washing step were performed to activate the C18 resin. Then the resin was washed twice with 200 µl of equilibration buffer (5% acetonitrile (ACN), 0.5% formic acid). A maximum of 150 µl of sample could be loaded at a time, so if the sample volume was larger than 150 µl, the sample was divided into aliquots of less than 150µl and these applied to the column sequentially. After sample loading, the column was washed repetitively with equilibration buffer. For desalting 8 M guanidine HCl, 4 cycles of 200µl washes were performed. Finally the two 20 µl 100% ACN elution steps were utilized to yield protein/peptide samples that were compatible with ESI-ToF mass spectrometry analysis.

5.2.11 Peptide mass determination

Peptide mass spectra were acquired using the method described in Section 3.2.17 with slight modifications. For each mass spectrum, the multiple charged mass peak was deconvoluted, and the peptide mass was assigned using the Masshunter program (Agilent).

5.2.12 Sbi-III-IV trypin digestion simulation

Sbi-III-IV trypic fragments were generated using the “PeptideMass” program

available on the ExPAsy bioinformatics resource portal (http://web.expasy.org/peptide_mass/). The primary sequence of Sbi-III-IV[28a] was submitted and trypic-digest peptide masses were calculated using the assumptions that peptide carries +1 positive charge and is monoisotopic. Considering the possible insufficient digestion of the Sbi-C3b adduct, trypic peptides containing up to 5 missed cleavage events were included in the final simulation report. The digestion simulation was shown in appendix Fig.9.8.

5.2.13 ELISA-C3 binding assay

For the C3 binding ELISA, 1µg/well of Sbi-III-IV or Sbi-III-IV mutants were coated on a Nunc MaxiSorp plate. After blocking (5% Skimmed milk-PBST), purified C3 was added for 1 hour at room temperature. The concentration of the analyte can be either a fixed value or a variable depending on the specific assay. After the C3 capturing step, polyclonal goat anti C3 antibody (1:100,000 dilution, Complementech, USA) was applied. After incubation and thorough washing of the plate, secondary antibody HRP conjugate against goat IgG (1:18,000 dilution) was added. Finally, 1-step Ultra TMB ELISA substrate solution was used to quantify C3/C3b binding.

5.2.14 Complement assay

A classical pathway complement assay was used to measure Sbi induced C3 consumption. The measurement and data analysis were carried out based on manufacture's instruction and as described in Section 3.2.3. Samples were taken as previously described (Section 3.2.2).

5.2.15 HSS C3 activation assay

The C3 activation assay was carried out based on a previously described protocol (Section 3.2.7).

5.2.16 Analysis of C3 consumption property of C3b and Sbi-C3b

The assay was inspired by the C3 consumption experiment described in (Fries *et al*. 1984), with necessary modifications. To compare the C3 consumption activity of C3b and Sbi-C3b, the first challenge was to eliminate free Sbi-III-IV[28a] (17.9 kDa) contamination from the Sbi-C3b sample. To overcome this handicap, Sbi-C3b (190 kDa) was repetitively concentrated and diluted using a 30 kDa cut-off Vivaspin concentrator. PBS supplemented with 1 M NaCl buffer was used during this process, until an equivalent of 3125× dilution (5 cycles of 5× dilution) was achieved. Then the Sbi-C3b sample was buffer exchanged to normal PBS buffer by the standard method.

Table 5.2.3 Composition of samples used to compare C3 consumption by C3b and Sbi-C3b

Group	C3b/Sbi-C3b added (µl)	PBS (µl)	2×MgEGTA-HSS (µl)	C3b/Sbi-C3b concentration (µM)
C3b	6	0	6	2.6
	4	2	6	1.7
	2	4	6	0.88
	1	6	6	0.44
Sbi-C3b	6	0	6	2.6
	4	2	6	1.7
	2	4	6	0.88
	1	5	6	0.44
No	0	6	6	0

Prior to the experiment, the protein concentrations of C3b and Sbi-C3b were determined, and adjusted to 5.2 µM (equivalent of 0.92 mg/ml of C3b, 1 mg/ml of Sbi-C3b). 2×HSS was reconstituted with 100 µl of water containing 10 mM $MgCl_2$ and 20 mM EGTA. To set up the C3 consumption reactions (Table 5.2.3), 2×MgEGTA-HSS was diluted once by adding various amount of C3b or Sbi-C3b

together with filtered PBS. Care was taken to mix the reaction mixture thoroughly and to start all the consumption experiments simultaneously. After incubation at 37°C for 1 hour in a thermocycler, C3 consumption was evaluated using the AP complement assay kit. At the same time, treated serum (1 µl) was added to 20µl of 1×SDS-PAGE loading buffer, 10µl of the sample was then analyzed by anti-Sbi, anti-C3a and anti-factor B Western blots.

5.2.17 Factor I depleted serum cleavage assay

The active C3 in factor I depleted serum was firstly consumed by incubating the serum with 0.5 mM $MgCl_2$ at 37°C for 1 hour. Afterward, Sbi-C3b adduct (0.24 µg/µl) or free C3b (0.24 µg/µl) molecule was added to C3 exhausted Factor I depleted serum. The incubation was divided into two groups according to whether Sbi-III-IV WT (3 µM) was added or not. Cleavage reaction was carried out at 50% v/v serum concentration, dilution was made by PBS-Mg^{2+}(PBS with 1 mM $MgCl_2$). At 0 min purified factor I was added to the final concentration of 4 ng/µl. Serum samples were retrieved at 0, 5, 10, 15, 30 and 60 min. An equivalent of 0.5 µl of 100% serum was analyzed using anti-Sbi or anti-C3d Western blots.

5.3 Results:

Previous studies have demonstrated that Sbi-III-IV is a prominent transacylation target of metastable C3b molecules. The Sbi-C3b adduct was also proposed to behave like an IgG-C3b adduct (Burman *et al*. 2008), by offering resistance to factor I mediated cleavage and facilitating the activation of the alternative pathway. The work described here also shows that the process of Sbi-C3b adduct formation synchronizes with the progression of C3 consumption (Fig.4.3.2). However, using our Western blot based C3 activation assay (Section 4.3.6.2), it would be premature to conclude whether the Sbi-C3b adduct is the prerequisite

condition of C3 consumption or the consequence of C3 consumption. Therefore purified Sbi-C3b adduct would be ideal for the performance of detailed biochemical analyzes.

Purification of the Sbi-C3b adduct from serum is hampered by the existence of other prominent transacylation target such as IgG and serum albumin, affecting the quantity and the purity of Sbi-C3b adduct derived by this method. We also experienced difficulties with the affinity of the Sbi-C3b adduct for the Ni^{2+} resin, and decided to introduce an additional (C-terminal) his-tag. The first part of this chapter describes the results of the re-cloning of Sbi-III-IV into a pET28a vector with a second his-tag. In addition, a protocol for making Sbi-C3b using a reconstituted alternative pathway was also provided.

5.3.1 Sbi-III-IV recloning to the pET28a vector

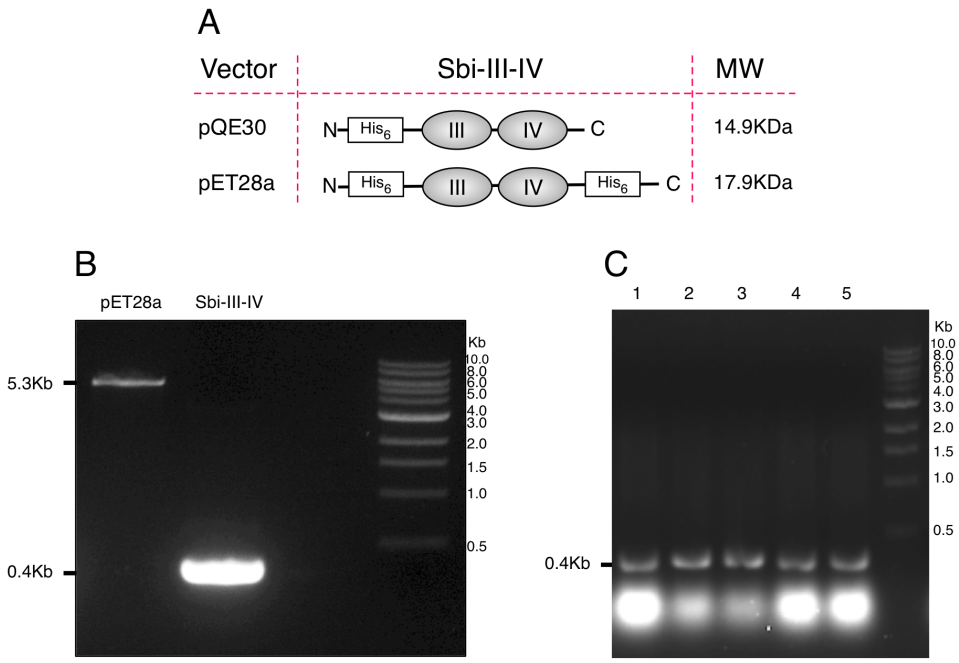

Figure 5.3.1: Cloning of the Sbi-III-IV gene into the pET28a vector. (A) Schematic diagram shows Sbi-III-IV constructs in two different vectors. **(B)** Agarose gel showing BamHI and HindIII double digested pET28a vector and the PCR product of Sbi-III-IV gene fragment. **(C)** Agarose gel analysis of colony PCR screening for Sbi-insert-containing colonies. The expected size of the PCR product is around 0.4 Kb.

Utilizing pQE30$^{Sbi\text{-}III\text{-}IV}$ as a template, the Sbi-III-IV gene fragment from I^{154} to V^{265} was amplified by PCR reaction using primers containing BamHI and HindIII restriction sites. An agarose gel electrophoresis analysis of the double-digested Sbi gene insert and pET28a vector is shown in Fig.5.3.1.B. After a standard T4 ligase reaction, the ligated pET28a$^{Sbi\text{-}III\text{-}IV}$ construct was then transformed into an *E.coli* DH5α cell line. The efficiency of the ligation reaction was then checked by colony PCR reaction. A total of 5 colonies were selected, which all contained the Sbi-III-IV gene insert (Fig.5.3.1.C). Clones 1, 2 and 3 were cultured overnight in LB medium and the expression vectors were purified by a standard miniprep protocol. The incorporation of the correct Sbi insert was verified by DNA sequencing (Appendix 9.1.1.6). Individual expression vectors were then transformed into *E.coli* strain BL21(DE3) and screened for the expression of Sbi-III-IV^{28a}. Fig.5.3.2 shows that after IPTG induction all three clones show over-expression of a recombinant protein corresponding to the size of Sbi-III-IV^{28a}.

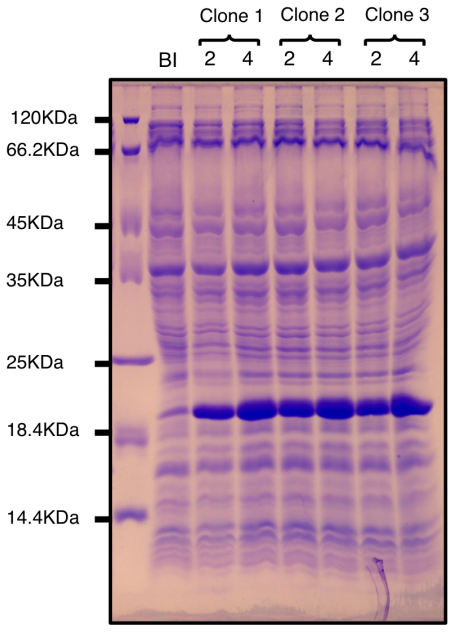

Figure 5.3.2: SDS-PAGE screening of Sbi-III-IV^{28a} expression conditions. After induction with 1 mM IPTG at 37°C. For every clone, 2-hour and 4-hour post-induction samples were analyzed. Before induction sample is labeled "BI". Sbi-III-IV^{28a}, with an expected size of 17.9 kDa is located slightly higher than the18.4 kDa weight marker.

Clone 1 was utilized for the large-scale production of Sbi-III-IV^{28a}. The soluble fraction of a 1 Liter induced culture was loaded on a 1ml Histrap FF column using a ÄKTA purifier. The bound protein was eluted with a gradient of HisB

buffer. Three peak fractions were collected and analyzed by SDS-PAGE. (Fig.5.3.3) The purified peak fraction of Sbi-III-IV^{28a} was subsequently concentrated and buffer exchanged to PBS.

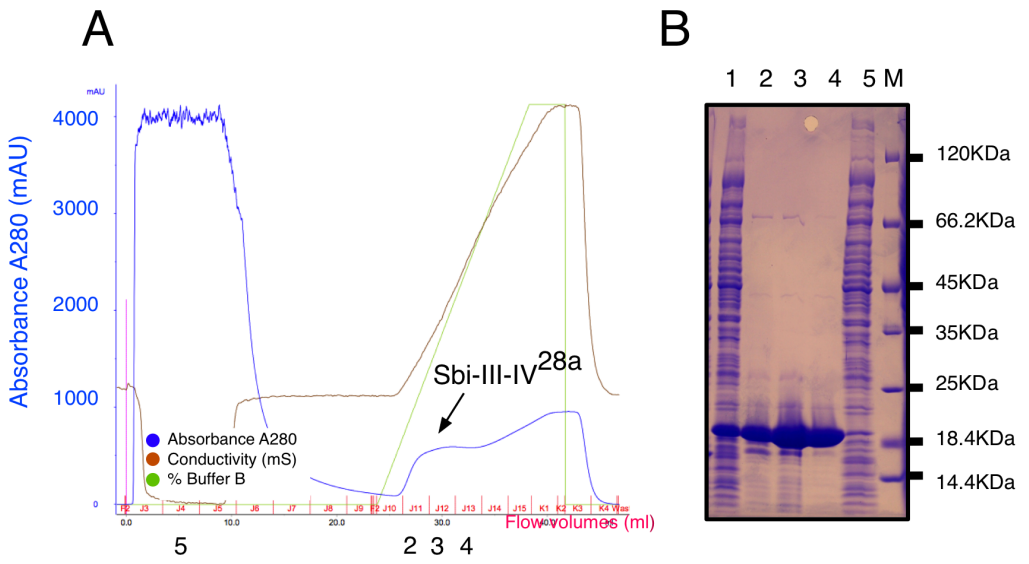

Figure 5.3.3: Ni^{2+} affinity chromatography and SDS-PAGE profile of Sbi-III-IV^{28a} purification. (A) A chromatogram of the Ni^{2+} affinity purification, volume (ml) and fractions are shown on X-axis. Peak fractions are labeled 2-4 and flow-through is labeled 5. Absorbance at 280 nm, solvent conductivity and percentage of buffer B are colour coded as shown on the graph. The protein was purified using a 1 ml Histrap FF column, eluted with 12 column volumes of HisB gradient. **(B)** Coomassie stained gel of Sbi-III-IV^{28a} purification, Lane 1 soluble fraction before purification, 2-4 purified peak fractions and 5 flow-through. pET28a$^{Sbi\text{-}III\text{-}IV}$, with an expected size of 17.9 kDa is located slightly higher than 18.4 kDa weight marker.

5.3.2 Molecular characterization of Sbi-C3b adduct

5.3.2.1 Generation and purification of Sbi-C3b adduct

The difficulty of purifying the Sbi-C3b adduct from serum prompted the development of an alternative route to prepare the Sbi-C3b adduct. There are several obstacles that are difficult to overcome when attempting to purify Sbi-C3b from serum. Firstly, large amounts of Sbi-III-IV are required, given that C3 serum concentration is not easily changeable. Secondly, due to the existence of C3b processing enzymes (e.g. factor I), Sbi-C3b rarely remains intact after

prolonged incubation. Thirdly, various metal binding serum proteins usually co-purify with the Sbi-C3b adduct. Finally, the presence of other prominent transacylation targets usually compete with Sbi-III-IV for C3b deposition, therefore only a fraction of the metastable C3b is actually deposited on Sbi-III-IV.

To overcome this inefficient and time-consuming procedure, Sbi-III-IV[28a] was added to purified C3 in combination with other alternative pathway components (e.g. factor B, D and P). Using this reconstituted AP system, a large amount of unprocessed Sbi-C3b adduct was generated in a considerably short period of time (Fig.5.3.4.A). The Sbi-C3b adduct was then purified using a N^{2+} affinity sepharose resin loaded in a spin-column (Fig.5.3.4.B). The purified Sbi-C3b adduct was also analyzed by anti-Sbi Western blot (Fig.5.3.4.C) to confirm the deposition of Sbi on C3b α' chain.

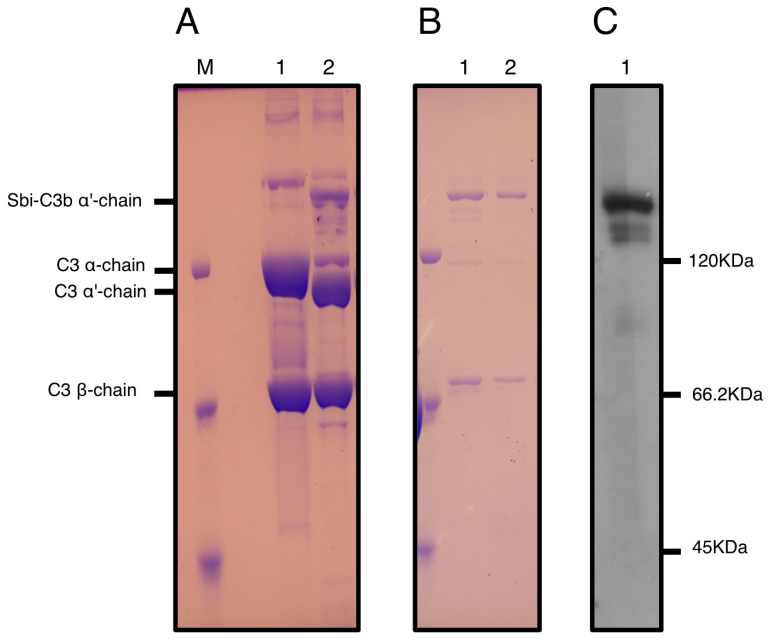

Figure 5.3.4: Generation and purification of Sbi-C3b adduct. (A) SDS-PAGE analysis of AP activation and C3b deposition processes. Lane 1, before AP activation. C3 α-chain appears as a single band. Lane 2, after AP activation. C3 α-chain converts to α'-chain and Sbi-C3b-α'-chain. **(B)** SDS-PAGE analysis of purified Sbi-C3b adduct. Lane 1-2, two elution fractions of N^{2+} affinity purification. Sbi-C3b adduct comprises of Sbi-C3b-α'-chain and C3 β chain. Small amount of C3b is indicated by the faint C3 α'-chain band. These two samples also contain non-deposited Sbi-III-IV protein, but this is not retained on the 8% acrylamide gel. **(C)** An anti-Sbi Western blot confirms the putative Sbi-C3b-α'-chain band contains Sbi.

5.3.2.2 Chemical properties of the covalent linkage between Sbi and C3b molecule

The human C3 thioester motif is described as preferring the formation of an ester bond with a hydroxyl group rather than the formation of amide linkage with an amine group (Law & Dodds 1997). Previous hydroxylamine sensitivity assays (Burman *et al*. 2008) of the Sbi-C3b adduct prepared by an immune precipitation technique suggested that C3b deposits on Sbi-III-IV through an ester linkage. In this part of the chapter, the chemical properties of the linkage between Sbi-III-IV and C3b molecule is further investigated. Firstly, the hydroxylamine sensitivity assay (Section 5.2.4) was repeated using Sbi-III-IV treated serum. A combination of two-dimensional gel and Western blot techniques were adopted to study the molecular weight changes caused by the ester bond hydrolyzing reagent hydroxylamine.

The hydroxylamine sensitivity assay demonstrated that the serum-derived Sbi-C3b and Sbi-iC3b adducts sustain the treatment of hydroxylamine; no mass decreases (off-diagonal spots) were detected (Fig.5.3.5.A). At the same time, as a control experiment the same sample was also analyzed by anti-C3d Western blot. This experiment (Fig.5.3.5.B) showed that a considerable amount of serum protein iC3b adduct was dissociated by incubation with hydroxylamine. In order to reach a decent separation of Sbi-C3b and Sbi-iC3b adducts, in Fig.5.3.5.A, an 8% acrylamide 2nd dimensional gel was used, but the small molecular weight Sbi-III-IV was not retainable on the gel. Therefore, the same sample was analyzed by a 12% 2nd dimensional gel (Fig.5.3.5.C) and anti-Sbi Western blot. Although free Sbi-III-IV was detected, no off-diagonal Sbi-III-IV was detected as a result of Sbi-C3b adduct disintegration.

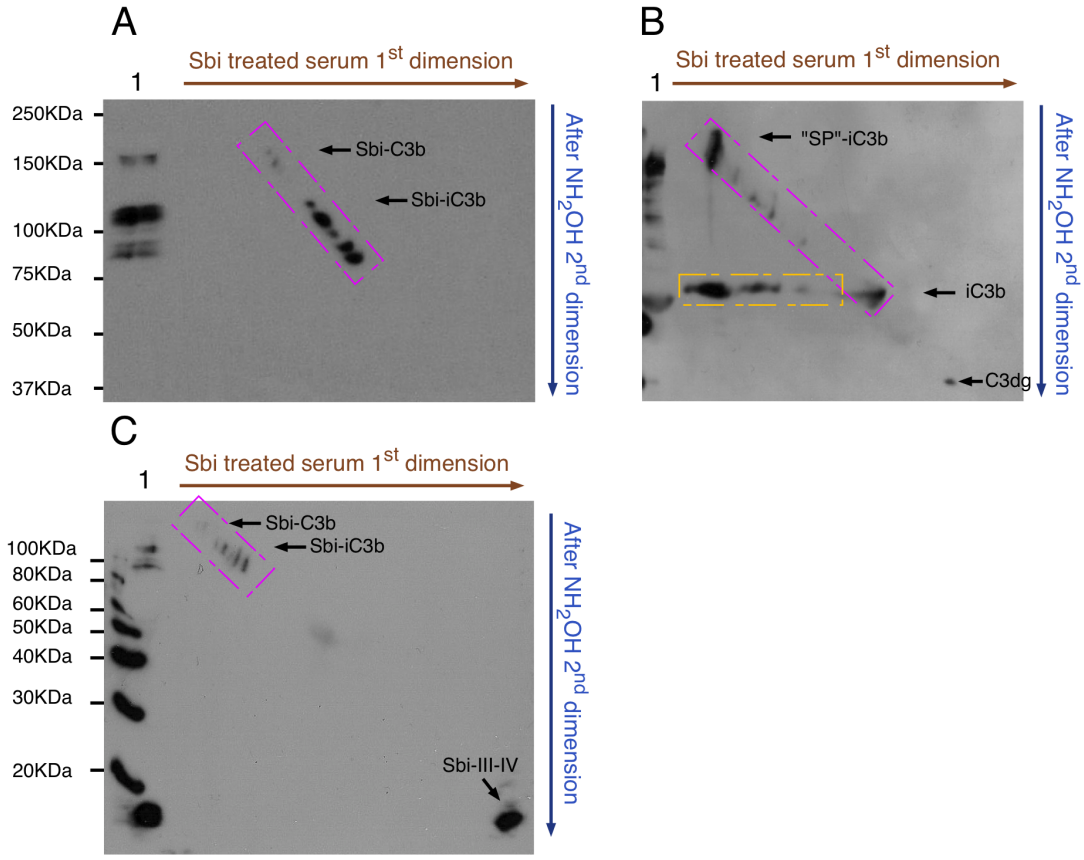

Figure 5.3.5: 2D gel and western blot analysis of the hydroxylamine treated Sbi-C3b adduct. (A) After hydroxylamine treatment the locations of the Sbi-C3b adduct were determined by anti-Sbi western blot. **(B)** After hydroxylamine treatment the locations of C3b/iC3b fragments were determined by anti-C3d Western blot. "SP-iC3b" is an abbreviation of serum protein iC3b adduct. **(C)** After hydroxylamine treatment the locations of Sbi-C3b adduct were determined by anti-Sbi western blot. The 2nd dimension was a 12% acrylamide gel that captures small molecular weight Sbi-III-IV. Lane 1 in all blots was Sbi treated serum sample without hydroxylamine treatment. On-diagonal spots are highlighted by pink dashed square. Off-diagonal spots are highlighted by yellow dashed square.

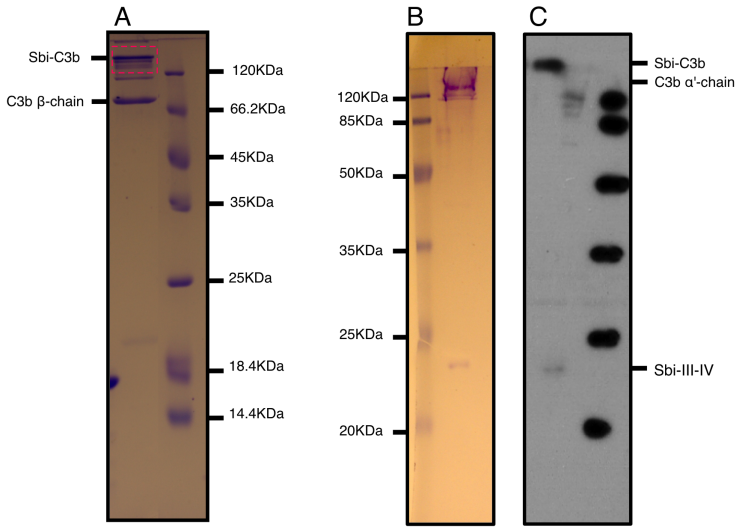

Figure 5.3.6: Hydroxylamine sensitivity assay using purified Sbi-C3b adduct. (A) SDS-PAGE profile of purified Sbi-C3b adduct. Before staining, the band highlighted by red dashed-line square was excised and treated with hydroxylamine. **(B)** 2nd dimension SDS-PAGE analysis of hydroxylamine treated Sbi-C3b α'-chain. **(C)** 2nd dimension anti-Sbi Western blot analysis of hydroxylamine treated Sbi-C3b α'-chain.

In the light of the newly developed method of *in vitro* production of Sbi-C3b adduct using the reconstituted AP pathway, the purified Sbi-C3b adduct was also subjected to a similar hydroxylamine sensitivity assay. Under the reconstituted AP condition, larger quantities of the Sbi-C3b adduct can be loaded on the gel, which decreases the difficulty of detection dramatically. This experiment demonstrated that a fraction of the purified Sbi-C3b adduct is dissociable (Fig.5.3.6.B) by hydroxylamine. However the anti-Sbi Western blot (Fig.5.3.6.C) also showed that the majority of the Sbi-C3b adduct remains intact.

5.3.2.3 The potential adduct formation sites on Sbi-III-IV

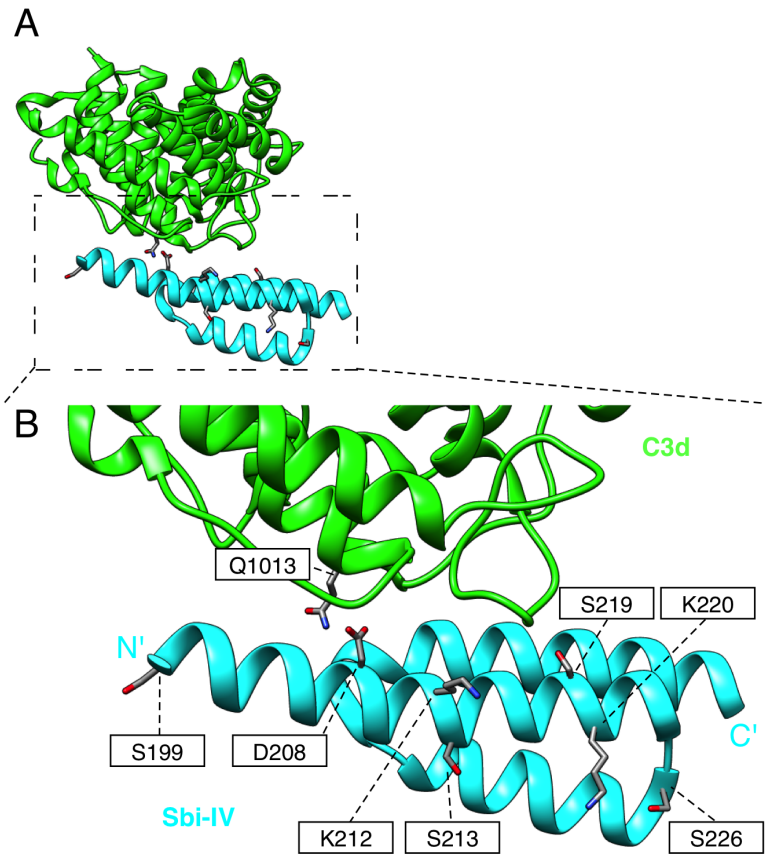

Figure 5.3.7: Crystal structure of the Sbi domain IV binding on the convex surface of C3d. (A) Sbi-IV (light blue) binding to the convex surface of C3d (green), the image was created using PDB file 2WY7. **(B)** A close-up image of the Sbi-IV:C3d interaction. Q1013 in the thioester region of C3d is able to form ester or amide linkages with hydroxyl or primary amine groups. On Sbi domain IV, K212 and S213 are the closest potential deposition targets. Other possible deposition targets in the vicinity are S199, S219, K220 and S226. In this structure, D208 is the closest residue to Q1013.

The exact adduct formation site(s) on Sbi-III-IV have been a subject of conjecture for years based on various circumstantial evidence. Initially, (Burman *et al*. 2008) proposed that the transacylation targets are the hydroxyl group containing residues located within Sbi domain III. This assumption was made based on the fact that neither C3 consumption nor covalent adduct formation occurred in the absence of Sbi-III. However, two years later, the crystal structure between Sbi-IV

and the C3d fragment prompted the emergence of an alternative possibility. In the crystal structure, two anti-parallel Sbi-IV molecules bind to both concave and convex surfaces of C3d, this dual binding model was supported by a NMR analysis (Clark *et al*. 2011) and an *in silico* protein binding dynamic modeling study (Gorham *et al*. 2014). The convex surface binding model (Fig.5.3.7) revealed Sbi-IV making a close contact with the thioester region of C3d, placing Sbi residues K^{212} and S^{213} in close proximity to the thiolactone ring component Q^{1013} in C3d.

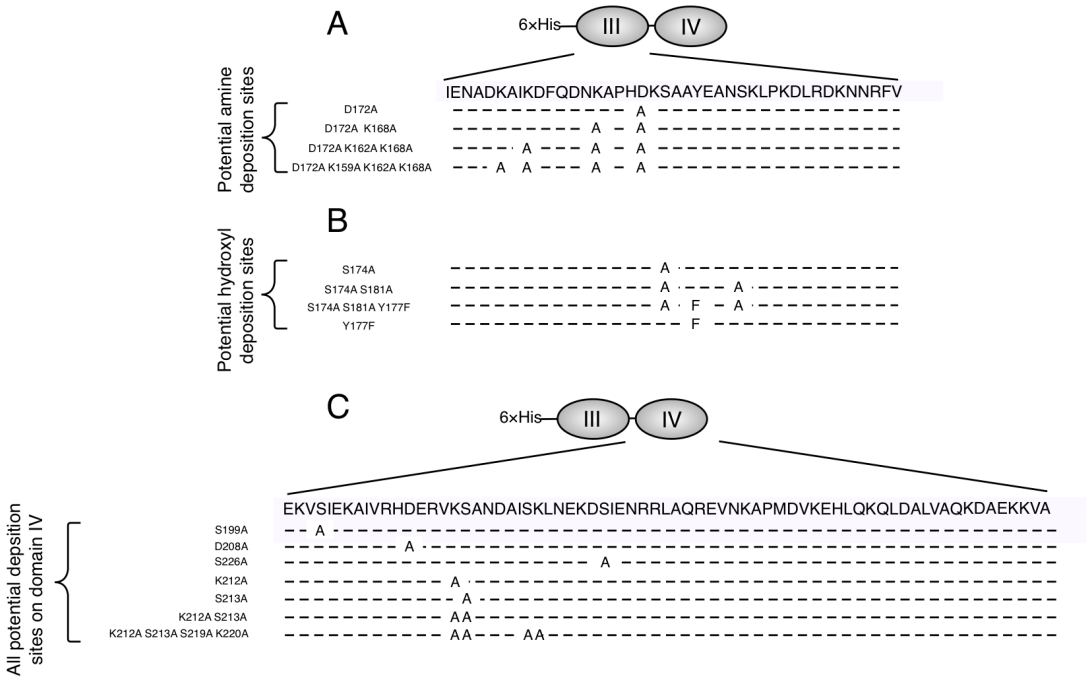

Figure 5.3.8: Sbi-III-IV single and multiple mutants used during the adduct formation site screening. (A) Sequential incorporation of domain III lysine mutation. **(B)** Sequential mutagenic depletion of domain III hydroxyl containing residues. **(C)** Sbi domain IV single mutants and multiple mutants.

Using the previous information and our recent finding that C3b deposition on Sbi-III-IV can occur on both hydroxyl and amine containing residues, one clear conclusion that emerges is that there could be multiple deposition sites on Sbi-III-IV. Therefore an accumulative mutagenesis strategy (Fig.5.3.8) was utilized to eliminate groups of potential transacylation targets on Sbi domain III

and IV, aiming to pinpoint the locations of adduct formation. Firstly a quadruple mutant of Sbi domain III residues (Fig.5.3.8.A) was made by the sequential substitution of D172, K168, K162 and K159 to alanine. Secondly, a triple mutant (Fig.5.3.8.B) of Sbi domain III hydroxyl residues was made by the sequential substitution of S174, S181 to alanine and Y177 to phenylalanine. Finally, according to the C3d convex surface binding of Sbi domain IV, a double mutant of K212A and S213A was made, based on which S219A and K220A mutations were then incorporated for the generation of a K212A-S213A-S219A-K220A quadruple mutant (Fig.5.3.8.C).

5.3.2.4 Mutagenic PCR reactions

Mutagenic PCR reactions were used to introduce multiple mutations to Sbi-III-IV constructs in a stepwise manner. As shown in Fig.5.3.9, the generation of three sets of Sbi-III-IV multiple mutants started with different templates. Using the single mutants (D172A, S174A and S212A) described in Section 4.3.6.1 as a template, further mutagenesis reactions were then carried out. Primers (Table 5.2.1) were designed based on the mutated DNA sequence after every cycle of mutagenesis reaction. To increase the possibility of mutation incorporation, for every mutation five PCR reactions were conducted using five distinct extension temperatures. The results of each PCR reaction were then analyzed by agarose gel electrophoresis. Fig.5.3.9 shows the PCR results for the incorporation of additional Sbi mutations. For every new mutation, at least two PCR conditions demonstrate significant amounts of PCR amplification products at the expected size. The majority of the mutagenesis reactions do not show bias over different extension temperatures. However when introducing Y177F to pQE30$^{\text{Sbi-III-IV S174A S181A}}$ plasmid, only relatively high extension temperatures (74.3°C and 75°C) produced PCR products. Despite the variation in the amount of PCR product, all mutagenesis experiments were successful. The incorporation of multiple mutations were confirmed by DNA sequencing (Appendix 9.1.2.2).

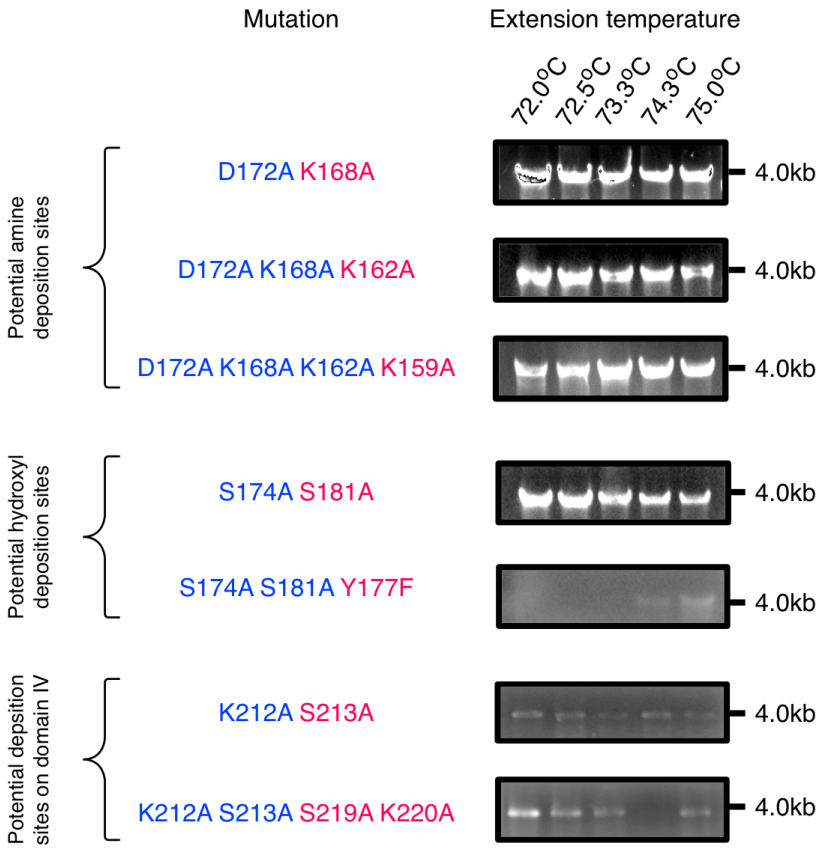

Figure 5.3.9: Agarose gel evaluation of the PCR amplification of mutations incorporated into the pQE30$^{Sbi\text{-}III\text{-}IV}$ plasmid. To generate accumulative mutants, for every cycle of PCR reaction a new PCR template was used. The pre-existing mutation in the PCR template is indicated by the blue colour, mutation intended to insert is indicated by the red colour. Mutagenic PCR reactions were carried out at five extension temperatures (72°C, 72.5°C, 73.3°C, 74.3°C and 75°C). The outcomes of mutation insertion and PCR amplification were represented by the intensity of the DNA band at 4.0 kb.

4.3.2.5 Expression and Purification of Sbi-III-IV accumulative mutants

After the successful incorporation of multiple mutations into the pQE30$^{Sbi\text{-}III\text{-}IV}$ plasmid, the mutated plasmids were extracted and transformed into the *E.coli* expression cell line BL21 (DE3). The mutant proteins were expressed and purified using the same protocol as the WT Sbi-III-IV (Section 3.2.1). After IPTG induced over-expression, *E.coli* cells were lysed and solubilized in HisA buffer. The soluble fraction of the cell was then loaded on a 1ml Histrap FF column. The purification of Sbi-III-IV multiple mutants is shown by a typical chromatogram

profile (Fig.5.3.10.A); with the Sbi-III-IV$^{S174A\ S181A\ Y177F}$ being the only exception. This mutant did not produce a significant elution peak (Fig.5.3.10.B). As discussed previously the mutation of the only UV 280nm absorptive residue (Y177) renders the protein undetectable. Three putative peak fractions were collected for each Sbi-III-IV mutant. The final and purest fraction was buffer exchanged to PBS. The purity of all the purified Sbi-III-IV multiple mutants was then assessed by SDS-PAGE analysis (Fig.5.3.11).

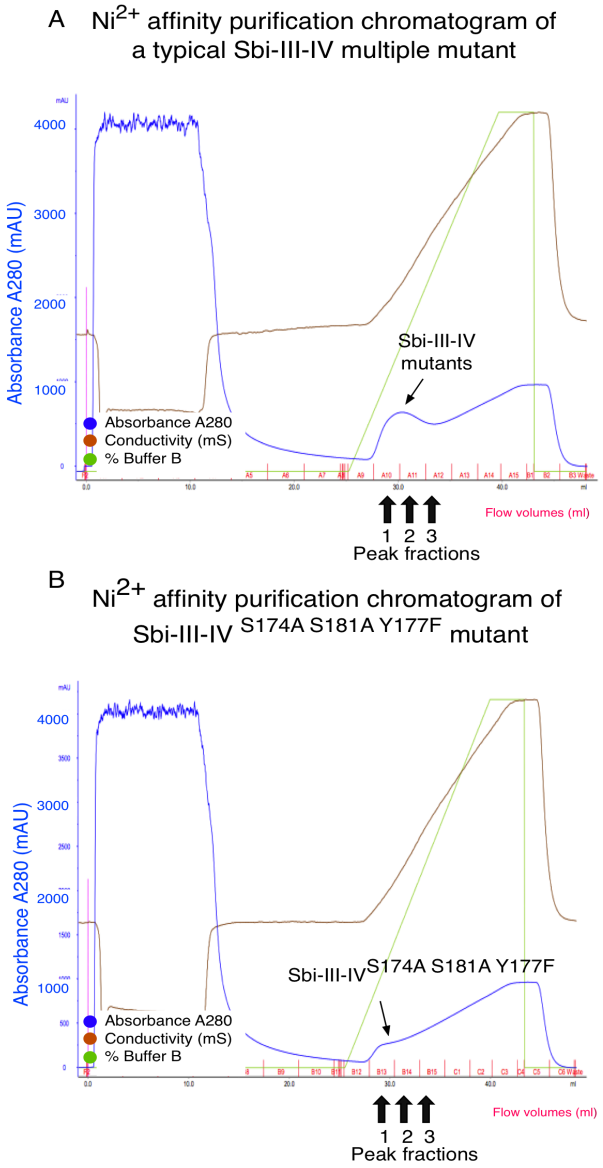

Figure 5.3.10: Ni^{2+} affinity purification of Sbi-III-IV multiple mutant. (A) A typical chromatogram for a Sbi-III-IV multiple mutant. After loading and intensive washing, every mutant protein was eluted with a 12 column volume gradient of HisB buffer. Peak fractions (1,2 and 3 as pointed by black arrows) of every Sbi multiple mutants were collected. **(B)** Chromatogram of Sbi-III-IV$^{S174A\ S181A\ Y177F}$. No significant elution peak was detected. However, the putative peak fractions 1-3 were collected.

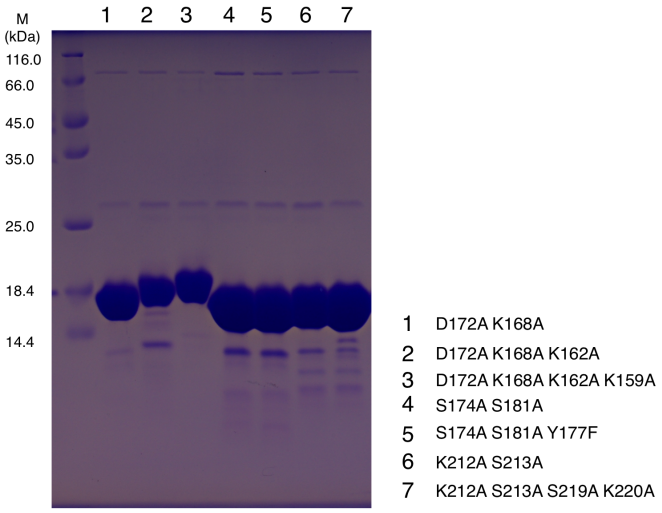

Figure 5.3.11: SDS-PAGE analysis of purified Sbi-III-IV multiple mutants. The purified Sbi-III-IV is generally located between 18.4 kDa and 14.4 kDa molecular weight markers. The sequential substitution of domain III lysines (lane 1-3) produces a series of Sbi-III-IV band up-shifts.

5.3.2.6 C3b deposition screening

As demonstrated in chapter 4 (Section 4.3.6.2), various mutations in Sbi-III-IV can cause different degrees of impact on Sbi-III-IV's activity. In addition, it was also shown in Chapter 4 that the Sbi-C3b adduct is subjected to factor I cleavage immediately after formation, and different Sbi-III-IV mutant:C3b adducts could also be degraded at different rates. These functional variations of Sbi-III-IV mutants inevitably cause fluctuations in the quantity of Sbi-C3b adduct formation in normal serum. Therefore, instead of performing quantitative assessments of Sbi-C3b adduct formation in normal serum, factor I depleted serum was utilized (Section 5.2.7). By depleting factor I from serum, the AP of complement system activates spontaneously in the presence of magnesium ions, and the resulting C3b molecules remain unprocessed. Under this experimental system, different Sbi-III-IV mutants are subjected to the same amount of complement activation, enabling a true assessment of their intrinsic ability to be deposited on by C3b.

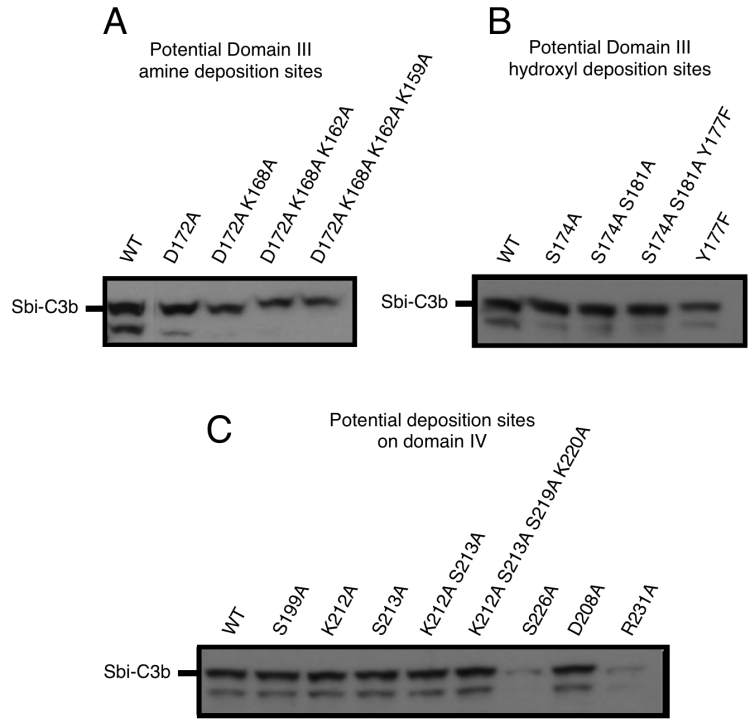

Figure 5.3.12: Anti-Sbi Western blot detection of Sbi-C3b adduct formation in Factor I depleted serum. (A) Adduct formation of Sbi-III-IV mutants designed to study potential amine deposition sites on domain III. **(B)** Adduct formation of Sbi-III-IV mutants designed to study potential hydroxyl deposition sites on domain III. **(C)** Adduct formation of Sbi-III-IV mutants designed to study potential deposition sites on domain IV.

Various Sbi-III-IV mutants (20 μM) were incubated with factor I depleted serum and the amount of Sbi-C3b adduct formation was subsequently assessed using polyclonal anti-Sbi Western blots. Fig.5.3.12.A demonstrates that with an increasing number of Sbi domain III lysine mutations, a decreasing trend of Sbi-C3b adduct formation was observed. At the same time, the sequential removal of Sbi domain III hydroxyl-containing residues shows no significant impact on adduct formation level (Fig.5.3.12.B). We also found that the residues that contribute the most to Sbi-C3b formation were located within domain IV (Fig.5.3.12.C). Based on the binding model of Sbi-IV on the convex surface of C3d (Fig.5.3.7), S199A, D208, K212A, S213A, S219A and K220 are the closest residues to the C3d thioester region. However substitutions of these residues do not produce any significant reduction in adduct formation levels. Conversely, the

substitution of S226 by an alanine residue does severely impair the adduct formation process, which correlates with the result presented in Fig.4.3.12. However, the analysis here suggests that S266A is able to form a minimal amount of the Sbi-C3b adduct. Another mutation that was found to also contribute to adduct formation is R231A. R231 is an essential residue for the interaction between the C3 TED domain and Sbi-III-IV.

5.3.2.7 C3b deposition site determination: a mass spectrometry approach

Adduct formation assays demonstrated that the S226A substitution dramatically reduces C3b deposition on Sbi-III-IV. But, no other significant deposition sites were identified; especially neither single nor multiple lysine mutants demonstrate significant reduction in adduct formation. However, the hydroxylamine sensitivity assays clearly suggested that the Sbi-C3b is also linked through an amide bond. Therefore, a mass spectrometry approach was developed and utilized to reveal the full repertoire of the adduct formation sites on Sbi-III-IV.

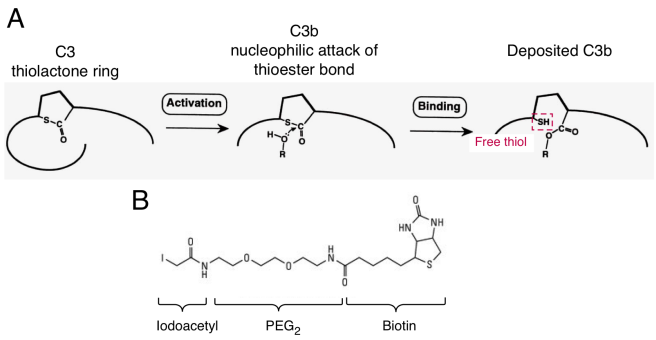

Figure 5.3.13: (A) Covalent binding reaction of C3. The free thiol group available after reaction is highlighted by red square. Image taken from (Law & Dodds 1997)
(B) Iodoactyl-PEG_2-Biotin label

It is known that after the hydrolysis of the thioester in C3 (Fig.5.3.13.A), a free thiol group (C^{1010}) emerges in hydrolyzed C3b and is available for labeling. Previous studies (Shohet *et al*. 1993; Sarrias *et al*. 2001) demonstrated that various functional experiments can be carried out based on the reactivity of this free thiol group.

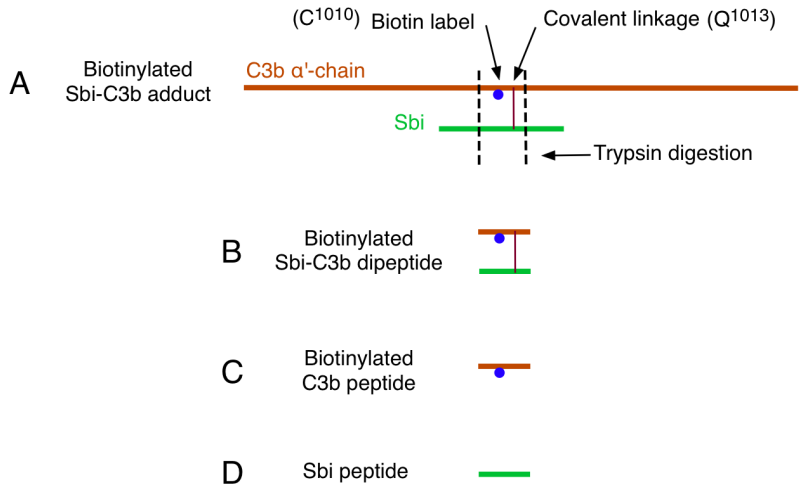

Figure 5.3.14: (A) Primary sequence presentations of biotinylated Sbi-C3b adduct, **(B)** Biotinylated Sbi-C3b adduct dipeptide, **(C)** Biotinylated C3b peptide and **(D)** Sbi peptide.

In this study, the free thiol group was labeled with an irreversible biotin tag (Fig.5.3.13.B) for the identification of C3b deposition sites on Sbi-III-IV. The primary sequence of the biotinylated Sbi-C3b adduct (Fig.5.3.14.A) shows that Q^{1013} in the C3b α' chain is linked covalently to an unknown residue in Sbi-III-IV. Given that there is no trypsin digestion site between C3 linkage site Q^{1013} and biotinylation site C^{1010}, it would be possible to purify the biotinylated Sbi-C3b trypic fragment (Fig.5.3.14.B) using biotin affinity resin and subsequently determine its molecular weight by mass spectrometry. By subtracting the mass of the biotinylated Sbi-C3b adduct peptide using the mass of the C3b peptide (Fig.5.314.C), the mass of the Sbi peptide (Fig.5.3.14.D) can be calculated. Finally, by referencing with the *in silico* Sbi-III-IV trypsin digestion simulation (Section 5.2.12), the mass of the Sbi peptide could then be interpreted as the peptide fragment of the Sbi primary sequence.

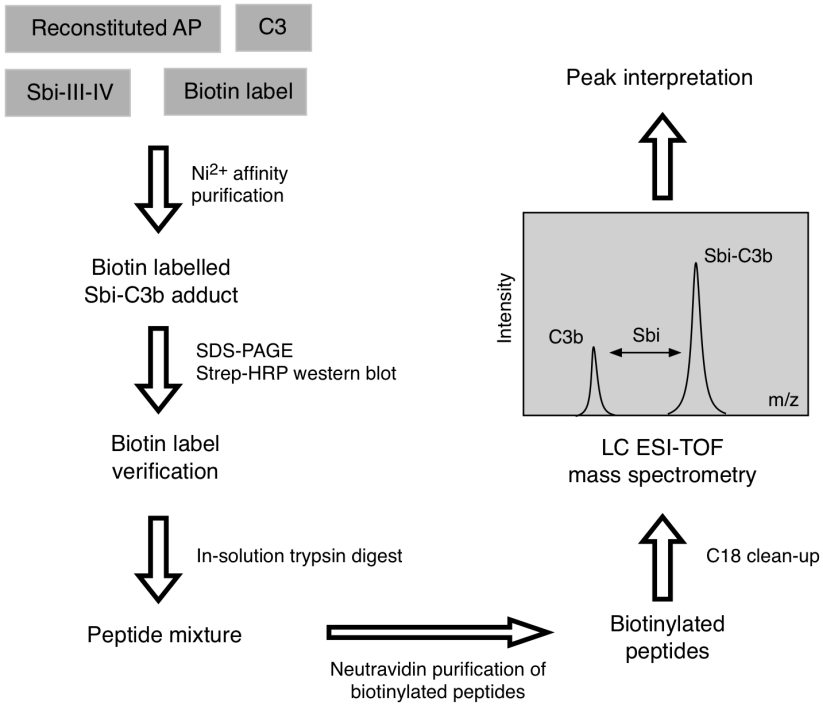

Figure 5.3.15: Experimental design for Sbi-C3b adduct peptide preparation

A flow chart detailing the experimental design of the adduct peptide purification is presented in Fig.5.3.15. Firstly, Sbi-C3b was generated with the previously described AP *in vitro* reconstitution method, but with slight modification (Section 5.2.2). Iodoacetyl-PEG2-Biotin label was added during incubation, to label the free thiol group immediately after it become available. After Ni^{2+} affinity purification, the purity and the labeling of Sbi-C3b adduct were evaluated by SDS-PAGE analysis and Strep-HRP Western blot. Fig.5.3.16 shows that the Sbi-C3b adduct was successfully produced and purified, at the same time the C3b α'chains in Sbi-C3b adduct and hydrolyzed C3b molecule were successfully labeled with a biotin molecule. As an internal control, the C3 α chain and β chain did not react to the biotin label, which suggested the labeling process was specific to a free thiol group at C^{1010}. The biotinylated Sbi-C3b adduct was then concentrated, reduced, denatured and subjected to prolonged in-solution trypsin digest (Section 5.2.8). From the resulting peptide mixture, neutravidin resin was used to purify the biotinylated peptide. After binding and intensive washing, the

biotinylated peptides were released from the resin using 6 M guanidine HCl pH 1.2 (Section 5.2.8). C18 spin columns were then used to de-salt the peptide sample, preparing the samples for mass spectrometry analysis (Section 5.2.10).

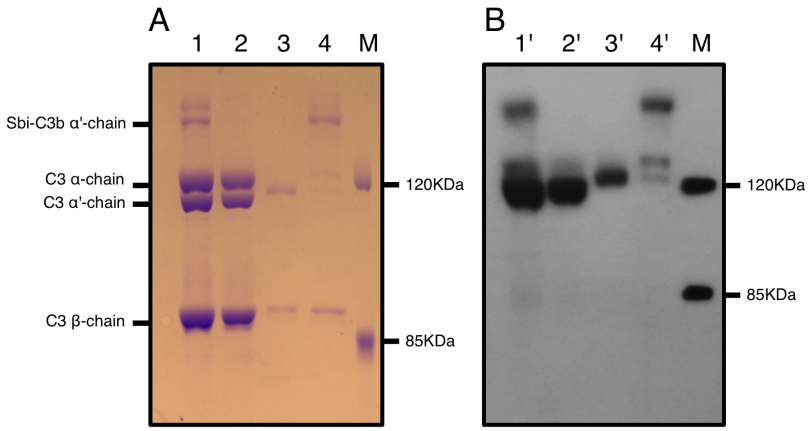

Figure 5.3.16: Producing, purifying and labeling of the Sbi-C3b adduct. (A) SDS-PAGE analysis of Sbi-C3b adduct purification. **(B)** Streptavidin-HRP western blot. Lane 1 After Sbi-C3b adduct formation, 2 Flow-through fraction, 3 Wash fraction, 4 Elution fraction.

The electrospray ionization time of flight mass spectrometry (ESI-ToF-MS) analysis of purified Sbi-C3b peptide sample yielded a variety of peptide masses from 4 kDa to 20 kDa (Fig.5.3.17 A-C). When compared with the mass spectrum of the C3b derived peptide (Fig.5.3.18), a similar peak of putative C3b monomeric peptide was also observed in the Sbi-C3b peptide spectrum (Fig.5.3.17.C). This suggested that a fraction of the covalent linked Sbi-C3b peptide was too fragile to survive the peptide preparation and the MS ionization processes, therefore only the vestigial C3b peptide peak was observed. In addition, it was also noticeable that there were a considerable number of peaks overlapping between Sbi-C3b and the neutravidin peptide (Fig.5.3.19) spectra. This is likely to be a consequence of the leaching of the neutravidin resin during the peptide elution process. However, there were three masses (5309.30 Da, 6516.4 Da and 6584.12 Da) that were unique to the Sbi-C3b peptide spectra (Fig.5.3.17 A-B) and could represent the possible Sbi-C3b adduct peptides.

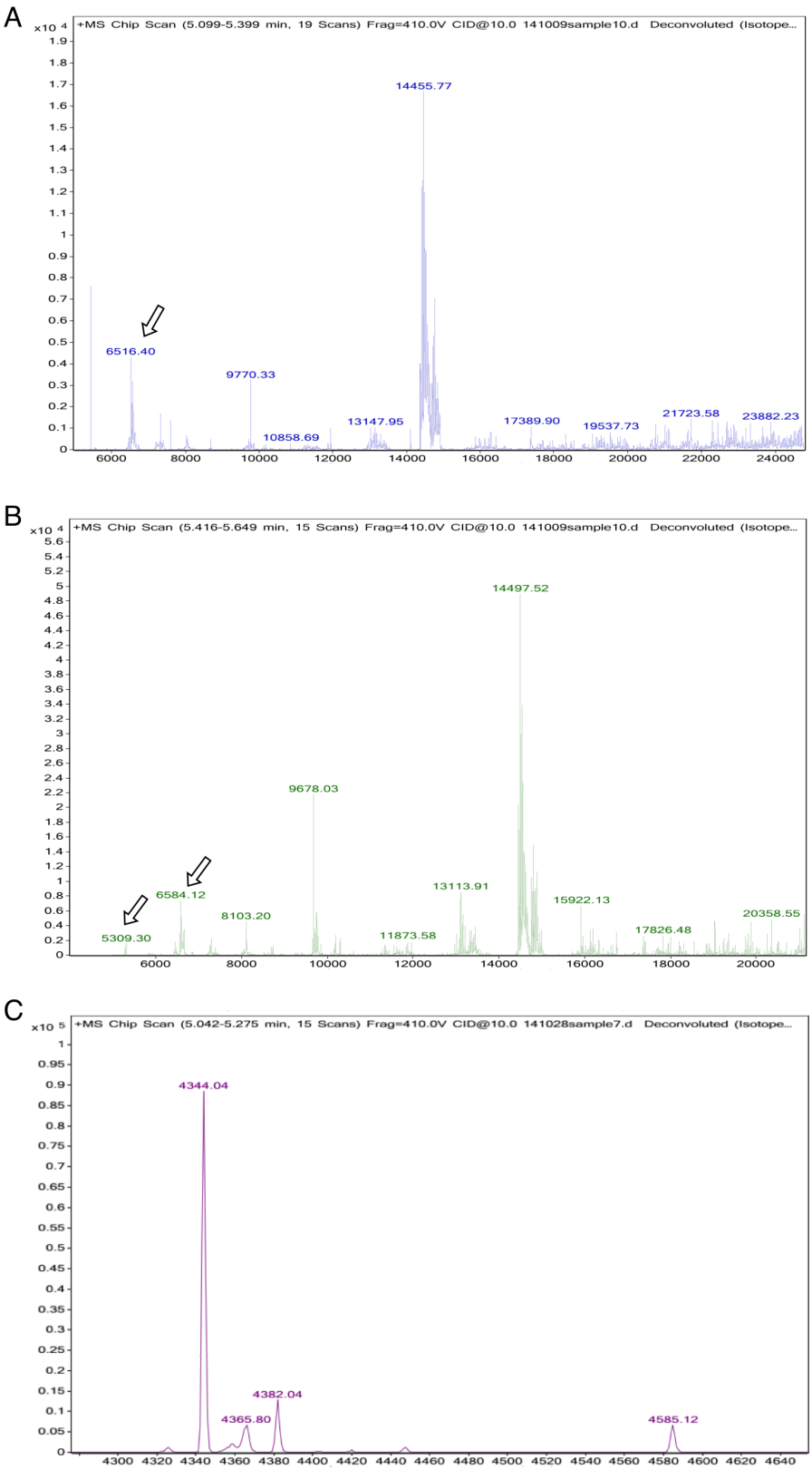

Figure 5.3.17: LC coupled ESI-ToF mass spectra of Sbi-C3b adduct peptides. **(A)** Peptides eluted between 5.099-5.399 min **(B)** Peptides eluted between 5.416-5.649 min **(C)** Mass spectra between 4200 Da to 4650 Da. Peptide masses (indicated by arrow) 6516.40 Da, 6584.12 Da and 5309.30 Da were selected for interpretation.

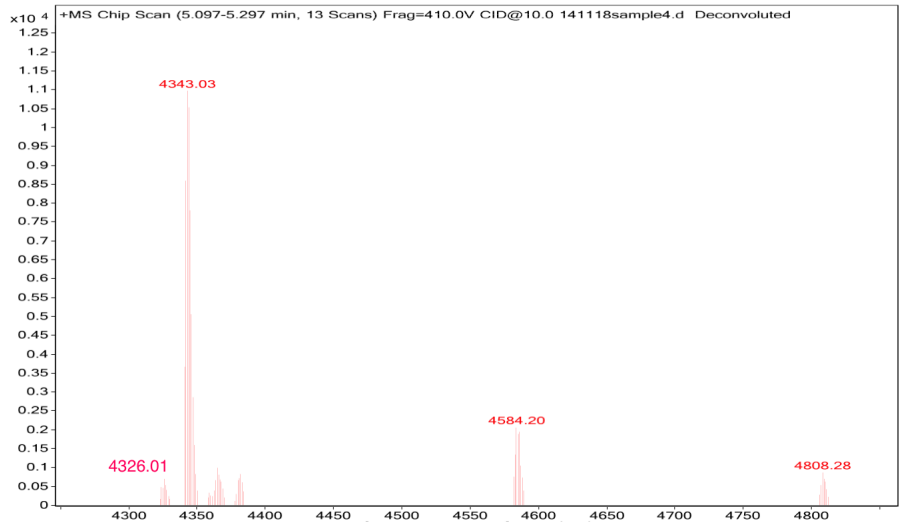

Figure 5.3.18: LC coupled ESI-ToF mass spectrum of the C3b peptide. Mass spectrum between 4200 Da to 5000 Da.

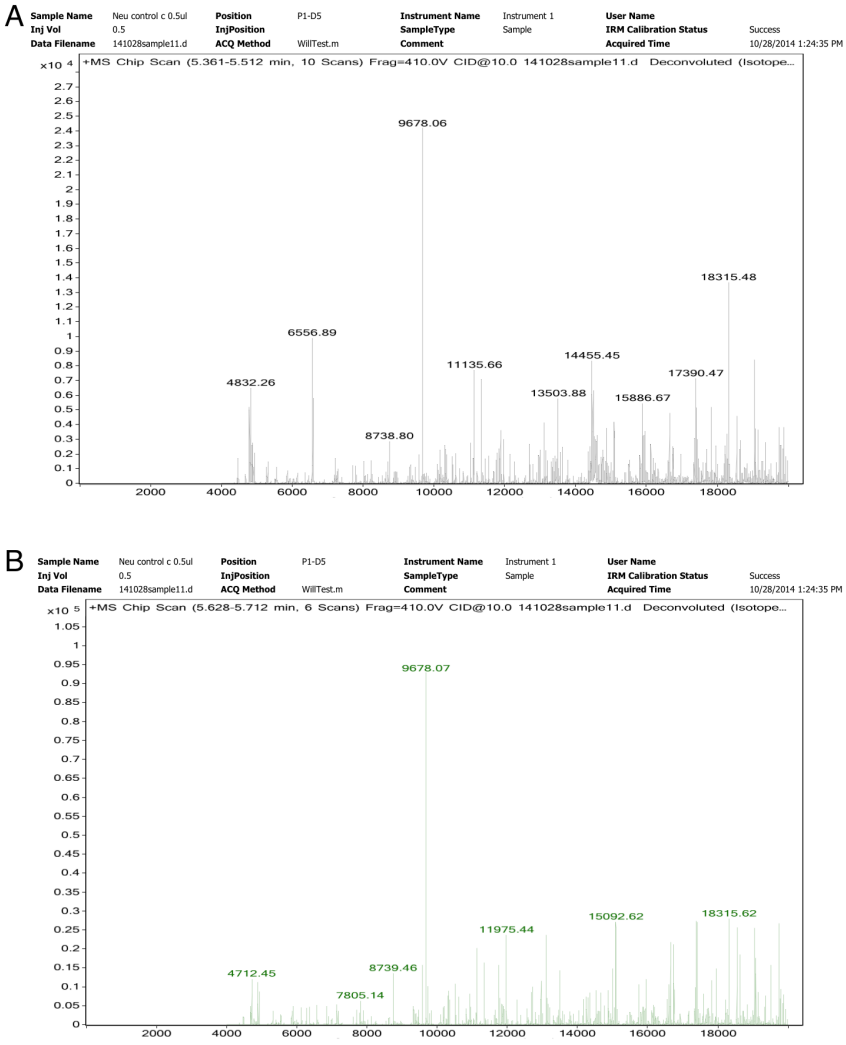

Figure 5.3.19: LC coupled ESI-TOF mass spectra of the neutravidin peptide. (A) Peptides eluted between 5.097-5.297 min (B) Peptides eluted between 5.628-5.712 min

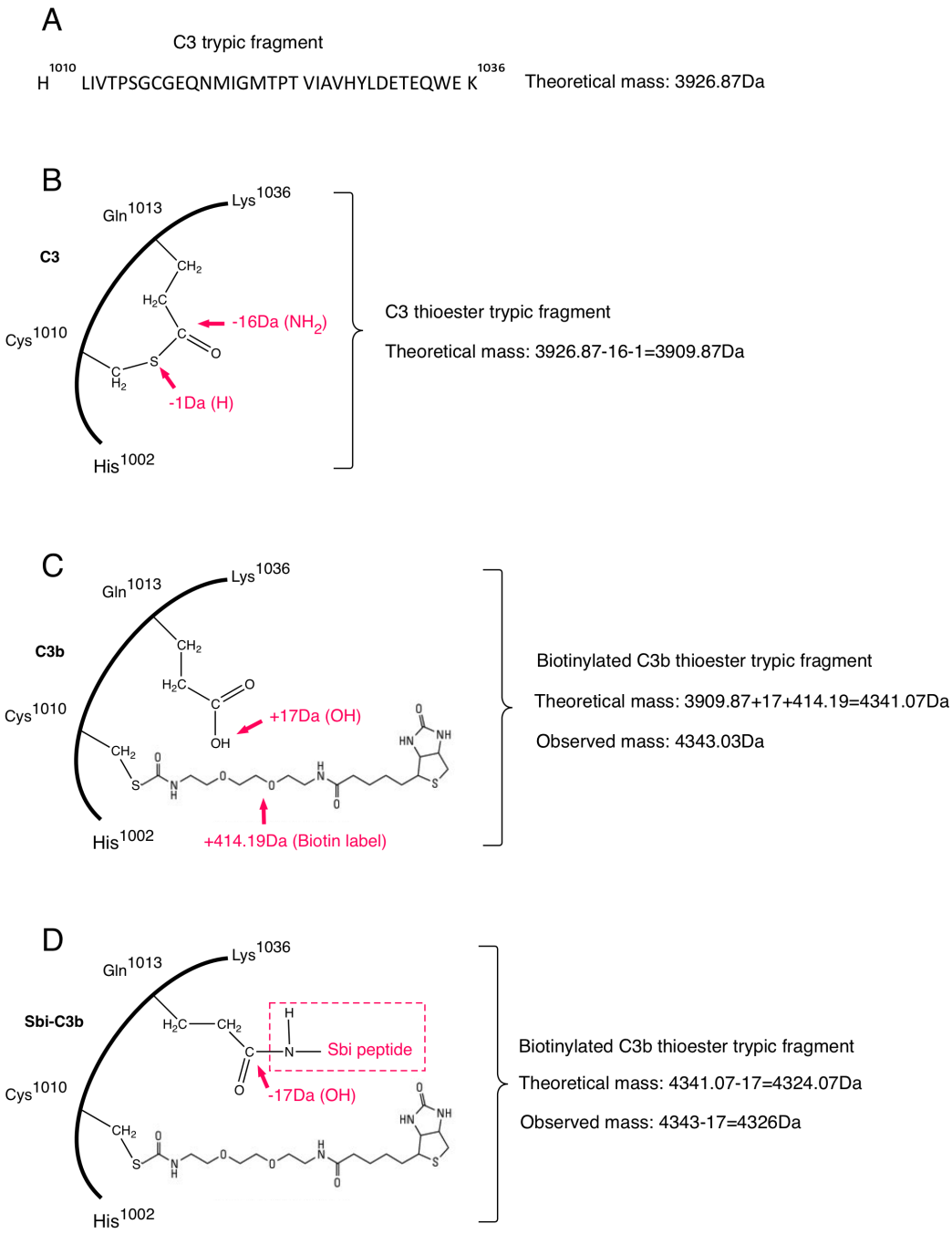

Figure 5.3.20: C3 thioester trypic peptide molecular weight variations.

In order to interpret the putative Sbi-C3b adduct peptide peaks, it was a prerequisite to establish the mass of the biotinylated C3b monomeric peptide. Firstly, the theoretical mass of the C3 thioester trypic fragment was calculated based on its primary sequence (Fig.5.3.20.A). Due to the formation of the thioester bond between the side chains of C^{1010} and Q^{1013}, the masses of an amine

group and a hydrogen atom were then subtracted (Fig.5.2.20.B). However, in the hydrolysed C3b molecule, the hydrolysis of the thioester results in the addition of a hydroxyl group and biotin label (Fig.5.3.20.C). But when C3b is covalently deposited on Sbi, the additional hydroxyl group is then replaced by the Sbi peptide (Fig.5.3.20.D).

The mass spectrum shown in Fig.5.3.18 demonstrates a major peak of 4343.03 Da, which is less than 2 mass units heavier than the theoretical mass of the hydrolysed C3b thioester fragment (Fig.5.3.20.C). This slight mass discrepancy could be the result of different protonation of the peptide or chemical modifications that occurred during preparation stage. Given that the C3b monomeric peptide and Sbi-C3b adduct peptide were derived from the same C3 sample and prepared using the same protocol, the peak of 4343.03 Da was utilized as the molecular weight of the hydrolysed monomeric C3b peptide. Based on this mass, the molecular weight of Sbi deposited C3b monomeric peptide (Fig.5.3.20.D) was calculated. The resulting mass of 4326 Da was utilized in following Sbi-C3b adduct peptide peak interpretation (Table 5.3.1).

Table 5.3.1: Sbi-C3b adduct peptide peak interpretation. 1Da was subtracted from all Sbi trypic fragments, due to the loss of one hydrogen atom during amide bond formation. Sbi trypic digestion simulation is presented in appendix Fig.9.8

Biotinylated C3b fragment (Da)	Sbi trypic fragment (-1Da)	**C**alculated peptide mass (Da)	**O**bserved peptide mass (Da)	Mass Differences ($\|\boldsymbol{C}-\boldsymbol{O}\|$Da)	Sbi domain & Residue$^{\text{Number}}$	Trypsin miss cleavage
4326	983.56	5309.56	5309.30	0.26	IV Q^{251}-K^{259}	0
4326	2191.20	6517.2	6516.4	0.8	IV E^{246}-K^{264}	3
4326	2260.16	6586	6584.12	1.88	IV A^{240}-K^{259}	2

Calculations involved in the Sbi-C3b adduct peptide peak interpretation are summarized in Table 5.3.1. Briefly, utilizing the observed masses of the putative

Sbi-C3b adduct peptide (Fig.5.3.17.A-B) and subtracting the mass of the C3b monomeric peptide, the masses of three possible Sbi peptides were identified with molecular weights: 983.56, 2191.2 and 2260.16 Da. Then, by cross-referencing with the Sbi-III-IV trypsin digestion simulation (Appendix Fig.9.8), three possible Sbi peptide trypic fragments were found. Two out of the three matches show less than 1 mass unit discrepancy from the calculated masses, however a possible peptide fragment larger by 2 mass units was also considered as a match.

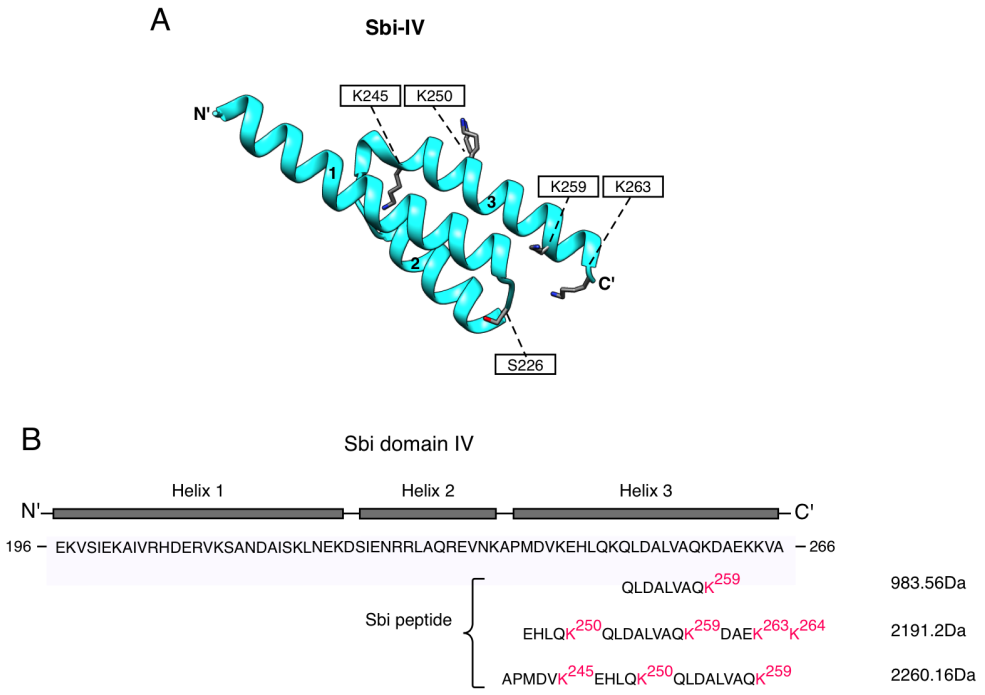

Figure 5.3.21: Amino acid and peptide mapping of Sbi peptide. (A) Potential lysine deposition sites on Sbi domain IV. **(B)** Mapping of Sbi peptide fragment on Sbi domain IV.

Peptide mapping shows that all three peptides are located at the C-terminal end of the Sbi domain IV, as part of helix 3 (Fig.5.3.21.B). The primary sequence of these peptides does not contain any hydroxyl-containing residues. However five lysine residues (K245, K250, K259, K263 and K264) are distributed over the 25 residue-long segment (Ala^{240} to Lys^{264}) corresponding to the identified peptides. Thus, in addition to the previously identified hydroxyl deposition site S226, this MS analysis suggested that multiple lysine deposition sites are also involved in the formation of Sbi-C3b adduct.

5.3.2.8 Lysine deposition sites verification via accumulative mutagenesis

As demonstrated in the above section, the MS results implicated that multiple Sbi domain IV lysine residues are likely to be involved in the adduct formation process. To verify this finding, all five lysine residues were mutated to alanine accumulatively. The effect of the stepwise mutations was then examined by the factor I depleted serum adduct formation assay. Prior to the mutagenesis experiment, the newly identified lysine deposition sites were mapped on the structure of Sbi-IV together with residues previously suspected as the potential adduct formation sites. In the structure, (Fig.5.3.22) the potential deposition sites (K212 S213 S219 and K220) are in close proximity to the newly discovered lysine deposition sites in helix 3, although as previous demonstrated (Fig.5.3.12.C), these four residues are not significantly involved in the process of adduct formation. But given that the nascent C3b thioester has a half-life of 100 μs and reacts nearly non-discriminately with hydroxyl and amine groups, it is possible that these four residues take on the role of targets for C3b deposition upon the mutagenic removal of the lysine residues in helix 3. Therefore, in this mutagenesis experiment the accumulative lysine to alanine substitution mutations were inserted based on both Sbi-III-IV^{WT} and Sbi-III-IV$^{K212A\ S213A\ S219A\ K220A}$ (KSSK) templates.

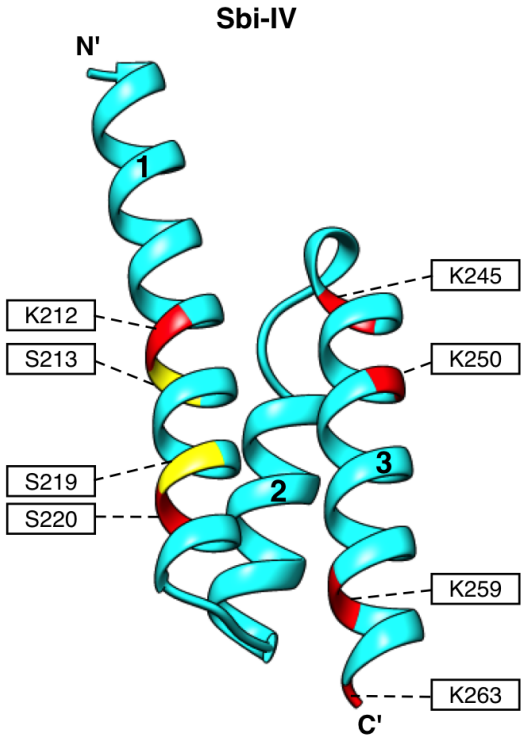

Figure 5.3.22: Potential C3b deposition sites on Sbi domain IV helix 1 and 3.

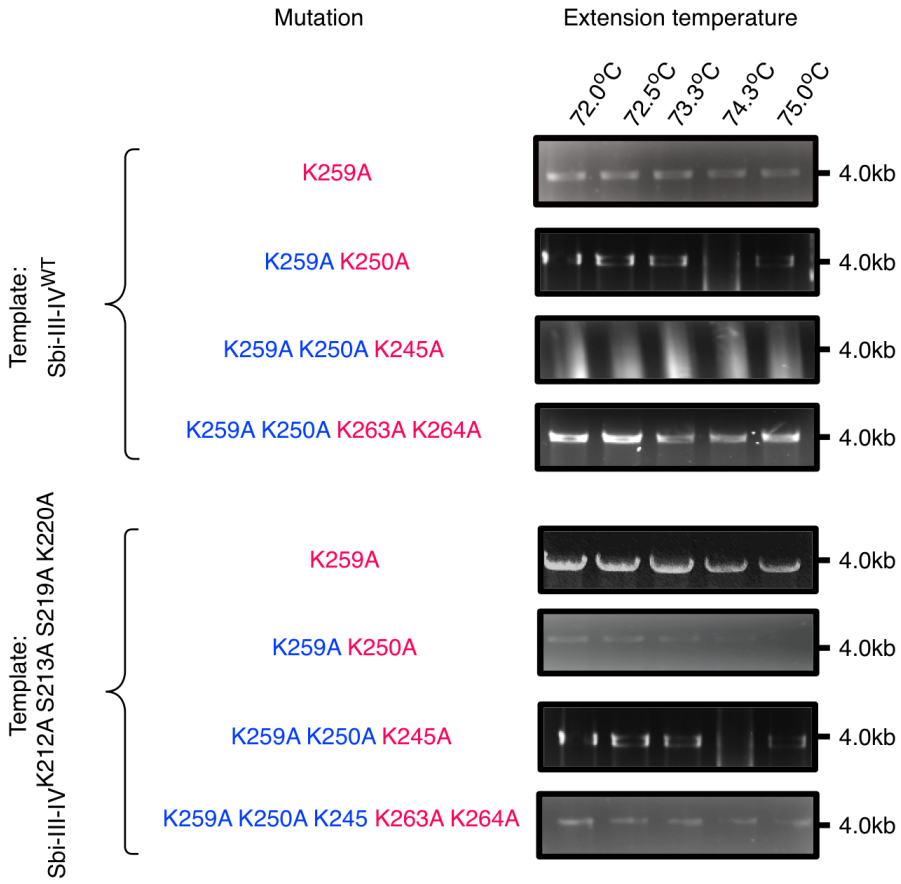

Figure 5.3.23: Agarose gel evaluation of the PCR amplification of mutation incorporated pQE30$^{Sbi\text{-}III\text{-}IV}$ plasmid. To generate accumulative mutants, for every cycle of PCR reaction a new PCR template was used. The pre-existing mutation in the PCR template is indicated by blue colour, mutation intended to insert is indicated by red colour. Mutagenic PCR reactions were carried out at five extension temperatures (72°C, 72.5°C, 73.3°C, 74.3°C and 75°C), the outcomes of mutation insertion and PCR amplification were represented as the intensity of the DNA band at 4.0 kb.

A series of lysine substitution mutations were inserted using mutagenic PCR reaction in a stepwise fashion. Based on pQE30$^{Sbi\text{-}III\text{-}IV}$ WT and KSSK templates, five lysine mutations were introduced in the order of K259A, K250A, K245A and finally K263A K264A (Fig.5.4.23). Primers (Table 5.2.2) were designed based on the mutated DNA sequence. Special primers were designed to mutate K263 and K264 at the same time. A similar extension temperature screen was also carried out. For every mutation five PCR reactions were conducted using five distinct extension temperatures and the results of each PCR reaction was then analyzed by agarose gel electrophoresis. Fig.5.3.23 shows the results for every mutagenic PCR reaction. Normally at least two PCR conditions demonstrate a significant

amount of PCR amplification products, and a preference of lower extension temperature was observed. But despite multiple attempts, the K245A mutation failed to be introduced into the Sbi-III-IV$^{K259A\ K250A}$ template, thus in total four lysine substitution mutations (K259A, K250A, K263A and K264A) were introduced to Sbi-III-IV WT template. Apart from this mutation, the rest of the mutagenesis experiments were successful, and the incorporation of multiple mutations was confirmed by DNA sequencing (Appendix 9.1.2.2). Expression and purification of Sbi-III-IV mutant were described in Section 4.2.1. Three peak fractions were collected according to the chromatograms and analyzed by SDS-PAGE (Fig.5.3.24). According to the SDS-PAGE analysis, the purest peak fraction of every mutant was selected and buffer exchanged to PBS buffer.

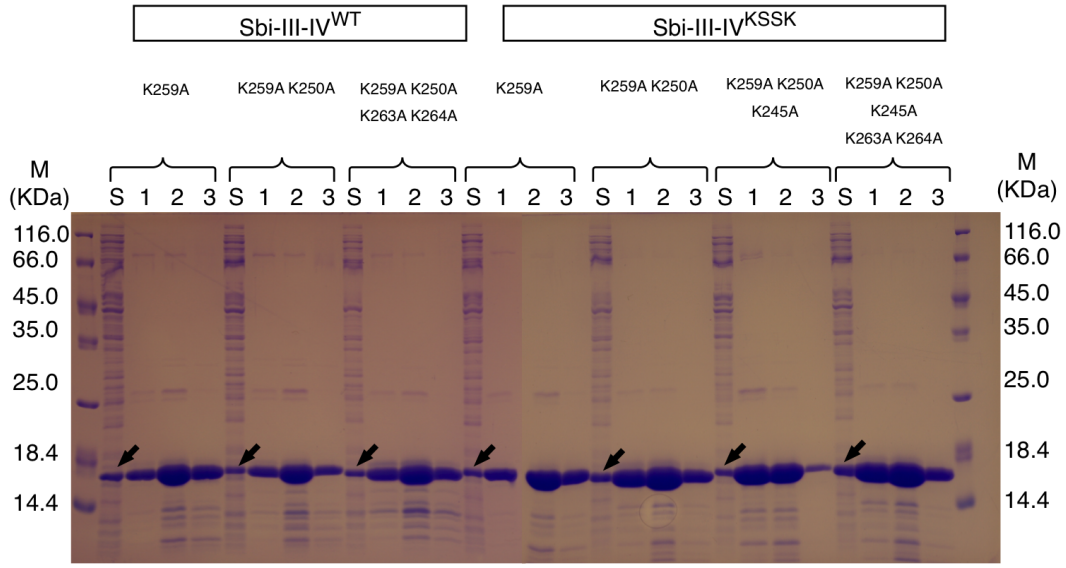

Figure 5.3.24: SDS-PAGE gel analysis of Sbi-III-IV mutant purifications. For every Sbi-III-IV mutant, four samples were analyzed, soluble fraction (S) and three peak fractions (1, 2 and 3). Expressions of the recombinant Sbi-III-IV mutant are indicated by black arrows. The majority of the recombinant protein was eluted in peak fractions 2 and 3.

5.3.2.9 Factor I depleted serum deposition assay of Sbi domain IV accumulative mutants

All accumulative lysine mutants (20 μM) were incubated with factor I depleted serum, then the amount of adduct formation was detected by Western blot

analysis. Anti-His tag antibody was utilized in this experiment, because the large number of mutations in the Sbi-III-IV could deform its epitope and affect anti-Sbi antibody recognition. Fig.5.3.25 shows that with the increasing number of lysine substitution mutations introduced, both series of mutant proteins become dramatically less likely to be deposited on by the C3b molecule. According to the gel densitometry quantification of the bands, on substitution of lysine 259, 250, 263 and 264 with alanine residues, a 70 percent decrease in adduct formation was observed (Fig.5.3.25.C). Even more dramatically, based on the template of Sbi-III-IV KSSK, the substitution of all five helix 3 lysine produced an 85 percent drop in the amount of adduct formation (Fig.5.3.25.D). These results correlate with the MS data, proving that lysine residues on Sbi domain IV helix 3 are the hydroxylamine insensitive covalent attachment sites for nascent C3b molecules.

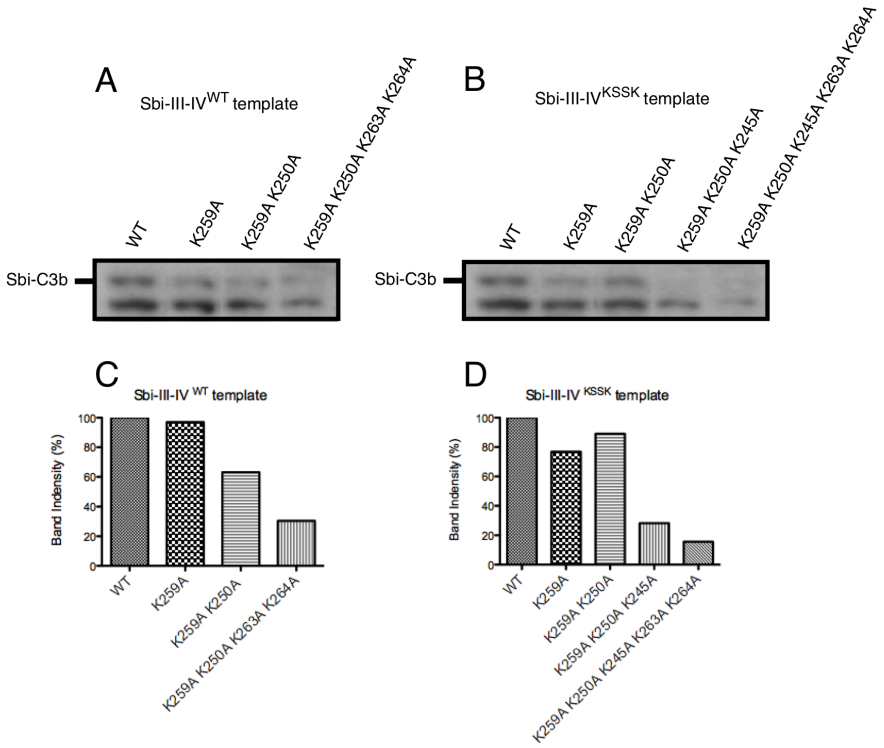

Figure 5.3.25: Anti-His tag Western blot detection of Sbi-C3b adduct formation in Factor I depleted serum. (A) Accumulative lysine mutants based on Sbi-III-IV^{WT} template **(B)** Accumulative lysine mutants based on Sbi-III-IV^{KSSK} template **(C)** Gel densitometry quantification of A. **(D)** Gel densitometry quantification of B.

5.3.2.10 C3 binding strength of Sbi-III-IV lysine accumulative mutants

As shown by the C3b deposition assay (Fig.5.3.25), the accumulation of lysine substitution mutations in the C-terminal of Sbi domain IV dramatically reduces the amount of C3b deposited on Sbi-III-IV. However, it was also known that Sbi-III-IV R231A with severely impaired C3 binding strength also leads to reduced adduct formation level (Fig.5.3.12.C). Given that Sbi domain IV mediates C3 binding, therefore the insertion of a considerable amount of lysine mutations could jeopardize the C3 binding property, thus leading to an artifact of adduct-formation reduction. To verify the C3 binding property of Sbi domain IV lysine mutants, ELISA C3 binding assays were performed.

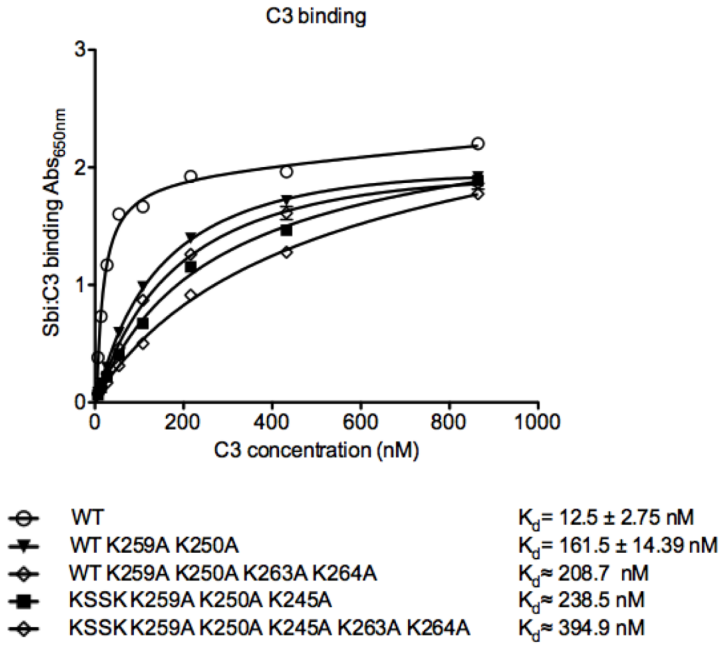

Figure 5.3.26: C3 binding curves of Sbi domain IV lysine mutants. Sbi-III-IV mutants were immobilized and for each type of Sbi the concentration dependent binding of C3 (0-900 nM) was measured by polyclonal anti-C3 antiserum. The K_d of C3 binding was determined from the fitted curve using GraphPad Prism.

Firstly, dose-dependent binding of C3 was measured. Fig.5.3.26 shows that all lysine mutants require increased C3 concentration to reach saturated binding compared to the WT protein. Estimated from the binding curve, the K_d for the Sbi-III-IV^{WT}:C3 interaction is around 12.47 nM. In comparison, Sbi-III-IV$^{KSSK\ K259A\ K250A\ K245A\ K263A\ K264A}$ shows the most impaired C3 binding with K_d decreased to 0.39 µM. However, despite the reduction in dissociation constant, all Sbi lysine

mutants could reach saturated binding when C3 concentration was higher than 0.8 μM. The factor I depleted serum deposition assay (Fig.5.3.25) was performed at half serum concentration. Given that serum C3 concentration is normally between 1-1.5 mg/ml (5.4-8.1 μM), therefore it is possible for all Sbi lysine mutants to achieve saturated C3 binding in serum despite the differences in C3 binding strength between various Sbi-III-IV proteins.

5.3.3 Functional characterization of Sbi-C3b adduct

5.3.3.1 Adduct formation defective Sbi-III-IV also shows functional defect

In this study, it was demonstrated that Sbi-C3b adduct formation is a unique feature of Sbi-III-IV triggered C3 consumption. Previously, there was speculation about the potential complement activation assisting role of the Sbi-C3b adduct, but experimental evidence for this claim was scarce. In this chapter, two Sbi-III-IV mutants with minimized adduct formation property were presented. Utilizing their unique characteristics, the functional role of Sbi-C3b adducts in the mechanism of C3 futile consumption was investigated.

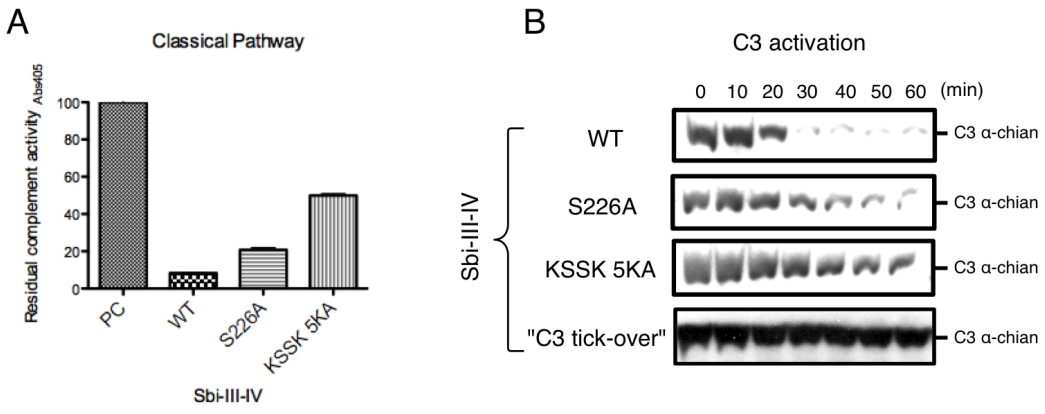

Figure 4.3.27: Consumption of C3 by Sbi-III-IV adduct formation mutants. (A) Different types of Sbi-III-IV were incubated with HSS for 30min at 37°C, then the consumption of C3 was assessed by the CP complement assay. Data shown represents means and standard errors from two experiments. KSSK 5KA is an abbreviation of "Sbi-III-IV KSSK K245A K250A K259A K263A K264A" **(B)** Anti-C3a Western blot analysis. Sbi-III-IV induced C3 consumption was marked by the gradual disappearance of the C3 α-chain.

Sbi-III-IV WT and the adduct formation mutants (5 μM) were incubated with HSS for 1 hour, treated serum samples were collected every 10 min and the C3 activation was followed by anti-C3a Western blot. As shown in Fig.5.3.27.B, although both mutants demonstrated minimal adduct formation level, they still function as an activator of C3. During the period of incubation, bands of C3 α-chain gradually reduce in size. However, when compared with the C3 activation profile of Sbi-III-IV^{WT}, the adduct formation mutants require prolonged incubation to achieve total depletion of intact C3 molecules.

A previously described method (Sections 4.2.2 & 4.2.3) was also utilized to evaluate the Sbi-III-IV induced consumption of complement. Briefly, HSS was treated with Sbi-III-IV proteins (5 μM) for 30 min, and then the residual CP activity was determined as an indicator for the level of C3 consumption. Fig.5.3.27.A shows that within the half-hour pre-incubation period, the Sbi-III-IV multiple lysine mutant consumed 50% of complement activity, the S226A mutant consumed 80% of complement activity, but the Sbi-III-IV WT protein reduced the residual CP activity by 92%. These measurements agree with the results of the C3 activation Western blot, and suggest that both adduct formation mutants of Sbi-III-IV are less potent C3 activators than the Sbi-III-IV WT protein.

5.3.3.2 Both ternary complexes and Sbi-C3b adduct extends serum C3b half-life

In chapter 4, it was demonstrated that Sbi-III-IV mediated ternary complex could extend C3b *in vitro* half-life. However, whether or not Sbi-C3b adducts also extend C3b half-life remained to be tested. Using the methods described in Section 5.2.3, free Sbi-III-IV molecule was removed from the Sbi-C3b adduct, using this sample the complement modulatory function of Sbi-C3b adduct alone is accessed.

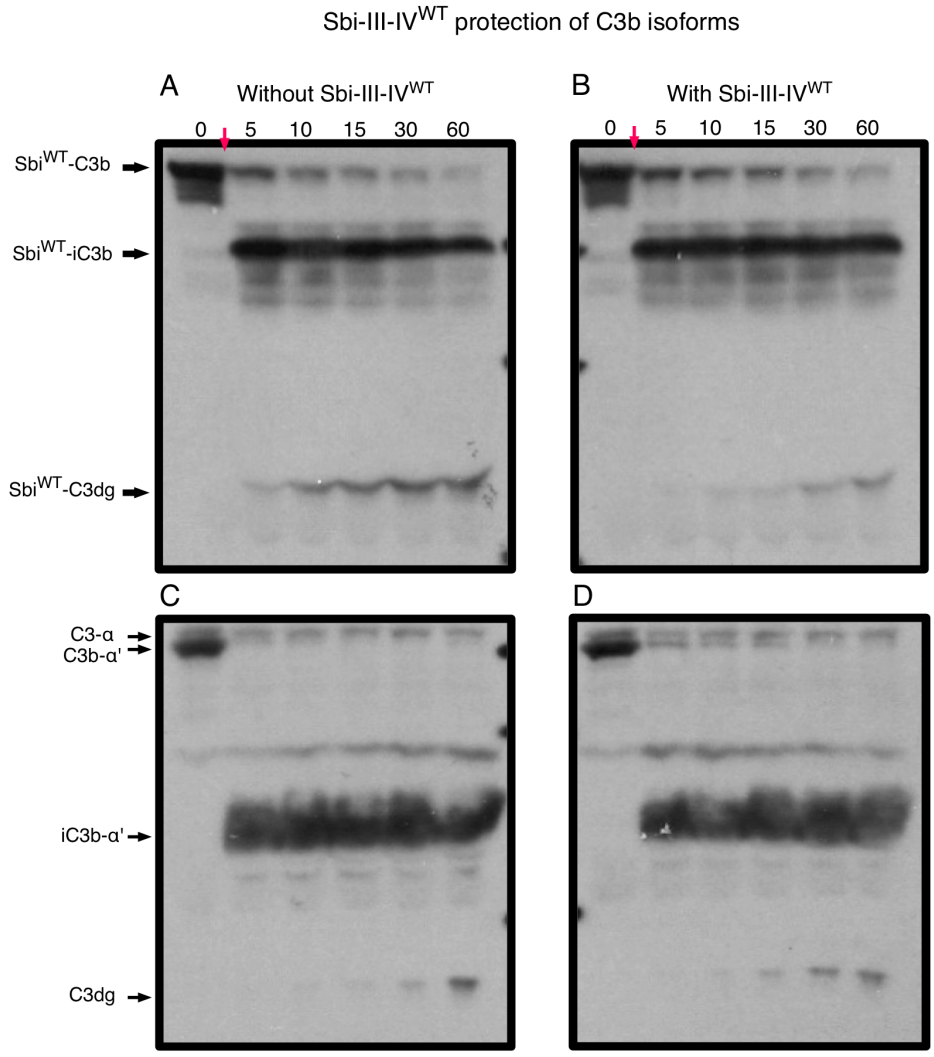

Figure 5.3.28: C3b conformation half-life is extended by free Sbi-III-IV^{WT} and the formation of Sbi-C3b adduct. The effect of free Sbi-III-IV^{WT} molecules on the degradation rate of Sbi^{WT}-C3b adduct and C3b molecule was conducted in C3 exhausted factor I depleted serum. Two sets of cleavage experiment were constituted, 6 µg of different C3b isoforms was incubated in the presence and absence of 3 µM of Sbi-III-IV^{WT}, factor I was added to 4 ng/µl to initiate the cleavage reaction. **(A-B)** Cleavage of Sbi^{WT}-C3b in the presence and absence of free Sbi-III-IV^{WT} **(C-D)** Cleavage of C3b in the presence and absence of free Sbi-III-IV^{WT}. Factor I addition was indicated by a red arrow.

To study if the free Sbi-III-IV^{WT} molecule is needed for the extended half-life of Sbi-C3b adduct, factor I depleted serum based cleavage assays (Section 5.2.17) were performed with the addition of either purified Sbi^{WT}-C3b adduct or C3b. Free Sbi-WT was also added to examine the effects of ternary complex formation. Fig.5.3.28 shows that the presence of free Sbi-III-IV^{WT} increases the C3b α' chain half-life of the Sbi-C3b adduct and C3b. However such protective effects were

most obvious in fluid phase C3b. In the case of the Sbi^{WT}-C3b adduct, with the presence of free Sbi molecule, only a slight protective effect was observed. In contrast, with free C3b, the Sbi^{WT}-C3b adduct alone (Fig.5.3.28.A) shows exceptional resistance to factor I mediated cleavage. Thus, both ternary complex formation and Sbi-C3b adduct formation contribute to the extension of C3b conformation half-life in serum. Additionally, for both iC3b species further cleavages of the iC3b α' chain were observed. This further proteolytic processing of the C3 fragment indicates the presence of sCR1 in the serum. As shown in Fig.5.2.28, Sbi-III-IV strongly protects Sbi-iC3b adduct than iC3b from sCR1 mediated cleavage.

5.3.3.3 Sbi-C3b adduct facilitates complement consumption

To directly assess the potential role of Sbi-C3b as a facilitator of AP pathway activation, the ability of free C3b and Sbi-C3b to mediate alternative pathway activation in serum was studied. HSS was reconstituted in Mg^{2+}-EGTA-water, and two types of C3b were added in various concentrations. After a 1 hour incubation at 37°C, the dose-dependent consumption of C3 was measured by the AP complement assay. At the same time, the treated serum samples were also analyzed by anti-Sbi, anti-FB and anti-C3a Western blot. As shown in Fig.5.3.29.A, both free C3b and Sbi-C3b demonstrated a dose-dependent consumption of serum C3 activity. However, while free C3b concentration of >2.5 μM was required for observable consumption of C3, Sbi-C3b yielded significant consumption of C3 at concentration higher than 1 μM. Without either type of C3b added, the control level of residual AP activity was 91%. With the addition of 1.8 and 2.6 μM of free C3b, the residual AP activities were reduced to 89.9 and 81.3%. In contrast, with the addition of 1.8 and 2.6 μM of Sbi-C3b, the residual AP activities were reduced to 69.4 and 51.0%.

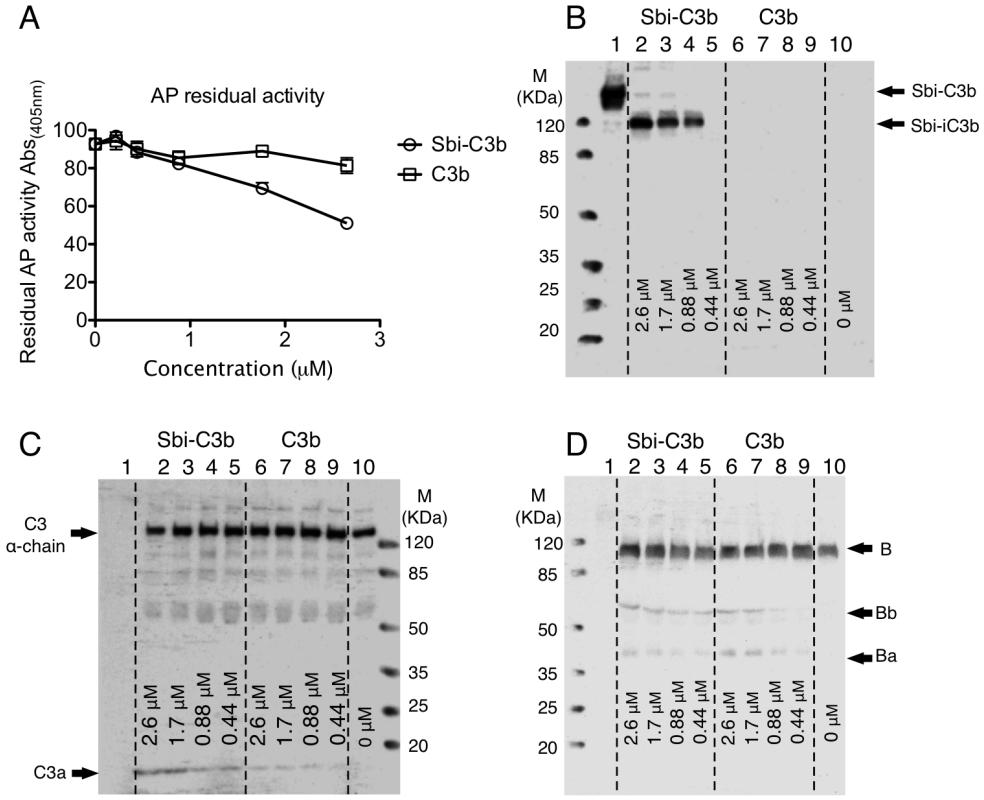

Figure 5.3.29: Consumption of C3 by C3b and Sbi-C3b. (A) Various amounts of C3b or Sbi-C3b were added to Mg^{2+}EGTA-HSS, and the consumption of C3 was assessed after 1 hour by the AP complement assay. Data shown represent means and standard errors from two experiments. **(B-D)** Anti-Sbi, anti-C3a and anti-factor B Western blot analysis. Each gel contains the following samples: 1 Sbi-C3b alone, 2-5 Sbi-C3b treated HSS samples (2.6, 1.7, 0.88 and 0.44 μM of Sbi-C3b), 6-9 C3b treated HSS samples (2.6, 1.7, 0.88 and 0.44 μM of C3b), 10 Mg^{2+}EGTA-HSS incubation alone. Complement assays were done in duplicate.

Western blot analyses of AP pathway activation markers revealed additional differences between C3b and Sbi-C3b triggered C3 consumption. As shown in Fig.5.3.29.D, at higher concentrations (2.6 and 1.8 μM) both C3b and Sbi-C3b induced similar levels of factor B activation. However, at lower concentrations (0.88 and 0.44 μM) no significant C3b induced factor B activation was detected. Although both C3b and Sbi-C3b can trigger factor B activation, dramatic differences in the amount of C3a production were observed (Fig.5.3.29.C), significantly more C3a release was induced by Sbi-C3b than C3b, and the release of C3a was dose-dependent on Sbi-C3b concentration. Finally, the anti-Sbi Western blot (Fig.5.3.29.B, lane 2-5) demonstrated that while the majority of

Sbi-C3b was converted to Sbi-iC3b, a small amount of Sbi-C3b remained intact after the incubation. More importantly, no free Sbi-III-IV was detected in Sbi-C3b samples (Fig.5.3.29.B, lane 1), which proves that the C3 consumption observed was not a consequence of free Sbi-III-IV contamination.

5.4 Discussion:

In this chapter, the freshly developed protocols aiming to generate, purify and label Sbi-C3b adducts are presented. The covalent deposition sites of C3b to Sbi-III-IV have been determined by means of mutant Sbi-III-IV and mass spectrometry. It was established that C3b could deposit covalently on both hydroxyl and amine containing amino acid residues predominantly located in Sbi domain IV. The complement modulatory function of Sbi-C3b adduct was also investigated; it was shown here for the first time that a Sbi-C3b adduct facilitates consumption of C3 through AP.

5.4.1 *in vitro* reconstitution of Sbi-C3b adduct

As introduced in result Section 5.3.1, previous attempts to purify Sbi-C3b adduct from serum had proved futile, both the quality and quantity of the Sbi-C3b adduct derived in these ways were less than satisfactory. It has been shown previously that the reconstituted AP pathway can be used to generate various types of C3b adduct (dextran, polysaccharide, insulin and IgG) (Pangburn 1989b; Shohet *et al*. 1991). Inspired by these early studies, protocols for the production of the Sbi-C3b adduct using the reconstituted AP were derived. As shown in Fig.5.3.4, Sbi-C3b was successfully produced by incubating Sbi-III-IV with purified AP components. This method is relatively easy to scale-up, as the main consumables in this procedure are purified C3 and factor B molecules. Moreover, the reaction conditions of this procedure can be subjected to small adjustments in order to meet special experimental conditions, for example when this procedure was adapted to produce the biotin labeled Sbi-C3b adduct, the

addition of iodoacetyl-PEG2-Biotin and increased pH value (pH 8.0) were found compatible with AP activation.

5.4.2 Determination of adduct formation sites

Prior to the mutagenesis and mass spectrometry studies, the chemical property of the covalent linkage between C3b and Sbi-III-IV was probed by a hydroxylamine sensitivity assay. I^{125} radioisotope labeled adducts are traditionally (Shohet *et al*. 1991) used in this type of assay, but here Western blots were used to follow the hydrolysis of the ester bond conjoined C3b adduct. In addition to the changes in detection methods, the 2D gel protocol was also modified to suit the detection of dissociated Sbi-III-IV. As shown in Fig.5.3.5, the treated serum was firstly separated on 1st dimensional 8% gel, treated with hydroxylamine, and then analyzed by the 2nd dimensional gel. Following this protocol, no dissociated Sbi-III-IV was detected. The potential technical problem could be that during hydroxylamine treatment of the 1st dimensional gel, the 8% gel slice remains unfixed and will be soaked for 1 hour. Thus the dissociated Sbi-III-IV could be lost significantly through diffusion due to its relative small molecular weight. Therefore in Section 5.3.3, an updated assay was utilized to minimize the loss of Sbi-III-IV. Together, these analyses suggested that the covalent attachment sites on Sbi-III-IV could be either hydroxyl or amine containing residues, which leads to the realization that there are multiple deposition sites on Sbi-III-IV.

In the next step of the study, the potential covalent attachment sites on Sbi-III-IV were proposed and investigated via site-directed mutagenesis. Having established that Sbi and C3b are linked by both ester and amide bonds, this broadened the potential covalent attachment sites on Sbi-III-IV to almost every serine and lysine residue. Furthermore, the possible existence of multiple deposition sites complicated the problem and prompted the generation of

accumulative mutants of Sbi-III-IV, by which the combined effect of these mutations can be revealed. The mutagenesis targets were decided based on both previous hypotheses and new discoveries. (Burman *et al*. 2008) proposed the earliest hypothesis that covalent attachment sites are located in Sbi-III, and the crystal structure of Sbi-IV binding to the C3d convex surface induced the emergence of another theory. But direct evidence supporting both hypotheses is scarce. Therefore to directly probe the covalent attachment sites, a study based on a mass spectrometry method was described here (Section 5.3.7), which provided a new list of possible covalent attachment residues.

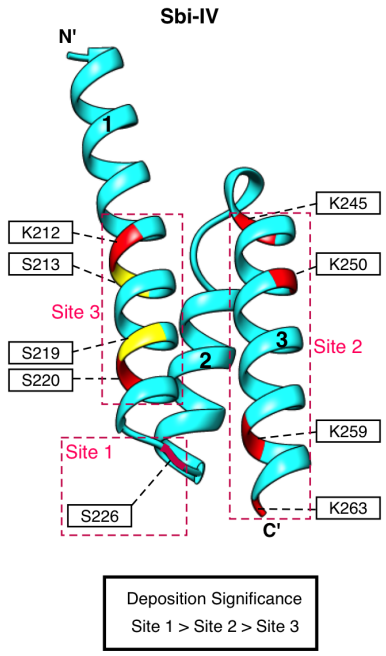

Figure 5.4.1: Summary of C3b covalent attachment sites on Sbi-IV

All possible covalent attachment residues and some residue combinations were mutated to alanine residues, and the resulting changes in adduct formation level were examined. Analyses of Sbi-III-IV mutant adduct formation was focused on selected groups of residues on Sbi-III and three putative deposition sites on Sbi-IV (Fig.5.4.1). No significant reduction in adduct formation was caused by mutations in domain III. In contrast, on Sbi-IV, the reduction in adduct formation level caused by the S226A mutation alone (Site 1) is almost the same as the total substitution of lysine residues included in site 2. Site 3 only takes on the role as the deposition target when other sites are seriously impaired. Therefore, three sites on Sbi-IV are responsible for C3b attachment. Ranked by their tendency to be deposited on: the most prominent site (Site 1) which consists of only the solvent-exposed S226 located in the loop region connecting Sbi-IV helix 1 to helix 2, Site 2 comprises C-terminal lysine residues that are implicated by the MS results and the least important site (Site 3) is located in the middle of Sbi-IV

helix-1.

The proposed multiple disposition sites on Sbi-III-IV agree with previous observations from hydroxylamine sensitivity assays that both serine and lysine residues are potential deposition residues. The miscellaneous and redundant nature of covalent attachment residues on Sbi-IV reflects firstly the semi-random nature of C3b deposition. Secondly the deposition process is probably not orchestrated by a defined protein-protein interaction but the formation of Sbi-C3b adduct is strongly encouraged. The obvious dominancy of Site 1 can be explained by the human C3 thioester preference for hydroxyl-containing deposition targets. However a structural transition mechanism might be involved to place S226 in close proximity to the metastable C3b thioester motif.

The combination of site-directed mutagenesis and C3b deposition assays were the common scheme utilized in numerous studies (Vidarte *et al*. 2001) to verify C3b covalent attachment sites on a protein. However, depending on the specific protein, a unique strategy is normally designed and executed in advance to narrow down the list of potential deposition sites. During the study of the IgG-C3b adduct, multiple strategies were shown able to locate the potential adduction formation sites. For example to roughly locate the area of interest, genetically engineered chimeric IgG molecules were used by which specific areas of the protein can be tested (Vidarte *et al*. 2001). To increase the detection resolution of the study, (Shohet *et al*. 1993) demonstrated that MS can be combined with radioisotope labeling, protease digestion and peptide purification to pinpoint the covalent attachment sites.

Inspired by these studies, the ESI-ToF MS technique was used in combination with biotin tag labeling, trypic digestion and biotin affinity purification to elucidate the covalent attachment sites on Sbi-III-IV. The results clearly indicated that five lysine residues at C-terminal of Sbi-IV are C3b deposition targets. However, surprisingly no serine residue is implicated by this method and large

amounts of C3b monomeric peptide was detected from the Sbi-C3b adduct sample. These observations could reflect the technical weakness of this method in detection of ester bond conjoined adduct. As described in Sections 5.2.9 and 5.2.10, during the purification and preparation of Sbi-C3b adduct peptides for MS analysis, the peptide sample was exposed to unavoidable acidic environment. This is a proven condition that catalyzes the hydrolysis of ester bonds, therefore making this method unsuitable for detection of ester bond mediated C3b adduct. Another imperfection of the current method is the leaching of the neutravidin peptide, which causes contamination of resulting peptide spectra. Although in this study, the source of the peptide peaks was verified by comparing with a neutravidin resin control. The existence of unnecessary peptide contaminations could still interfere with the ionization of the targeting peptides. However this method also displays advantages such as high efficiency, high detection accuracy and theoretically having the potential to reveal the entire repertoire of covalent attachment sites. Thus, improvements could be considered to make this method applicable to various types of C3b adducts. Firstly, it may be useful to use an affinity resin with relatively weaker biotin binding strength, by which the bound molecule could be eluted without exposure to very harsh conditions. Secondly, although the use of ion pair reagents (e.g. formic acid and TFA) are not avoidable during the MS procedure, during preparation and storage of the peptide sample the exposure to these reagents should be minimized.

5.4.3 Putative mechanism of Sbi-C3b adduct formation

So far, it has been demonstrated that the Sbi-C3b adduct formation process is virtually synchronized with the activation of C3. A simplified explanation for this phenomenon is based on the binding affinity between Sbi and C3, which means the majority of the C3 is presented to C3 convertase in the Sbi bound form. Therefore after the conversion to C3b, the Sbi in close proximity becomes a prominent deposition target. In addition, it was shown that the intact C3 binding

property is a prerequisite for Sbi molecule to become covalently deposited on by C3b. As the C3 binding mutant of Sbi-III-IV (R231A) demonstrates minimal adduct formation, it seems likely that the same Sbi molecule is responsible for both C3 binding and adduct formation. This theory fits with the observations that C3b preferentially deposits on its interaction ligands (e.g. C3b and IgG).

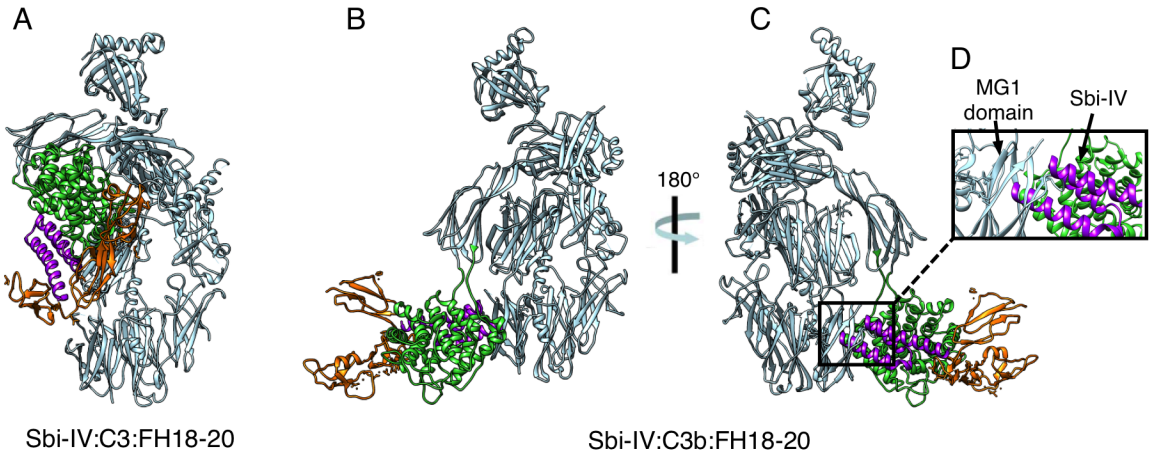

Figure 5.4.2: Structural transition from C3 to C3b bound ternary complexes. (A) Putative model of Sbi-IV:C3:FH18-20 ternary complex. C3: Light blue. C3d: Green. FH 18-20:orange. Sbi-IV: Purple. **(B-C)** Putative model of Sbi-IV:C3b:FH18-20 ternary complex. C3b: Light blue. C3d: Green. FH 18-20:orange. Sbi-IV: Purple. **(D)** Steric clash between C3b MG1 domain and Sbi-IV.

However, several mechanistic details of the Sbi-C3b adduction formation remain to be fully explained. Firstly, as shown in chapter 4, before AP activation, Sbi-III-IV predominantly exists in either FH or FHR-1 containing ternary complexes in combination with C3. Therefore, rather than the Sbi:C3 binary complex being presented to C3 convertase, it could be proposed that the majority of the C3 substrate presented is in the form of ternary complexes (Fig.5.4.2.A). This updated version of the Sbi-C3b adduct formation mechanism correlates with the observation that Sbi-III is not a major deposition target, since Sbi-III is normally interacting with FH or FHR-1 in the context of ternary complexes, by which Sbi-III is shielded from C3b deposition.

Secondly, as proposed earlier the same molecules involved in Sbi:C3 non-covalent interaction are highly likely to be converted to Sbi-C3b covalent adducts as a consequence of C3 activation. In this chapter, the majority of the covalent attachment sites have been located within Sbi-IV. Together, these results imply that the C3 bound Sbi-IV has to become temporarily dissociated after the formation of C3b and undergoes a repositioning process by which S226 (Site 1) on Sbi-IV is placed in close proximity to the metastable thioester motif. The structural analysis of C3b bound Sbi-IV reveals a severe steric clash between the MG1 domain of C3b and C-terminal region of Sbi-IV (Fig.5.4.2.D). Therefore it may be that this steric clash could detach the Sbi-IV binding on the concave surface of C3d and trigger the repositioning of Sbi-IV.

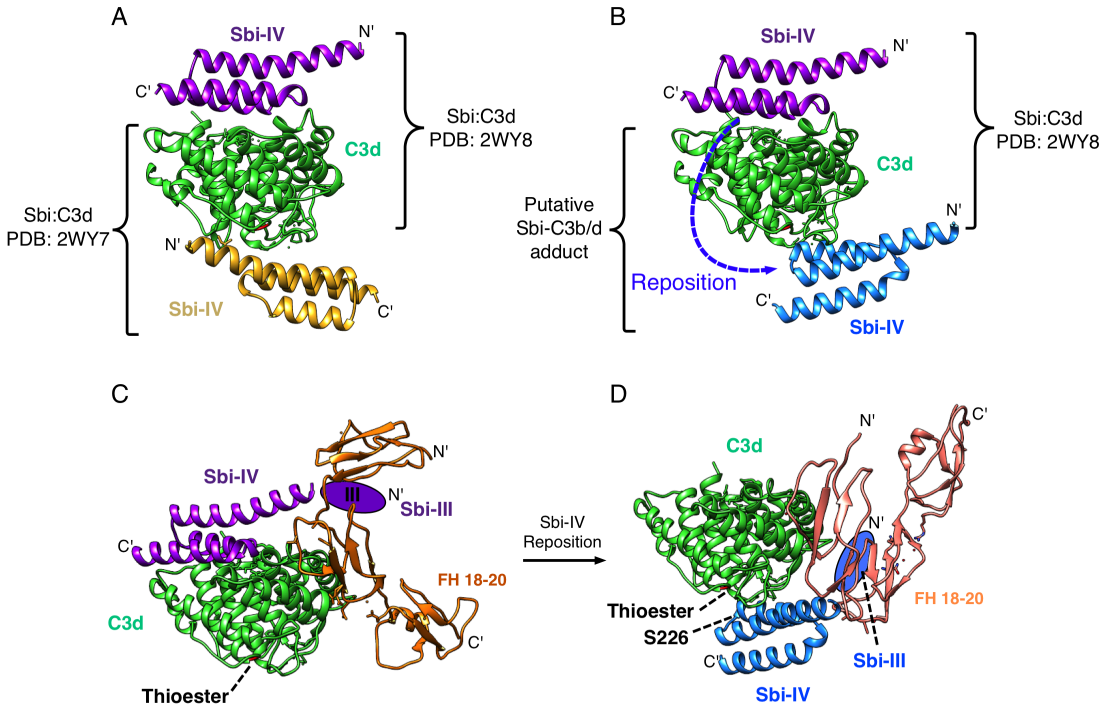

Figure 5.4.3: Molecular models of deposited Sbi-III-IV. (A) Two Sbi-IV binding modes on C3d. **(B)** Putative structural model of Sbi-IV reposition, the concave surface bound Sbi-IV (purple) repositions to the new location (blue) on convex surface. **(C-D)** Putative structural model of Sbi-IV reposition within Sbi-III-IV:C3d:FH18-20 ternary complex.

To provide further molecular details for this repositioning process, the crystal structures of Sbi-IV binding on both concave (PDB: 2WY8) and convex (PDB: 2WY7) surfaces of C3d have been analyzed (Fig.5.4.3.A). Since the elucidation of Sbi-IV:C3d convex surface binding mode, this structure is generally believed to reveal how the C3d domain covalently attaches onto Sbi-IV. However the covalent attachment data presented in this chapter contradict with this view. Furthermore, in respect of the putative Sbi-IV repositioning process, one would expect that the Sbi-IV molecule detached from the concave surface would maintain the same general orientation. But Sbi-IV was found binding in a completely opposite direction in the crystal structure 2WY7. Thus, this binding mode is less likely to be involved in the currently proposed Sbi-IV repositioning mechanism.

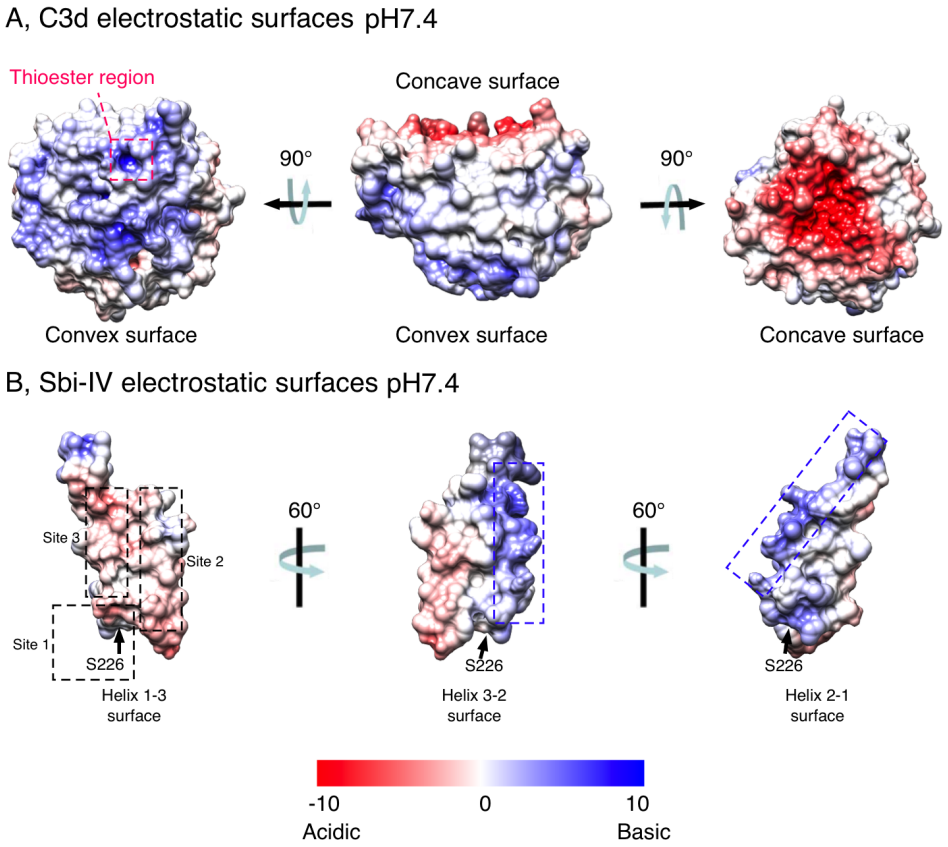

Figure 5.4.4: Electrostatic presentation of C3d and Sbi-IV. (A) Electrostatic surfaces of C3d at pH 7.4. **(B)** Electrostatic surfaces of Sbi-IV at pH 7.4. Thioester region of C3d is indicated by red dashed box. Deposition sites on Sbi-IV are indicated by black dashed box. The Sbi-IV region responsible for C3d concave surface binding is indicated by blue dashed box. The electrostatic surfaces were calculated by the APBS sever (Baker et al. 2001).

Although the crystal structure 2WY7 does not fit within the current Sbi-IV repositioning hypothesis, it does provide structural insight into the Sbi-IV binding interface on convex surface of C3d. The 2WY7 crystal structure (Fig.5.4.3) reveals that the acidic surface made up by the Sbi-IV helix 1-3 (Fig.5.4.4.B Sbi-IV helix 1-3) contacts with the largely basic C3d convex surface (Fig.5.4.4.A C3d convex surface). Based on the crystal structure, deposition site 3 (Fig.5.4.4.1) should be the most prominent deposition site, but site 1 (S226) was proven as the predominant covalent attachment site in reality. Therefore, it is reasonable to hypothesize that the acidity of Sbi-IV helix 1-3 surface offers the general electrostatic attraction to the convex surface of C3d, but there could be other forms of constraints that increase the tendency of S226 to be the covalent attachment residue.

Considering the new discoveries such as the ternary complexes and covalent attachment sites described in this thesis, a putative molecular model of Sbi-C3b adduct formation was shown in Fig.5.4.3.B. In this model, Sbi-IV repositions from the concave surface of C3d to the convex surface, during which the general orientation of Sbi-IV remains unchanged and the verified major covalent attachment residue S226 is placed in close proximity to the C3d thioester region. As depicted in Fig.5.4.3.C, ternary complexes could also play a role during the repositioning of Sbi-IV, the interaction between Sbi-III and FH 18-20 may act as a pivot point that restrains the general orientation of the moving Sbi-IV. It is also likely that after Sbi-IV deposits, the ternary complex could adapt a loosely packed alternative configuration (Fig.5.4.3.D). This is supported by the discovery of the binary binding between Sbi-III-IV and FH or FHR-1 (Section 4.3.10.3).

5.4.4 Complement modulatory function of Sbi-C3b adduct

In addition to the biophysical characterizations, the potential complement modulatory function of Sbi-C3b adduct was also investigated in this study. The results demonstrate that both ternary complex and Sbi-C3b adduct are protective mechanisms against C3b inactivation. As shown in Fig.5.3.28, compared with the free C3b molecule, Sbi-C3b on its own displays remarkable serum half-life. After the addition of free Sbi-III-IV, hence the formation of ternary complexes, the protective effect is much more obvious on free C3b than Sbi-C3b adduct. As discussed above, the C3b deposited Sbi-III-IV could remain FHR-1 bound, thereby extending the Sbi-C3b serum half-life. The observation of an extended serum half-life leads to the hypothesis that the Sbi-C3b adduct could be a potent AP C3 convertase precursor. In Section 5.3.3.1 and 5.3.3.3, it was shown that Sbi-III-IV mutants with minimal adduct formation properties demonstrate impaired C3 consumption activity, and a strong dose-dependent relationship between the amount of the Sbi-C3b adduct and the level of C3 consumption is observed. The functional significance of the Sbi-C3b adduct implicates that rather than a simple by-product of C3 activation the adduct formation is most likely a deliberate and advantageous step within the Sbi mediated C3 consumption mechanism.

Chapter 6: Structural analysis of Sbi ligand binding mechanism

6.1 Introduction

In chapter 4, the functional significances of Sbi N-terminal domain III have been demonstrated for the first time. This domain is essential for Sbi to bind FH or FHR-1 in combination with C3 isoforms. The resulting ternary complexes demonstrate unique immune-regulatory characteristics that could provide fresh molecular insights into the regulation of AP. Although numerous Sbi domain III amino acid residues have been determined that are crucial for the assembly of these complexes, molecular details of the structure of the ternary complexes remain elusive.

Structural characterization of the protein complexes comprising *staphylococcal* immune evasion proteins and complement components have made crucial contributions to the current understanding of immune evasion and complement regulation mechanisms (Serruto *et al.* 2010; Garcia *et al.* 2009). The B-cell activation inhibitory functions of Efb-C (Hammel *et al.* 2007b), Ehp (Hammel *et al.* 2007a) and Sbi (Clark *et al.* 2011) have been elucidated by the crystal structures of these proteins in complex with C3 fragment C3d. In addition, the crystal structure of SCIN in complex with C3b and a factor Bb fragment (Rooijakkers *et al.* 2009) not only resolved the mystery of the SCIN inhibitory mechanism but also offered unprecedented information about the molecular architecture of the active alternative pathway C3 convertase.

Previously, utilizing conventional structural biology methods (X-ray crystallography, Small-angle X-ray scattering and NMR spectroscopy), it was demonstrated that the extracellular region of Sbi adopts a modular domain organization to form an elongated structure (Burman *et al*. 2008). Among those four N-terminal domains, only the structure of Sbi-IV was solved, and this three-helix bundle domain was later shown to bind both the concave and convex

surfaces of C3d. However, when conventional structural biology methods were applied to Sbi domain III, very limited information was yielded. Several attempts to crystallize Sbi-III and Sbi-III-IV have so far been unsuccessful. The reason for those fruitless attempts became clear later when attempts were made to solve those puzzles by NMR spectroscopy. The resulting NMR spectra suggested that Sbi-III could be an intrinsically unfolded domain or at least extremely flexible (Upadhyay *et al.*, 2008). Therefore in this study, the I-TASSER structure prediction method in combination with single-molecule FRET spectroscopy and small angle X-ray scattering were used to generate a comprehensive model explaining the interaction between Sbi-III-IV and its complement component partners.

Given the novelty associated with some of the structural biology methods included in this chapter, I will briefly introduce the methodologies and justify the reasons for employing them.

6.2 Methodology

6.2.1 I-TASSER structural prediction

As presented in previous chapters, various analyses were performed to deepen our understanding about Sbi-III-IV. CD spectroscopy (Section 4.3.8.1) revealed the secondary structure composition, SwitchSENSE analysis (Section 4.3.8.2) provided information regarding to the hydrodynamic diameter, and Sbi mutant ternary complex formation assays (Section 4.3.10) pinpointed crucial interaction residues. On their own, these analyses only reflect individual aspects of Sbi-III-IV, however if these data can be considered together with structural models of Sbi-III-IV, this would make an in-depth structural analysis possible. In two previous publications (Burman *et al.*, 2008; Gorham, Rodriguez & Morikis, 2014), structural models for the entire Sbi-I-IV were presented, but no in-depth structural prediction analysis was performed on Sbi-III-IV. Therefore in the

beginning of this chapter, structural modeling studies of Sbi-III and Sbi-III-IV are presented.

Currently the computational methods for predicting three-dimensional protein structures have been classified into three categories, based on the availability of template structures in the PDB database. Homology modeling method is most suitable for those sequences that have structural template similarity of more than 80%. Threading methods are designed to match the query sequence directly onto the 3D structure of other solved proteins, with the goal of identifying and exploiting similar folds even when there is no evolutionary relationship between the query and template proteins. Finally, for proteins without apparent structurally related template in the PDB database, *ab initio* modeling method can be attempted. However, the sheer computational power needed limits this method to be only applied on small proteins with less than 120 amino acids (Zhang, 2008).

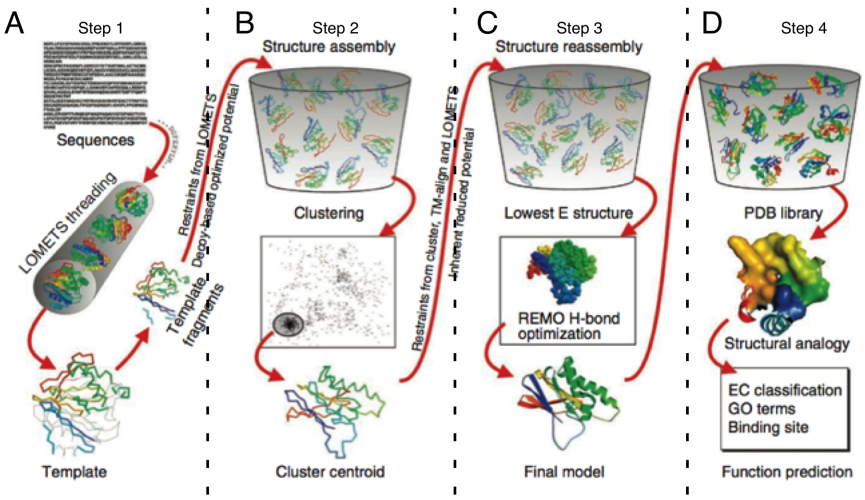

Figure 6.2.1: Schematic representation of the I-TASSER protocol for protein structure and function predication. **(A-D)** Predication step 1-4. Image taken from (Roy, Kucukural & Zhang, 2010).

Previous PDB database searches demonstrated that Sbi domain III does not share significant sequence identity to any proteins with known 3D structures. However the structure of Sbi domain IV has been solved on several occasions. Therefore to predict the 3D structure of Sbi-III and Sbi-III-IV, an iterative

threading assembly refinement (I-TASSER) method (Roy, Kucukural & Zhang, 2010) was utilized. I-TASSER is a composite protein structure predication approach, which combines numerous techniques such as threading, *ab initio* modeling and atomic-level structure refinement approaches. The query protein sequence is submitted through the I-TASSER server, the program then performs a four-stage protocol (Fig.6.2.1) to predict the 3D structure of a protein. The first stage (Fig.6.2.1.A) involves matching the query sequence against a non-redundant protein structure database through position-specific iterated BLAST (Altschul *et al.*, 1997) to find template proteins with similar structures or motifs. At the same time, using the query sequence and its predicted secondary structure profile, a threading procedure is also performed against PDB database utilizing LOMETS (Wu & Zhang, 2007), which is a locally installed meta-threading server consisting of seven high performance new threading programs. At the end of stage one, all templates are ranked according to specific score criteria, and the top template hits are selected for further consideration. The second stage (Fig.6.2.1.B) involves extracting threading alignments of fragments from the template structure in order to assemble regions that align well into a structural conformation. However, for these unaligned structural fragments (e.g. loops), structural information is supplied by a built-in *ab initio* modeling program. Once all the fragments are assigned with structural information, assembly is performed utilizing the replica-exchange Monte Carlo simulation technique (Zhang, Kihara & Skolnick, 2002). From the newly generated structural pool, the similar 3D coordinates are clustered by SPICKER (Zhang & Skolnick, 2004), which averages all the clustered structures by superposition to produce the "Cluster Centroids". At this stage, the cluster centroids generally have substantial internal steric clash and can be structurally distorted (Wu, Skolnick & Zhang, 2007). Therefore in the third stage (Fig.6.2.1.C), starting with cluster centroids, fragment assembly simulation is performed again. But this time, structural constraints are introduced to remove steric clashes and to refine the global topology. Therefore, at the end of this stage only a limited

number of cluster centroids remain, since under the newly introduced constraints, some cluster centroids have to be abandoned. These final models are then refined by REMO (Li & Zhang, 2009), which decorates the crude Cα trace models (cluster centroid) with an optimized hydrogen bonding network. In the final stage (Fig.6.2.1.D), functional annotation prediction takes place by comparing the predicted model with proteins of known structure and function from the PDB database.

Every stage is evaluated by multiple categories of scores that propel the model building process: energy scores, confidence scores, identity scores and statistical scores, etc. The primary scores for evaluating the final 3D model outputs are C-score (Equation 6.2.1).

$$\mathrm{C-score} = \ln\left(\frac{M}{M_{tot}} \times \frac{1}{\langle RMSD \rangle} \times \frac{1}{7}\sum_{i=1}^{7} \frac{Z(i)}{Z_0(i)}\right) \quad \text{[Equation 6.2.1]}$$

The M is the number of structure decoys in the cluster an M_{tot} is the total number of decoys generated during the I-TASSER simulation. <*RMSD*> is the average RMSD of the decoy to the cluster centroid. Z(i) is the Z-score of the best template generated by LOMETS program. $Z_0(i)$ is the program specific Z-score cut-off for distinguishing between good and bad templates. The C-score is a confidence score for estimating the quality of predicted models by I-TASSER, it normally varies from 2 to -5, where a higher value indicates a model with a higher confidence.

6.2.2 ALEX smFRET protein conformation dynamic analysis

Apart from structure predication methods, another novel structural biology approach described in this chapter is single molecule alternating laser excitation (ALEX) fluorescence resonance energy transfer (FRET) (Doose, Margeat & Weiss, 2004). This method has been shown to be particularly powerful in capturing different conformational states of biological molecules (Santoso *et al.*, 2010). Therefore, by utilizing this technique the conformational dynamics of Sbi-III-IV in response to ligand binding events could be investigated.

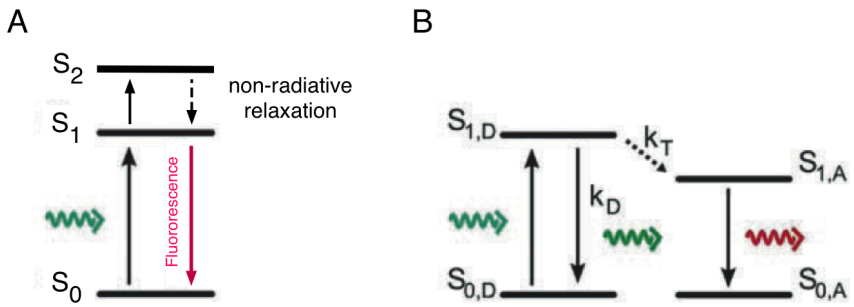

Figure 6.2.2: Principles of fluorescence and fluorescence resonance energy transfer (FRET). (A) External light source (green) directly excites an orbital electron from a fluorescent molecule ground state (S_0) to energy level S_2. The high-energy electron relaxes from S_2 to S_1 level vibrationally, and then the energy is released (S_1 to S_0) in the form of a photon. **(B)** After the excitation of the fluorescent donor, two processes can occur: the donor electron can either relax to ground state by emitting a photon or the energy can be transferred to a nearby acceptor where the energy is finally released as a photon (red). Figures taken from (Hinterdorfer & Van Oijen, 2009).

Fluorescence was first described and studied in the middle of the 19th century by Sir John Frederic William Herschel. It is a special form of luminescence and characterized by the emission of light from a substance that has absorbed light or electromagnetic radiation. The physical basis of this process is summarized by a Jablonski diagram (Fig.6.2.2.A), which involves the transition of an electron from an excited higher quantum state to the ground state by emission of a photon or energy. It was later discovered that the energy emitted from a fluorophore could be harvested by another fluorophore as a consequence of long-range dipole-dipole coupling. This phenomenon was defined as fluorescence resonance energy transfer (FRET) or Förster resonance energy transfer after Theodor Förster who developed the main FRET theory in the middle of the 20th century. Fig.6.2.2.B is used to explain the physical basis of this phenomenon.

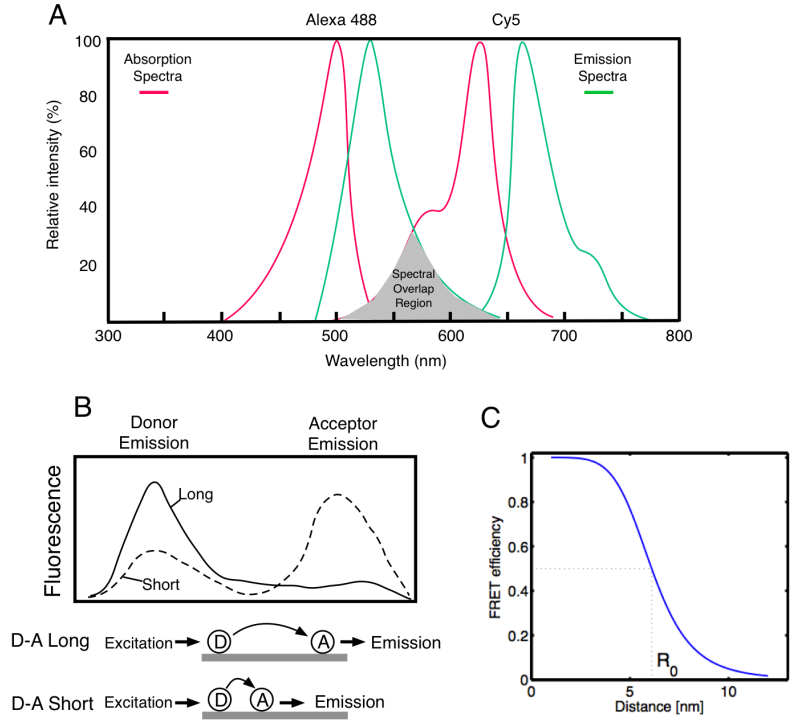

Figure 6.2.3 FRET spectra: **(A)** Overlap region of emission spectrum of Alexa 488 and absorption spectrum of Cy5 is coloured in grey. **(B)** FRET efficiency is dependent on the distance between donor and acceptor fluorophores. **(C)** Förster radius R_0 is the distance where E=0.5.

In a FRET event (Fig.6.2.3.B), an external light source was used to excite a high-energy fluorophore (donor, D), the energy can be then transferred to a

low-energy fluorophore (acceptor, A). However, two prerequisite conditions have to be fulfilled: first, both fluorophores must be in close proximity (<10 nm); and second the emission spectrum of the donor must overlap with the adsorption spectrum of the acceptor (Fig.6.2.3.A). As a result of energy transfer, the emission intensity of the donor decreases, and the emission intensity of the acceptor increases.

As stated by one of the FRET preconditions, FRET is a distance dependent energy transfer process. According to Equation 6.2.2 stated by Förster, FRET efficiency *E* is inversely proportional to the sixth power of the distance *R* between two fluorophores.

$$E = \frac{1}{1+(R/R_0)^6} \qquad \text{[Equation 6.2.2]}$$

The Förster radius R_0 (Fig.6.2.3.C), which describes the donor-to-acceptor distance where FRET efficiency equals 50%, normally varies between 2 and 6 nm (Selvin 2000) for common pairs of fluorophores. It can be calculated using Equation 6.2.3.

$$R_0{}^6 = \frac{9000(\ln 10)\Phi_D k^2 J}{128\pi^5 N n^4} \qquad \text{[Equation 6.2.3]}$$

The quantum yield of the fluorophore donor in the absence of acceptor Φ_D, Avogadro' number *N*, refractive index of the sample *n*. The relative orientation factor k^2 can take values between 0 (for perpendicular dipoles) and 4 (for collinear dipoles). *J* is an integral that described the overlap between the donor emission and acceptor absorption spectra, it is calculated by Equation 6.2.4 as a function of the wavelength λ using $\varepsilon_A(\lambda)$ as the molar extinction coefficient of the acceptor and $f_D(\lambda)$ as the normalized emission spectrum of the donor.

$$J = \int_0^\infty f_D(\lambda)\varepsilon_A(\lambda)\lambda^4 d\lambda \qquad \text{[Equation 6.2.4]}$$

Given the relationship between FRET efficiency and the distance between fluorophores, the FRET phenomenon has been developed intensively to be applied to the structural studies of biological molecules. Using poly-L-proline (Stryer & Haugland 1967) and double-stranded DNA (Clegg *et al*. 1993) as model molecules, the potential of FRET as a type of "spectroscopic ruler" has been firmly established. However, in most biological applications, FRET measurement has been found more appropriate for detecting the changes in distance rather than reporting the absolute distances between fluorophores. As shown in Equation 6.2.3, the fluorophore orientation factor k^2 plays a key role in the determination of R_0, but measuring it experimentally is often error prone (Selvin 2000).

FRET technology has evolved rapidly in the past two decades; today it has become an invaluable tool for characterization of conformational dynamics associated with biological molecules. In the traditional FRET experiment, the molecule under study is labeled on two locations with a pair of fluorophores, and then the energy transfer efficiency is determined. Although this type of ensemble FRET measurements provide structural insight about a molecule, this method only reflects the mean properties of populations of billions of molecules. Therefore the internal heterogeneity of the sample can skew the mean FRET efficiency to a degree that complicates the interpretation of experiments. This effect is particularly worrying when large, unstable or dynamic biomolecules are analyzed (Haas *et al*. 1975).

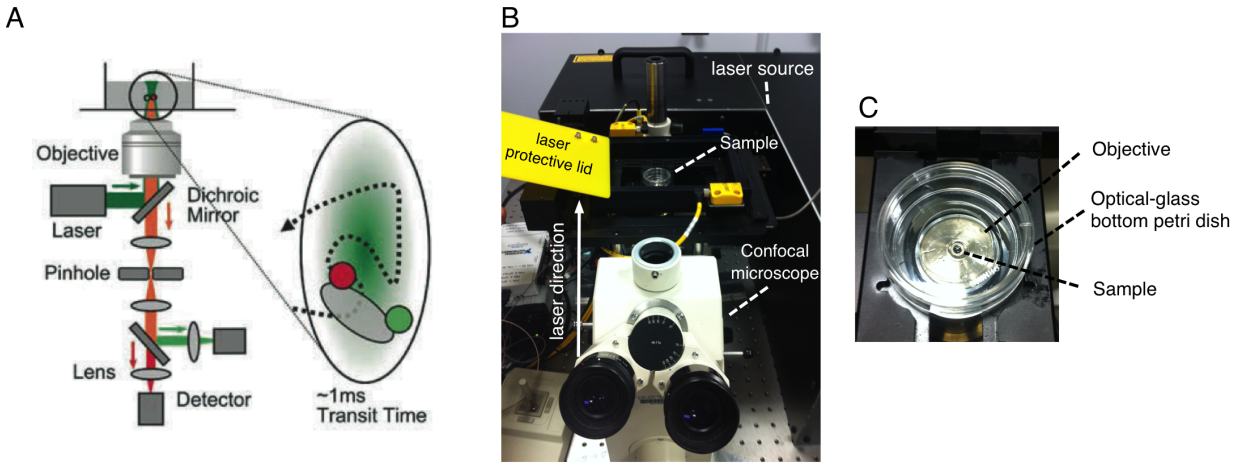

Figure 6.2.4: Instrumentation for single molecule FRET. (A) Simplified confocal microscopy set-up for FRET detection of single molecules diffusing in solution. **(B)** Single molecule FRET confocal microscopy set-up. **(C)** Sample loading of real single molecule FRET. Figure A adapted from (Hinterdorfer & Van Oijen 2009).

Some of these drawbacks of ensemble FRET experiment were overcome by single molecule FRET (smFRET), which is principally the measurement of FRET at the level of single molecule. The concept of smFRET was firstly demonstrated in 1996 (Ha *et al*. 1996), but it was not until 1999 (Ting *et al*. 1999) that it was developed to measure biological molecules in liquid buffer. Since then a consensus of smFRET experimental conditions has been established (Fig.6.2.4.A). In a typical smFRET experiment, the sample concentration is adjusted to between 50 and 100 pM, and a laser beam is utilized to excite the high-energy fluorophore. However, the laser beam is focused by a microscope's objective, thereby an extremely small excitation/detection volume (<1 femtoliter) is created. The smFRET instrument utilized in this study is shown in Fig.6.2.4.B-C. It was shown that given the extremely low sample concentration and extremely small focus volume, the probability of single-molecule occupancy is roughly 1% and it is several orders of magnitude greater than the chance of more than one molecule residing simultaneously within the focus (Nie *et al*. 1994). To derive the smFRET energy transfer efficiency E, photons emitted are counted separately using donor- or acceptor-emission channel detectors. Upon excitation of the donor fluorophore, two types of photon emission were counted, $f_{\mathrm{Dex,Dem}}$ and

$f_{Dex,Aem}$ where $f_{Xex,Yem}$ is the photon count for X-excitation-based Y-emission. The resulting smFRET efficiency *E* is then expressed as:

$$E = f_{Dex,Aem} / (f_{Dex,Aem} + f_{Dex,Dem}) \qquad \text{[Equation 6.2.5]}$$

In most smFRET studies, the conformational dynamic of a protein is usually directly reported by changes in the smFRET efficiency *E*, the variation in absolute distance between two fluorophores is only considered as an approximation. This is because of the numerous correction steps needed to determine accurate FRET efficiencies within single molecules. Moreover when R>6-8 nm the presence of chemically or photo-physically induced species also would obscure FRET measurements (Doose *et al*. 2004).

During the last decade, the latest improvement in smFRET measurement was the development of alternative laser excitation (ALEX) smFRET (Doose *et al*. 2004). In this method (Fig.6.2.5), the laser rapidly alternates between two wavelengths by which both donor and acceptor fluorophores are excited regularly (Fig.6.2.5.A-B). In combination with advanced photon detectors, not only donor excitation associated photon emissions ($f_{Dex,Dem}$ and $f_{Dex,Aem}$) are recorded, but also acceptor excitation associated photon emissions ($f_{Aex,Dem}$ and $f_{Aex,Aem}$,) (Fig.6.2.5.C-D). The donor excitation provides standard information about smFRET efficiency *E*, but it is the direct excitation of the acceptor that allows the relative fluorophore stoichiometry, *S*, to be measured (Equation 6.2.6).

$$S = (f_{Dex,Aem} + f_{Dex,Dem}) / (f_{Dex,Aem} + f_{Dex,Dem} + f_{Aex,Aem} + f_{Aex,Dem}) \qquad \text{[Equation 6.2.6]}$$

S can be considered as an indicator for the quality of fluorophore labeling. A stoichiometry reading of 1 indicates that the molecule under observation is only donor fluorophore labeled, which will display an *E* value of 0. On the other hand, when the stoichiometry reading of a molecule biases toward 0, this indicates that

the molecule is only acceptor labeled, which would give an *E* reading of 1.When the molecule is labeled with both donor and acceptor fluorophores, a *S* value close to 0.5 is expected. Only under this circumstance can the variation in *E* value be interpreted as changes in donor to acceptor distance ($R_{D\text{-}A}$).

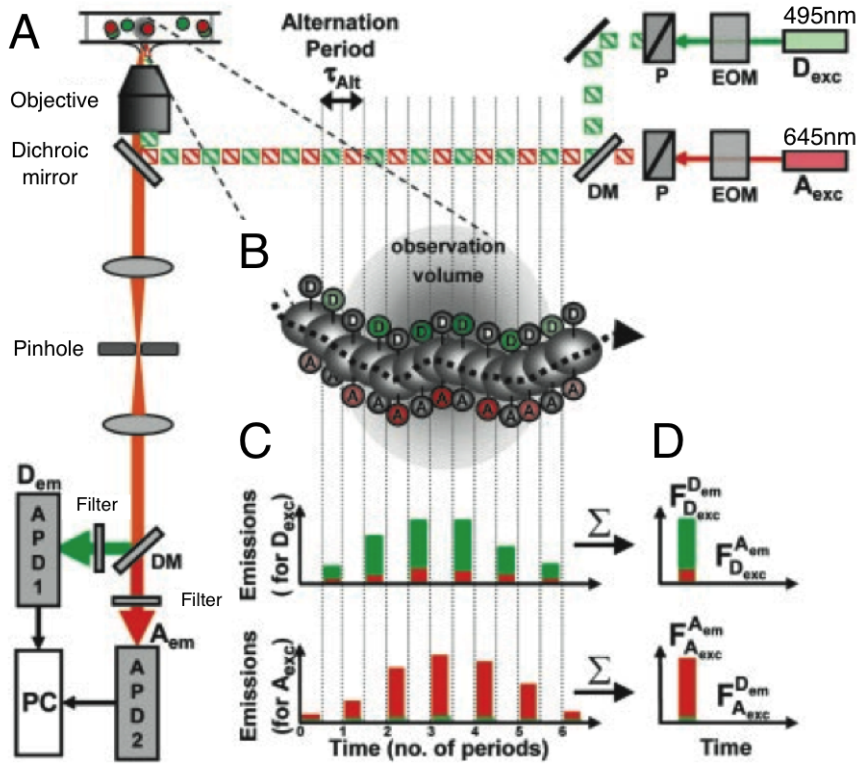

Figure 6.2.5: Alternative laser excitation (ALEX) smFRET. (A) Simplified presentation of ALEX microscopy set-up. APD, avalanche photodiode; DM, dichroic mirror; EOM, electro-optical modulator; P, polarizer. When the EOM and polarizer are used in combination, lasers rapidly alternate between two excitation wavelengths (D_{ex}=495 nm and A_{ex}=645 nm) with period defined as τ_{Alt}. The resulting fluorescence emission (orange) is collected in D_{em} and A_{em} channels. **(B)** Excitation of a single diffusing molecule across the microscopic focus point. The travel time is defined as a single "burst" **(C)** When excited at 495 nm, donor-excitation based D- and A-emissions (green and red columns, respectively). When excited at 645 nm, acceptor-excitation based emissions are collected. **(D)** The integration of the four excitation/emission streams yields four emissions for a single burst from which transfer efficiency (*E*) and stoichiometry (*S*) are calculated. Figure adapted from (Doose *et al*. 2004)

6.2.3 SAXS analysis of macro-molecular assembly

Small angle X-ray scattering (SAXS) is an established structural biology method for low-resolution characterization of biological molecules. It utilizes the isotropic scattering pattern of a molecule. By applying mathematical transformations on the scattering data, low-resolution (1-2 nm) molecular models can be constructed for various types of biological molecules. This method has been intensively exploited in the studies of protein structural properties such as overall topology, oligomeric state, flexibility and even folding status. Nowadays, taking advantages of modern high-brilliance synchrotron X-ray sources, polypeptides in the range of 1-10 kDa, macro-molecular complexes and large virus particles up to several hundred MDa can all be analyzed by this method (Mertens & Svergun 2010). Normally, for a complete set of measurements, 1-2 mg of protein sample is needed, and the experiments can be performed in most common biological buffer systems.

In this thesis, exploratory SAXS experiments were carried out, aiming to pave the way for the detailed characterization of the Sbi:C3d:FHR-1 ternary complex in the future. By combining the results of *in silico* structural modeling, ALEX smFRET and SAXS analysis, we hope the molecular organization of the Sbi:C3d:FHR-1 ternary complex can be revealed for the first time. In the following sections, the methodology of SAXS and its data analysis methods will be described.

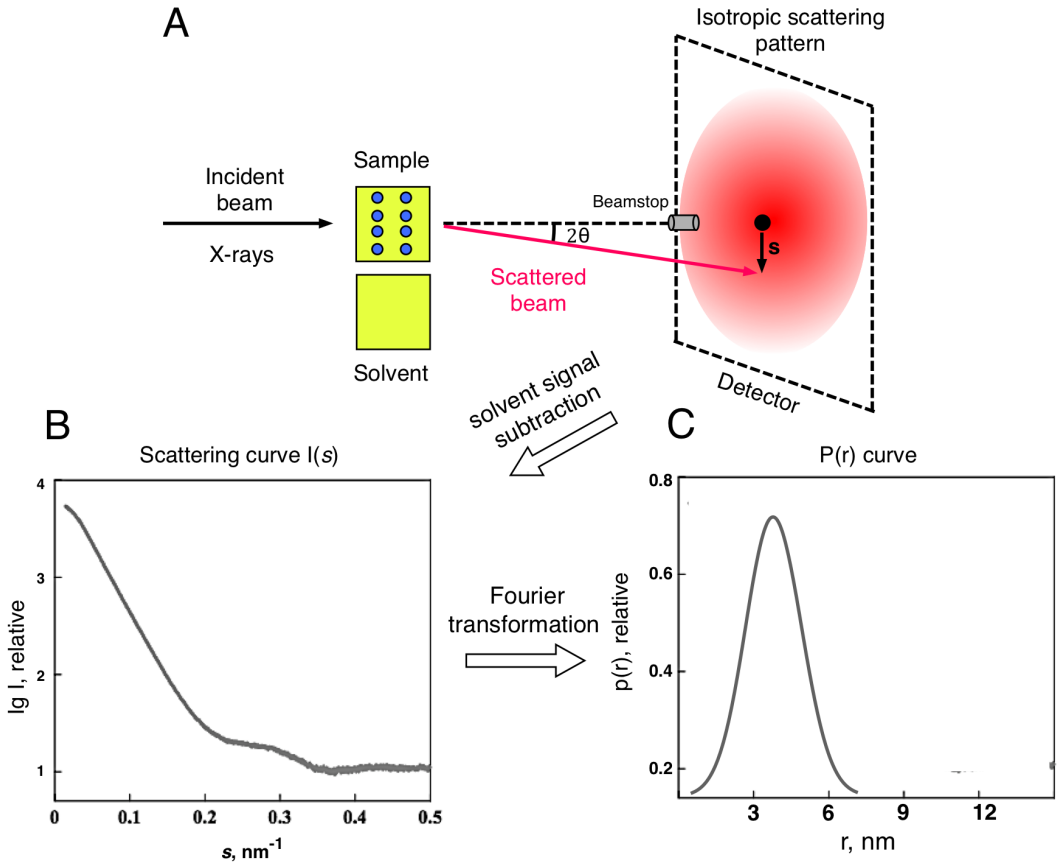

Figure 6.2.6: Schematic presentation of a typical SAXS experiment and subsequent data processing steps. (A) Scattering data acquisition **(B)** Scattering curve, *I(s)*, of a hypothetical protein **(B)** Pair distance distribution function.

During SAXS measurements (Fig.6.2.6.A), the sample is exposed to a collimated monochromatic X-ray beam. The incipient beam is scattered by the tumbling sample molecules, the resulting angle between incipient and scattering beams is defined as 2θ. The scattering of macromolecules such as protein or nucleic acid in the aqueous solution normally gives rise to an isotropic intensity (Mertens & Svergun 2010), which depends on the modulus of the momentum transfer *s*. Therefore mathematically, the scattering pattern is described by the intensity (*I*) as a function of *s*. Based on this mathematical relationship, the scattering pattern is transformed to an radially averaged one dimensional scattering curve (Fig.6.2.6.B). Although this curve could provide several important indications related to the size, shape and oligomeric state of the molecule, the reciprocal relationship between *I(s)* and *s* prevents it from being used in quantitative

descriptions of molecular structures. Thus, to interpret a scattering profile in terms of a structure, it is useful to Fourier transform the scattering curve to obtain a pair distance distribution function (P(r)) (Glatter 1977), which is a real space representation of the scattering profile (Fig.6.2.6.C). The shape of the P(r) function gives strong indications about the symmetry and domain structure of the sample molecule, but more informatively, several quantitative structural parameters can also be derived from the P(r) function. These include D_{max} (maximum particle diameter), Rg (radius of gyration) and V*p* (hydrated particle volume)(Porod 1982). Through these parameters, a basic understanding about the shape and weight of the scattering particle can be established, which is invaluable information for downstream sophisticated 3D model building processes.

Although all biological samples in solution would scatter X-ray beam, for SAXS analysis several stringent sample requirements have to be satisfied. Firstly, sample buffer has to be coherent, when a sample solution is illuminated by X-ray beam, not only the sample molecules causes scattering of the incipient beam but also the solvent molecules. Therefore, experimentally the scattering intensities of both sample solution and buffer solution are measured; the scattering intensity for sample molecules alone is then derived by subtraction. As a result, a consistent buffer environment is essential for the generation of a credible sample scattering curve.

$$I(s)=F(s)\times S(s) \qquad \text{[Equation 6.2.7]}$$

After subtraction of the buffer contribution from the total scattering intensity, the scattering intensity of the sample is derived. However, the Equation 6.2.7 that defines the composition of the sample intensity elicits an additional requirement for SAXS sample, monodispersity. Equation 6.2.7 shows that the sample scattering intensity comprises the form factor (F(*s*)), which describes the

structure of the molecule and the structural factor (S(*s*)), which describes the inter-molecular interactions (e.g. attractions and repulsions). In a monodisperse sample, where molecules are subject to minimal levels of inter-molecular interactions, the S(*s*) should be approximately equal to 1. Only under this condition can the sample scattering intensity (I(*s*)) be considered the same as the form factor (F(*s*)) and can be used for accurate structural modeling process.

In other structural biology techniques (e.g. Crystallography and NMR spectroscopy), solvable data are usually only obtained when the sample is appropriately prepared. But small-angle scattering pattern can always be produced from samples of any quality (Jacques & Trewhella 2010); therefore verification of scattering particles' purity and monodispersity is essential before structural modeling can proceed. Numerous complementary analyses are recommended to verify the sample quality independently such as SDS-PAGE, dynamic light scattering and size exclusion chromatography multi-angle laser light scattering (Mertens & Svergun 2010). However, for preliminary sample quality inspection, the scattering intensity function *I(s)* can be re-arranged and plotted again using Guinier analysis (Guinier 1939). Based on the linearity of the best-fit line, the presence of aggregation in the scattering sample could be detected. A non-linear Guinier plot is a strong indicator of poor sample quality. Apart from its use in data evaluation, using the scattering profile in the very small angle region ($s < 1.3/Rg$), Guinier analysis could also function as a useful means for estimating values for Rg.

Nowadays, *ab initio* reconstruction of low-resolution 3D models strictly from SAXS data is a common procedure. Most modeling programs are based on the concept of "spherical harmonics representation"(Stuhrmann 1970), which defines the model structure as a sum of independent contributions from the substructures corresponding to different spherical harmonics. This allows the calculation of scattering patterns of the model, which then can be compared with

experimental scattering patterns. By applying algorithms (Equation 6.2.8) to minimize the discrepancy between the calculated and experimented data, 3D SAXS models can be generated with some confidence (Fig.6.2.7). In this study, the modeling program DAMMIF (Franke & Svergun 2009) was used, which is the latest addition to the automated bead-modeling program family.

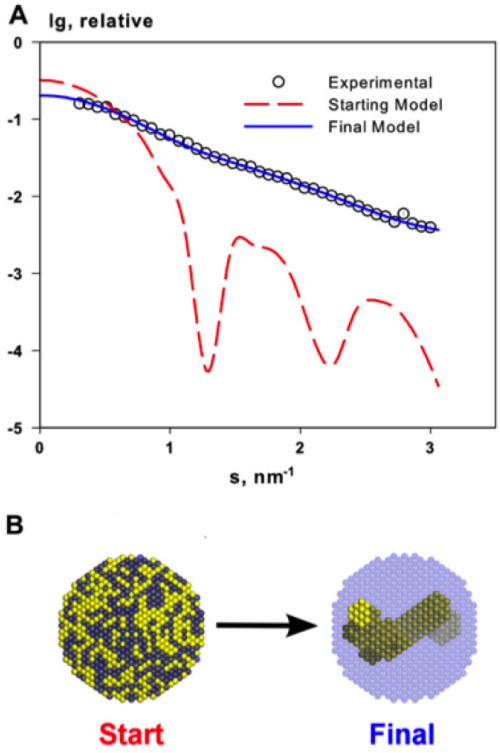

Figure 6.2.7: Principal of *ab initio* reconstruction. (A) Starting from a bead filled spherical search volume, a fitting process is performed until a model is produced that correlates not only to the experimental data but also has been shaped into a compact and connected model of beads **(B)** The spherical search volume with beads that represent particle (yellow) and solvent (blue). Images taken from (Mertens & Svergun 2010).

DAMMIF represents the particle as a collection of densely packed beads inside an adaptable and loosely constrained search volume (Fig.6.2.7.B) defined by experimentally determined *R*g. The latest version of the DAMMIF program utilizes an unrestricted search volume that can expand and reduce in size during simulated annealing processes, avoiding undesired boundary effects that may occur in the case of asymmetrical particles. Each bead is randomly assigned to solvent (assigned "0") or solute (assigned "1"), and the particle structure in solution is described by a binary string of length M. Only connected strings of beads are considered as a possible model, and the scattering amplitudes are

calculated. The simulated annealing process is described by Equation 6.2.8, aiming to search for a compact model with minimal discrepancy (x^2).

$$\chi^2 = \sum_k \frac{1}{N-1} \sum_j \left[\frac{I_{exp}(Sj) - cI_{calc}(Sj)}{\sigma(Sj)} \right] \qquad \text{[Equation 6.2.8]}$$

Where N is the number of experimental points; $I_{exp}(S_j)$ and $I_{calc}(S_j)$ are the experimental and calculated intensities respectively; c is a scaling factor; and $\sigma(S_j)$ is the experimental error at the momentum transfer S_j.

As the *ab initio* 3D structure modeling is an approximation process, therefore based on a 1D scattering pattern numerous 3D shapes could be obtained as reasonable structural solutions. The comparison of these models could be essential for identifying the most persistent features and variations shared by various *ab initio* models. Thus, by averaging these models, the intrinsic ambiguity of SAXS modeling can be reduced and a reliable average model can be produced. In this study, the comparison of the SAXS models was performed by DAMAVER (Volkov & Svergun 2003), which averages superposed models and produces a smoothed model presenting the most persistent features in the input models.

6.3 Material and methods:

6.3.1 Amino acid sequences used in structural prediction

Sbi-III^{WT}
N'-GSERQNIENADKAIKDFQDNKAPHDKSAAYEANSKLPKDLRDKNNRFVEK-C'

Sbi-III^{K173A}
N'-GSERQNIENADKAIKDFQDNKAPHDASAAYEANSKLPKDLRDKNNRFVEK-C'

Sbi-III-IV^{WT}
N'-GSERQNIENADKAIKDFQDNKAPHDKSAAYEANSKLPKDLRDKNNRFVEKVSIEK AIVRHDERVKSANDAISKLNEKDSIENRRLAQREVNKAPMDVKEHLQKQLDALVAQK DAEKKVA-C'

Sbi-III-IV^{K173A}

N'-GSERQNIENADKAIKDFQDNKAPHDASAAYEANSKLPKDLRDKNNRFVEKVSIEK AIVRHDERVKSANDAISKLNEKDSIENRRLAQREVNKAPMDVKEHLQKQLDALVAQK DAEKKVA-C'

6.3.2 I-TASSER structure prediction method

For prediction of protein tertiary structure, the primary sequence of the target protein was submitted to the I-TASSER on-line server (http://zhanglab.ccmb.med.umich.edu/I-TASSER/).

6.3.3 Cysteine substitution in Sbi-III-IV-cys

N'-MRGSHHHHHHGSER^{14}QNIENADKAIKDFQDNKAPHDKSAAYEANSKLPKDLRD KNNRFVEKVSIEKAIVRHDERVKSANDAISKLNEKDSIENRRLAQREVNKAPMDVKE HLQKQLDALVAQKDAEKKVAC^{130}-C'

Primary sequence of Sbi-III-IV-cys

A single substitution mutation of R14C was introduced using the method described in Section 2.2.2, slight modifications were made including the PCR template (pQE30$^{Sbi\text{-}III\text{-}IV\text{-}cys}$) and mutagenic primers (Forward 5'-3': atcaccatcacggatccgaatgtcaaaatattgaaaatgcg; Reverse 5'-3': cgcattttcaatattttgacatt cggatccgtgatggtgat). The mutated plasmids were verified with DNA sequencing service.

6.3.4 Protein expression & purification of Sbi-III-IV$^{dual\text{-}cys}$

The expression and purification procedures of Sbi-III-IV$^{dual\text{-}cys}$ were largely unmodified from the protocol described in Section 3.2.1. However, minor modifications were made to the recipe of Ni^{2+} affinity chromatography buffers. For the purification of Sbi-III-IV$^{dual\text{-}cys}$, 3 mM β-mercaptoethanol was added to both HisA and HisB buffer. The purified protein was stored in PBS buffer supplemented with 5 mM β-mercaptoethanol.

6.3.5 Fluorescent labeling

Labeling of the Sbi-III-IV$^{dual\text{-}cys}$ with sulfhydryl specific fluorophores was carried out according to the manufacturer's instructions. Prior to the labeling process, after a 30 min room temperature incubation, β-mercaptoethanol was removed using a protein-desalting spin-column (Section 2.3.5). The protein sample was buffer exchanged into phosphate-TCEP buffer (10 mM sodium phosphate pH 7.0, 5 mM TCEP). To label Sbi-III-IV$^{dual\text{-}cys}$ with the fluorescent donor and acceptor simultaneously, the protein concentration was adjusted to 150 μM (final volume of 200 μl), and then 2-fold molar excess of both maleimide derivative of Cy5 (GE healthcare) and Alexa Fluor 488 (Invitrogen) was added. The labeling reaction was flushed with nitrogen gas and maintained at room temperature for 2 hours shielded from light. Assuming that both maleimide fluorescent derivatives have similar reactivity to the reduced Cys side-chain on both ends of Sbi-III-IV$^{dual\text{-}cys}$, this way a single protein molecule became double labeled by both donor and acceptor. After the labeling reaction, the unincorporated fluorophores were removed by PD10 desalting column. The labeled proteins were concentrated (100 μM) and stored at -80°C in PBS buffer.

6.3.6 Fluorescence labeling verification using mass spectrometry

The molecular weights of unlabeled Sbi-III-IV$^{dual\text{-}cys}$ and fluorescent double-labeled Sbi-III-IV$^{dual\text{-}cys}$ were determined by ESI-MS. Before mass spectrometry analysis, both proteins were buffer exchanged into water, the mass determination procedure was as described in Section 3.2.13.

6.3.7 Single molecule confocal experiment

Single-molecule fluorescence analyses were performed at the Central Laser Facility (CLF), Rutherford Appleton laboratory. For each measurement, 100 pM of double-labeled Sbi-III-IV$^{dual\text{-}cys}$ was prepared in combination with various protein ligands (Appendix Table 9.8) and PBS buffer to a final volume of 25 μl.

Single molecule FRET was measured at room temperature using a confocal microscope with alternating-laser excitation at 495 nm and 645 nm. Photon arrival times were recorded and processed using customized software written in MATLAB (MathWorks, Natick) and Python (Python Software Foundation). Alternating laser excitation (ALEX) experiments produce four photon streams: $f_{\mathrm{Dex,Dem}}$, $f_{\mathrm{Dex,Aem}}$, $f_{\mathrm{Aex,Dem}}$ and $f_{\mathrm{Aex,Aem}}$, where $f_{\mathrm{Xex,Yem}}$ is the photon count for X-excitation-based Y-emission. To calculate the fluorescence transfer efficiency E of a single molecule, a data acquisition period is defined as a fluorescence burst, which putatively corresponds to the time of a single molecule diffusing across the force point of the confocal microscope. Within this period, the photon numbers based on the donor-excitation were counted to generate $f_{\mathrm{Dex,Dem}}$ and $f_{\mathrm{Dex,Aem}}$. Using these data that report the relative distance between D and A, calculation of transfer efficiency E is based on Equation 6.2.5.

A unique feature of single molecule ALEX FRET is that during a fluorescence burst, not only the total emission due to donor excitation is recorded but also the total emission results from the excitation of the fluorescent acceptor. Using this feature two emission parameters ($f_{\mathrm{Aex,Aem}}$ and $f_{\mathrm{Aex,Dem}}$) are derived and report on the D-A stoichiometry. Using the Equation 6.2.6 the stoichiometry of the each burst was calculated. For the data presentation, stoichiometry, S, and FRET efficiency, E, were calculated for each fluorescence burst, resulting in 2-dimensional E-S histograms.

6.3.8 Analysis of *E* histograms

The peak positions of various Sbi-III-IV ligand complexes were obtained by iteratively fitting the E histograms to a single-Gaussian function. Fitting the E histogram yielded the mean E for each Sbi-III-IV conformation, which was then used for the calculation of inter-fluorophore (inter-terminal) distances.

$R_{\mathrm{D\text{-}A}}$ calculation was based on Equation 6.2.2. A Förster radius (R_0) of 5.2nm was

used in the calculation, as R_0 is a fluorophore-pair specific value, therefore the Förster radius determined for the Alexa 488-Cy5 fluorophore pair in previous study (Grubmüller & Seidel 2008; Kalinin *et al*. 2012) was utilized.

6.3.9 Preparation of Sbi-III-IV interaction ligands

The preparation of Sbi-III-IV interaction ligands was described in chapter 3.

6.3.10 Preparation of sample for small-angle X-ray scattering (SAXS)

Purified Sbi-III-IV, C3d and rFHR-1 were buffer exchanged to PBS buffer separately. Recombinant FHR-1 (rFHR-1) provided by Dr Kevin Marchbank was used in this experiment. The protein concentrations were determined by the UV absorption method as described in Section 2.3.6. The extinction coefficients at A_{280} are as follows: Sbi-III-IV 1490 $M^{-1}cm^{-1}$, C3d 45505 $M^{-1}cm^{-1}$, and rFHR-1 69090 $M^{-1}cm^{-1}$. The ternary complex sample was made shortly prior to the SAXS experiment to prevent aggregation and precipitation. Various amounts of the ternary complex constituents were added to achieve final molar ratio of 1:1:1. The final concentration of Sbi:C3d:FHR-1 ternary complex (monomer theoretical MW 86 kDa) sample was 2 mg/ml, determined using extinction coefficients ε_{280} of 116085 $M^{-1}cm^{-1}$ (1490 $M^{-1}cm^{-1}$ +45505 $M^{-1}cm^{-1}$ +69090 $M^{-1}cm^{-1}$).

6.3.11 Small-angle X-ray scattering

SAXS data of the complex comprising the three proteins: Sbi-III-IV, C3d and FHR-1 were collected at I711 beamline in Max-lab in Lund, Sweden. The wavelength of 0.9 Å was used and a sample-to-detector distance of around 1996mm. The range of momentum transfer $0.01 < s < 0.55$ $Å^{-1}$ was covered ($s = 4\pi \sin\theta/\lambda$, where 2θ is the scattering angle). A cell with mica windows was used. The acquisition time was 2 minutes. The volume between the sample and the detector was kept under vacuum during data collection to minimize the

background scattering. The automated sample changer was employed to load the samples and oscillate the sample through the observation capillary during the exposure period to constantly remove the irradiated sample. 4 successive exposures of 30 second exposure time were collected and compared to detect and discard radiation damage effects. Only one sample concentration (2 mg/ml) was measured at 10°C in PBS buffer. These primary data processing steps were performed using appropriate programs for the ATSAS 2.6 package ((Petoukhov *et al*. 2012); http://www.embl-hamburg.de/biosaxs/download.html). The forward scattering *I*(0) and the radius of gyration Rg were extracted from the Guinier approximation calculated with the AutoRG function within PRIMUS (Konarev *et al*. 2003; Petoukhov *et al*. 2007). These parameters were also computed from the entire scattering patterns using the indirect transform package GNOM (Svergun 1992), providing the pair distribution function, p(r), and the maximum size D_{max} of the particle as well. To evaluate the flexibility of the two dimer species, dimensionless Kratky plots were generated (Kratky 1964; Durand *et al*. 2010). The molecular weight (MW) of the solute was evaluated by comparison of the forward scattering with that from a reference solution of bovine serum albumin. The MW estimations were cross-validated using the particle excluded (Porod) volumes as previously described (Petoukhov *et al*. 2012).

6.3.12 *Ab initio* shape determination and molecular modeling

The *ab initio* reconstructions were generated with the program DAMMIF (Franke & Svergun 2009). To check the stability of the solution the ten independent DAMMIF runs performed for each dimer were superimposed onto each other by SUPCOMB (Kozin & Svergun 2001). Using DAMAVER (Volkov & Svergun 2003) common structural features were determined and an averaged model was generated for the complex with the most persistent features of all reconstructions.

6.4 Results:

6.4.1 I-TASSER structural prediction of Sbi-III

In chapter 3, based on comparative CD analyses (Section 4.3.8.1) and hydrodynamic diameter measurements (Section 4.3.8.2), we demonstrated that Sbi-III-IV^{K173A} could be more structurally ordered and compacted than Sbi-III-IV^{WT}. Therefore in this chapter, the I-TASSER structural prediction server was used to predict the structure of Sbi-III and Sbi-III-IV of both WT and K173A proteins (Section 6.3.2).

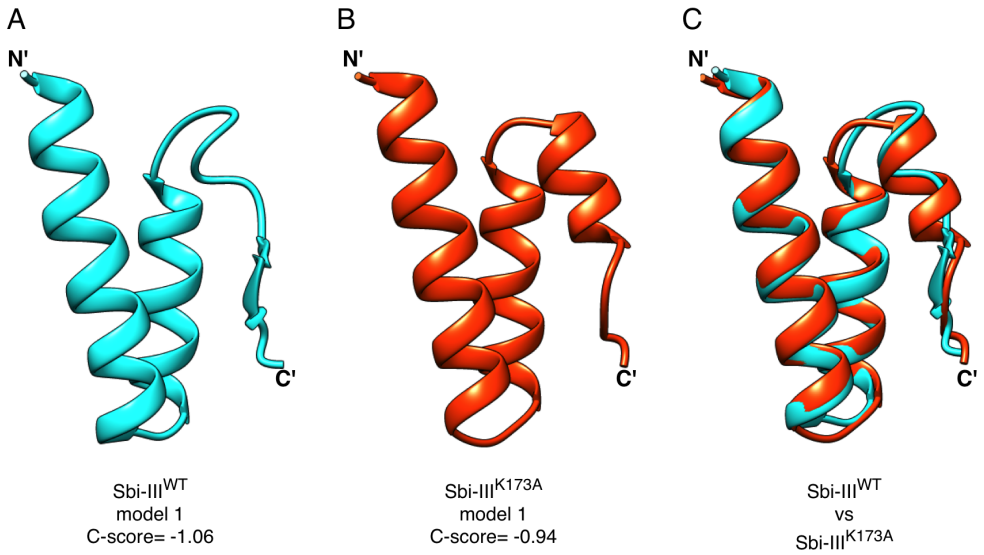

Figure 6.4.1: I-TASSER predictions of Sbi-III^{WT} and Sbi-III^{K173A}. (A) The best model for Sbi-III^{WT} (Cyan). **(B)** The best model for Sbi-III^{K173A} (Orange). **(C)** Superposition of Sbi-III^{WT} and Sbi-III^{K173A} models. C-score varies from 2 to -5, where a higher value indicates a model with a higher confidence.

According to the I-TASSER confidence score (C-score) the best models for WT and K173A Sbi-III are shown in Fig.6.4.1. The C-scores for both models are around -1, which is in the middle between two extremes of modeling quality. The tertiary structure organization of these models (Fig.6.4.1.A and B) is nearly identical, it was predicted that Sbi domain III could start with two N-terminal α-Helices and then finished with a C-terminal loop. Together, these three

secondary structure segments organize to a compact bundle-like tertiary structure. The only noticeable difference between WT and K173A models is the secondary structure of the C-terminal predicted loop region, as the superimposed presentation (Fig.6.4.1.C) indicated that this region is replaced by a partial helical structure in K173A mutant.

A slight difference in secondary structure was also detected, when Ramachandran analyses were used to validate both models. The resulting plots (Appendix Fig.9.9 A & B) demonstrate that some residues adopt different φ and ψ angles in WT or K173A models, but the majority of the residues from both Sbi-III models are located in the favorable region. Although the Ramachandran analyses support the viability of both models, since Sbi domain III lacks a homologous protein as modeling template, the modeling process uses the structural information that is mainly extracted from aligned peptide fragments and *ab initio* modeling processes. Therefore, fluctuations in local modeling accuracy are expected. Fig.6.4.2 shows that the mean estimated accuracy for both Sbi-III models is about 3 Å, the helical segments demonstrate highest accuracy (less than 3 Å), the loop regions between helices have slightly lower accuracy, and the accuracy decreases dramatically for the last seven residues approaching the C-terminus of the molecule.

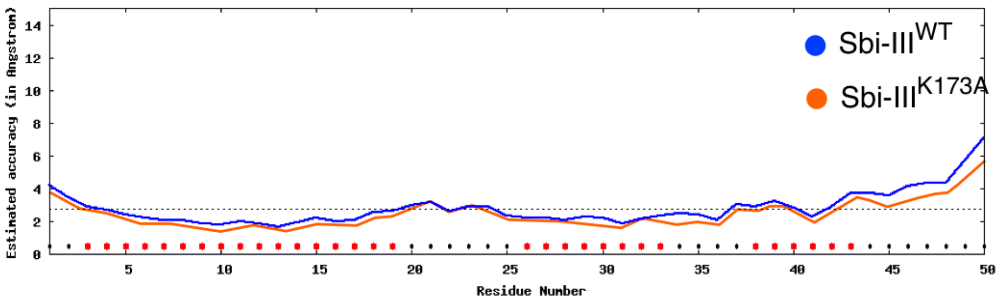

Figure 5.4.2: Local modeling accuracy of Sbi-III. Residue-level distance error estimation for Sbi-III. The solid lines are predicted error. The dashed line represents the predicted error level of 3 Å. The α helical secondary structural segments are indicated by red dots, the loops are indicated by black dots.

6.4.2 I-TASSER structural prediction of Sbi-III-IV

Under the assumption that the folding of Sbi-III could be influenced by the presence of Sbi-IV, the primary sequences of WT and K173A Sbi-III-IV were submitted to the I-TASSER structural prediction server. The best models are presented according to the C-score (Fig.6.4.4.A & B). These models demonstrate that the insertion of K173A mutation has no significant structural impact on the predicted overall topology of Sbi-III-IV, and both models are mainly composed of α-helix secondary structure.

However, unlike the previously presented models of Sbi-III, the predicted structure of Sbi domain III in Sbi-III-IV appears as a loosely packed helical domain. In Sbi-III-IV^{WT} model, starting from the N-terminus of the molecule, two α-Helix segments and a loop segment are connected to Sbi-IV through two 90° turns. Also in this model, rather than modeling Sbi-III-IV as an elongated protein consisting of two domains, Sbi-III is folded toward Sbi-IV resulting an overall arrangement similar to a globular protein.

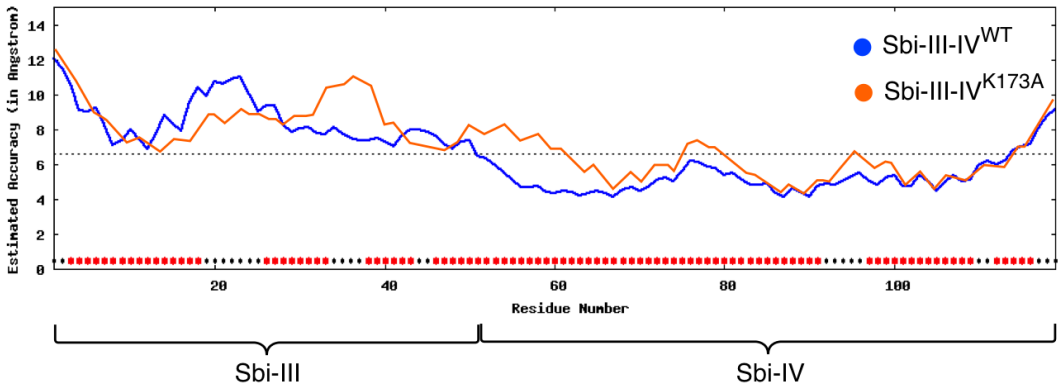

Figure 6.4.3: Local modeling accuracy of Sbi-III-IV. Residue-level distance error estimation for Sbi-III-IV. The solid lines are predicted error. The dashed line represents the predicted error level of 7 Å. The α helical secondary structural segments are indicated by red dots, the loops are indicated by black dots.

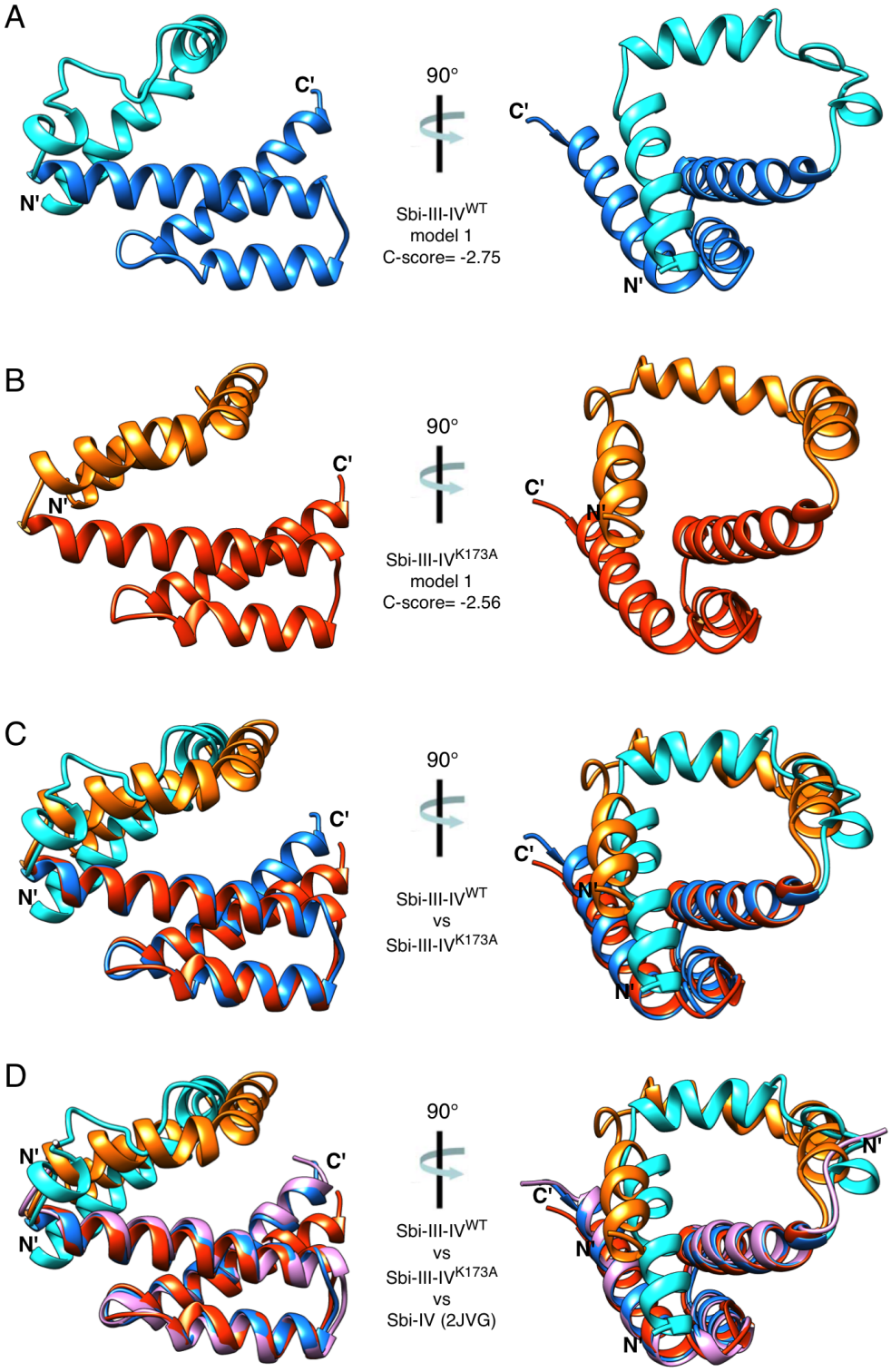

Figure 6.4.4: I-TASSER predictions of Sbi-III-IV^{WT} and Sbi-III-IV^{K173A}. (A) The best model for Sbi-III-IV^{WT} (Sbi-III: Cyan, Sbi-IV: Blue). **(B)** The best model for Sbi-III-IV^{K173A} (Sbi-III: Gold, Sbi-IV: Orange). **(C)** Superimposed models of Sbi-III-IV^{WT} and Sbi-III-IV^{K173A}. **(D)** Superimposed models of Sbi-III-IV^{WT}, Sbi-III-IV^{K173A} and Sbi-IV NMR structure (PDB: 2JVG, Pink). C-score varies from -5 to 2, where a higher value indicates a model with a higher confidence.

The structural alignment of the WT and K173A Sbi-III-IV models is presented in Fig.6.4.4.C. The majority of the structural discrepancies are located in domain III, as the domain IV segments from both models are nearly superimposable. The mean structural difference is the secondary structure of the C-terminal segment of Sbi domain III, this segment was predicted as a loop in the WT model but in the K173A model it was predicted as a helical segment.

In comparison with the results of the Sbi-III single domain modeling process (Fig.6.4.1), the best models generated for Sbi-III-IV demonstrate considerably lower C-scores: WT -2.75 and K173A -2.56. Although the Ramachandran plots (Appendix Fig.9.9.C & D) indicate that in both Sbi-III-IV models the majority of the residues adopted feasible φ and ψ angles, the analyses of the local modeling accuracy reveal that the mean estimated accuracy (Fig.6.4.3) of both models is about 7 Å. It was also noticed that the local modeling accuracy fluctuates heavily across Sbi-III-IV, the modeling accuracy for Sbi-III is much poorer than that of Sbi-IV. This bias is most likely a result of lacking homologous template for Sbi-III. As shown by Fig.6.4.4.D, using Sbi-IV NMR structure as the template, the Sbi-IV segment of the molecule was predicted with reasonably high accuracy.

Taken together, the modeling statistics indicate that the Sbi-III models generated with only the Sbi-III primary sequence are probably more accurate than the Sbi-III conformation as part of Sbi-III-IV. However, all structural predications agree that Sbi-III is mainly comprised of α-helices and loops. Another consensus reached is that the mutation of K173 to alanine causes an increase in α-helicity of the C-terminal segment of Sbi-III, this increase in the structural order might be the reason for the devastating effect of the K173A mutation.

6.4.3 ALEX Single-molecular FRET

6.4.3.1 Sbi-III-IV$^{dual-cys}$ preparation and verification

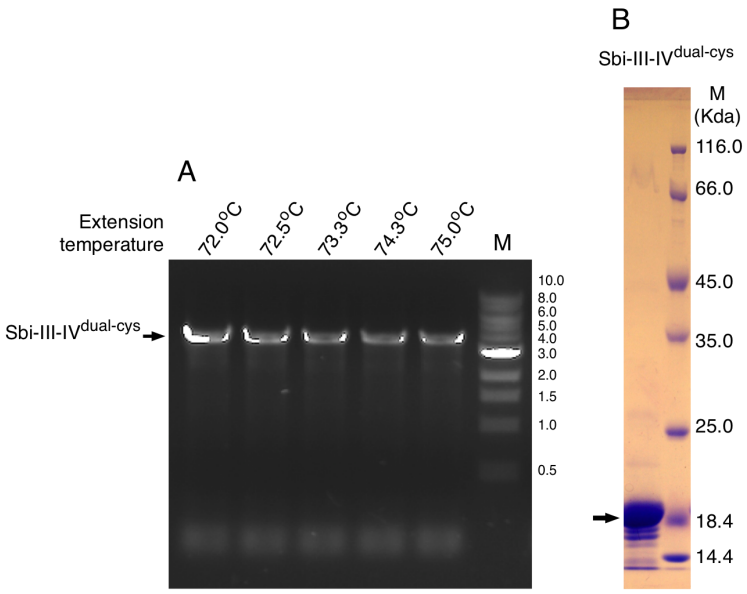

Figure 6.4.5: Preparation of Sbi-III-IV$^{dual-cys}$. (A) Agarose gel evaluation of the PCR amplification of mutation incorporated pQE30$^{Sbi-III-IV\ dual-cys}$ plasmid. The mutagenic PCR reactions were carried out 5 extention temperatures. The outcomes of mutation insertion and PCR amplification were represented as the intensity of the DNA band at 4.0kb. **(B)** SDS-PAGE profile of Ni^{2+} affinity purified Sbi-III-IV$^{dual-cys}$ (black arrow).

Prior to the smFRET experiment, Sbi-III-IV has to be labeled by both donor and acceptor fluorophores on both ends of the protein. Therefore based on pQE30$^{Sbi-III-IV-Cys}$ construct, one additional cysteine was introduced to the N-terminus of the Sbi-III-IV by substituting arginine at location 14 to a cysteine, and the resulting protein is named Sbi-III-IV$^{dual-cys}$. The mutagenic PCR reaction was carried out as described in Section 6.3.3. Essentially five PCR reactions were conducted using five distinct extension temperatures, and the results of each PCR condition were then analyzed by agarose gel electrophoresis. After PCR amplification was detected, the mutated plasmids were processed and purified. The incorporation of the correct mutation was confirmed by DNA sequencing (Appendix 9.1.1.7). The expression and purification of Sbi-III-IV$^{dual-cys}$ were described in Section 3.2.1. The purity of the protein sample was analyzed using SDS-PAGE (Fig.6.4.5.B).

Labeling verification via ESI-ToF mass spectrometry

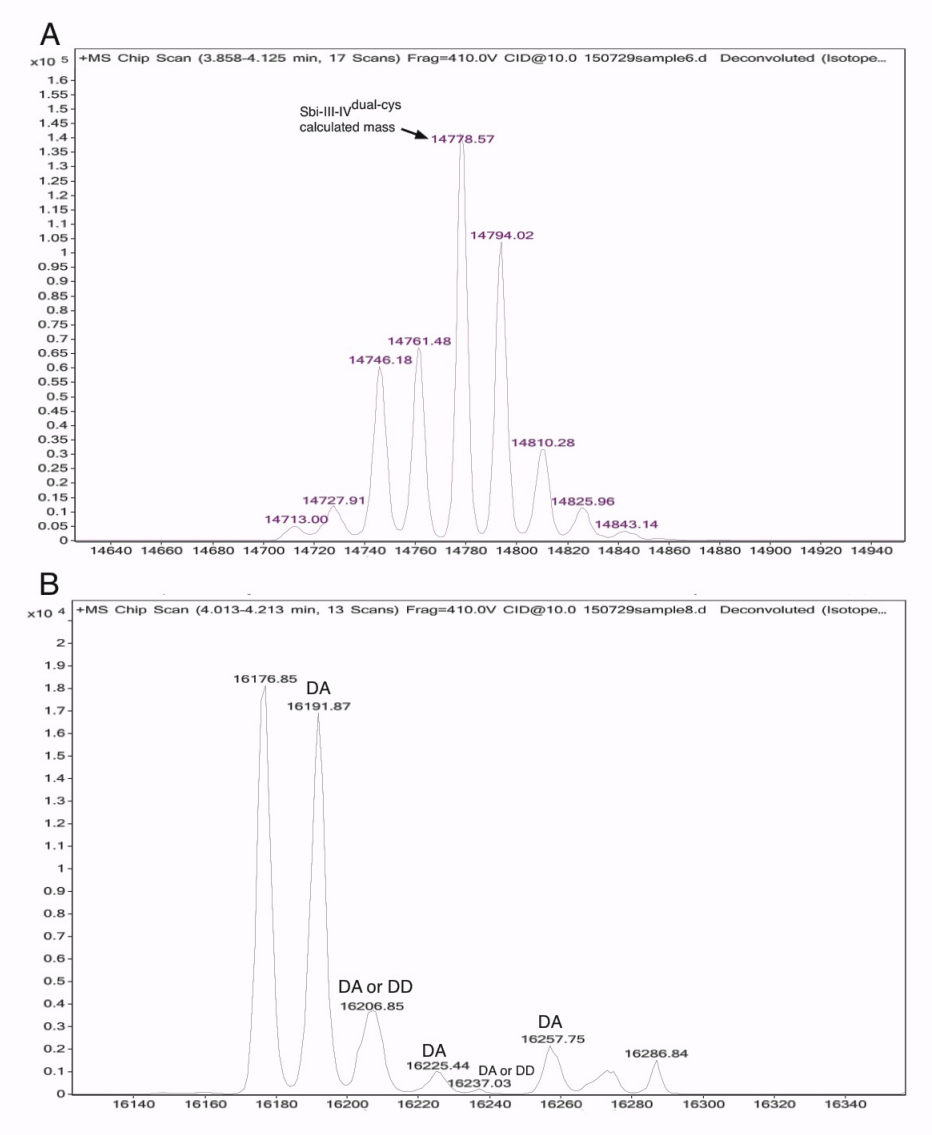

Figure 6.4.6: MS analysis of fluorophore double labeled Sbi-III-IV. (A) ESI-ToF mass spectrum of unlabeled Sbi-III-IV$^{dual\text{-}cys}$. The theoretical mass based on primary sequence is indicated. **(B)** ESI-ToF mass spectrum of double-labeled Sbi-III-IV$^{dual\text{-}cys}$. "DA" indicates the peaks resulted from the labeling of Sbi-III-IV by both donor and acceptor fluorophore. "DD" indicates the peaks resulted from the labeling of Sbi-III-IV by two donor fluorophores. Donor: Alexe 488; Acceptor: Cy5

The protocol for labeling of Sbi-III-IV$^{dual\text{-}cys}$ with both Alexa 488 (donor) and Cy5 (acceptor) was described in Section 6.3.5. To confirm the simultaneous labeling of Sbi-III-IV$^{dual\text{-}cys}$ with both donor and acceptor fluorophore molecules, protein mass changes before and after the labeling process were detected by ESI-ToF mass spectrometry.

Fig.6.4.6.A shows the MS spectrum of Sbi-III-IV$^{dual\text{-}cys}$ before labeling, the mass 14478.57 Da was detected and presented as a major peak in the spectrum, this mass is nearly identical to the calculated mass of Sbi-III-IV$^{dual\text{-}cys}$ (14778.06 Da, reducing condition). Therefore, this result demonstrates that firstly Sbi-III-IV$^{dual\text{-}cys}$ was correctly engineered via mutagenesis; secondly the majority of the Sbi-III-IV$^{dual\text{-}cys}$ molecule was in its reduced state. Along with this peak, several other peaks were also detected that could be derivatives of Sbi-III-IV$^{dual\text{-}cys}$ molecule as the consequences of a range of chemical modifications.

Analysis of double-labeled Sbi-III-IV$^{dual\text{-}cys}$ (Fig.6.4.6.B) demonstrates several peaks that could be the results of fluorophore labeling. To interpret these peaks, mass modifications caused by DA (1476 Da) DD (1554 Da) and AA (1394 Da) labeling were subtracted from these peaks and then compared with the unlabeled Sbi-III-IV$^{dual\text{-}cys}$ spectrum. The interpretable peaks were indicated in Fig.6.4.6.B and listed in Table 6.4.1 A&B. It was found that majority of the peaks are the result of double labeling of DA. However, there are a couple of peaks that could be the result of labeling with two donors. No peaks representing double labeling of the acceptor were detected. There were two masses (16176.85 and16286.84 Da) from Fig.6.4.6.B that were not directly interpretable. The 16176.85 Da peak represents the most abundant double labeled Sbi-III-IV$^{dual\text{-}cys}$ species in the sample, it was 15 Da lighter than the DA double-label Sbi-III-IV$^{dual\text{-}cys}$ (16191.87 Da), this could suggest that the 16176.85 Da peak also represents DA labeled Sbi-III-IV$^{dual\text{-}cys}$, the 15 Da mass discrepancy was the result of de-amidation.

Table 6.4.1: Interpretation of MS spectra. L-DA and L-DD masses match with one of the Sbi-III-IV$^{dual\text{-}cys}$ masses.

A

*L*abelled Sbi (Da)	Sbi-III-IV$^{dual\text{-}cys}$ (Da)	*L-DA* masses (Da)
16191.87	14713.00	14713.87
16206.85	14727.91	14728.85
16225.44	14746.18	14747.44
16237.03	14761.48	14759.03
16257.75	14778.57	14779.75

B

Labelled Sbi (Da)	Sbi-III-IV$^{dual\text{-}cys}$ (Da)	L-DD masses (Da)
16206.85	14810.28	14812.85
16237.03	14843.14	14843.03

6.4.3.2 Unliganded Sbi-III-IV demonstrates a single conformation in solution

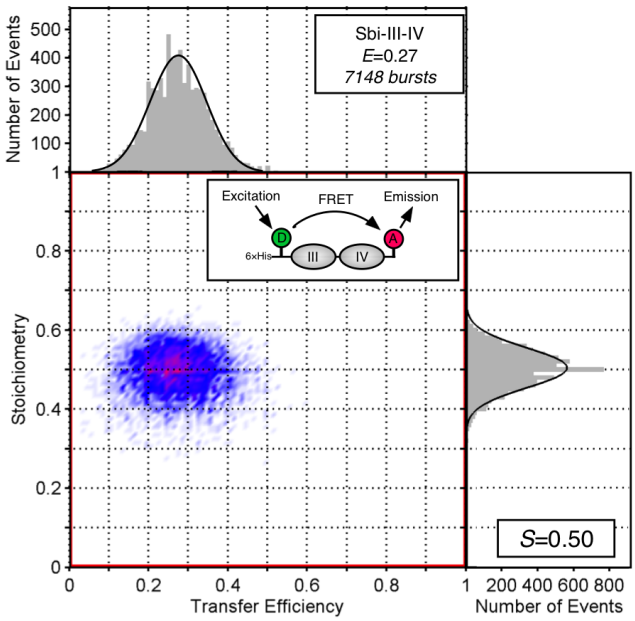

Figure 6.4.7: FRET related histograms for Sbi-III-IV. The sample is described by two histograms: a histogram of transfer efficiency (*E*) versus a histogram of stoichiometry (*S*). Individual burst are plotted in an *E* vs *S* graph, which is colour coded to describe overlapping in the data population, the high density region is coloured red, low density region is coloured blue. Both *E* and *S* distributions were fitted into a single-Gaussian distribution (black solid line), the mean values derived from the fitting were provided on the graph. The number of bursts measured was also indicated on the graph.

Single molecule FRET study of unliganded Sbi-III-IV was performed on free diffusing molecules through a femtoliter observation volume defined by the focused laser beam and confocal microscope. In combination with alternating laser excitation (ALEX), the status of both donor and acceptor fluorophores on the diffusing molecule were reported, using the methods described in Section 6.3.8. Two parameters were derived, relative donor:acceptor stoichiometry (*S*) and FRET efficiency (*E*).

The distribution of *E* (Fig.6.4.7) obtained for Sbi-III-IV reveals an unbiased distribution that fits into a single Gaussian function with the mean *E* = 0.27. This indicates that unliganded Sbi-III-IV molecule largely exists in one major conformation. The internal flexibility of the molecule is reflected by the

broadness of the E distribution. Using Equation 6.2.2 and a previously determined R_0 of 52 Å (Kalinin *et al*. 2012), the estimated $R_{D\text{-}A}$ between two fluorophores is calculated as 61.3 Å. Because the fluorophore labeling sites are designed on either end of the Sbi-III-IV, therefore the distance $R_{D\text{-}A}$ is utilized to represent the inter-terminus distance of the Sbi-III-IV molecule. The single Gaussian fitting of S distribution yields the mean S of 0.5, suggesting that the majority of the single molecules analyzed are double labeled by donor and acceptor fluorophores.

6.4.3.3 Ligand induced conformational changes in Sbi-III-IV

Sbi-III-IV was shown to be able to bind various C3d containing fragments, and the main binding site was located in Sbi domain IV. In Chapter 3, it was demonstrated that C3d fragment binding is a prerequisite condition for the high affinity ternary complex assembly mediated by Sbi domain III. A hypothesis that could account for this phenomenon is that Sbi-III-IV undergoes binding induced conformation changes, through which a new Sbi domain III conformation forms which is favorable for FH/FHR-1 binding. In the following sections, single molecule FRET measurements of ligand bound Sbi-III-IV are presented to provide new molecular insights into ligand binding triggered Sbi-III-IV conformation changes. During each experiment, an excess amount of ligand molecule was added to ensure the binding status of Sbi-III-IV (Section 6.3.7). Only smFRET measurements with $S \approx 0.5$ were presented in following sections.

Firstly, the FRET efficiency changes induced by binding of various TED domain containing C3 fragments were determined. In Fig.6.4.8 a single Gaussian function was fitted in the E distribution of C3d, $C3_{(H2O)}$, C3b and C3 bound Sbi-III-IV, the mean E determined are 0.30, 0.34, 0.27 and 0.31 respectively. Therefore apart from binding of C3b, all other C3 fragments trigger an increase in transfer efficiency, hence a decrease in $R_{D\text{-}A}$. Disparate E values also indicate that although

Sbi-III-IV binds to the same TED domain interaction interface, the average conformation of bound Sbi-III-IV is also sensitive to the overall shape of the C3 fragments.

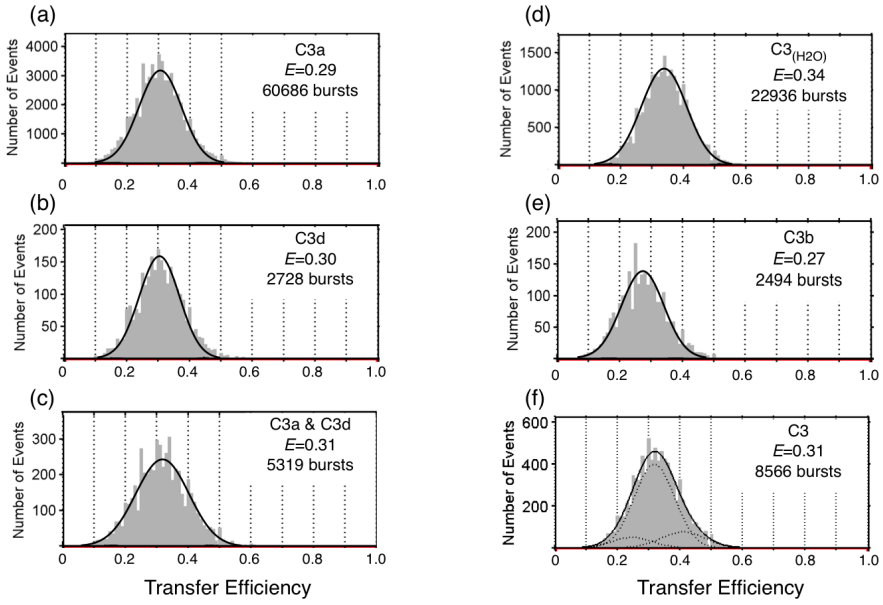

(g)

Ligand	*E*	$R_{D\text{-}A}$ (Å)	$\Delta R_{D\text{-}A}$ (Å)
No	0.27	61.3	0
C3a	0.29	60.3	-1.0
C3d	0.30	59.8	-1.4
C3a & C3d	0.31	59.4	-1.9
C3(H2O)	0.34	58.0	-3.3
C3b	0.27	61.3	0
C3	0.31	59.4	-1.9

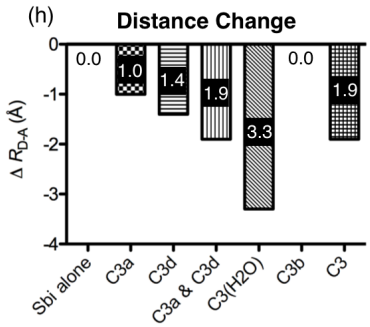

Figure 6.4.8: Single molecule FRET experiments reveal conformational flexibility of ligand bound Sbi-III-IV. (a-f) *E* histograms for ligand bound Sbi-III-IV. Single-Gaussian fit (black solid line), the mean values derived from the fitting were provided on the graph. The number of bursts measured was also indicated on the graph. **(g)** Table summarizing mean *E* values for various bound Sbi-III-IV. Based on the mean E value, $R_{D\text{-}A}$ was derived. The changing in interprobe distance $\Delta R_{D\text{-}A}$ was calculated as $R_{D\text{-}A\ liganded}$ - $R_{D\text{-}A\ unliganded}$. **(h)** A bar chart presentation of ligand induced interprobe distance changes. The negative values indicate relative shortening of Sbi-III-IV molecule.

Secondly, in addition to prominent TED domain interactions, previously Sbi-III-IV was also shown to bind C3 activation fragment C3a (Burman *et al*. 2008). This interaction with a K_d of 19.8 μM was shown to be much weaker then

the TED domain mediated interaction, and the structural basis of this interaction is still elusive. To unravel the mysterious nature of this interaction, smFRET *E* was obtained by challenging Sbi-III-IV with C3a alone and C3a in combination with C3d. In both cases, the resulting *E* distributions were fitted into single Gaussian functions, by which the mean *E* value was derived, 0.29 for C3a alone, 0.31 for C3a in combination with C3d. Compared with unliganded Sbi-III-IV, no significant *E* change was caused by C3a binding (E_{alone}=0.27 vs E_{c3a}=0.29). When applied together with a more prominent ligand C3d, the result *E* distribution resembles that of C3d bound Sbi-III-IV ($E_{C3a\ C3d}$=0.31 vs E_{C3d}=0.30). Thus, the binding of C3a does not induce a significant Sbi-III-IV conformational change event. It is also likely that the presence of prominent interaction ligands could displace the relatively weak C3a interaction.

To compare the changes in conformation of various ligand bound Sbi-III-IV, $R_{D\text{-}A}$ for ligand bound Sbi-III-IV were calculated from *E* as described in Section 6.3.8. Fig.6.4.8.g shows that the C3 fragment binding induces changes of $R_{D\text{-}A}$ to a different degree, and the amplitudes of the distance changes are generally modest. By subtraction of unliganded $R_{D\text{-}A}$ from ligand bound $R_{D\text{-}A}$, $\Delta R_{D\text{-}A}$ was calculated and utilized to evaluate the amplitude of changes in inter-probe distance. As shown by Fig.6.4.8.h, the most significant change in $R_{D\text{-}A}$ was induced by $C3_{(H2O)}$ (3.3 Å), by contrast the addition of C3a fragment yielded the most subtle change (1 Å) in $R_{D\text{-}A}$.

6.4.3.4 Sbi-III-IV binds to FH and FHR-1 in different conformations

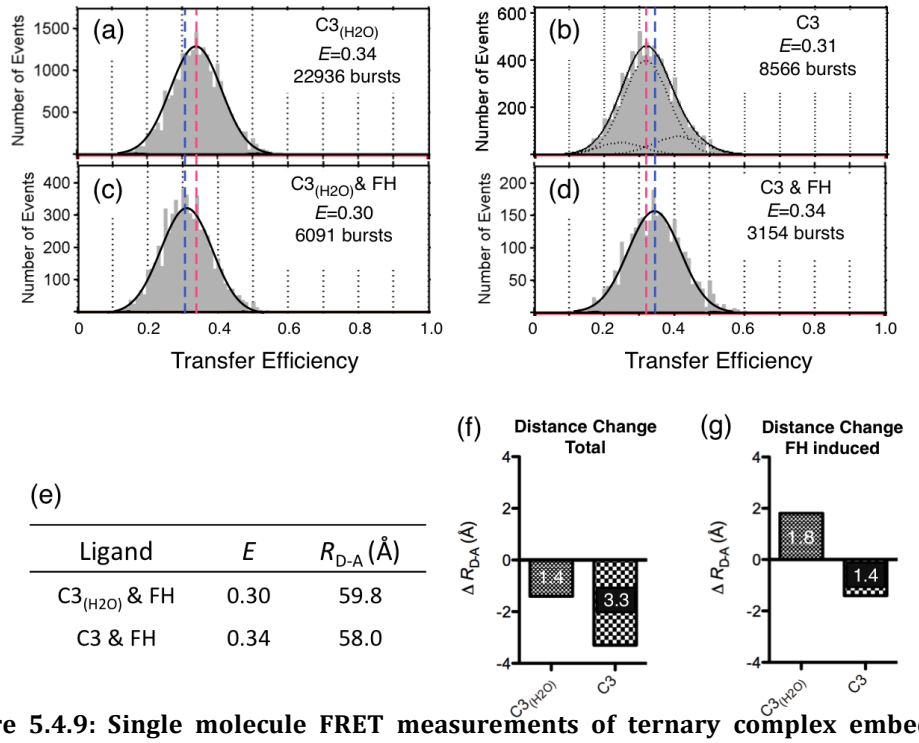

Figure 5.4.9: Single molecule FRET measurements of ternary complex embedded Sbi-III-IV. (a-b) *E* histograms for secondary ligand bound Sbi-III-IV. **(c-d)** *E* histograms for ternary complex embedded Sbi-III-IV. Red dashed line: Before FH recruitment, Blue dashed line: After FH recruitment. Using a single-Gaussian fit (black solid line), the mean values derived from the fitting were provided on the graph as well as the total number of bursts. **(e)** A table summarizing the detected *E* and the resulting $R_{D\text{-}A}$ values. **(f)** A bar chart presentation of changes in interprobe distance, calculated as $R_{D\text{-}A\ ternary\ complex}$ - $R_{D\text{-}A\ unliganded}$. **(g)** A bar chart presentation of changes in interprobe distance, calculated as $R_{D\text{-}A\ ternary\ complex}$ - $R_{D\text{-}A\ dimeric\ complex}$. For $\Delta R_{D\text{-}A}$, positive values indicate relaxation of Sbi-III-IV molecule, negative values indicate relative shortening of Sbi-III-IV molecule.

As shown in previous sections, the Sbi-III-IV binding to C3 fragments induces subtle shortening of the inter-terminus distance. Although the changes in $R_{D\text{-}A}$ are modest, this could still imply the existence of a new domain III conformation that is ready to recruit FH/FHR-1 as the third component of a ternary complex. Based on the flexible and elongated domain structure of FH and FHR-1, by binding to these proteins, the Sbi domain III could be subjected to more conformational influences. Therefore with the recruitment of FH or FHR-1 further FRET efficiency changes would be expected.

The single molecule FRET measurements demonstrated that in combination with different C3 fragments, Sbi-III-IV could bind to FH in distinct conformations. Fig.6.4.9.a-d shows two comparisons of E distributions, before and after the recruitment of FH. Using $C3_{(H2O)}$ as the secondary ligand, the binding of FH induces a decrease in E from $E_{C3(H20)}$= 0.34 to $E_{C3(H20)+FH}$= 0.30. However, the separate measurement using C3 as the secondary ligand shows that the FH recruitment increases E from E_{C3}= 0.31 to E_{C3+FH}= 0.34. After conversion of E to $R_{D\text{-}A}$, the inter-terminus distances of the ternary complex embedded Sbi-III-IV were compared with the unliganded Sbi-III-IV and secondary ligand bound Sbi-III-IV. As shown in Fig.6.4.9.f, compared to unliganded Sbi-III-IV, the assembly of ternary complexes shortens the inter-terminus distance of Sbi-III-IV in both cases. However, the FH induced distance changes are dependent on the type of C3 isoform. Based on the $C3_{(H2O)}$:Sbi complex a subsequent relaxation was observed, but based on the C3:Sbi complex a further shortening process was detected. These observations suggest that in order to recruit FH, Sbi-III-IV has to adopt different conformations to accommodate the requirements of using structurally different C3 isoforms as the secondary component of the ternary complex.

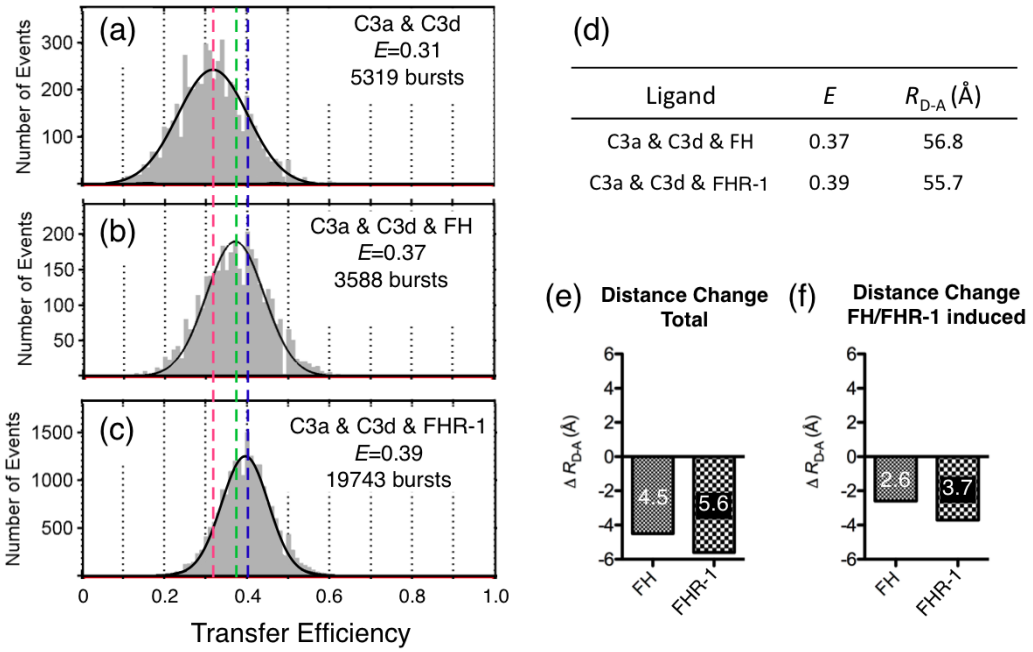

Figure 5.4.10: Single molecule FRET measurements of ternary complex embedded Sbi-III-IV. (a) *E* histograms for secondary ligands (C3a and C3b) bound Sbi-III-IV. **(b-c)** *E* histograms for ternary complex embedded Sbi-III-IV. Red dashed line: Before FH/FHR-1, Green dashed line: After FH recruitment, Blue dashed line: After FHR-1 recruitment. Using a single-Gaussian fit (Black solid line), the mean values derived from the fitting were provided on the graph as well as the total number of bursts. **(d)** Table summarizing the detected *E* and the resulting $R_{D\text{-}A}$ values. **(e)** A bar chart presentation of changes in inter-probe distance, calculated as $R_{D\text{-}A\ ternary\ complex}$ - $R_{D\text{-}A\ unliganded}$. **(f)** A bar chart presentation of changes in interprobe distance, calculated as $R_{D\text{-}A\ ternary\ complex}$ - $R_{D\text{-}A\ C3a\ +C3d}$. For $\Delta R_{D\text{-}A}$, negative values indicate relative shortening of Sbi-III-IV molecule.

FH or FHR-1 have been shown to be able to form ternary complexes with Sbi-III-IV in combination with multiple types of C3 isoform. However, when using the same type of C3 isoform, Sbi-III-IV mediates a much stronger binding to FHR-1 than FH (Section 4.3.10.2). This observation is especially hard to comprehend, as the putative binding regions of FHR-1 and FH are almost identical in primary sequence. Using single molecule FRET, the FH and FHR-1 binding modes of Sbi-III-IV were studied. To perform the experiment, an *E* distribution of Sbi-III-IV incubated with C3d and C3a was firstly acquired (Fig.6.4.10.a). As previously established, E_{C3d} is almost the same as $E_{C3a+C3d}$, therefore in this series of measurement an excess amount of C3a was also supplemented, firstly as a negative control molecule and secondly to help

prevent fluctuations in ligand concentration. Based on this platform, the *E* distribution of FH ternary complex embedded Sbi-III-IV was determined; the single Gaussian fitting provides the mean *E* value of 0.37 (Fig.6.4.10.b). Furthermore, when FHR-1 was added instead of FH, the single Gaussian fitting derived mean *E* is 0.39 (Fig.6.4.10.c). The converted $R_{D\text{-}A}$ values are presented in Fig.6.4.10.d, when compared with all previous measurements, the Sbi-III-IV molecules embedded in these two type of ternary complexes are much more compact. In comparison with unliganded Sbi-III-IV, FH together with C3d induces a 4.5 Å decrease in $R_{D\text{-}A}$ which accounts for 7.3% of the original length of Sbi-III-IV. More dramatically, FHR-1 in combination with C3d shortens Sbi-III-IV by 5.6 Å, which accounts for 9.1% of the original length of Sbi-III-IV. Although when compared with the C3d bound Sbi-III-IV, the FH induced distance change is reduced to 2.6 Å and the FHR-1 induced distance change is reduced to 3.7 Å. This still shows that the Sbi-III-IV molecules embedded in these ternary complexes adopt unprecedentedly compact conformations. Because of the discrepancies between FH and FHR-1 induced $R_{D\text{-}A}$, it is reasonable to suggest that Sbi domain III binds FH and FHR-1 in two slightly different manners.

6.4.4 SAXS analysis of the ternary Sbi:C3d:FHR-1 complex

To date, multiple crystallographic studies have determined the 3D structures of Sbi-IV (Upadhyay *et al*. 2008), C3d (Nagar *et al*. 1998), Sbi-IV:C3d complex (Clark *et al*. 2011), FHR-1_{1-2} (Goicoechea de Jorge *et al*. 2013) and FHR-1_{4-5} (Bhattacharjee *et al*. 2015), but little information is available on the arrangement of these components in the ternary complex. Although a putative molecular model of the ternary complex is proposed in Section 4.4.3, further experimental validations are needed. Therefore small-angle X-ray scattering (SAXS) was used to determine the structural contours of the Sbi-III-IV:C3d:FHR-1 ternary complex. Ternary complex components were mixed as described in Section 6.3.10, until a final molar ratio of 1:1:1 was achieved. The scattering profile was acquired at a protein concentration of 2.0 mg/ml (SDS-PAGE analysis is presented in Appendix Fig.9.10.A).

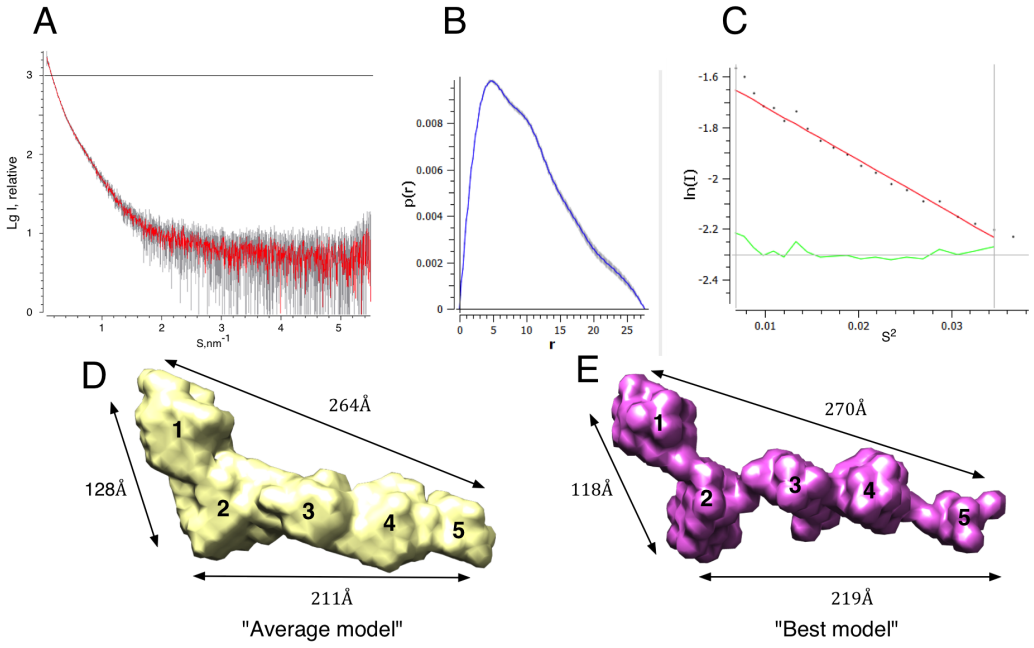

Figure 6.4.11: Small-angle X-ray scattering (SAXS) of Sbi-III-IV:C3d:FHR-1 ternary complex. (A) Buffer subtracted scattering curve of the ternary complex. (*I* is a relative unit, s is expressed in nm^{-1}). **(B)** Pair distance distribution function P(r). **(C)** Guinier approximation. **(D)** An average model of 10 independent calculated models. **(E)** Single model with highest score. B and C were calculated using PRIMUS program package. *Ab initio* scattering models were generated with DAMMIF and averaged in DAMAVER. The surface presentations were prepared by Chimera.

During the SAXS experiment, the scattering profiles of protein with buffer and buffer alone were collected (Appendix Fig.9.10.B), after subtraction of the buffer signal, the differential scattering profile of the protein sample alone was derived (Fig.6.4.11.A). The scattering profile was subsequently converted to a $P(r)$ function and Guiner plot (Fig.6.4.11.B-C), through which structural parameters were calculated. As a preliminary indication of the sample quality, the linear fit at the low *s* region of the Guiner plot suggests that the protein scattering profile is eligible for downstream structural modeling processes. As shown in Table 6.4.2, the SAXS parameters of the FHR-1 ternary complex are compared with previously published data of the Sbi-III-IV:C3d complex (Clark *et al*. 2011). According to the volume, the ternary complex is about 4-5 times larger than the Sbi-III-IV:C3d binary complex, which demonstrates an unexpected large size for the monomeric ternary complex. At the same time, significant increases in *Rg* and D_{max} are also observed. Therefore, these data indicate that, in solution, the FHR-1 ternary complex probably exists as a dimer with an elongated conformation.

Table 6.4.2: Overall parameters of SAXS data. Sbi-III-IV:C3d SAXS data was retrieved from (Clark *et al*. 2011). *Rg*, D_{max}, V_p and V_{ex} are radius of gyration, maximum size, Porod volumn and excluded volume derived by experimental SAXS data.

	$\mathbf{Rg_{(Guinier)}}$	$\mathbf{Rg_{(P(r))}}$	$\mathbf{D_{max}}$	$\mathbf{V_p}$	$\mathbf{V_{ex}}$
Sbi-III-IV:C3d	3 nm	3.3 nm	12 nm	90 nm^3	104 nm^3
Sbi-III-IV:C3d:FHR-1	7.8 nm	8.2 nm	27nm	400 nm^3	490 nm^3

The low-resolution *ab initio* models of the ternary complex reconstructed using the bead-fitting program DAMMIF. An "average model" of 10 independently calculated models is presented in Fig.6.4.11.D, and the "best model" with lowest χ^2=1.34 is shown in Fig.6.4.11.E. Both average and best models are very similar in shape and size, and adopt an asymmetrical "L" shape, which comprises 5

distinct globular domains (Fig.6.4.11.D-E). The first density domain is related to the other four density-domains through an angle of 120°. The "best model" shows clear domain boundaries and decreased densities in the connecting region, which indicates that the protein domains are likely to be connected through flexible loops.

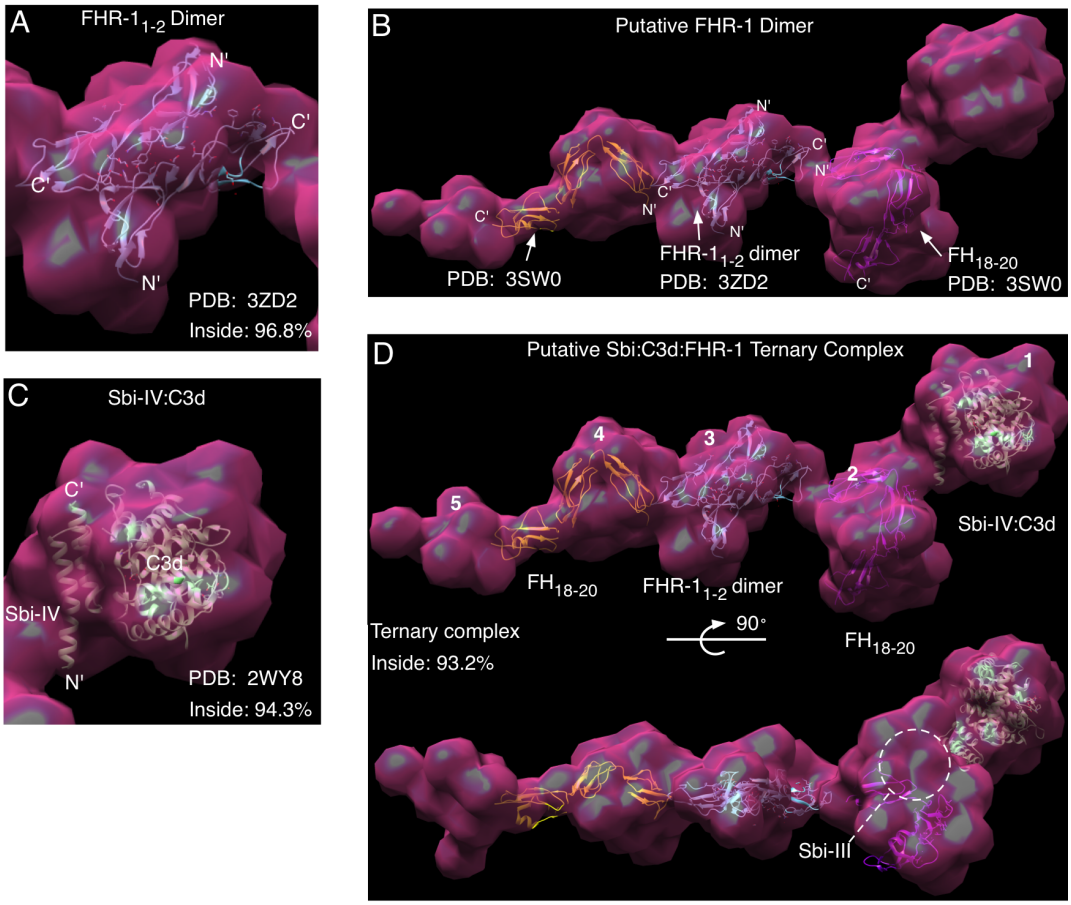

Figure 6.4.12: Model fitting of Ternary complex. **(A)** Fitting of the FHR-1_{1-2} dimer. **(B)** Fitting of full-length FHR-1 dimer. **(C)** Fitting of the Sbi-IV:C3d binary complex. **(D)** An overview of fitted Sbi-III-IV:C3d:FHR-1 1:1:2 dimer. Inside percentage indicates the percentage of the structural model that is included in the SAXS envelope. PDB files used were indicated on the figure. Model fitting and graphic presentation were performed with Chimera program.

Using the determined low-resolution structural envelopes, semi-automatic fitting processes were performed to generate the putative molecular model of FHR-1 containing ternary complexes. Using the program Chimera (Pettersen *et al*. 2004), individual structural components of the ternary complex were fitted into the "Best model", under the principal of maximal occupancy. Then small

manual adjustments were made based on established structural characteristics of FHR-1 and the Sbi-IV:C3d complex. As introduced in Section 1.4.3, FHR-1 was shown to dimerize in serum, therefore it could be that the elongated SAXS model contains a pair of dimerized FHR-1 proteins, with the dimerization region located in middle of the model, and Sbi:C3d complex bound on either end of the model.

Using the "best model" generated by DAMMIF as the search density, the highest occupancy was achieved by fitting the crystal structure of FHR-$1_{1\text{-}2}$ dimer into the density domain 3 (Fig.6.4.12.A). Based on the location and orientation of the fitted FHR-$1_{1\text{-}2}$ dimer, two $FH_{18\text{-}20}$ ($FH_{18\text{-}20}$≈FHR-$1_{3\text{-}5}$) domains were manually fitted into the SAXS envelope, flanking the dimerization region. The resulting putative model of the FHR-1 dimer occupies density domains 2-5 of the SAXS envelope (Fig.6.4.12.B). Finally, a space fitting search was performed again using Sbi-IV:C3d crystal structure. It was found that density domain 1 provides best occupancy to this binary complex (Fig.6.4.12.C).

Thus, this putative ternary complex model suggests that although the FHR-1 dimer provides two Sbi:C3d binding sites, but only one site is bound in the current model. Another surprising discovery is that unlike the previously proposed idea that Sbi-IV:C3d:$FH_{18\text{-}20}$ is a tightly packed globular complex (Section 4.4.3), the new SAXS based model suggests that the C3d is not necessarily interacting with FHR-$1_{4\text{-}5}$ in the ternary complex. Instead the connection between C3d and FHR-1 could be solely maintained by Sbi-III-IV, which is strongly supported by the newly discovered binary binding between Sbi and FH/FHR-1 (Section 4.3.10.3). As shown by Fig.6.4.12.D, using current structural information, a considerable amount of space (Fig.6.4.12.D, white dash line circle) in density-domain 2 was unable to be explained, but given the close proximity of this space to the N-terminus of Sbi-IV, it is possible that Sbi-III occupies this space and makes contact with $FH_{18\text{-}20}$/FHR-$1_{3\text{-}5}$.

6.5 Discussion

In this chapter, the structural aspects of Sbi-III-IV and its ligand binding properties were investigated. Firstly, the protein structure prediction server I-TASSER was used to construct putative models of Sbi-III^{WT} and Sbi-III^{K173A}. Comparisons of these models indicate a slight secondary structure difference in the C-terminal of Sbi-III could cause a decrease in Sbi-III's activity. In the second part of this chapter, the conformational flexibility of Sbi-III-IV was studied by ALEX smFRET. These results suggest that un-liganded Sbi-III-IV adopts one major conformation, but sequential changes in conformation are inducible by binding with various ligands. The FHR-1 binding of Sbi-III-IV:C3d complex causes a reduction of 9% in Sbi-III-IV's inter-terminal distance indicating a significant structural compaction. The final results section of this chapter, Section 6.4.4, provides the first structural insight into the Sbi-III-IV:C3d:FHR-1 ternary complex. The molecular model derived from SAXS analysis confirms the dimerization state of FHR-1 in solution, suggesting that the molar ratio of the ternary complex in the current model is 1:1:2, and supports an alternative packing mechanism of the ternary complex that is different from the putative model proposed in Section 4.4.3.

6.5.1 Evaluation of current structural data against Sbi-III-IV:C3d SAXS analysis

Like most structure prediction studies, despite the sophisticated algorisms and self-evaluating scores, discrepancies from the real structure are unavoidable; therefore experimental verification is essential before further exploitation of the model. To evaluate the Sbi-III^{WT} model presented in this chapter, the model of Sbi-III^{WT} (Fig.6.4.1.A) and the crystal structure of Sbi-IV:C3d were fitted manually into the SAXS envelope of Sbi-III-IV:C3d binary complex that had been determined previously. By comparing the theoretical scattering intensity curve

of the model against the experimental scattering curve, the accuracy of the current Sbi-III^{WT} model can be tested.

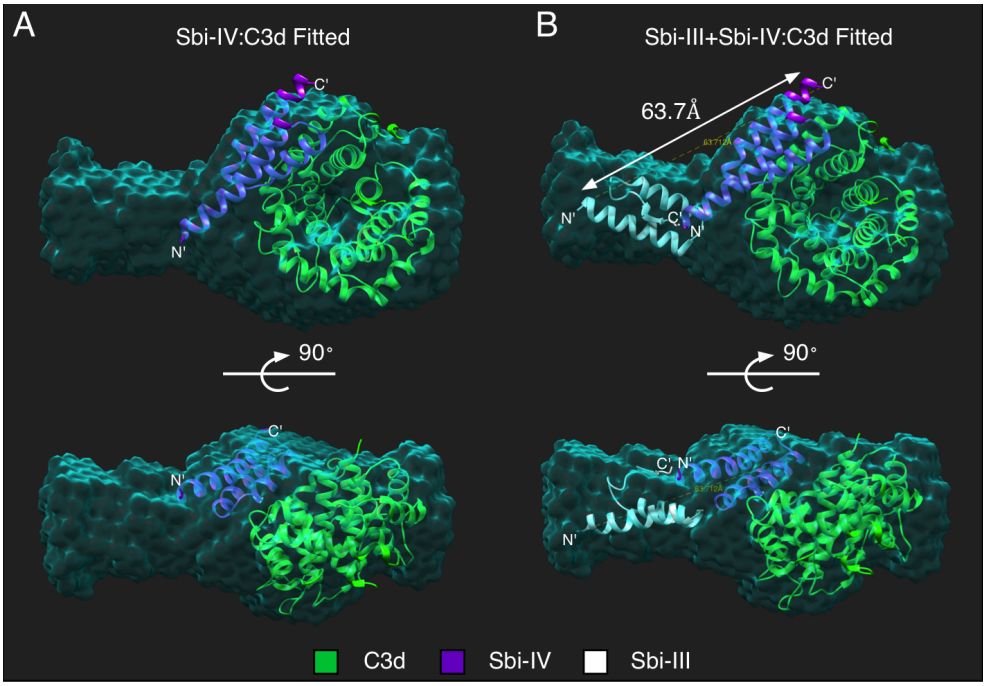

Figure 6.5.1: Reconstruction of the Sbi-III-IV:C3d complex based on the Sbi-III-IV:C3d SAXS envelope using the Sbi-III^{WT} model and the Sbi-IV:C3d crystal structure. **(A)** Before Sbi-III fitting and **(B)** after fitting. The identity of the structural components is indicated by colour key. The SAXS envelope is depicted in translucent Cyan colour. Guided by the SAXS envelope, Sbi-III^{WT} was manually fitted, and the distance between the N-terminus of Sbi-III and the C-terminus of Sbi-IV was determined by Chimera. The Sbi-IV:C3d complex (PDB: 2WY8) was used to construct this model.

As shown by Fig.6.5.1, guided by the Sbi-III-IV:C3d SAXS envelope, the model of Sbi-III^{WT} fits neatly into SAXS *ab initio* density. The theoretical scattering curve of the model was then calculated and compared with experimental scattering curve using CRYSOL (Svergun *et al*. 1995). Fig.6.5.2 shows that the overall discrepancy between two set of data is χ^2=4.7. At the low *s* region of the plot, the scattering curve of the Sbi-III-IV:C3d theoretical model nearly superimposes with the experimental data, but large discrepancies were detected at the high *s* region of the plot (Fig.6.5.2, blue dash box). The high correlation at low *s* suggests that the model genuinely reflects the size and shape properties of the real structure (Svergun & Koch 2002). However in terms of internal structure (reflected by the

high *s* region) this model still can be improved, which indicates the difficulty of accurately predicting the 3D structure of Sbi-III using structural prediction methods. The distance between the Sbi-III-IV's termini, based on the SAXS model is 63.7 Å (Fig.6.5.1.B). This is similar to the distance determined by smFRET (59.8 Å, Fig6.4.8.g). Although no large discrepancy is revealed, a difference of 3.9 Å is observed which could be the result of the modeling error of Sbi-III^{WT} or smFRET's inherent technical shortcoming in measuring absolute distance.

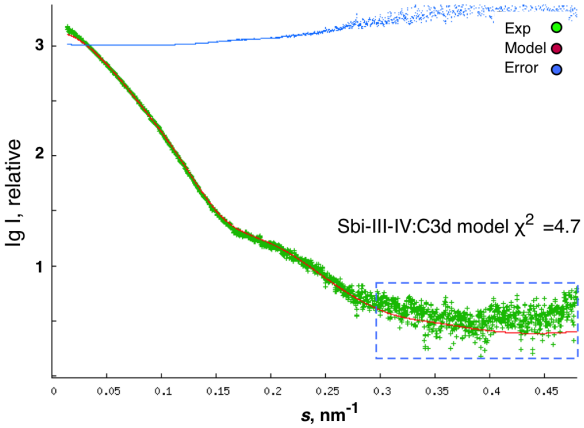

Figure 6.5.2: Experimental vs theoretical scattering curve. Sbi-III-IV:C3d model was used for theoretical scattering curve calculation and compared to experimental data using CRYSOL. Large discrepancy is highlighted by blue dashed box.

Thus, here we provided a Sbi-III-IV:C3d model with reliable size and shape characteristics, which could be exploited further for the modeling of Sbi-III-IV ligand induced conformation changes.

6.5.2 Hypothesis of Sbi-III-IV ternary complex binding mode

It was demonstrated in Section 6.4.3.3 that Sbi-III-IV changes in inter-terminus distance upon binding of various protein ligands. The conformational flexibility seems highly related to the complement modulatory function of Sbi-III-IV, as the CD studies (Section 4.3.8.1) demonstrated that both K173A and S199A mutants contain increased α-helix content. The modeling study (Section 6.4.1) indicates that C-terminal segment of Sbi-III that connects to Sbi-IV could be responsible for the flexibility of Sbi-III-IV. The flexibility of the peptide segment connecting Sbi-IV to Sbi-III was also previously illustrated by a NMR study of Sbi-IV (Upadhyay *et al.* 2008). As shown in Fig.6.5.3.A, the N-terminal loop region of the 20 solution NMR structures of Sbi-IV demonstrates three general orientations. The majority of the loop adopts the orientation coloured in blue in Fig.6.5.3.A, the purple and yellow loop orientations are less

common. Based on this previously unexploited information, we propose that the three observed Sbi-IV N-terminal loop orientations could be translated into three Sbi-III orientations, depicted in Fig.6.5.3.B as O1, O2 and O3. The orientation changes of Sbi-III from O1 to O2 and O3 involve two iso-planar rotations of 90°, due to the rotations being centred around the N-terminus of Sbi-IV, therefore only slight inter-terminus distance changes are produced (Fig.6.5.3.C). Changing from O1 (61.5 Å) to O2 (60.4 Å) produces an inter-terminus distance change of 1 Å, and from O1 to O3 (55.6 Å) a larger decrease in distance (5 Å) is observed. Among these three Sbi-III orientations, the O1 orientation is found able to fit neatly in the Sbi-III-IV:C3d SAXS envelope shown in Fig.6.5.1.A.

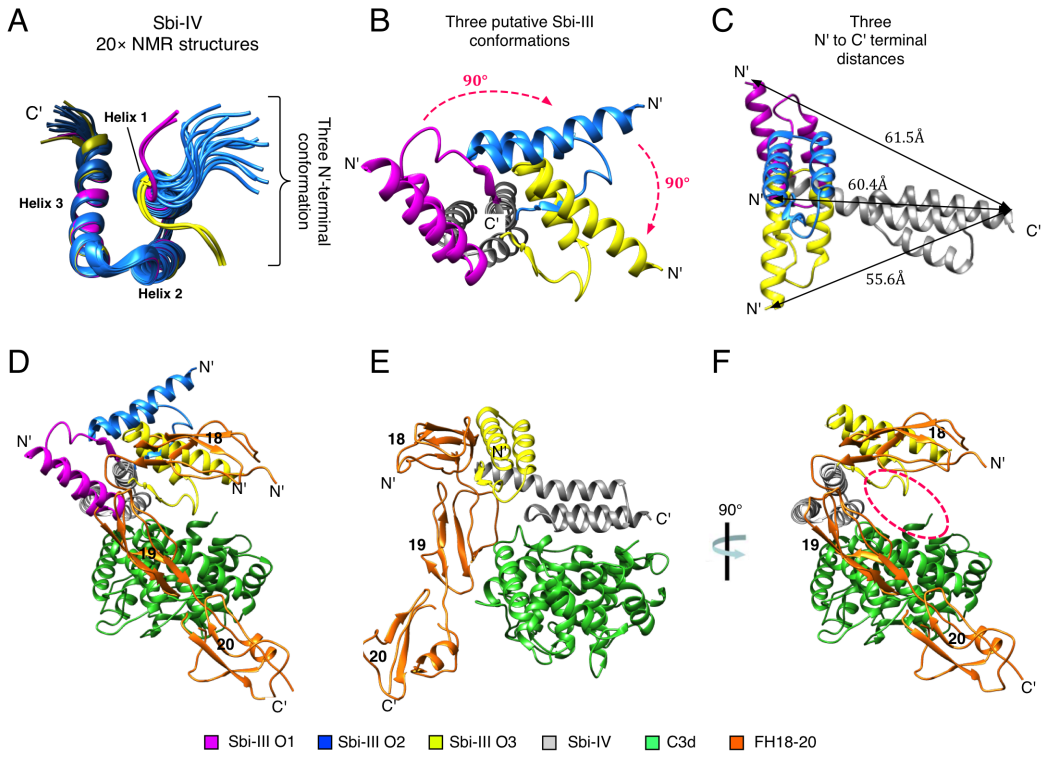

Figure 6.5.3. Sbi-III's orientation flexibility: (A) 20 solution NMR structures of Sbi-IV.PDB:2JVG **(B)** Three extrapolated Sbi-III orientations based on the NMR structures. **(C)** The inter-terminus distances of Sbi-III-IV. Distances are determined using Chimera **(D)** Putative structural relationship between Sbi-III's orientations and ternary complex formation. **(E-F)** Putative structural relationship between Sbi-III O3 orientation and $FH_{18\text{-}19}$≈$CFHR1_{3\text{-}4}$. The proposed Sbi-III binding region is indicated in a red dashed oval. Structural analysis and presentation were performed using Chimera.

The subtle decreasing trend in inter-terminus distances (O1>O2>O3, Fig.6.5.3.C), fits with our smFRET results (Section 6.4.3.3 & 6.4.3.4), which shows that Sbi-III-IV decreases in inter-terminus distances upon step-wise ligand-binding events. Therefore, we propose that the changing of Sbi-III orientations could be the underlying molecular requirement for Sbi-III-IV ligand binding events. This theory is evaluated in the context of ternary complex formation, which has been proven to be predominantly a Sbi-III mediated event. Using Sbi-IV as a reference, three Sbi-III orientations were modelled into the previously proposed Sbi-IV:C3d:FH_{18-20} complex (Fig.4.4.2.B). It is shown (Fig.6.5.3.D) that the Sbi-III O1 and O2 orientation is not in a favourable location to make contact with FH_{18-19}. By adopting the O3 orientation, however Sbi-III is hypothetically placed in close contact with FH_{18-19} (Fig.6.5.3.E-F).

6.5.3 "Loose" and "Tight" binding model of ternary complex

In this study, based on the SAXS analysis, a putative model for the Sbi-III-IV:C3d:FHR-1 ternary complex was generated (Fig.6.4.12.D), based on which the previous report regarding the dimerization state of FHR-1 was confirmed. The model also suggests a previously unexpected molar ratio and a novel loosely packed ternary complex binding mode. These observations not only prompt new hypotheses about ternary complex formation, but also pave the way for further in-depth structural studies.

Sbi and Ecb are two *Staphylococcal* immune evasion proteins that form ternary complexes. In this thesis, it was found that although similar complement constituents are used, the assembly mechanisms of the ternary complexes are totally different. The previous bioinformatic analysis (Hammel *et al.* 2007a) shows that Ecb has no Sbi-III-like domain, the author (Amdahl *et al*. 2013) proposes a model for the Ecb ternary complex (Fig.6.5.4.A) by matching the Ecb:C3d crystal structure (Hammel *et al.* 2007a) with the C3d:FH_{19-20} crystal

structure (Kajander *et al.* 2011). Using C3d as the reference structure, their model suggests that the Ecb binds FH_{19}, which increases the affinity between FH and C3b. Notably, the proposed Ecb residues interacting with FH_{19} are not conserved in Sbi-IV structure.

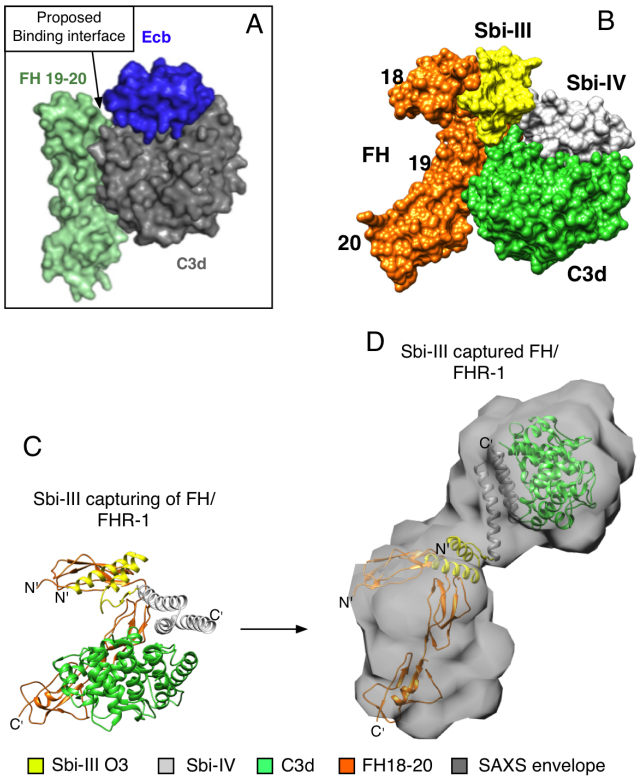

Figure 6.5.4: "Loose" and "Tight" packing models of ternary complex. (A) The surface representation of Ecb:C3d:FH19-20 ternary complex. **(B)** The surface representation of Sbi-III^{O3}-IV:C3d:FH18-20. **(C)** Hypothesized structural model of Sbi-III^{O3}-IV:C3d:FH18-20, "Tightly packed model". **(D)** SAXS model of Sbi-III-IV:C3d:FH18-20, the "Loosely packed model". Figure A taken from (Amdahl et al. 2013).

Inspired by their methodology, in Section 4.4.3 a putative Sbi-IV:C3d: FH_{18-20} model was generated, based on which Sbi-III O3 was added to generate a Sbi-III-IV:C3d: FH_{18-20} model (Fig.6.5.3.E-F) and the putative Sbi-III binding site was proposed. The updated model shows that the Sbi-III-IV:C3d: FH_{18-20} ternary complex is extremely tightly packed (Fig.6.5.4.B), therefore raising concern over steric hindrance and accessibility to the binding site. A possible answer for this issue is provided in Section 6.4.4, in which a loosely packed ternary complex configuration (Fig.6.4.12.D and Fig.6.5.4.D) is implicated by the SAXS study.

This new discovery triggers a rethink of the mechanistic detail about ternary complex formation. It has been shown in this study that C3 isoform binding is a

prerequisite condition for Sbi-III-IV to acquire enhanced binding affinity to FH and FHR-1. This firmly supports two arguments regarding the role of C3 isoform binding. The first is to prepare Sbi-III structurally to a presumably FH/FHR-1 welcoming orientation/conformation, the second is to provide the initial FH/FHR-1 binding interface. Thus, the existence of the tightly packed configuration may be an unavoidable part of the ternary complex formation mechanism. Therefore, the relationship between these the "tightly packed" and "loosely packed" models (Fig.6.5.4.C and Fig.6.5.4.D) may not necessarily be contradictory, but synergistic; together they could depict a sequential event. The tightly packed model (Fig.6.5.4.C) could represent how Sbi-III-IV captures C3 isoforms and FH/FHR-1 at the same time. However after the both Sbi-III and Sbi-IV are bound, the ternary complex could dissemble into a loosely packed configuration (Fig.6.5.4.D).

Taken all observations together, a summary for the molecular events during the formation of Sbi ternary complex could contain following steps. Initially, the Sbi-III adopts the O2 orientation, but after Sbi-III-IV binds to a C3 isoform, Sbi-III switches the to O1 orientation. As shown in Fig.6.5.3.D, in the O1 orientation, the potential steric clash between Sbi-III and FH_{18} is avoided; therefore the O1 orientation is a FH/FHR-1 welcoming orientation. Next, using the interaction interface on C3d, FH/FHR-1 docks on the C3d containing C3 isoforms in a weak and transient fashion. Then, Sbi-III flips into the orientation O3, although in this orientation there could be considerable steric clashes, but the decrease in distance facilitates Sbi-III reaching its binding site. After the binding of Sbi-III, the steric clash could induce the ternary complex to adopt a loosely packed configuration.

It is indicated by the hydrodynamic diameter analysis (Section 4.3.8.2) that Sbi-III-IV^{K173A} adopts a more compact conformation. Thus, it is possible that Sbi-III-IV^{K173A} adopts an "O3 like" conformation naturally, which could

accidentally hamper the capturing of FH/FHR-1.

6.5.4 Role of glycosylation in the differential binding of Sbi-III-IV to FH and FHR-1

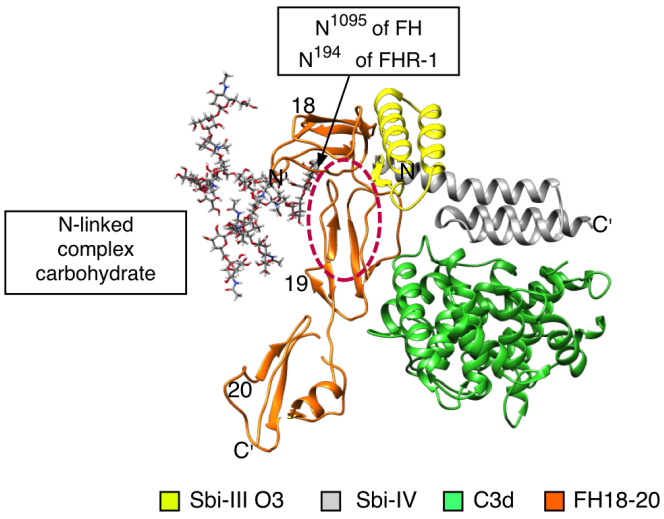

Figure 6.5.5: Impact of glycosylation on ternary complex formation. The putative Sbi-III binding site (red dashed circle) is in close proximity to the differential glycosylated site on both FH and FHR-1. Complex N-linked carbohydrate glycosylated FH18-20 is modelled using GlyProt (Bohne-Lang & Lieth 2005).

In chapter 4 (Section 4.3.10.2), it was demonstrated that Sbi-III-IV preferentially binds FHR-1 over FH in combination with various C3 isoforms. Although this binding preference is one of the theoretical foundations for Sbi triggered C3 consumption, given the extremely high sequence identity between $FH_{18\text{-}20}$ and $FHR\text{-}1_{3\text{-}5}$, how this selectivity is achieved remains elusive. In this section, an explanation for this question is discussed based on the differential glycosylation status of FH and FHR-1. Despite the sequence identity between $FH_{18\text{-}19}$ and $FHR\text{-}1_{3\text{-}4}$, biochemical differences could still be introduced via post-translational modifications. The *N*-linked glycosylation site in FH_{18} (N^{1095}) has been shown to always have a carbohydrate chain attached (Fenaille *et al.* 2007), but the post-translational modification on the equivalent glycosylation site in $FHR\text{-}1_3$ (N^{194}) is less strict. Two glycosylated forms of FHR-1 were found in human serum (Skerka *et al.* 1991), FHR-1β has two and FHR-1α has one carbohydrate chain attached (Skerka & Zipfel 2008). FHR-1α could represent the FHR-1 protein with no glycosylation on N^{194}. As shown in Fig.6.5.5, this potentially

decisive glycosylation site is located in close proximity to the putative Sbi-III binding site, in the presence of a complex carbohydrate chain the accessibility of the surrounding protein surface could be significantly hampered. Therefore, Sbi-III-IV could bind FHR-1α with a distinct binding kinetic profile, leading to preference for FHR-1 over FH. Although, as shown in Fig.4.3.19.B, it appears that Sbi-III-IV binds FHR-1β better than FHR-1α, but this result may be an artifact caused by recognition bias of the polyclonal FH antibody (Skerka *et al*. 2013).

6.5.5 ALEX smFRET as a tool to study protein conformation flexibility

In this study, using ALEX smFRET the conformational flexibility of Sbi-III-IV has been demonstrated in great detail. Although the *E* histogram (Fig.6.4.7) only suggests one major inter-terminal distance of unliganded Sbi-III-IV, based on the model proposed in Fig.6.5.3.C, changes in Sbi-III orientation could still occur without significant impact on the inter-terminal distance. The smFRET data indicated step-wise changes in Sbi-III-IV's inter-terminal distance during the assembly of ternary complex. The binding of secondary ligand (e.g. C3 isoforms) generally induces relatively small decreases in inter-terminal distance, followed by big distance decreases induced by binding of tertiary ligand (e.g. FH/FHR-1). This fits with the previous arguments that Sbi-III undergoes orientational changes and then binds to FH/FHR-1. Corresponding to the differential binding affinity, it is also revealed that Sbi-III-IV binds to FH/FHR-1 in slightly different manners (Section 6.4.3.4). This could reflect differences in the overall structure between $FH_{18\text{-}20}$ and $FHR\text{-}1_{3\text{-}5}$ in solution. But at the same time, the differential glycosylation status could also cause this difference.

6.5.6 Further experiments

Based on current structural data, a putative model for the ternary complex formation is constructed in this chapter. This leads to multiple lines of further

work that will not only validate the findings but also provide new molecular insights. Further SAXS analysis of Sbi:C3d:FHR-1 is required for improved data quality and modeling accuracy. Ternary complexes of different C3 isoforms could be used, as the distinct shape of C3 isoforms could simplify the interpretation of the ternary complex SAXS envelope. smFRET measurement of Sbi-III-IV mutants could also provide invaluable information. Potential crystallographic studies on the Sbi K173A mutant should also be considered. With proven increased structure stability, the Sbi-III or Sbi-III-IV version of this mutant could eventually be crystalized. Finally, the most informative further work of all, could be the crystallographic study of the Sbi-III-IV:C3d:FHR-1_{3-5} ternary complex. In this experiment the different glycosylation status of FHR-1_{3-5} should be included in order to investigate the impact of glycosylation on Sbi-III binding.

Chapter 7: General discussion

7.1 Immune evasion mechanism of Sbi

Within the arsenal of *S. aureus* immune evasion proteins, there are numerous small and secreted proteins that interfere with the function of the central complement component, C3. Although these *Staphylococcal* proteins have different modes of action, the goals of the previously determined mechanisms are the same: to block complement activation, to prevent opsonization, and to neutralize the complement effector molecules (e.g. C3a and C5a). The discovery that Sbi triggers C3 consumption fits with the long-term objections of these goals, but also demonstrates the unique mechanistic signatures of Sbi. Rather than direct inhibition, Sbi exploits the host's AP activation and regulation mechanisms to achieve immune evasion.

At first it may seem counter-intuitive that an immune evasion protein such as Sbi promotes C3 activation, but detailed scrutiny of the mechanism suggests otherwise. The significance of a distal C3 activation resembles an anti-missile flare that consumes active C3 before it can reach the bacterium. The metastable C3b only has a finite lifetime, therefore only the microbial surfaces in close proximity are under threat of opsonization. Furthermore, if the complement activation is not well orchestrated, the metastable C3b will more likely react with water and subsequently be degraded by complement regulators. Clearly, Sbi has evolved to minimize self-inflicted opsonization on the bacteria, doing so by directing the metastable C3b molecules to host targets such as IgG. Sbi expression correlates with the presence of IgG (Zhang *et al*. 2000), and it deliberately attracts IgG to the site of C3 consumption. The IgG molecule may be exploited as a molecular mop for metastable C3b. The Sbi-I-II:IgG interaction was shown to form large insoluble immune complexes (Atkins *et al*. 2008), which

potentially offer enough C3b deposition sites to neutralize the amount of C3b generated from a C3 convertase. Under physiological circumstances, a single C3 convertase has a half-life of 90 s, and is able to turn 160 C3 molecules into C3b (Pangburn 1986). In addition, (Smith *et al*. 2012) demonstrated that Sbi-III-IV is only active after becoming secreted ,which is another protective mechanism to tackle the C3 consumption "back-firing".

Given that Sbi triggered C3 consumption is distanced from the location of the bacteria, the resulting release of C3a probably would not cause harm to the bacteria, but could direct the leukocytes to irrelevant sites. On the contrary, the release of the much more potent chemoattractant C5a is strongly suppressed by Sbi.

Through the means of ternary complexation, Sbi achieves the goal of destroying active C3 before they can reach the bacteria. Although the mechanistic detail of Sbi is surprising, proteolytic degradation of C3 as an immune evasion strategy has been described before. *Streptococcal* cysteine protease SpeB (Terao *et al*. 2008) degrades C3 to inhibit bacterial clearance. Both Gelatinase E (GelE) (Park *et al*. 2008) from *Enterococcus faecalis* and *Staphylococcal* metalloprotease aureolysin (Laarman *et al*. 2011) cleave the C3 α-chain at a site close to the C3 convertase cleavage site, exposing the resulting C3b molecule to the host complement proteases. Sbi shares a very similar immune evasion philosophy with GelE and aureolysin, converting C3 to its activated conformation C3b in distal fluid phase, where C3b can be disposed of by host protease factor I. However, Sbi is clearly designed to deal with the explosive C3 activation event resulting from C3 convertase, as discussed earlier, the use of IgG could be a guarantee that the activated C3b will not harm the bacteria. The proteolytic reactions catalyzed by GelE and aureolysin are generally slower, therefore the factor I mediated C3b inactivation is unlikely to be overwhelmed.

A more prevalent immune evasion strategy involves recruiting FH onto microbial surfaces. This strategy is used by several bacteria, some yeasts and even some viruses (Lambris *et al*. 2008). The surface acquisition of FH is beneficial for the survival of the pathogens, and the surface associated FH makes the microbial surfaces like the non-activator surface, which is hostile for complement AP amplification. Various microbial proteins have evolved convergently to target two binding sites on FH, which suggests that the FH needs to be maintained in a specific orientation in order to be functionally active (Meri *et al*. 2013).

Recently, this traditional view of FH's role in immune evasion is being reinvestigated, as an increasing number of secreted immune evasion proteins have been shown able to recruit FH as well. Sbi is the first secreted *Staphylococcal* immune evasion protein discovered that sequesters FH family proteins in combination with C3 isoforms (Burman *et al*. 2008; Haupt *et al*. 2008). Similar activity was later associated with another two *Staphylococcal* C3 binding proteins Ecb-C (Ecb-C, C3d binding domain of Ecb)(Amdahl *et al*. 2013) and Efb-C (Efb-C, C3d binding domain of Efb)(Chen *et al*. 2010; Amdahl *et al*. 2013). Although all three proteins (Sbi-IV, Ecb-C and Efb-C) share a high level of structural similarity and are able to form similar FH ternary complexes, the mechanisms of ternary complex formation and the immunological outcomes differ significantly from each other. An in-depth discussion of the similarities and differences of these three *staphylococcal* proteins was presented in Sections 3.4.6.2. These three proteins present a perfect example of the functional significances of the C3 binding and ternary complex formation. The inhibition of C3 convertase is positively related to the avidity to C3b, the inhibition of C5 convertase is positively related to the ability to form ternary complexes. We propose that Sbi organizes more stable ternary complexes than the ones mediated by Ecb-C and Efb-C, because Sbi dedicates a separate domain (Domain III) to FH/FRH1 binding, while the other two proteins only provide a limited

interaction interface. Apart from Sbi, the other two proteins fit with the general expectation of immune evasion proteins. They significantly inhibit both C3 and C5 convertases, blocking the activation of complement. Ecb was also associated with recruiting FH to the *S. aureus* surface. At least 98% of the clinical isolates express Ecb, 85% express Efb (Jongerius *et al*. 2007) and the majority express Sbi (Smith *et al*. 2011). This suggests that despite the functional overlap, these proteins may have differential roles in *S.aureus* immune evasion.

The C3 activating function of Sbi could be attributed to 1) altered C3 binding kinetic properties, 2) the preference for FHR-1 containing ternary complex formation 3) Sbi-C3b adduct formation.

Comparing the binding kinetics of Sbi-IV and Efb-C with C3 fragments reveals the molecular adaptions Sbi has undergone to become a less potent inhibitor of AP C3 convertase. The kinetic of Efb-C binding to C3 fragments (Hammel *et al*. 2007b) demonstrates quick complex formation rates and very slow complex dissociation rates; same kinetic profile holds for the interactions between Efb-C to C3, $C3_{H2O}$, C3b and C3d. However, previous SPR analysis (Burman *et al*. 2008) have shown that Sbi binds strongly to C3 and C3d, and only weakly interacts with other C3 fragments. Sbi:C3 isoform complexes demonstrate a quick binding rate and quick dissociation rate. It could be argued that the dramatic decrease in stability from Sbi:C3 to Sbi:C3b, causes Sbi domain IV to dissociate from C3 after cleavage by C3 convertase. This type of transient interaction to C3b reduces Sbi's ability as an allosteric C3 convertase inhibitor, compared with Efb (Chen *et al*. 2010). This reduction in C3b binding avidity also agrees with the "Sbi-IV repositioning" mechanism proposed in Section 5.4.3.

Table 7.1: Complement modulators that simultaneously recruit FH and FHR-1

Genus and species	FH/FHR-1 binding proteins	C3 isoforms binding	C3 activation	References
S. pyogenes	Scl1.6 and Scl1.55	No	No	(Reuter *et al*. 2010)
S.aureus	Sbi	Yes	Yes	(Burman *et al*. 2008; Haupt *et al*. 2008)
B. burgdorferi	CRASP-3, CRASP-4, CRASP-5,	No	No	(Haupt *et al*. 2007) (Kunert *et al*. 2007)
P. aeruginosa	Tuf, Lpd	No	No	(Hallstrom *et al*. 2012)
E. coli	Stx2	No	Yes	(Orth *et al*. 2009) (Poolpol *et al*. 2014)

The simultaneous binding of FHR-1 and FH is not an exclusive feature of Sbi. Numerous bacterial proteins (Table 7.1) have been identified that can bind FH and FHR-1 at the same time. Similar to Sbi, FH and FHR-1 compete for binding to these proteins, among which Scl and CRASP have been shown able to reduce fluid phase C3b degradation. This C3b protective property is attributed to the FHR-1 binding, as FHR-1 does not possess factor I cofactor activity. The majority of these proteins are not able to trigger C3 activation. But, Stx2 is the only other protein that shares the C3 activation outcome with Sbi. This protein is unique in its ability to bind both FH_{6-8} and FH_{18-20} regions of FH, unlike the majority of the proteins described here that only target the FH_{18-20} region. The AP pathway activation process triggered by Stx2 is able to proceed until the formation of the membrane attack complex, which releases anaphylotoxins C3a and C5a. Therefore, Stx2 is proposed as a bacterial toxin, which could be a major cause of hemaolytic uremic syndrome (HUS). The molecular mechanism of Stx2 induced AP activation remains to be elucidated.

In many aspects, these FH family binding proteins behave in a strikingly similar

fashion to Sbi, however Sbi is the only protein that binds FH and FHR-1 in combination with C3 isoforms. C3, C3b and C3d are all eligible constituents for Sbi ternary complex assembly. This suggests that Sbi recruits FHR-1 before, during and after the C3 activation. Sbi decreases the physical distance between C3b and FHR-1, and this could be another reason for the enhanced C3b protection. It was also demonstrated that Sbi prefers to bind FHR-1 over FH during ternary complex assembly. Under physiological conditions, where the FHR-1:FH ratio is 0.5:1, only 40% of C3b is FH bound. Together, these unique features make Sbi a better protector of fluid phase C3b than any other known bacterial complement modulator (Table 7.1).

Another truely unique feature of Sbi is its ability to form the Sbi-C3b adduct. It has been demonstrated that this is a deliberate mechanism of Sbi in order to extend the serum half-life of the C3b conformation (Section 5.3.3.2). By covalent deposition on polysaccharides or proteins, a 10-fold reduction (S. Meri & Pangburn 1990) in FH affinity for C3b can be achieved. This phenomenon is normally exploited by the host immune system. To assist AP signal amplification, IgG molecules have evolved to behave as a prominent deposition target for C3b. The resulting IgG-C3b adduct demonstrates a long serum half-life (Fries *et al*. 1984) and has been accredited as the most potent C3 convertase precursor in the blood (Lutz & Jelezarova 2006). A mutation at the major IgG C3b deposition site (S132A) abolishes the ability of the Fab region to bind C3b and to activate the AP of complement (Vidarte *et al*. 2001). These observations correlate with the results here that adduct-formation defective Sbi-III-IV mutants are poor initiators of C3 consumption.

The Sbi-C3b adduct alone can consume AP activity in a dose-dependent manner. In Section 5.3.3.3, it was proposed that the Sbi-III-IV in Sbi:C3:FHR-1 ternary complex embedded mode is convertible to C3b deposited mode, during which the domain III interaction with FHR-1 could be maintained. The resulting

Sbi-C3b:FHR-1 complex could be another explanation for the exceptional resilience of the Sbi-C3b adduct against factor I mediated inactivation. All these observations taken together could suggest that an orchestrated C3b deposition process is another secret of the success of Sbi as a C3 activator. After the conversion of C3 to C3b, the nascent C3b molecule needs to be stabilized immediately by forming a covalent adduct. Instead of allowing C3b to become deposited in a semi-random and inefficient natural process, Sbi deliberately offers itself as the deposition target. By this route, the resulting Sbi-C3b adduct stands a better chance of eventually developing into a functional C3 convertase.

7.2 Structural aspects of the ternary complexes

In this study, the smFRET study of Sbi-III-IV and its ligand binding properties indicates: 1) Free Sbi-III-IV demonstrates one major inter-terminal distance 2) Sbi-III-IV only demonstrates limited inter-terminal distance flexibility, 3) Sbi-III-IV undergoes a step-wise structural change process to assemble the ternary complex. In addition, using the predicted Sbi-III model, previous NMR data, the Sbi-III-IV:C3d and the Sbi-III-IV:C3d:FHR-1 SAXS envelopes, two Sbi ternary complex models were constructed. The “tight” packed model is believed to represent the “capturing” phase of ternary complex formation, the “loose” packed model could represent the “captured” ternary complex.

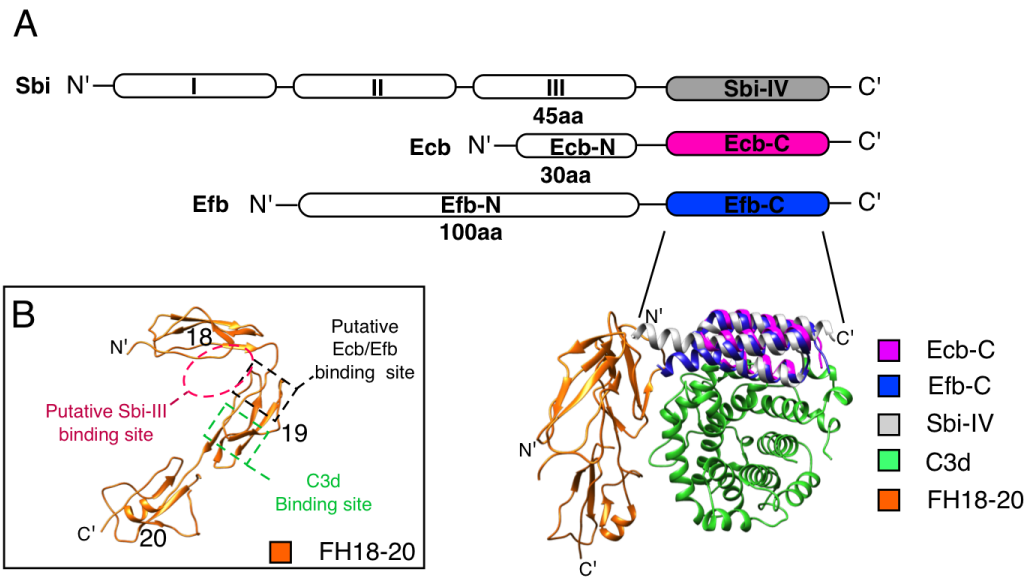

Figure 7.1: Putative models of *Staphylococcal* immune evasion protein mediated ternary complex. (A) Sequence and structural alignments of Sbi, Ecb and Efb. In Section 4.4.3 details of putative ternary complex modeling are provided. Sbi-IV, Ecb-C and Efb-C present the C3d binding region shown in the structural model. **(B)** Proposed bacterial protein binding sites on FH_{18-20}.

So far multiple attempts have been made to construct structural models of the ternary complexes. A detailed discussion of the modelling process is presented in Sections 4.4.3 and 6.5.2. The putative models of Sbi-IV, Ecb-C and Efb-C ternary complexes are shown in Fig.7.1. According to these models, the C3d binding Ecb-C and Efb-C could form ternary complex with C3d and FH with minimal steric clashes. However, if the N-terminal regions of these C3d binding proteins were taken into account, an alternative conclusion would be more reasonable. As shown in Fig.7.1.A, there are considerable lengths of extra polypeptide chains in the N-terminal segments of Ecb-C and Efb-C, which are not associated with FH binding activity. The N-terminal region of Efb-C is responsible for fibrinogen binding(Bodén & Flock 1994), and the function of the N-terminal domain of Ecb-C is unknown. Therefore, under physiological circumstances, whether the full-length Ecb and Efb will achieve the same level of ternary complex formation as their recombinant truncated counterparts remains in doubt. As pointed out in Section 5.5.3, if the N-terminal region of a C3d binding domain is not correctly positioned, the ternary complex formation will be significantly jeopardized.

However, Sbi does not pose the same problem, since Sbi-III is designed to bind FH or FHR-1. More interestingly, in this study a loosely packed Sbi ternary complex model was proposed based on the SAXS analysis. This result offers us an answer of how Sbi solves the problem of potential steric clash once the ternary complex has formed.

7.3 Therapeutic potential of Sbi

The complement system is often considered as a double-edge sword. An intact complement cascade is essential for protection against invading pathogens and for developing long-term adaptive immunity of the host. Whereas, an imbalanced, excessive or deregulated complement activation is hugely problematic to the host. As described in this thesis, Sbi demonstrates duplicitous complement modulatory functions, activating C3 with great efficiency and at same time potently suppressing C5 activation. These features could be delicately exploited, thereby unleashing the therapeutic potential of Sbi.

7.3.1 Vaccine adjuvant

Firstly, this immune evasion protein from *S.aureus* could be exploited as a new type of vaccine adjuvant. Vaccination has been proven as the most successful method of eradicating infectious diseases. Traditionally, attenuated or inactivated pathogens were used as antigens. Despite their success in modern day disease control, their inherent safety flaws undermine the potential of these relatively simple and robust methods to be exploited further. Nowadays, the therapeutic industry is increasingly interested in the development of subunit vaccines, which are based on a purified antigenic subunit. This pinpointed antigen presentation scheme allows vaccination to be utilized not only as a way to fight infectious pathogens, but also deadly human diseases that are associated with aberrant biochemical epitopes. However, not all purified antigenic subunits

are sufficiently immunogenic (Coffman *et al*. 2010); therefore adjuvants generally need to be added to subunit vaccines to enhance the immune response. In recent years, the attention of new adjuvant research is shifting from the activators of Toll-like receptors (TLRs) to activators of the complement system (Reddy *et al*. 2007; Liu *et al*. 2013). Although the complement system was conventionally considered as a defense mechanism, there is mounting evidence suggesting that complement also plays a role in promoting B cell (Dempsey *et al*. 1996) and T cell (Kemper & Atkinson 2006; Kopf *et al*. 2002) immunities. (Dempsey *et al*. 1996) has demonstrated that by conjugating up to three C3d molecules per antigen, the threshold of antigen specific B-cell activation can be dramatically reduced by 1000 times.

As a C3 activator, Sbi fits with the general goal of vaccine adjuvant. By co-injection or conjugated with an antigen, the Sbi induced local activation of C3 could increase the efficiency of C3b opsonization of antigen, thereby decreasing the antigen specific B-cell activation threshold. At the same time, the resulting C3a production could simulate the leukocytes chemotaxis toward the site of complement activation, facilitating the antigen presentation. New evidence also suggests that the activation of C3a receptor up-regulates the inflammatory cytokine production (Zhang *et al*. 2007). Despite the theoretical possibility of Sbi as an adjuvant, there are a several problems that are worth considering. 1) To achieve the best C3b opsonization efficiency, whether to co-inject or pre-conjugate Sbi with antigen remains to be tested. 2) Potential complement receptor 2 (CR2) inhibition of Sbi, as illustrated by crystal structures of Sbi-IV:C3d (Clark *et al*. 2011) and CR2:C3d (van den Elsen & Isenman 2011), Sbi-IV is an inhibitor of the C3d:CR2 interaction (Burman *et al*. 2008), which is the molecular basis of B-cell activation. Sbi-III-IV mutant with decreased C3d binding avidity could be used to avoid this problem. As demonstrated in Section 4.3.9.4, the R231A mutant of Sbi-III-IV has a very low affinity for C3, but it is still a potent activator of C3, although increased Sbi concentration and prolonged

incubation are needed. 3) It is optimistic to assume that Sbi is directly usable as a molecular adjuvant. Since Sbi is derived from a commensal human pathogen, pre-existing antibodies might further complicate this approach.

7.3.2 Anti-cancer drug

In addition to vaccine adjuvants, Sbi could also contribute to the effort of conquering cancer. Immune-targeted treatment is a contemporary trend of cancer treatment. Antibodies are raised against aberrant cancerous cell surface epitopes. The binding of antibody to these epitopes would trigger the activation of the complement classical pathway, which links antibody-dependent cellular cytotoxicity (ADCC) (Perlmann 1981) to complement-dependent cellular cytotoxicity (CDCC) (Bara & Lint 1987). However, a high density of the surface epitope are required for the efficient initiation of CP, and the cancer cells normally overexpress complement regulators on the cell surface (Fishelson *et al*. 2003), therefore the antibody mediated killing can hardly achieve its ideal level. As Sbi is a strong activator of complement AP, it would be reasonable to speculate that by conjugating the Sbi together with an antibody, the antibody mediated killing of cancerous cell could be significantly enhanced. The conjugated antibody could simultaneously trigger the activation of both CP and AP, so the resulting complement activation would be significantly harder to contain. Since Sbi is a bacterial protein, modifications may be necessary before this protein totally complies with the designated function. Some of the concerns mentioned in the above paragraph still apply here. In addition, another potential obstacle for this particular application is the C5 activation suppressive activity of Sbi. C5 activation leads to the formation of the membrane attack complex, which is the direct killing mechanism for cancer cells. This study demonstrated that the formation of ternary complexes is vital for both the activation of AP and inhibition of C5 activation. Thus, potentially, the Sbi-III-IV mutants could be screened for mutants and concentrations that are able to trigger AP activation,

but with low C5 inhibitory activity. Alternatively, *E.coli* toxin Stx2 could be a more suitable candidate for this purpose, as Stx2 is an activator of entire AP.

7.3.3 Anti-inflammatory drug

So far, the potential applications of Sbi have been suggested based on its C3 activating function. However, in this study it was also shown that Sbi is an inhibitor of C5. Given these multifaceted complement modulatory activities, native Sbi might not be a suitable candidate for potential anti-inflammatory therapeutics. But, with slight genetic manipulation Sbi-III-IV could be transformed into a protein that strongly inhibits both C3 and C5 activation. In Section 4.4.6.2, it was elucidated that two positive relationships exist, one is between C3 binding strength and C3 convertase inhibitory activity, and another one is between ternary complex formation and C5 convertase inhibitory activity. The native Sbi-III-IV demonstrates relatively loosened C3b binding strength, therefore only causing limited inhibition of C3 convertase. Thus, it would be reasonable to speculate that by swapping the C3d binding region of Sbi-III-IV with the similar region of Efb, the resulting fusion protein of Sbi-III and Efb-C could be an extremely potent inhibitor of the entire complement cascade.

Improperly-regulated complement activation is a major cause of numerous human diseases (Ricklin & Lambris 2007), such as AMD, aHUS, rheumatoid arthritis, and systemic lupus erythematosus. But given the complexity of the complement cascade and the sheer amount of complement components in the blood, the development of drugs targeting complement seems very frustrated. To date, there are only a handful of clinically-approved complement inhibitors on the market. The most successful one is the anti-C5 monoclonal antibody eculizumab (Alexion, Cheshire, CT, USA), which inhibits the terminal pathway by binding to C5. Reflected by the success of eculizumab, antibody-based therapeutics appear to be the general trend in the pharmaceutical industry for

complement related diseases. Despite the demonstration of the inhibitory potency of *staphylococcal* immune modulatory proteins (e.g. SCIN, Efb, Ecb and Sbi), so far only their inhibitory mechanisms (Rooijakkers *et al*. 2007; Laarman *et al*. 2010; Jongerius *et al*. 2007; Chen *et al*. 2010) are inspirational for potential new therapeutics. Thus, in the light of this in-depth study of Sbi mediated ternary complex formation, a bi-specific antibody that binds to C3d and FHR-1_{4-5} simultaneously could be a potential Sbi inspired C5 inhibition solution.

7.4 Conclusion

This study shows that Sbi binds directly to FH and FHR-1, and in complex with isoforms of complement component C3, the resulting FH and FHR-1 ternary complexes are significantly stronger in avidity. Specifically, Sbi domain III was identified as the domain responsible for the binding of FH and FHR-1. Systematic mutagenesis studies pinpointed K173 as the key residue for the activity of Sbi-III. Comparative assays using Sbi-III-IV WT and K173A mutants lead to following conclusions: 1) The formation of the FHR-1 containing ternary complex is essential for the Sbi triggered C3 consumption mechanism, 2) The formation of the FHR-1 ternary complex protects C3b from FH mediated inactivation, and 3) The C3 consumption is controlled to avoid activation of C5. Despite the sequence identity of FH_{18-20} and FHR-1_{3-5}, Sbi prefers FHR-1 over FH during the assembly of the ternary complex. This binding preference could further increase the stability of C3b species (e.g. C3b, $C3_{H20}$ and Sbi-C3b) in the serum, and as a result, disrupting the regulation of AP, which leads to the local consumption of C3.

Ternary complex formation is only one of the factors contributing to the increased C3b stability. It is also shown in this study that by covalently attaching C3b to Sbi-III-IV, the resulting Sbi-C3b adduct demonstrates a prolonged half-life in the serum compared with free C3b molecule. Moreover, a stronger dose-dependent relationship was observed between the Sbi-C3b adduct

concentration and the consumption of AP activity. The deposition process was shown to be a non-random process, C3b selectively attaches on S226 and the lysine residues on Sbi-IV. The preference for the covalent attachment site suggests that Sbi-IV repositions from the C3d concave surface to convex surface through a defined mechanism yet to be fully explained.

Therefore, this study confirms the previous description of the C3 futile consumption mechanism. More importantly, mechanistic details were elucidated for to this novel microbial immune evasion mechanism, which paves the way for future exploitations of Sbi as novel vaccine adjuvant, anti-cancer drug and anti-inflammatory reagent.

Chapter 8: References

Alcorlo, M., Martínez-Barricarte, R., Fernández, F.J., Rodríguez-Gallego, C., Round, A., Vega, M.C., Harris, C.L., de Córdoba, S.R. & Llorca, O. (2011) Unique structure of iC3b resolved at a resolution of 24 Å by 3D-electron microscopy. *Proceedings of the National Academy of Sciences of the United States of America*. 108 (32), pp. 13236–13240.

Alcorlo, M., Tortajada, A., Rodríguez de Córdoba, S. & Llorca, O. (2013) Structural basis for the stabilization of the complement alternative pathway C3 convertase by properdin. *Proceedings of the National Academy of Sciences*. 110 (33), pp. 13504–13509.

Alitalo, A., Meri, T., Chen, T., Lankinen, H., Cheng, Z.Z., Jokiranta, T.S., Seppala, I.J.T., Lahdenne, P., Hefty, P.S., Akins, D.R. & Meri, S. (2004) Lysine-Dependent Multipoint Binding of the Borrelia burgdorferi Virulence Factor Outer Surface Protein E to the C Terminus of Factor H. *Journal of immunology*. 172 (10), pp. 6195–6201.

Alper, C.A., Johnson, A.M., Birtch, A.G. & Moore, F.D. (1969) Human C'3: evidence for the liver as the primary site of synthesis. *Science*. 163 (3864), pp. 286–288.

Alsenz, J., Avila, D., Huemer, H.P., Esparza, I., Becherer, J.D., Kinoshita, T., Wang, Y., Oppermann, S. & Lambris, J.D. (1992) Phylogeny of the third component of complement, C3: analysis of the conservation of human CR1, CR2, H, and B binding sites, concanavalin A binding sites, and thiolester bond in the C3 from different species. *Developmental and comparative immunology*. 16 (1), pp. 63–76.

Alsenz, J., Schulz, T.F., Lambris, J.D., Sim, R.B. & Dierich, M.P. (1985) Structural and functional analysis of the complement component factor H with the use of different enzymes and monoclonal antibodies to factor H. *Biochemical Journal*. 232pp. 841–850.

Altschul, S.F., Madden, T.L., Schäffer, A.A., Zhang, J., Zhang, Z., Miller, W. & Lipman, D.J. (1997) *Gapped BLAST and PSI-BLAST: a new generation of protein database search programs*. 25 (17), pp. 3389–3402.

Amdahl, H., Jongerius, I., Meri, T., Pasanen, T., Hyvarinen, S., Haapasalo, K., van Strijp, J.A., Rooijakkers, S.H. & Jokiranta, T.S. (2013) Staphylococcal Ecb Protein and Host Complement Regulator Factor H Enhance Functions of Each Other in Bacterial Immune Evasion. *The Journal of Immunology*. 191 (4), pp. 1775–1784.

Andoh, A., Fujiyama, Y., Bamba, T. & Hosoda, S. (1993) Differential cytokine regulation of complement C3, C4, and factor B synthesis in human intestinal epithelial cell line, Caco-2. *The Journal of Immunology*. 151 (8), pp. 4239–4247.

Arlaud, G.J. & Thielens, N.M. (2001) *Complement: Classical and Lectin Pathways*. Chichester, UK: John Wiley & Sons, Ltd.

Atkins, K.L., Burman, J.D., Chamberlain, E.S., Cooper, J.E., Poutrel, B., Bagby, S., Jenkins, A.T.A., Feil, E.J. & van den Elsen, J.M.H. (2008) S. aureus IgG-binding proteins SpA and Sbi: Host specificity and mechanisms of immune complex formation. *Molecular Immunology*. 45 (6), pp. 1600–1611.

Baker, N.A., Sept, D., Joseph, S., Holst, M.J. & McCammon, J.A. (2001) Electrostatics of nanosystems: Application to microtubules and the ribosome. *Proceedings of the National Academy of Sciences*. 98 (18), pp. 10037–10041.

Bara, S. & Lint, T.F. (1987) The third component of complement (C3) bound to tumor target cells enhances their sensitivity to killing by activated macrophages. *The Journal of Immunology*. 138 (4), pp. 1303–1309.

Barthel, D., Schindler, S. & Zipfel, P.F. (2012) Plasminogen Is a Complement Inhibitor. *Journal of Biological Chemistry*. 287 (22), pp. 18831–18842

Bhattacharjee, A., Reuter, S., Trojnár, E., Kolodziejczyk, R., Seeberger, H., Hyvärinen, S., Uzonyi, B., Szilágyi, Á., Prohászka, Z., Goldman, A., Józsi, M. & Jokiranta, T.S. (2015) The Major Autoantibody Epitope on Factor H in Atypical Hemolytic Uremic Syndrome Is Structurally Different from Its Homologous Site in Factor H-related Protein 1, Supporting a Novel Model for Induction of Autoimmunity in This Disease. *Journal of Biological Chemistry*. 290 (15), pp. 9500–9510.

Blandin, S. (2004) Thioester-containing proteins and insect immunity. *Molecular Immunology*. 40 (12), pp. 903–908.

Blaum, B.A.R.S., Hannan, J.P., Herbert, A.P., Kavanagh, D., scaron an Uhr iacute n, Du & Stehle, T. (2014) Structural basis for sialic acid–mediated self-recognition by complement factor H. *Nature Chemical Biology*. pp. 1–7.

Bodén, M.K. & Flock, J.-I. (1994) Cloning and characterization of a gene for a 19kDa fibrinogen-binding protein from *Staphylococcus aureus*. *Molecular Microbiology*. 12 (4), pp. 599–606.

Bohne-Lang, A. & Lieth, von der, C.W. (2005) GlyProt: in silico glycosylation of proteins. *Nucleic Acids Research*. 33 (Web Server), pp. W214–W219.

Bunkenborg, J., Pilch, B.J., Podtelejnikov, A.V. & Wiśniewski, J.R. (2004) Screening forN-glycosylated proteins by liquid chromatography mass spectrometry. *Proteomics*. 4 (2), pp. 454–465.

Burman, J.D., Leung, E., Atkins, K.L., O'Seaghdha, M.N., Lango, L., Bernadó, P., Bagby, S., Svergun, D.I., Foster, T.J. & Isenman, D.E. (2008) Interaction of human complement with Sbi, a staphylococcal immunoglobulin-binding protein indications of a novel mechanism of complement evasion by Staphylococcus aureus. *Journal of Biological Chemistry*. 283 (25), pp. 17579–17593.

Carroll, M.C. (2004) The complement system in regulation of adaptive immunity. *Nature Immunology*. 5 (10), pp. 981–986.

Chabelskaya, S., Gaillot, O. & Felden, B. (2010) A Staphylococcus aureus Small RNA Is Required for Bacterial Virulence and Regulates the Expression of an Immune-Evasion Molecule Pascale Cossart. *PLoS Pathogens*. 6 (6), pp. e1000927.

Chambers, H.F. (2001) The changing epidemiology of Staphylococcus aureus? *Emerging Infectious Diseases*. 7 (2), pp. 178.

Chen, H., Ricklin, D., Hammel, M., Garcia, B.L., McWhorter, W.J., Sfyroera, G., Wu, Y.-Q., Tzekou, A., Li, S., Geisbrecht, B.V., Woods, V.L. & Lambris, J.D. (2010) Allosteric inhibition of complement function by a staphylococcal immune evasion protein. *Proceedings of the National Academy of Sciences*. 107 (41), pp. 17621–17626.

Cheung, G.Y.C., Wang, R., Khan, B.A., Sturdevant, D.E. & Otto, M. (2011) Role of the Accessory Gene Regulator agr in Community-Associated Methicillin-Resistant Staphylococcus aureus Pathogenesis. *Infection and Immunity*. 79 (5), pp. 1927–1935.

Clark, E.A., Crennell, S., Upadhyay, A., Zozulya, A.V., Mackay, J.D., Svergun, D.I., Bagby, S. & van den Elsen, J.M.H. (2011) A structural basis for Staphylococcal complement subversion: X-ray structure of the complement-binding domain of *Staphylococcus aureus* protein Sbi in complex with ligand C3d. *Molecular Immunology*. 48 (4), pp. 452–462.

Clegg, R.M., Murchie, A.I., Zechel, A. & Lilley, D.M. (1993) Observing the helical geometry of double-stranded DNA in solution by fluorescence resonance energy transfer. *Proceedings of the National Academy of Sciences of the United States of America*. 90 (7), pp. 2994–2998.

Coffman, R.L., Sher, A. & Seder, R.A. (2010) Vaccine Adjuvants: Putting Innate Immunity to Work. *Immunity*. 33, pp. 492–503.

Corrigan, R.M., Miajlovic, H. & Foster, T.J. (2009) Surface proteins that promote adherence of Staphylococcus aureus to human desquamated nasal epithelial cells. *BMC Microbiology*. 9 (1), pp. 22.

Dalmasso, A.P. & Müller-Eberhard, H.J. (1967) Physico-chemical characteristics of the third and fourth component of complement after dissociation from complement—cell complexes. *Immunology*. 13, pp. 293–305.

Darmstadt, G.L. & Lane, A.T. (1994) Impetigo: an overview. *Pediatric dermatology*. 11 (4), pp. 293–303.

Daum, R.S., Ito, T., Hiramatsu, K., Hussain, F., Mongkolrattanothai, K., Jamklang, M. & Boyle-Vavra, S. (2002) A Novel Methicillin-Resistance Cassette in Community-Acquired Methicillin-Resistant Staphylococcus aureus Isolates of Diverse Genetic Backgrounds. *Journal of Infectious Diseases.* 186, pp. 1344–1347.

Davis, A.E., III, Mejia, P. & Lu, F. (2008) Biological activities of C1 inhibitor. *Molecular Immunology*. 45 (16), pp. 4057–4063.

de Bruijn, M.H. & Fey, G.H. (1985) Human complement component C3: cDNA coding sequence and derived primary structure. *Proceedings of the National Academy of Sciences of the United States of America*. 82, pp. 708–712.

Dempsey, P.W., Allison, M.E., Akkaraju, S., Goodnow, C.C. & Fearon, D.T. (1996) C3d of complement as a molecular adjuvant: bridging innate and acquired immunity. *Science*. 271 (5247), pp. 348–350.

DiScipio, R.G. (1992) Ultrastructures and interactions of complement factors H and I. *The Journal of Immunology*. 149 (8), pp. 2592–2599.

Doose, S., Margeat, E. & Weiss, S. (2004) Fluorescence-aided molecule sorting: analysis of structure and interactions by alternating-laser excitation of single molecules. *Proceedings of the National Academy of Sciences of the United States of America*. 101 (24), pp. 8936–8941.

Durand, D., Vivès, C., Cannella, D. & Pérez, J. (2010) NADPH oxidase activator p67phox behaves in solution as a multidomain protein with semi-flexible linkers. *Journal of structural Biology.* 169 (1), pp. 45–53.

Eiff, von, C., Becker, K., Machka, K., Stammer, H. & Peters, G. (2001) Nasal Carriage as a Source of Staphylococcus aureusBacteremia. *New England Journal of Medicine*. 344 (1), pp. 11–16.

Endo, Y., Matsushita, M. & Fujita, T. (2011) The International Journal of Biochemistry & Cell Biology. *International Journal of Biochemistry and Cell Biology*. 43 (5), pp. 705–712.

England-Public- Health (2014) *Voluntary reporting of Staphylococcus aureus bacteraemia in England, Wales and Northern Ireland, 2013*. 8, pp. 1–11.

Fearon, D.T. & Austen, K.F. (1975) Properdin: binding to C3b and stabilization of the C3b-dependent C3 convertase. *The Journal of experimental medicine*. 142 (4), pp. 856–863.

Fenaille, F., Le Mignon, M., Groseil, C., Ramon, C., Riandé, S., Siret, L. & Bihoreau, N. (2007) Site-specific N-glycan characterization of human complement factor H. *Glycobiology*. 17 (9), pp. 932–944.

Fishelson, Z. & Müller-Eberhard, H.J. (1982) C3 convertase of human complement: enhanced formation and stability of the enzyme generated with nickel instead of magnesium. *The Journal of Immunology*. 129 (6), pp. 2603–2607.

Fishelson, Z., Donin, N., Zell, S., Schultz, S. & Kirschfink, M. (2003) Obstacles to cancer immunotherapy: expression of membrane complement regulatory proteins (mCRPs) in tumors. *Molecular Immunology*. 40 (2-4), pp. 109–123.

Foster, T.J., Geoghegan, J.A., Ganesh, V.K. & Höök, M. (2014) Adhesion, invasion and evasion: themany functions of the surface proteinsof Staphylococcus aureus. *Nature Reviews Microbiology*. 12 (1), pp. 49–62.

Fowler, V.G., Miro, J.M., Hoen, B., Cabell, C.H., Abrutyn, E., Rubinstein, E., Corey, G.R., Spelman, D., Bradley, S.F., Barsic, B., Pappas, P.A., Anstrom, K.J., Wray, D., Fortes, C.Q., et al. (2005) *Staphylococcus aureus* Endocarditis: A Consequence of Medical Progress. *JAMA*. 293 (24), pp. 3012–3021.

Franke, D. & Svergun, D.I. (2009) DAMMIF, a program for rapid *ab-initio* shape determination in small-angle scattering. *Journal of Applied Crystallography*. 42 (2), pp. 342–346.

Fraser, J., Arcus, V., Kong, P., Baker, E. & Proft, T. (2000) Superantigens - powerful modifiers of the immune system. *Molecular medicine today*. 6 (3), pp. 125–132.

Fries, L.F., Gaither, T.A., Hammer, C.H. & Frank, M.M. (1984) C3b covalently bound to IgG demonstrates a reduced rate of inactivation by factors H and I. *Journal of Experimental Medicine*. 160 (6), pp. 1640–1655.

Friese, M.A., Hellwage, J., Jokiranta, T.S., Meri, S., Peter, H.H., Eibel, H. & Zipfel, P.F. (1999) FHL-1/reconectin and factor H: two human complement regulators which are encoded by the same gene are differently expressed and regulated. *Molecular Immunology*. 36 (13-14), pp. 809–818.

Fujita, T. (2002) Evolution of the lectin–complement pathway and its role in innate immunity. *Nature reviews immunology*. 2 (5), pp. 346–353.

Gale, D.P., De Jorge, E.G., Cook, H.T. & Martinez-Barricarte, R. (2010) Identification of a mutation in complement factor H-related protein 5 in patients of Cypriot origin with glomerulonephritis. *The Lancet*. 376 (9743), pp. 794–801.

Garcia, B.L., Tzekou, A., Ramyar, K.X., McWhorter, W.J., Ricklin, D., Lambris, J.D. & Geisbrecht, B.V. (2009) Crystallization of human complement component C3b in the presence of a staphylococcal complement-inhibitor protein (SCIN). *Acta Crystallographica Section F Structural Biology and Crystallization Communications*. 65 (5), pp. 482–485.

Ghannam, A., Pernollet, M., Fauquert, J.L., Monnier, N., Ponard, D., Villiers, M.B., Peguet-Navarro, J., Tridon, A., Lunardi, J., Gerlier, D. & Drouet, C. (2008) Human C3 Deficiency Associated with Impairments in Dendritic Cell Differentiation, Memory B Cells, and Regulatory T Cells. *Journal of immunology*. 181 (7), pp. 5158–5166.

Gharavi, A.G., Kiryluk, K., Choi, M., Li, Y., Hou, P., Xie, J., Sanna-Cherchi, S., Men, C.J., Julian, B.A., Wyatt, R.J., Novak, J., He, J.C., Wang, H., Lv, J., et al. (2011) Genome-wide association study identifies susceptibility loci for IgA nephropathy. *Nature Genetics*. 43 (4), pp. 321–327.

Gigli, I., Fujita, T. & Nussenzweig, V. (1979) Modulation of the classical pathway C3 convertase by plasma proteins C4 binding protein and C3b inactivator. *Proceedings of the National Academy of Sciences of the United States of America*. 76 (12), pp. 6596–6600.

Glatter, O. (1977) Data evaluation in small angle scattering: calculation of the radial electron density distribution by means of indirect Fourier transformation. *Acta Physica Austriaca*. 47 (1-2), pp. 83–102.

Goicoechea de Jorge, E., Caesar, J.J.E., Malik, T.H., Patel, M., Colledge, M., Johnson, S., Hakobyan, S., Morgan, B.P., Harris, C.L., Pickering, M.C. & Lea, S.M. (2013) Dimerization of complement factor H-related proteins modulates complement activation in vivo. *Proceedings of the National Academy of Sciences*. 110 (12), pp. 4685–4690.

Gorham, R.D., Jr, Rodriguez, W. & Morikis, D. (2014) Molecular Analysis of the Interaction between Staphylococcal VirulenceFactor Sbi-IV and Complement C3d. *Biophysj*. 106 (5), pp. 1164–1173.

Grigg, J.C., Ukpabi, G. & Gaudin, C. (2010) Structural biology of heme binding in the Staphylococcus aureus Isd system. *Journal of Inorganic Biochemistry.* 104, pp. 341–348.

Gros, P., Milder, F.J. & Janssen, B.J.C. (2008) Complement driven by conformational changes. *Nature Reviews Immunology*. 8 (1), pp. 48–58.

Grubmüller, H. & Seidel, C. (2008) Single-molecule FRET measures bends and kinks in DNA. I *Proceedings of the National Academy of Sciences of the United States of America*. 105 (47), pp. 18337–18342.

Guinier, A. (1939) La diffraction des rayons X aux tres petits angles : applications a l'etude de phenomenes ultramicroscopiques. *Annales de physique.* 11(12), pp. 161–237.

Ha, T., Enderle, T., Ogletree, D.F., Chemla, D.S., Selvin, P.R. & Weiss, S. (1996) Probing the interaction between two single molecules: fluorescence resonance energy transfer between a single donor and a single acceptor. *Proceedings of the National Academy of Sciences of the United States of America*. 93 (13), pp. 6264–6268.

Haas, E., Wilchek, M., Katchalski-Katzir, E. & Steinberg, I.Z. (1975) Distribution of end-to-end distances of oligopeptides in solution as estimated by energy transfer. *Proceedings of the National Academy of Sciences of the United States of America*. 72 (5), pp. 1807–1811.

Hair, P.S., Foley, C.K., Krishna, N.K., Nyalwidhe, J.O., Geoghegan, J.A., Foster, T.J. & Cunnion, K.M. (2013) Complement regulator C4BP binds to *Staphylococcus aureus* surface proteins SdrE and Bbp inhibiting bacterial opsonization and killing. *Results in Immunology*. 3pp. 114–121.

Hakobyan, S., Harris, C.L., Tortajada, A., de Jorge, E.G., García-Layana, A., Fernández-Robredo, P., de Córdoba, S.R. & Morgan, B.P. (2008) Measurement of Factor H Variants in Plasma Using Variant-Specific Monoclonal Antibodies: Application to Assessing Risk of Age-Related Macular Degeneration. 49 (5), pp. 1983–1990.

Hallstrom, T., Morgelin, M., Barthel, D., Raguse, M., Kunert, A., Hoffmann, R., Skerka, C. & Zipfel, P.F. (2012) Dihydrolipoamide Dehydrogenase of *Pseudomonas aeruginosa* Is a Surface-Exposed Immune Evasion Protein That Binds Three Members of the Factor H Family and Plasminogen. *Journal of immunology*. 189 (10), pp. 4939–4950.

Hammel, M., Sfyroera, G., Pyrpassopoulos, S., Ricklin, D., Ramyar, K.X., Pop, M., Jin, Z., Lambris, J.D. & Geisbrecht, B.V. (2007a) Characterization of Ehp, a

Secreted Complement Inhibitory Protein from Staphylococcus aureus. *Journal of Biological Chemistry*. 282 (41), pp. 30051–30061.

Hammel, M., Sfyroera, G., Ricklin, D., Magotti, P., Lambris, J.D. & Geisbrecht, B.V. (2007b) A structural basis for complement inhibition by Staphylococcus aureus. *Nature Immunology*. 8 (4), pp. 430–437.

Harper, S. & Speicher, D.W. (2010) Purification of Proteins Fused to Glutathione S-Transferase. In: *Methods in Molecular Biology*. Methods in Molecular Biology. Totowa, NJ: Humana Press. pp. pp. 259–280. doi:10.1007/978-1-60761-913-0_14.

Hartman, B.J. & Tomasz, A. (1984) Low-affinity penicillin-binding protein associated with beta-lactam resistance in Staphylococcus aureus. *Journal of Bacteriology*. 158(2), pp. 513–516.

Hase, S.,Kikuchi, N.,Ikenaka, T. & Inoue, K. (1985) Structures of Sugar Chains of the Third Component of Human Complement. *Journal of biochemistry*. 98, pp. 863–874.

Haupt, K., Kraiczy, P., Wallich, R., Brade, V., Skerka, C. & Zipfel, P.F. (2007) Binding of human factor H-related protein 1 to serum-resistant *Borrelia burgdorferi* is mediated by borrelial complement regulator-acquiring surface proteins. *Journal of Infectious Diseases*. 196, pp. 124–133.

Haupt, K., Reuter, M., van den Elsen, J., Burman, J., Hälbich, S., Richter, J., Skerka, C. & Zipfel, P.F. (2008) The *Staphylococcus aureus* Protein Sbi Acts as a Complement Inhibitor and Forms a Tripartite Complex with Host Complement Factor H and C3b. *PLoS Pathogens*. 4 (12), pp. e1000250.

Hebecker, M. & Jozsi, M. (2012) Factor H-related Protein 4 Activates Complement by Serving as a Platform for the Assembly of Alternative Pathway C3 Convertase via Its Interaction with C3b Protein. *Journal of Biological Chemistry*. 287 (23), pp. 19528–19536.

Heinen, S., Hartmann, A., Lauer, N., Wiehl, U., Dahse, H.M., Schirmer, S., Gropp, K., Enghardt, T., Wallich, R., Halbich, S., Mihlan, M., Schlotzer-Schrehardt, U., Zipfel, P.F. & Skerka, C. (2009) Factor H-related protein 1 (CFHR-1) inhibits complement C5 convertase activity and terminal complex formation. *Blood*. 114 (12), pp. 2439–2447.

Hellwage, J., Kühn, S. & Zipfel, P.F. (1997) The human complement regulatory factor-H-like protein 1, which represents a truncated form of factor H, displays cell-attachment activity. *Biochemical Journal*. 326 (Pt 2)pp. 321–327.

Hellwage, J., Meri, T., Heikkila, T., Alitalo, A., Panelius, J., Lahdenne, P., Seppala, I.J.T. & Meri, S. (2001) The Complement Regulator Factor H Binds to the Surface Protein OspE of Borrelia burgdorferi. *Journal of Biological Chemistry*. 276 (11), pp. 8427–8435.

Hinterdorfer, P. & Van Oijen, A. (2009) Handbook of single-molecule biophysics.

Hiramatsu, K. (2001) Whole genome sequencing of meticillin-resistant *Staphylococcus aureus*. *The Lancet*. 357, pp. 1225–1240.

Horstmann, R.D., Sievertsen, H.J., Knobloch, J. & Fischetti, V.A. (1988) Antiphagocytic activity of streptococcal M protein: selective binding of complement control protein factor H. *Proceedings of the National Academy of Sciences of the United States of America*. 85 (5), pp. 1657–1661.

Hourcade, D.E. (2008) Properdin and Complement Activation: A Fresh Perspective. *Current drug targets*. 9 (2), pp. 158–164.

Hourcade, D.E. (2006) The role of properdin in the assembly of the alternative pathway C3 convertases of complement. *The Journal of biological chemistry*. 281 (4), pp. 2128–2132.

Huber, R., Scholze, H., Paques, E.P. & Deisenhofer, J. (1980) Crystal Structure Analysis and Molecular Model of Human C3a Anaphylatoxin. *Hoppe-Seyler´s Zeitschrift für physiologische Chemie*. 361 (2), pp. 1389–1400.

Hughes, A.E., Orr, N., Esfandiary, H., Diaz-Torres, M., Goodship, T. & Chakravarthy, U. (2006) A common CFH haplotype, with deletion of CFHR1 and CFHR3, is associated with lower risk of age-related macular degeneration. *Nature Genetics*. 38 (10), pp. 1173–1177.

Isenman, D.E. & Young, J.R. (1984) The molecular basis for the difference in immune hemolysis activity of the Chido and Rodgers isotypes of human complement component C4. *The Journal of Immunology*. 132 (6), pp. 3019–3029.

Isenman, M.C.D. & Isenman, D.E. (2012) Regulation of Humoral Immunity by Complement. *Immunity*. 37 (2), pp. 199–207.

Jacques, D.A. & Trewhella, J. (2010) Small-angle scattering for structural biology-Expanding the frontier while avoiding the pitfalls. *Protein Science*. 19 (4), pp. 642–657.

Janssen, B.J.C., Christodoulidou, A., McCarthy, A., Lambris, J.D. & Gros, P. (2006) Structure of C3b reveals conformational changes that underlie complement activity. *Nature*. 444 (7116), pp. 213–216.

Janssen, B.J.C., Huizinga, E.G., Raaijmakers, H.C.A., Roos, A., Daha, M.R., Nilsson Ekdahl, K., Nilsson, B. & Gros, P. (2005) Structures of complement component C3 provide insights into the function and evolution of immunity. *Nature*. 437 (7058), pp. 505–511.

Jelezarova, E. & Lutz, H.U. (1999) Assembly and regulation of the complement amplification loop in blood: the role of C3b-C3b-IgG complexes. *Molecular Immunology*. 36 (13), pp. 837–842.

Jones, R.C., Deck, J., Edmondson, R.D. & Hart, M.E. (2008) Relative Quantitative Comparisons of the Extracellular Protein Profiles of Staphylococcus aureus UAMS-1 and Its sarA, agr, and sarA agr Regulatory Mutants Using One-Dimensional Polyacrylamide Gel Electrophoresis and Nanocapillary Liquid Chromatography Coupled with Tandem Mass Spectrometry. *Journal of Bacteriology*. 190 (15), pp. 5265–5278.

Jongerius, I., Kohl, J., Pandey, M.K., Ruyken, M., van Kessel, K.P.M., van Strijp, J.A.G. & Rooijakkers, S.H.M. (2007) Staphylococcal complement evasion by various convertase-blocking molecules. *Journal of Experimental Medicine*. 204 (10), pp. 2461–2471.

Kajander, T., Lehtinen, M.J., Hyvärinen, S., Bhattacharjee, A., Leung, E., Isenman, D.E., Meri, S., Goldman, A. & Jokiranta, T.S. (2011) Dual interaction of factor H with C3d and glycosaminoglycans in host-nonhost discrimination by complement. *Proceedings of the National Academy of Sciences*. 108 (7), pp. 2897–2902.

Kalinin, S., Peulen, T., Sindbert, S., Rothwell, P.J., Berger, S., Restle, T., Goody, R.S., Gohlke, H. & Seidel, C.A.M. (2012) A toolkit and benchmark study for FRET-restrained high-precision structural modeling. *Nature Publishing Group*. 9 (12), pp. 1218–1225.

Katayama, Y., Ito, T. & Hiramatsu, K. (2000) A New Class of Genetic Element, Staphylococcus Cassette Chromosome mec, Encodes Methicillin Resistance in Staphylococcus aureus. *Antimicrobial Agents and Chemotherapy*. 44 (6), pp. 1549–1555.

Kemper, C. & Atkinson, J.P. (2006) T-cell regulation: with complements from innate immunity. *Nature Reviews Immunology*. 7 (1), pp. 9–18.

Kemper, C., Pangburn, M.K. & Fishelson, Z. (2014) Complement Nomenclature 2014. *Molecular Immunology*. 61 (2), pp. 56–58.

Kluytmans, J., van Belkum, A. & Verbrugh, H. (1997) Nasal carriage of *Staphylococcus aureus*: epidemiology, underlying mechanisms, and associated risks. *Clinical microbiology reviews*. 10 (3), pp. 505–520.

Knezevic, J., Langer, A., Hampel, P.A., Kaiser, W., Strasser, R. & Rant, U. (2012) Quantitation of Affinity, Avidity, and Binding Kinetics of Protein Analytes with a Dynamically Switchable Biosurface. *Journal of the American Chemical Society*. 134 (37), pp. 15225–15228.

Koch, T.K., Reuter, M., Barthel, D., Böhm, S., van den Elsen, J., Kraiczy, P., Zipfel, P.F. & Skerka, C. (2012) Staphylococcus aureus Proteins Sbi and Efb Recruit Human Plasmin to Degrade Complement C3 and C3b Stefan Bereswill (ed.). *PLoS ONE*. 7 (10), pp. e47638.

Konarev, P.V., Volkov, V.V., Sokolova, A.V., Koch, M.H.J. & Svergun, D.I. (2003) PRIMUS: a Windows PC-based system for small-angle scattering data analysis. *Journal of Applied Crystallography*. 36 (5), pp. 1277–1282.

Kopf, M., Abel, B., Gallimore, A., Carroll, M. & Bachmann, M.F. (2002) Complement component C3 promotes T-cell priming and lung migration to control acute influenza virus infection. *Nature Medicine*. 8 (4), pp. 373–378.

Kozin, M.B. & Svergun, D.I. (2001) Automated matching of high- and low-resolution structural models. *Journal of Applied Crystallography*. 34 (1), pp. 33–41.

Kraiczy, P., Hellwage, J., Skerka, C., Becker, H., Kirschfink, M., Simon, M.M., Brade, V., Zipfel, P.F. & Wallich, R. (2004) Complement resistance of Borrelia burgdorferi correlates with the expression of BbCRASP-1, a novel linear plasmid-encoded surface protein that interacts with human factor H and FHL-1 and is unrelated to Erp proteins. *The Journal of biological chemistry*. 279 (4), pp. 2421–2429.

Kratky, O. (1964) Die Messung der Absolutintensität der diffusen Röntgenkleinwinkelstreuung- ein Verfahren zur "Wägung " in makromolekularen Systemen. *Fresenius' Zeitschrift für Analytische Chemie*. 201 (3), pp. 161–194.

Kulics, J., Rajnavölgyi, E., Füst, G. & Gergely, J. (1983) Interaction of C3 and C3b with immunoglobulin G. *Molecular Immunology*. 20 (8), pp. 805–810.

Kunert, A., Losse, J., Gruszin, C., Huhn, M., Kaendler, K., Mikkat, S., Volke, D., Hoffmann, R., Jokiranta, T.S., Seeberger, H., Moellmann, U., Hellwage, J. & Zipfel, P.F. (2007) Immune Evasion of the Human Pathogen *Pseudomonas aeruginosa*: Elongation Factor Tuf Is a Factor H and Plasminogen Binding Protein. *Journal of immunology*. 179 (5), pp. 2979–2988.

Kwan, W.-H., van der Touw, W. & Heeger, P.S. (2012) Complement regulation of T cell immunity. *Immunologic Research*. 54 (1-3), pp. 247–253.

Laarman, A., Milder, F., Strijp, J. & Rooijakkers, S. (2010) Complement inhibition by gram-positive pathogens: molecular mechanisms and therapeutic implications. *Journal of Molecular Medicine*. 88 (2), pp. 115–120.

Laarman, A.J., Ruyken, M., Malone, C.L., van Strijp, J.A.G., Horswill, A.R. & Rooijakkers, S.H.M. (2011) Staphylococcus aureus Metalloprotease Aureolysin Cleaves Complement C3 To Mediate Immune Evasion. *The Journal of Immunology*. 186 (11), pp. 6445–6453.

Lachmann, P.J., Halbwashs. L. (1975) The influence of C3b inactivator (KAF) concentration on the ability of serum to support complement activation. *Clinical and Experimental Immunology*. 21 (1), pp. 109-104.

Lachmann, P.J. & Hughes-Jones, N.C. (1984) Initiation of complement activation. *Springer Seminars in Immunopathology*. 7 (2-3), pp. 143–162.

Lambris, J.D., Ricklin, D. & Geisbrecht, B.V. (2008) Complement evasion by human pathogens. *Nature Reviews Microbiology*. 6 (2), pp. 132–142.

Langer, A., Hampel, P.A., Kaiser, W., Knezevic, J., Welte, T., Villa, V., Maruyama, M., Svejda, M., hner, S.J.A., Fischer, F., Strasser, R. & Rant, U. (2013) Protein analysis by time-resolved measurements with an electro-switchable DNA chip. *Nature Communications*. 4 pp. 1–8.

Law, S.K. & Dodds, A.W. (1997) The internal thioester and the covalent binding properties of the complement proteins C3 and C4. *Protein science : a publication of the Protein Society*. 6 (2), pp. 263–274.

Law, S.K., Lichtenberg, N.A. & Levine, R.P. (1979) Evidence for an ester linkage between the labile binding site of C3b and receptive surfaces. *The Journal of Immunology*. 123 (3), pp. 1388–1394.

Lee, L.Y.L., Höök, M., Haviland, D., Wetsel, R.A., Yonter, E.O., Syribeys, P., Vernachio, J. & Brown, E.L. (2004) Inhibition of complement activation by a secreted Staphylococcus aureus protein. *The Journal of infectious diseases*. 190 (3), pp. 571–579.

Lee, S.M., Ender, M., Adhikari, R., Smith, J.M.B., Berger-Bachi, B. & Cook, G.M. (2007) Fitness Cost of Staphylococcal Cassette Chromosome mec in Methicillin-Resistant Staphylococcus aureus by Way of Continuous Culture. *Antimicrobial Agents and Chemotherapy*. 51 (4), pp. 1497–1499.

Le Friec, G., Sheppard, D., Whiteman, P., Karsten, C.M., Shamoun, S.A.-T., Laing, A., Bugeon, L., Dallman, M.J., Melchionna, T., Chillakuri, C., Smith, R.A., Drouet, C., Couzi, L., Fremeaux-Bacchi, V., et al. (2012) The CD46-Jagged1 interaction is critical for human TH1 immunity. *Nature Immunology*. 13 (12), pp. 1213–1221.

Li, Y. & Zhang, Y. (2009) REMO: A new protocol to refine full atomic protein models from C-alpha traces by optimizing hydrogen-bonding networks. *Proteins: Structure, Function, and Genetics*. 76 (3), pp. 665–676.

Liszewski, M.K., Kemper, C., Price, J.D. & Atkinson, J.P. (2005) Emerging roles and new functions of CD46. *Springer Seminars in Immunopathology*. 27 (3), pp. 345–358.

Liszewski, M.K., Kolev, M., Le Friec, G., Leung, M., Bertram, P.G., Fara, A.F., Subias, M., Pickering, M.C., Drouet, C., Meri, S., Arstila, T.P., Pekkarinen, P.T., Ma, M., Cope, A., et al. (2013) Intracellular Complement Activation Sustains T Cell Homeostasis and Mediates Effector Differentiation. *Immunity*. 39 (6), pp. 1143–1157.

Liu, T., Qian, W.-J., Gritsenko, M.A., Camp, D.G., Monroe, M.E., Moore, R.J. & Smith, R.D. (2005) Human Plasma N-Glycoproteome Analysis by Immunoaffinity Subtraction, Hydrazide Chemistry, and Mass Spectrometry. *Journal of Proteome Research*. 4 (6), pp. 2070–2080.

Liu, Y., Yin, Y., Wang, L., Zhang, W., Chen, X., Yang, X., Xu, J. & Ma, G. (2013) Engineering Biomaterial-Associated Complement Activation to Improve Vaccine Efficacy. *Biomacromolecules*. 14 (9), pp. 3321–3328.

Lowy, F.D. (1998) Staphylococcus aureus infections. *The New England journal of medicine*. 339 (8), pp. 520–532.

Lutz, H.U. & Jelezarova, E. (2006) Complement amplification revisited. *Molecular Immunology*. 43 (1-2), pp. 2–12.

McRae, J.L., Duthy, T.G., Griggs, K.M., Ormsby, R.J., Cowan, P.J., Cromer, B.A., McKinstry, W.J., Parker, M.W., Murphy, B.F. & Gordon, D.L. (2005) Human Factor H-Related Protein 5 Has Cofactor Activity, Inhibits C3 Convertase Activity, Binds Heparin and C-Reactive Protein, and Associates with Lipoprotein. *The Journal of Immunology*. 174 (10), pp. 6250–6256.

Meri, S. & Pangburn, M.K. (1990) Discrimination between activators and nonactivators of the alternative pathway of complement: regulation via a sialic acid/polyanion binding site on factor H. *Proceedings of the National Academy of Sciences of the United States of America*. 87 (10), pp. 3982–3986.

Meri, T., Amdahl, H., Lehtinen, M.J., Hyvarinen, S., McDowell, J.V., Bhattacharjee, A., Meri, S., Marconi, R., Goldman, A. & Jokiranta, T.S. (2013) Microbes Bind Complement Inhibitor Factor H via a Common Site Frank R DeLeo (ed.). *PLoS Pathogens*. 9 (4), pp. e1003308.

Mertens, H.D.T. & Svergun, D.I. (2010) Structural characterization of proteins and complexes using small-angle X-ray solution scattering. *Journal of Structural Biology*. 172 (1), pp. 128–141.

Miki, K., Ogata, S., Misumi, Y. & Ikehara, Y. (1986) Carbohydrate structures of the third component of rat complement. *Biochemical Journal*. 240, pp. 691–698.

Moore, I., Strain, L., Pappworth, I., Kavanagh, D., Barlow, P.N., Herbert, A.P., Schmidt, C.Q., Staniforth, S.J., Holmes, L.V., Ward, R., Morgan, L., Goodship, T.H.J. & Marchbank, K.J. (2010) Association of factor H autoantibodies with deletions of CFHR1, CFHR3, CFHR4, and with mutations in CFH, CFI, CD46, and C3 in patients with atypical hemolytic uremic syndrome. *Blood*. 115 (2), pp. 379–387.

Morgan, B.P. (2000) Complement methods and protocols. *Methods in Molecular Biology.* Volume 150.

Morgan, H.P., Mertens, H.D.T., Guariento, M., Schmidt, C.Q., Soares, D.C., Svergun, D.I., Herbert, A.P., Barlow, P.N. & Hannan, J.P. (2012) PLOS ONE: Structural Analysis of the C-Terminal Region (Modules 18–20) of Complement Regulator Factor H (FH) Andreas Hofmann. *PLoS ONE*. 7 (2), pp. e32187.

Morgan, H.P., Schmidt, C.Q., Guariento, M., Blaum, B.S., Gillespie, D., Herbert, A.P., Kavanagh, D., Mertens, H.D.T., Svergun, D.I., Johansson, C.M., Uhrín, D., Barlow, P.N. & Hannan, J.P. (2011) Structural basis for engagement by complement factor H of C3b on a self surface. *Nature Structural & Molecular Biology*. 18 (4), pp. 463–470.

Mölkänen, T., Tyynelä, J., Helin, J., Kalkkinen, N. & Kuusela, P. (2002) Enhanced activation of bound plasminogen on Staphylococcus aureus by staphylokinase. *FEBS Letters*. 517, pp. 72–78.

Müller-Eberhard, H.J. (1988) Molecular organization and function of the complement system. *Annual review of biochemistry*. 57, pp. 321–347.

Müller-Eberhard, H.J. (1966) The reaction mechanism of 1C-Globulin (C'3) in immune hemolysis. *Journal of Experimental Medicine*. 123 (1), pp. 33–54.

Nagar, B., Jones, R.G., Diefenbach, R.J., Isenman, D.E. & Rini, J.M. (1998) X-ray crystal structure of C3d: a C3 fragment and ligand for complement receptor 2. *Science*. 280 (5367), pp. 1277–1281.

Nie, S., Chiu, D.T. & Zare, R.N. (1994) Probing individual molecules with confocal fluorescence microscopy. *Science*. 266 (5187), pp. 1018–1021.

Nishida, N., Walz, T. & Springer, T.A. (2006) Structural transitions of complement component C3 and its activation products. *Proceedings of the National*

Academy of Sciences of the United States of America. 103 (52), pp. 19737–19742.

Nonaka, M., Nakayama, K., Yeul, Y.D. & Takahashi, M. (1985) Complete nucleotide and derived amino acid sequences of the fourth component of mouse complement (C4). Evolutionary aspects. *Journal of Biological Chemistry*. 260 (20), pp. 10936–10943.

O'Riordan, K. & Lee, J.C. (2004) *Staphylococcus aureus* Capsular Polysaccharides. *Clinical microbiology reviews*. 17 (1), pp. 218–234.

Ogston, A. (1882) Micrococcus Poisoning. *Journal of anatomy and physiology*. 17 (Pt 1), pp. 24–58.

Orth, D., Khan, A.B., Naim, A., Grif, K., Brockmeyer, J., Karch, H., Joannidis, M., Clark, S.J., Day, A.J., Fidanzi, S., Stoiber, H., Dierich, M.P., Zimmerhackl, L.B. & Wurzner, R. (2009) Shiga Toxin Activates Complement and Binds Factor H: Evidence for an Active Role of Complement in Hemolytic Uremic Syndrome. *Journal of immunology.* 182 (10), pp. 6394–6400.

Otto, M. (2013) Community-associated MRSA: What makes them special? *International Journal of Medical Microbiology*. 303 (6-7), pp. 324–330.

Palma, M., Shannon, O., Quezada, H.C., Berg, A. & Flock, J.-I. (2001) Extracellular Fibrinogen-binding Protein, Efb, from Staphylococcus aureus Blocks Platelet Aggregation Due to Its Binding to the alpha -Chain. *Journal of Biological Chemistry*. 276 (34), pp. 31691–31697.

Pangburn, M.K., Müller-Eberhard, H.J. (1986) The C3 convertase of the alternative pathway of human complement. Enzymic properties of the bimolecular proteinase. *Biochemical Journal*. 235 (3), pp. 723.

Pangburn, M.K. (1989a) Analysis of recognition in the alternative pathway of complement. Effect of polysaccharide size. *The Journal of Immunology*. 142 (8), pp. 2766–2770.

Pangburn, M.K. (1989b) Analysis of the mechanism of recognition in the complement alternative pathway using C3b-bound low molecular weight polysaccharides. *The Journal of Immunology*. 142 (8), pp. 2759–2765.

Pangburn, M.K. (1989c) Analysis of the natural polymeric forms of human properdin and their functions in complement activation. *The Journal of Immunology*. 142 (1), pp. 202–207.

Pangburn, M.K., Schreiber, R.D. & Müller-Eberhard, H.J. (1981) Formation of the initial C3 convertase of the alternative complement pathway. Acquisition of

C3b-like activities by spontaneous hydrolysis of the putative thioester in native C3. *The Journal of experimental medicine*. 154 (3), pp. 856–867.

Pangburn, M.K., Schreiber, R.D. & Müller-Eberhard, H.J. (1977) Human complement C3b inactivator: isolation, characterization, and demonstration of an absolute requirement for the serum protein beta1H for cleavage of C3b and C4b in solution. *The Journal of experimental medicine*. 146 (1), pp. 257–270.

Park, S.Y., Shin, Y.P., Kim, C.H., Park, H.J., Seong, Y.S., Kim, B.S., Seo, S.J. & Lee, I.H. (2008) Immune Evasion of Enterococcus faecalis by an Extracellular Gelatinase That Cleaves C3 and iC3b. *Journal of immunology*. 181 (9), pp. 6328–6336.

Pasch, M.C., Van Den Bosch, N.H., Daha, M.R., Bos, J.D. & Asghar, S.S. (2000) Synthesis of complement components C3 and factor B in human keratinocytes is differentially regulated by cytokines. *The Journal of investigative dermatology*. 114 (1), pp. 78–82.

Peacock, S.J., de Silva, I. & Lowy, F.D. (2001) What determines nasal carriage of *Staphylococcus aureus*? *Trends in Microbiology*. 9 (12), pp. 605–610.

Perlmann, H. (1981) Interaction of target cell-bound C3bi and C3d with human lymphocyte receptors. Enhancement of antibody-mediated cellular cytotoxicity. *Journal of Experimental Medicine*. 153 (6), pp. 1592–1603.

Petoukhov, M.V., Franke, D., Shkumatov, A.V., Tria, G., Kikhney, A.G., Gajda, M., Gorba, C., Mertens, H.D.T., Konarev, P.V., Svergun, D.I.IUCr (2012) New developments in the ATSAS program package for small-angle scattering data analysis. *Journal of Applied Crystallography*. 45 (2), pp. 342–350.

Petoukhov, M.V., Konarev, P.V., Kikhney, A.G. & Svergun, D.I. (2007) ATSAS2.1 – towards automated and web-supported small-angle scattering data analysis. *Journal of Applied Crystallography*. 40 (s1), pp. s223–s228.

Pettersen, E.F., Goddard, T.D., Huang, C.C., Couch, G.S., Greenblatt, D.M., Meng, E.C. & Ferrin, T.E. (2004) UCSF Chimera?A visualization system for exploratory research and analysis. *Journal of Computational Chemistry*. 25 (13), pp. 1605–1612.

Pilpa, R.M., Robson, S.A., Villareal, V.A., Wong, M.L., Phillips, M. & Clubb, R.T. (2009) Functionally Distinct NEAT (NEAr Transporter) Domains within the Staphylococcus aureus IsdH/HarA Protein Extract Heme from Methemoglobin. *Journal of Biological Chemistry*. 284 (2), pp. 1166–1176.

Poolpol, K., Orth-Höller, D., Speth, C., Zipfel, P.F., Skerka, C., de Córdoba, S.R., Brockmeyer, J., Bielaszewska, M. & Würzner, R. (2014) Interaction of Shiga

toxin 2 with complement regulators of the factor H protein family. *Molecular Immunology*. 58 (1), pp. 77–84.

Porod, G. (1982) Physics of elementary particals and fields*. Small angle X-ray scattering.* pp. 17–51.

Prosser, B.E., Johnson, S., Roversi, P., Herbert, A.P., Blaum, B.S., Tyrrell, J., Jowitt, T.A., Clark, S.J., Tarelli, E., Uhrin, D., Barlow, P.N., Sim, R.B., Day, A.J. & Lea, S.M. (2007) Structural basis for complement factor H linked age-related macular degeneration. *Journal of Experimental Medicine*. 204 (10), pp. 2277–2283.

Ram, S., McQuillen, D.P., Gulati, S., Elkins, C., Pangburn, M.K. & Rice, P.A. (1998) Binding of complement factor H to loop 5 of porin protein 1A: a molecular mechanism of serum resistance of nonsialylated *Neisseria gonorrhoeae*. *The Journal of experimental medicine*. 188 (4), pp. 671–680.

Reddy, S.T., van der Vlies, A.J., Simeoni, E., Angeli, V., Randolph, G.J., O'Neil, C.P., Lee, L.K., Swartz, M.A. & Hubbell, J.A. (2007) Exploiting lymphatic transport and complement activation in nanoparticle vaccines. *Nature Biotechnology*. 25 (10), pp. 1159–1164.

Reid, K. & Porter, R.R. (1981) The proteolytic activation systems of complement. *Annual review of biochemistry*. 50, pp. 433–464.

Reuter, M., Caswell, C.C., Lukomski, S. & Zipfel, P.F. (2010) Binding of the Human Complement Regulators CFHR1 and Factor H by Streptococcal Collagen-like Protein 1 (Scl1) via Their Conserved C Termini Allows Control of the Complement Cascade at Multiple Levels. *Journal of Biological Chemistry*. 285 (49), pp. 38473–38485.

Ricklin, D. & Lambris, J.D. (2007) Complement-targeted therapeutics. *Nature Biotechnology*. 25 (11), pp. 1265–1275.

Rooijakkers, S.H.M., Milder, F.J., Bardoel, B.W., Ruyken, M., van Strijp, J.A.G. & Gros, P. (2007) Staphylococcal Complement Inhibitor: Structure and Active Sites. *Journal of immunology.* 179 (5), pp. 2989–2998.

Rooijakkers, S.H.M., Ruyken, M., Roos, A., Daha, M.R., Presanis, J.S., Sim, R.B., van Wamel, W.J.B., van Kessel, K.P.M. & van Strijp, J.A.G. (2005a) Immune evasion by a staphylococcal complement inhibitor that acts on C3 convertases. *Nature Immunology*. 6 (9), pp. 920–927.

Rooijakkers, S.H.M., van Wamel, W.J.B., Ruyken, M., van Kessel, K.P.M. & van Strijp, J.A.G. (2005b) Anti-opsonic properties of staphylokinase. *Microbes and Infection*. 7 (3), pp. 476–484.

Rooijakkers, S.H.M., Wu, J., Ruyken, M., van Domselaar, R., Planken, K.L., Tzekou, A., Ricklin, D., Lambris, J.D., Janssen, B.J.C., van Strijp, J.A.G. & Gros, P. (2009) Structural and functional implications of the alternative complement pathway C3 convertase stabilized by a staphylococcal inhibitor. *Nature Immunology*. 10 (7), pp. 722–728.

Roy, A., Kucukural, A. & Zhang, Y. (2010) I-TASSER: a unified platform for automated protein structure and function prediction. *Nature Protocols*. 5 (4), pp. 725–738.

Santoso, Y., Joyce, C.M., Potapova, O., Le Reste, L., Hohlbein, J., Torella, J.P., Grindley, N.D.F. & Kapanidis, A.N. (2010) Conformational transitions in DNA polymerase I revealed by single-molecule FRET. *Proceedings of the National Academy of Sciences*. 107 (2), pp. 715–720.

Sarrias, M.R., Franchini, S., Canziani, G., Argyropoulos, E., Moore, W.T., Sahu, A. & Lambris, J.D. (2001) Kinetic analysis of the interactions of complement receptor 2 (CR2, CD21) with its ligands C3d, iC3b, and the EBV glycoprotein gp350/220. *The Journal of Immunology*. 167 (3), pp. 1490–1499.

Scharfstein, J., Ferreira, A., Gigli, I. & Nussenzweig, V. (1978) Human C4-binding protein. I. Isolation and characterization. *The Journal of experimental medicine*. 148 (1), pp. 207–222.

Schmidt, C.Q., Herbert, A.P., Kavanagh, D., Gandy, C., Fenton, C.J., Blaum, B.S., Lyon, M., Uhrín, D. & Barlow, P.N. (2008) A new map of glycosaminoglycan and C3b binding sites on factor H. *Journal of immunology.* 181 (4), pp. 2610–2619.

Selvin, P.R. (2000) The renaissance of fluorescence resonance energy transfer. *Nature structural biology*. 7 (9), pp. 730–734.

Serruto, D., Rappuoli, R., Scarselli, M., Gros, P. & van Strijp, J.A.G. (2010) Molecular mechanisms of complement evasion: learning from staphylococci and meningococci. *Nature reviews microbiology*. 8, pp. 393–399.

Sharma, A.K. & Pangburn, M.K. (1996) Identification of three physically and functionally distinct binding sites for C3b in human complement factor H by deletion mutagenesis. *Proceedings of the National Academy of Sciences of the United States of America*. 93 (20), pp. 10996–11001.

Sharp, J.A., Echague, C.G., Hair, P.S., Ward, M.D., Nyalwidhe, J.O., Geoghegan, J.A., Foster, T.J. & Cunnion, K.M. (2012) Staphylococcus aureus Surface Protein SdrE Binds Complement Regulator Factor H as an Immune Evasion Tactic Brian Stevenson. *PLoS ONE*. 7 (5), pp. e38407.

Shohet, J.M., Bergamaschini, L., Davis, A.E. & Carroll, M.C. (1991) Localization of the human complement component C3 binding site on the IgG heavy chain. *Journal of Biological Chemistry*. 266 (28), pp. 18520–18524.

Shohet, J.M., Pemberton, P. & Carroll, M.C. (1993) Identification of a major binding site for complement C3 on the IgG1 heavy chain. *Journal of Biological Chemistry*. 268 (8), pp. 5866–5871.

Skerka, C. & Zipfel, P.F. (2008) Complement factor H related proteins in immune diseases. *Vaccine*. 26pp. I9–I14.

Skerka, C., Chen, Q., Fremeaux-Bacchi, V. & Roumenina, L.T. (2013) Complement factor H related proteins (CFHRs). *Molecular Immunology*. 56 (3), pp. 170–180.

Skerka, C., Horstmann, R.D. & Zipfel, P.F. (1991) Molecular cloning of a human serum protein structurally related to complement factor H. *Journal of Biological Chemistry*. 266 (18), pp. 12015–12020.

Skerka, C., Timmann, C., Horstmann, R.D. & Zipfel, P.F. (1992) Two additional human serum proteins structurally related to complement factor H. Evidence for a family of factor H-related genes. *Journal of Biological Chemistry*. 148 (10), pp. 3313–3318.

Skinner, D. (1941) Significance of bacteremia caused by Staphylococcus aureus. *Archives of Internal Medicine*. 68 (5), pp. 851–875.

Skjoedt, M.O., Hummelshoj, T., Palarasah, Y., Honore, C., Koch, C., Skjodt, K. & Garred, P. (2010) A Novel Mannose-binding Lectin/Ficolin-associated Protein Is Highly Expressed in Heart and Skeletal Muscle Tissues and Inhibits Complement Activation. *Journal of Biological Chemistry*. 285 (11), pp. 8234–8243.

Smith, E.J., Corrigan, R.M., van der Sluis, T., Gründling, A., Speziale, P., Geoghegan, J.A. & Foster, T.J. (2012) The immune evasion protein Sbi of Staphylococcus aureus occurs both extracellularly and anchored to the cell envelope by binding lipoteichoic acid. *Molecular Microbiology*. 83 (4), pp. 789–804.

Smith, E.J., Visai, L., Kerrigan, S.W., Speziale, P. & Foster, T.J. (2011) The Sbi Protein Is a Multifunctional Immune Evasion Factor of *Staphylococcus aureus*. *Infection and Immunity*. 79 (9), pp. 3801–3809.

Stryer, L. & Haugland, R.P. (1967) Energy transfer: a spectroscopic ruler. *Proceedings of the National Academy of Sciences of the United States of America*. 58 (2), pp. 719–726.

Stuhrmann, H.B. (1970) Interpretation of small-angle scattering functions of dilute solutions and gases. A representation of the structures related to a one-particle scattering function. *Acta Crystallographica Section A*. 26 (3), pp. 297–306.

Svergun, D., Barberato, C. & Koch, M.H.J. (1995) CRYSOL– a Program to Evaluate X-ray Solution Scattering of Biological Macromolecules from Atomic Coordinates. *Journal of Applied Crystallography*. 28 (6), pp. 768–773.

Svergun, D.I. (1992) Determination of the regularization parameter in indirect-transform methods using perceptual criteria. *Journal of Applied Crystallography*. 25 (4), pp. 495–503.

Svergun, D.I. & Koch, M. (2002) Advances in structure analysis using small-angle scattering in solution. *Current opinion in structural biology*. 12 (4), pp. 654–660.

Terao, Y., Mori, Y., Yamaguchi, M., Shimizu, Y., Ooe, K., Hamada, S. & Kawabata, S. (2008) Group A Streptococcal Cysteine Protease Degrades C3 (C3b) and Contributes to Evasion of Innate Immunity. *Journal of Biological Chemistry*. 283 (10), pp. 6253–6260.

Ting, A.Y., Liang, J., Chemla, D.S., Schultz, P.G. & Weiss, S. (1999) Temporal fluctuations of fluorescence resonance energy transfer between two dyes conjugated to a single protein. *Chemical physics*. 247, pp. 107–118.

Upadhyay, A., Burman, J.D., Clark, E.A., Leung, E., Isenman, D.E., van den Elsen, J.M.H. & Bagby, S. (2008) Structure-Function Analysis of the C3 Binding Region of Staphylococcus aureus Immune Subversion Protein Sbi. *Journal of Biological Chemistry*. 283 (32), pp. 22113–22120.

Verbrugh, H. A., Willemien, C.V, Peters, D.R., Marijke, E.V.D.T. & Verhoef, J. (1979) The role of *Staphylococcus aureus* cell-wall peptidoglycan, teichoic acid and protein A in the processes of complement activation and opsonization. *Immunology*. 37 (3), pp. 615.

Villa, V. (2012) Electro-switchable DNA layers for the analysis of antibody-antigen and p53-DNA interactions. PhD thesis, Technische Universität München

van Belkum, A. & Melles, D.C. (2009) Not All Staphylococcus aureus Strains Are Equally Pathogenic. *Discovery Medicine*. 5 (26), pp. 148–152.

van den Elsen, J.M.H. & Isenman, D.E. (2011) A Crystal Structure of the Complex Between Human Complement Receptor 2 and Its Ligand C3d. *Science*. 332 (6029), pp. 608–611.

Verbrugh, H.A., Peterson, P.K., Nguyen, B.Y., Sisson, S.P. & Kim, Y. (1982) Opsonization of encapsulated Staphylococcus aureus: the role of specific antibody and complement. *Journal of immunology*. 129 (4), pp. 1681–1687.

Vidarte, L., Pastor, C., Mas, S., Blázquez, A.B., De los Rios, V., Guerrero, R. & Vivanco, F. (2001) Serine 132 is the C3 covalent attachment point on the CH1 domain of human IgG1. *Journal of Biological Chemistry*. 276 (41), pp. 38217–38223.

Volkov, V.V. & Svergun, D.I. (2003) Uniqueness of ab initioshape determination in small-angle scattering. *Journal of Applied Crystallography*. 36 (3), pp. 860–864.

Voyich, J.M., Braughton, K.R., Sturdevant, D.E., Whitney, A.R., Said-Salim, B., Porcella, S.F., Long, R.D., Dorward, D.W., Gardner, D.J., Kreiswirth, B.N., Musser, J.M. & DeLeo, F.R. (2005) Insights into Mechanisms Used by Staphylococcus aureus to Avoid Destruction by Human Neutrophils. *Journal of immunology*. 175 (6), pp. 3907–3919.

Walport, M.J. (2001) Complement. First of two parts. *The New England journal of medicine*. 344 (14), pp. 1058–1066.

Wenzel, R.P. & Perl, T.M. (1995) The significance of nasal carriage of Staphylococcus aureus and the incidence of postoperative wound infection. *The Journal of hospital infection*. 31 (1), pp. 13–24.

Wertheim, H.F., Vos, M.C., Ott, A., van Belkum, A., Voss, A., Kluytmans, J.A., van Keulen, P.H., Vandenbroucke-Grauls, C.M., Meester, M.H. & Verbrugh, H.A. (2004) Risk and outcome of nosocomial Staphylococcus aureus bacteraemia in nasal carriers versus non-carriers. *The Lancet*. 364 (9435), pp. 703–705.

Whaley, K. & Ruddy, S. (1976) Modulation of the alternative complement pathways by beta 1 H globulin. *The Journal of experimental medicine*. 144 (5), pp. 1147–1163.

Wiesmann, C., Katschke, K.J., Yin, J., Helmy, K.Y., Steffek, M., Fairbrother, W.J., McCallum, S.A., Embuscado, L., DeForge, L., Hass, P.E. & van Lookeren Campagne, M. (2006) Structure of C3b in complex with CRIg gives insights into regulation of complement activation. *Nature*. 444 (7116), pp. 217–220.

Wu, J., Wu, Y.-Q., Ricklin, D., Janssen, B.J.C., Lambris, J.D. & Gros, P. (2009) Structure of complement fragment C3b–factor H and implications for host protection by complement regulators. *Nature immunology*. 10 (7), pp. 729–734.

Wu, S. & Zhang, Y. (2007) LOMETS: A local meta-threading-server for protein structure prediction. *Nucleic Acids Research*. 35 (10), pp. 3375–3382.

Wu, S., Skolnick, J. & Zhang, Y. (2007) Ab initio modeling of small proteins by iterative TASSER simulations. *BMC Biology*. 5 (1), pp. 17-27.

Zhang, H., Li, X.-J., Martin, D.B. & Aebersold, R. (2003) Identification and quantification of N-linked glycoproteins using hydrazide chemistry, stable isotope labeling and mass spectrometry. *Nature Biotechnology*. 21 (6), pp. 660–666.

Zhang, L., Jacobsson, K., Ström, K., Lindberg, M. & Frykberg, L. (1999) Staphylococcus aureus expresses a cell surface protein that binds both IgG and β2-glycoprotein I. *Microbiology*. 145 (1), pp. 177–183.

Zhang, L., Jacobsson, K., Vasi, J., Lindberg, M. & Frykberg, L. (1998) A second IgG-binding protein in Staphylococcus aureus. *Microbiology*. 144 (4), pp. 985–991.

Zhang, L., Rosander, A., Jacobsson, K., Lindberg, M. & Frykberg, L. (2000) Expression of staphylococcal protein Sbi is induced by human IgG. *FEMS immunology and medical microbiology*. 28 (3), pp. 211–218.

Zhang, Y., Skolnick,J. (2004) SPICKER: a clustering approach to identify near-native protein folds. *Journal of Computational Chemistry*. 25 (6), pp. 865–871.

Zhang, X., Kimura, Y., Fang, C., Zhou, L., Sfyroera, G., Lambris, J.D., Wetsel, R.A., Miwa, T. & Song, W.C. (2007) Regulation of Toll-like receptor-mediated inflammatory response by complement in vivo. *Blood*. 110 (1), pp. 228–236.

Zhang, Y. (2008) Progress and challenges in protein structure prediction. *Current opinion in structural biology*. 18, pp. 342–348.

Zhang, Y., Kihara, D. & Skolnick, J. (2002) Local energy landscape flattening: Parallel hyperbolic Monte Carlo sampling of protein folding. *Proteins: Structure, Function, and Genetics*. 48 (2), pp. 192–201.

Zhao, J., Wu, H., Khosravi, M., Cui, H., Qian, X. & Kelly, J.A. (2011) Association of Genetic Variants in Complement Factor H and Factor H-Related Genes with Systemic Lupus Erythematosus Susceptibility. *PLoS Genetics,* 7 (5), pp. e1002079

Zipfel, P.F. & Skerka, C. (2009) Complement regulators and inhibitory proteins. *Nature Reviews Immunology*. 9 (10), pp. 729–740.

Zipfel, P.F. & Skerka, C. (1999) FHL-1/reconectin: a human complement and immune regulator with cell-adhesive function. *Immunology Today*. 20 (3), pp. 135–140.

Chapter 9: Appendices

9.1: DNA sequencing results and protein sequences

9.1.1 Constructs:

9.1.1.1pQE30$^{Sbi\text{-}III\text{-}IV}$ sequence

```
ATG AGA GGA TCG CAT CAC CAT CAC CAT CAC GGA TCC GAA CGT CAA AAT ATT GAA AAT GCG  < 60
M   R   G   S   H   H   H   H   H   H   G   S   E   R   Q   N   I   E   N   A
            10          20          30          40          50

GAT AAA GCA ATT AAA GAT TTC CAA GAT AAC AAA GCA CCA CAC GAT AAA TCA GCA GCA TAT  < 120
D   K   A   I   K   D   F   Q   D   N   K   A   P   H   D   K   S   A   A   Y
            70          80          90          100         110

GAA GCT AAC TCA AAA TTA CCT AAA GAT TTA CGC GAT AAA AAT AAC CGC TTT GTA GAA AAA  < 180
E   A   N   S   K   L   P   K   D   L   R   D   K   N   N   R   F   V   E   K
            130         140         150         160         170

GTT TCA ATT GAA AAA GCA ATC GTT CGT CAT GAT GAG CGT GTG AAA TCA GCA AAT GAT GCA  < 240
V   S   I   E   K   A   I   V   R   H   D   E   R   V   K   S   A   N   D   A
            190         200         210         220         230

ATC TCA AAA TTA AAT GAA AAA GAT TCA ATT GAA AAC AGA CGT TTA GCA CAA CGT GAA GTT  < 300
I   S   K   L   N   E   K   D   S   I   E   N   R   R   L   A   Q   R   E   V
            250         260         270         280         290

AAC AAA GCA CCT ATG GAT GTA AAA GAG CAT TTA CAG AAA CAA TTA GAC GCA TTA GTA GCT  < 360
N   K   A   P   M   D   V   K   E   H   L   Q   K   Q   L   D   A   L   V   A
            310         320         330         340         350

CAA AAA GAT GCT GAA AAG AAA GTG GCG TAA  < 390
Q   K   D   A   E   K   K   V   A   *
            370         380
```

9.1.1.2 pQE30$^{Sbi\text{-}III\text{-}IV\text{-}cys}$ sequence

```
ATG AGA GGA TCG CAT CAC CAT CAC CAT CAC GGA TCC GAA CGT CAA AAT AT  < 50
M   R   G   S   H   H   H   H   H   H   G   S   E   R   Q   N   I
            10          20          30          40

T GAA AAT GCG GAT AAA GCA ATT AAA GAT TTC CAA GAT AAC AAA GCA CCA C  < 100
  E   N   A   D   K   A   I   K   D   F   Q   D   N   K   A   P   H
            60          70          80          90

AC GAT AAA TCA GCA GCA TAT GAA GCT AAC TCA AAA TTA CCT AAA GAT TTA  < 150
   D   K   S   A   A   Y   E   A   N   S   K   L   P   K   D   L
            110         120         130         140

CGC GAT AAA AAT AAC CGC TTT GTA GAA AAA GTT TCA ATT GAA AAA GCA AT  < 200
R   D   K   N   N   R   F   V   E   K   V   S   I   E   K   A   I
            160         170         180         190

C GTT CGT CAT GAT GAG CGT GTG AAA TCA GCA AAT GAT GCA ATC TCA AAA T  < 250
  V   R   H   D   E   R   V   K   S   A   N   D   A   I   S   K   L
            210         220         230         240

TA AAT GAA AAA GAT TCA ATT GAA AAC AGA CGT TTA GCA CAA CGT GAA GTT  < 300
   N   E   K   D   S   I   E   N   R   R   L   A   Q   R   E   V
            260         270         280         290

AAC AAA GCA CCT ATG GAT GTA AAA GAG CAT TTA CAG AAA CAA TTA GAC GC  < 350
N   K   A   P   M   D   V   K   E   H   L   Q   K   Q   L   D   A
            310         320         330         340

A TTA GTA GCT CAA AAA GAT GCT GAA AAG AAA TGC GCG TAA  < 390
  L   V   A   Q   K   D   A   E   K   K   C   A   *
            360         370         380
```

C-terminal cystine

9.1.1.3 pET15b-C3d^{17A} sequence

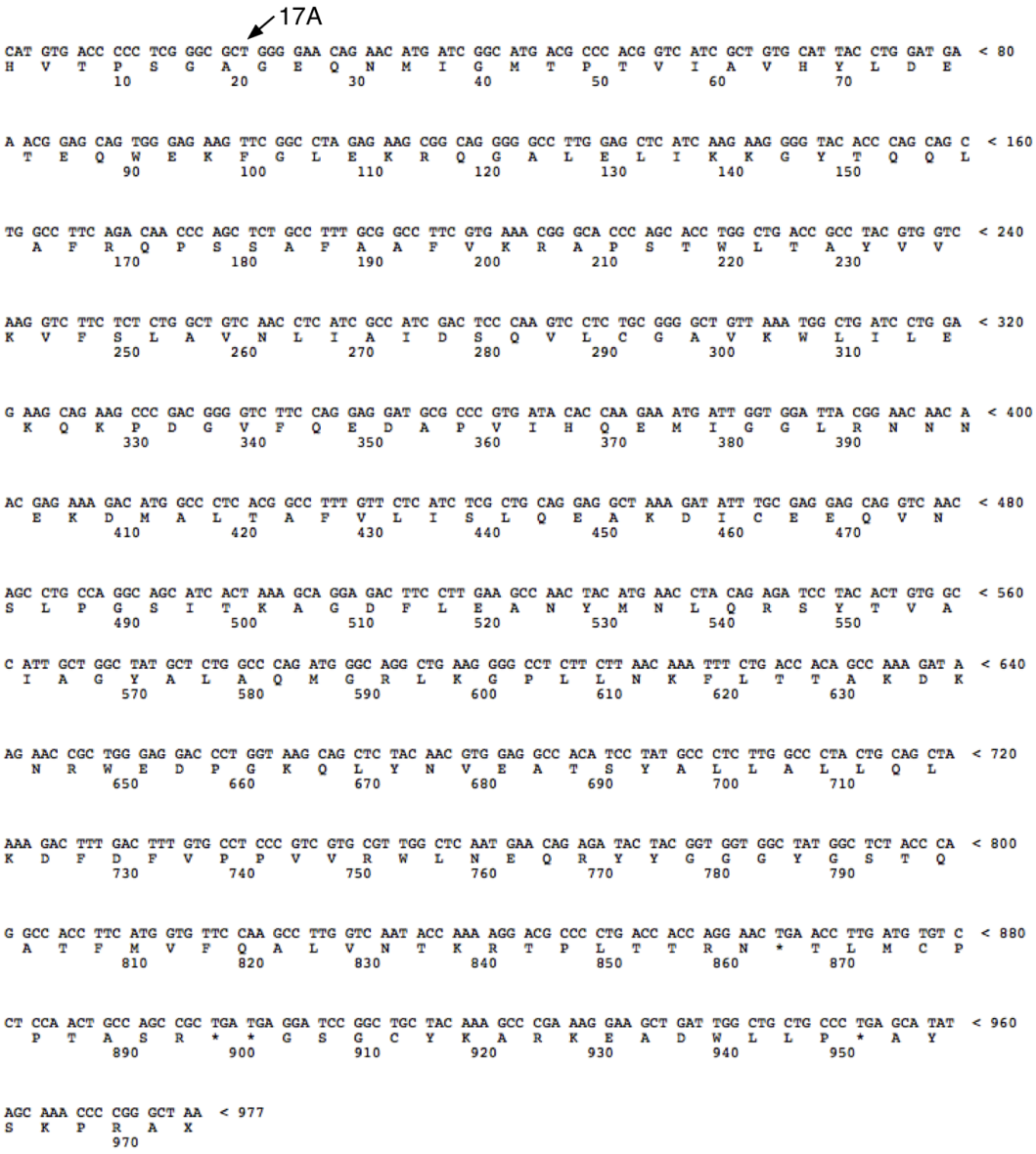

9.1.1.4 pMA-T-C3a sequence

9.1.1.5 pGEX-C3a

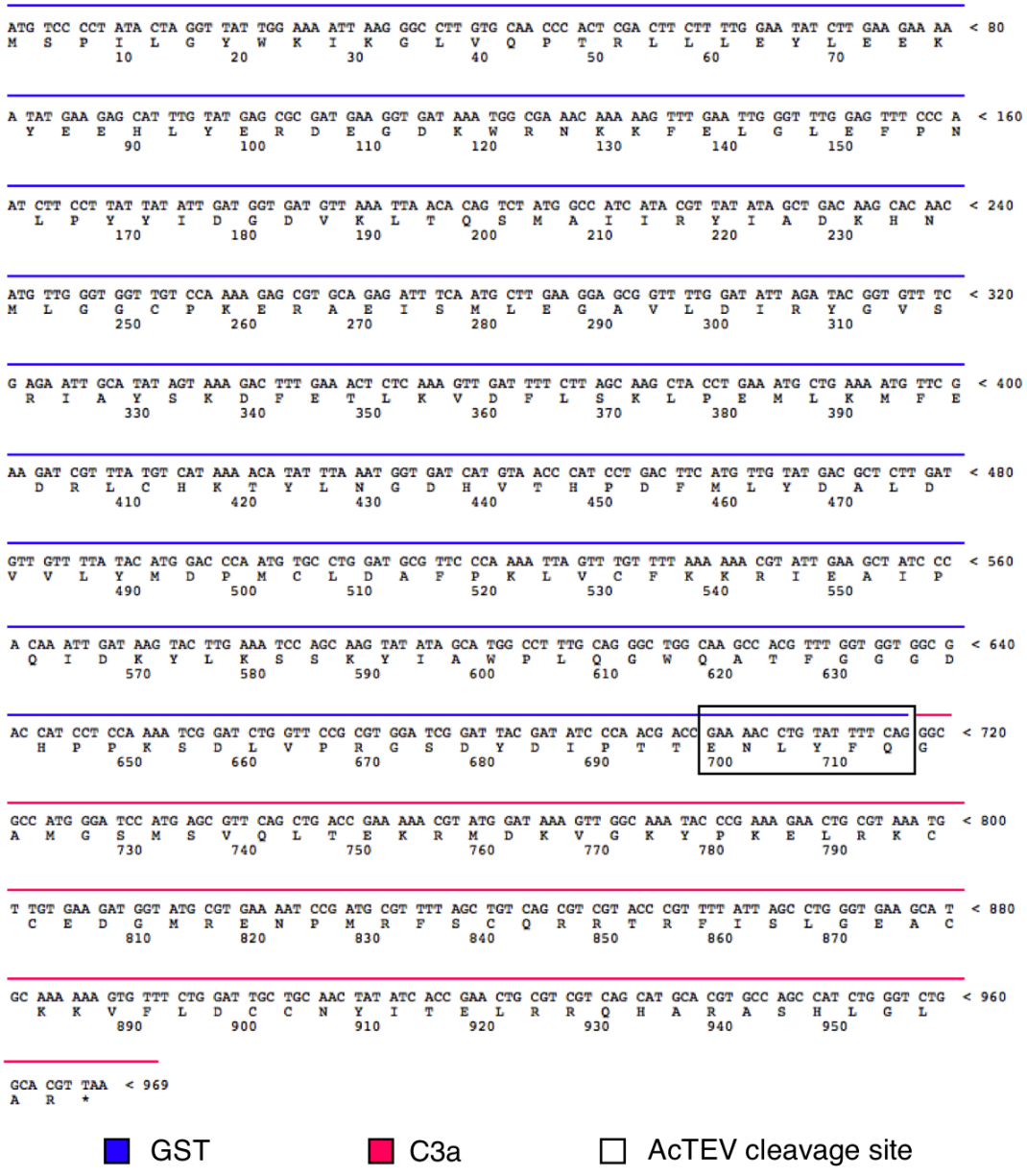

9.1.1.6 pET28$^{Sbi\text{-}III\text{-}IV}$

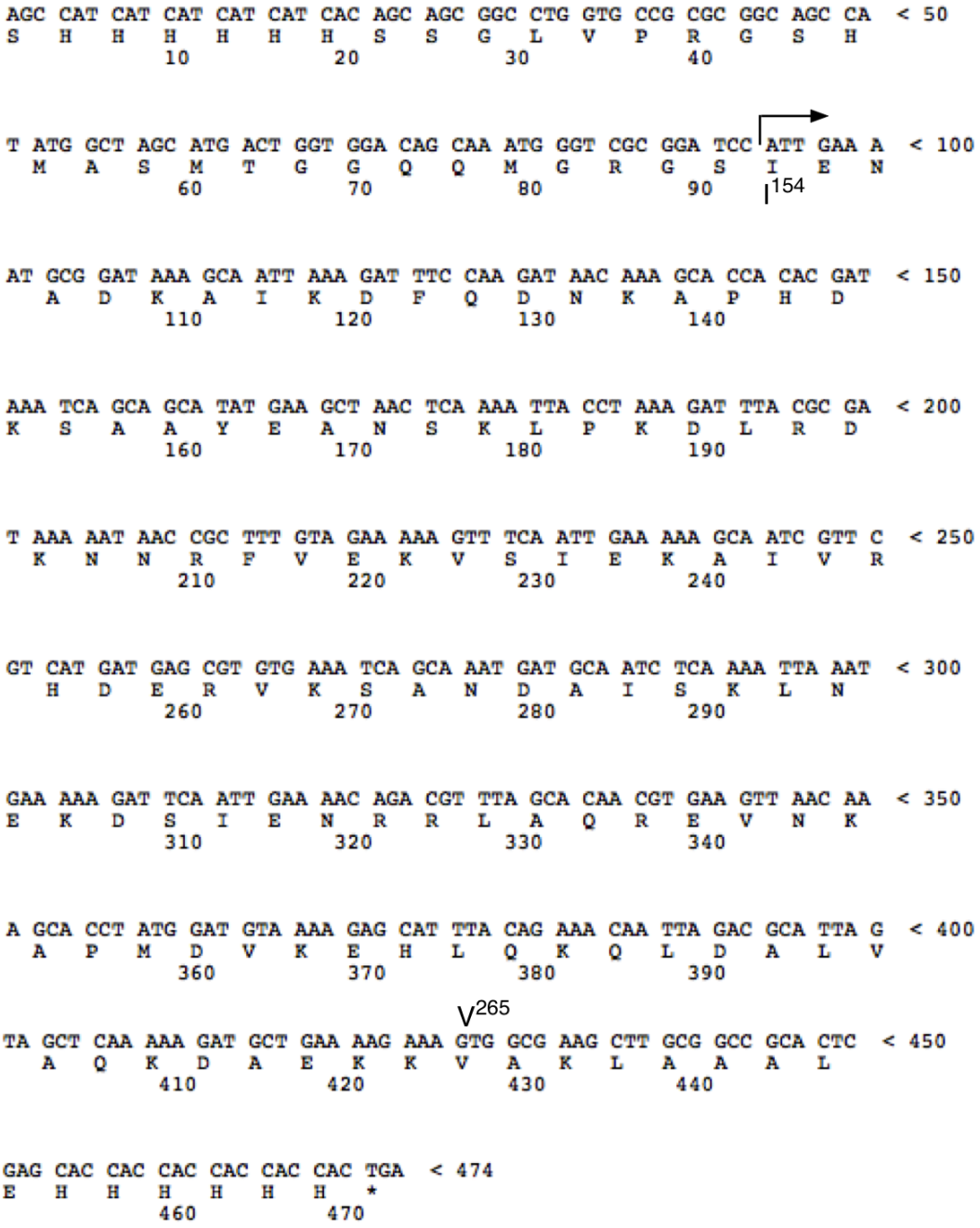

9.1.1.7 pQE30$^{Sbi\text{-}III\text{-}IV\text{-}dual\text{-}cys}$

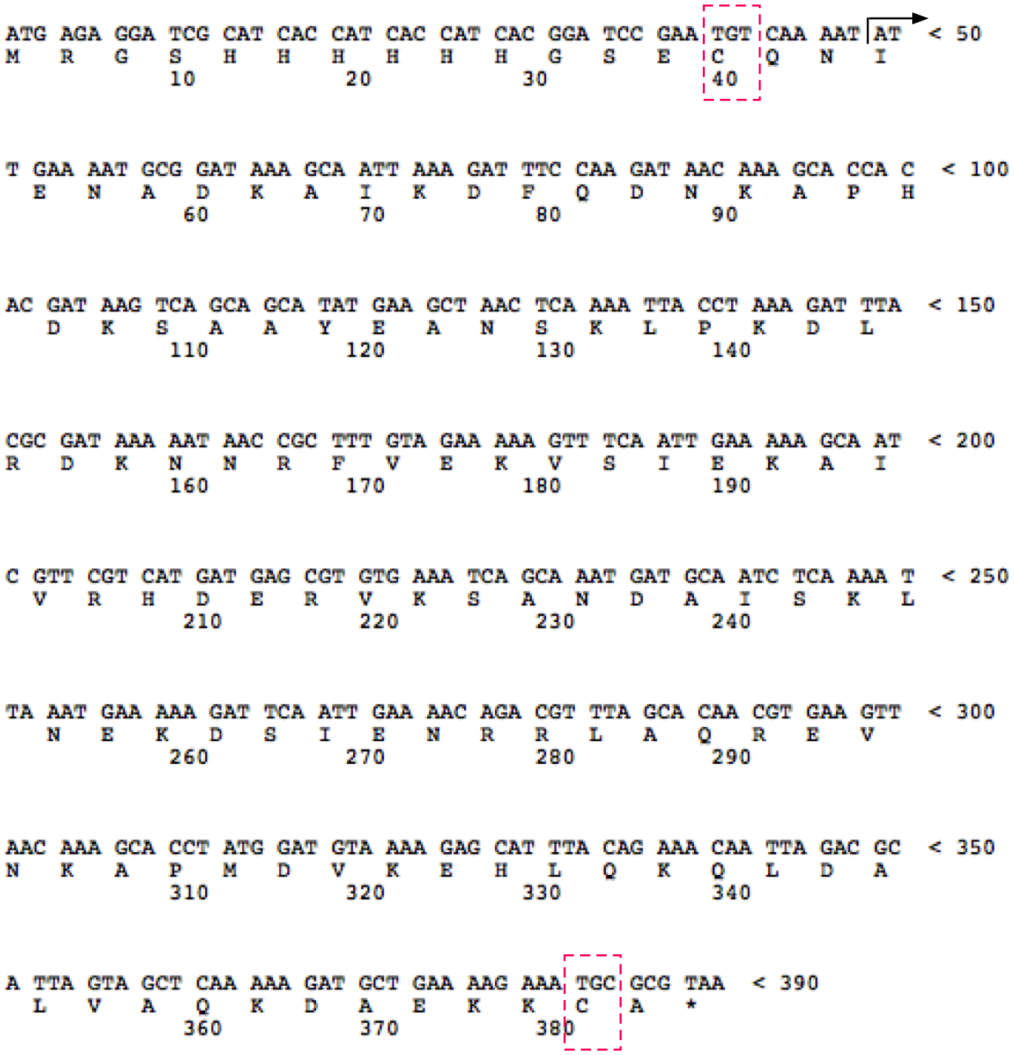

9.1.2 DNA sequencing results

9.1.2.1 pQE30$^{Sbi\text{-}III\text{-}IV}$ Single mutants

Alanine mutations are highlighted in red, phenylalanine mutation is highlighted in green.

N156A

ATGAGAGGATCGCATCACCATCACCATCACGGATCCGAACGTCAAAATATTGAA**GCT**GCGGATAAAGCAATTAAAG
ATTTCCAAGATAACAAAGCACCACACGATAAATCAGCAGCATATGAAGCTAACTCAAAATTACCTAAAGATTTACG
CGATAAAAATAACCGCTTTGTAGAAAAAGTTTCAATTGAAAAAGCAATCGTTCGTCATGATGAGCGTGTGAAATCA
GCAAATGATGCAATCTCAAAATTAAATGAAAAAGATTCAATTGAAAACAGACGTTTAGCACAACGTGAAGTTAACA
AAGCACCTATGGATGTAAAAGAGCATTTACAGAAACAATTAGACGCATTAGTAGCTCAAAAAGATGCTGAAAAGAA
AGTGGCGTAA

K159A

ATGAGAGGATCGCATCACCATCACCATCACGGATCCGAACGTCAAAATATTGAAAATGCGGATGCAGCAATTAAAG
ATTTCCAAGATAACAAAGCACCACACGATAAATCAGCAGCATATGAAGCTAACTCAAAATTACCTAAAGATTTACG
CGATAAAAATAACCGCTTTGTAGAAAAAGTTTCAATTGAAAAAGCAATCGTTCGTCATGATGAGCGTGTGAAATCA
GCAAATGATGCAATCTCAAAATTAAATGAAAAAGATTCAATTGAAAACAGACGTTTAGCACAACGTGAAGTTAACA
AAGCACCTATGGATGTAAAAGAGCATTTACAGAAACAATTAGACGCATTAGTAGCTCAAAAAGATGCTGAAAAGAA
AGTGGCGTAA

K162A

ATGAGAGGATCGCATCACCATCACCATCACGGATCCGAACGTCAAAATATTGAAAATGCGGATAAAGCAATTGCAG
ATTTCCAAGATAACAAAGCACCACACGATAAATCAGCAGCATATGAAGCTAACTCAAAATTACCTAAAGATTTACG
CGATAAAAATAACCGCTTTGTAGAAAAAGTTTCAATTGAAAAAGCAATCGTTCGTCATGATGAGCGTGTGAAATCA
GCAAATGATGCAATCTCAAAATTAAATGAAAAAGATTCAATTGAAAACAGACGTTTAGCACAACGTGAAGTTAACA
AAGCACCTATGGATGTAAAAGAGCATTTACAGAAACAATTAGACGCATTAGTAGCTCAAAAAGATGCTGAAAAGAA
AGTGGCGTAA

K168A

ATGAGAGGATCGCATCACCATCACCATCACGGATCCGAACGTCAAAATATTGAAAATGCGGATAAAGCAATTAAAG
ATTTCCAAGATAACGCAGCACCACACGATAAATCAGCAGCATATGAAGCTAACTCAAAATTACCTAAAGATTTACG
CGATAAAAATAACCGCTTTGTAGAAAAAGTTTCAATTGAAAAAGCAATCGTTCGTCATGATGAGCGTGTGAAATCA
GCAAATGATGCAATCTCAAAATTAAATGAAAAAGATTCAATTGAAAACAGACGTTTAGCACAACGTGAAGTTAACA
AAGCACCTATGGATGTAAAAGAGCATTTACAGAAACAATTAGACGCATTAGTAGCTCAAAAAGATGCTGAAAAGAA
AGTGGCGTAA

P170A

ATGAGAGGATCGCATCACCATCACCATCACGGATCCGAACGTCAAAATATTGAAAATGCGGATAAAGCAATTAAAG
ATTTCCAAGATAACAAAGCAGCACACGATAAATCAGCAGCATATGAAGCTAACTCAAAATTACCTAAAGATTTACG
CGATAAAAATAACCGCTTTGTAGAAAAAGTTTCAATTGAAAAAGCAATCGTTCGTCATGATGAGCGTGTGAAATCA
GCAAATGATGCAATCTCAAAATTAAATGAAAAAGATTCAATTGAAAACAGACGTTTAGCACAACGTGAAGTTAACA
AAGCACCTATGGATGTAAAAGAGCATTTACAGAAACAATTAGACGCATTAGTAGCTCAAAAAGATGCTGAAAAGAA
AGTGGCGTAA

D172A

ATGAGAGGATCGCATCACCATCACCATCACGGATCCGAACGTCAAAATATTGAAAATGCGGATAAAGCAATTAAAG
ATTTCCAAGATAACAAAGCACCACACGCCAAATCAGCAGCATATGAAGCTAACTCAAAATTACCTAAAGATTTACG
CGATAAAAATAACCGCTTTGTAGAAAAAGTTTCAATTGAAAAAGCAATCGTTCGTCATGATGAGCGTGTGAAATCA
GCAAATGATGCAATCTCAAAATTAAATGAAAAAGATTCAATTGAAAACAGACGTTTAGCACAACGTGAAGTTAACA
AAGCACCTATGGATGTAAAAGAGCATTTACAGAAACAATTAGACGCATTAGTAGCTCAAAAAGATGCTGAAAAGAA
AGTGGCGTAA

K173A

ATGAGAGGATCGCATCACCATCACCATCACGGATCCGAACGTCAAAATATTGAAAATGCGGATAAAGCAATTAAAG
ATTTCCAAGATAACAAAGCACCACACGATGCATCAGCAGCATATGAAGCTAACTCAAAATTACCTAAAGATTTACG
CGATAAAAATAACCGCTTTGTAGAAAAAGTTTCAATTGAAAAAGCAATCGTTCGTCATGATGAGCGTGTGAAATCA

GCAAATGATGCAATCTCAAAATTAAATGAAAAAGATTCAATTGAAAACAGACGTTTAGCACAACGTGAAGTTAACA
AAGCACCTATGGATGTAAAAGAGCATTTACAGAAACAATTAGACGCATTAGTAGCTCAAAAAGATGCTGAAAAGAA
AGTGGCGTAA

S174A

ATGAGAGGATCGCATCACCATCACCATCACGGATCCGAACGTCAAAATATTGAAAATGCGGATAAAGCAATTAAAG
ATTTCCAAGATAACAAAGCACCACACGCCAAA**GCA**GCAGCATATGAAGCTAACTCAAAATTACCTAAAGATTTACG
CGATAAAAATAACCGCTTTGTAGAAAAAGTTTCAATTGAAAAAGCAATCGTTCGTCATGATGAGCGTGTGAAATCA
GCAAATGATGCAATCTCAAAATTAAATGAAAAAGATTCAATTGAAAACAGACGTTTAGCACAACGTGAAGTTAACA
AAGCACCTATGGATGTAAAAGAGCATTTACAGAAACAATTAGACGCATTAGTAGCTCAAAAAGATGCTGAAAAGAA
AGTGGCGTAA

Y177F

ATGAGAGGATCGCATCACCATCACCATCACGGATCCGAACGTCAAAATATTGAAAATGCGGATAAAGCAATTAAAG
ATTTCCAAGATAACAAAGCACCACACGATAAATCAGCAGCA**TTT**GAAGCTAACTCAAAATTACCTAAAGATTTACG
CGATAAAAATAACCGCTTTGTAGAAAAAGTTTCAATTGAAAAAGCAATCGTTCGTCATGATGAGCGTGTGAAATCA
GCAAATGATGCAATCTCAAAATTAAATGAAAAAGATTCAATTGAAAACAGACGTTTAGCACAACGTGAAGTTAACA
AAGCACCTATGGATGTAAAAGAGCATTTACAGAAACAATTAGACGCATTAGTAGCTCAAAAAGATGCTGAAAAGAA
AGTGGCGTAA

N180A

ATGAGAGGATCGCATCACCATCACCATCACGGATCCGAACGTCAAAATATTGAAAATGCGGATAAAGCAATTAAAG
ATTTCCAAGATAACAAAGCACCACACGATAAATCAGCAGCATATGAAGCT**GCC**TCAAAATTACCTAAAGATTTACG
CGATAAAAATAACCGCTTTGTAGAAAAAGTTTCAATTGAAAAAGCAATCGTTCGTCATGATGAGCGTGTGAAATCA
GCAAATGATGCAATCTCAAAATTAAATGAAAAAGATTCAATTGAAAACAGACGTTTAGCACAACGTGAAGTTAACA
AAGCACCTATGGATGTAAAAGAGCATTTACAGAAACAATTAGACGCATTAGTAGCTCAAAAAGATGCTGAAAAGAA
AGTGGCGTAA

K182A

ATGAGAGGATCGCATCACCATCACCATCACGGATCCGAACGTCAAAATATTGAAAATGCGGATAAAGCAATTAAAG
ATTTCCAAGATAACAAAGCACCACACGATAAATCAGCAGCATATGAAGCTAACTCA**GCA**TTACCTAAAGATTTACG
CGATAAAAATAACCGCTTTGTAGAAAAAGTTTCAATTGAAAAAGCAATCGTTCGTCATGATGAGCGTGTGAAATCA
GCAAATGATGCAATCTCAAAATTAAATGAAAAAGATTCAATTGAAAACAGACGTTTAGCACAACGTGAAGTTAACA
AAGCACCTATGGATGTAAAAGAGCATTTACNGAAACAATTAGACGCNTTAGTAGCTCAAAAAGATGCTGAAAAGA
AAGTGGCGTAG

K185A

ATGAGAGGATCGCATCACCATCACCATCACGGATCCGAACGTCAAAATATTGAAAATGCGGATAAAGCAATTAAAG
ATTTCCAAGATAACAAAGCACCACACGATAAATCAGCAGCATATGAAGCTAACTCAAAATTACCT**GCA**GATTTACG
CGATAAAAATAACCGCTTTGTAGAAAAAGTTTCAATTGAAAAAGCAATCGTTCGTCATGATGAGCGTGTGAAATCA
GCAAATGATGCAATCTCAAAATTAAATGAAAAAGATTCAATTGAAAACAGACGTTTAGCACAACGTGAAGTTAACA
AAGCACCTATGGATGTAAAAGAGCATTTACAGAAACAATTAGACGCATTAGTAGCTCAAAAAGATGCTGAAAAGAA
AGTGGCGTAA

R188A

ATGAGAGGATCGCATCACCATCACCATCACGGATCCGAACGTCAAAATATTGAAAATGCGGATAAAGCAATTAAAG
ATTTCCAAGATAACAAAGCACCACACGATAAATCAGCAGCATATGAAGCTAACTCAAAATTACCTAAAGATTTA**GC**
CGATAAAAATAACCGCTTTGTAGAAAAAGTTTCAATTGAAAAAGCAATCGTTCGTCATGATGAGCGTGTGAAATCA
GCAAATGATGCAATCTCAAAATTAAATGAAAAAGATTCAATTGAAAACAGACGTTTAGCACAACGTGAAGTTAACA
AAGCACCTATGGATGTAAAAGAGCATTTACAGAAACAATTAGACGCATTAGTAGCTCAAAAAGATGCTGAAAAGAA
AGTGGCGTAA

K190A

ATGAGAGGATCGCATCACCATCACCATCACGGATCCGAACGTCAAAATATTGAAAATGCGGATAAAGCAATTAAAG
ATTTCCAAGATAACAAAGCACCACACGATAAATCAGCAGCATATGAAGCTAACTCAAAATTACCTAAAGATTTACG
CGAT**GCA**AATAACCGCTTTGTAGAAAAAGTTTCAATTGAAAAAGCAATCGTTCGTCATGATGAGCGTGTGAAATCA
GCAAATGATGCAATCTCAAAATTAAATGAAAAAGATTCAATTGAAAACAGACGTTTAGCACAACGTGAAGTTAACA
AAGCACCTATGGATGTAAAAGAGCATTTACAGAAACAATTAGACGCATTAGTAGCTCAAAAAGATGCTGAAAAGAA
AGTGGCGTAA

N191A

ATGAGAGGATCGCATCACCATCACCATCACGGATCCGAACGTCAAAATATTGAAAATGCGGATAAAGCAATTAAAG
ATTTCCAAGATAACAAAGCACCACACGATAAATCAGCAGCATATGAAGCTAACTCAAAATTACCTAAAGATTTACG
CGATAAA**GCT**AACCGCTTTGTAGAAAAAGTTTCAATTGAAAAAGCAATCGTTCGTCATGATGAGCGTGTGAAATCA
GCAAATGATGCAATCTCAAAATTAAATGAAAAAGATTCAATTGAAAACAGACGTTTAGCACAACGTGAAGTTAACA
AAGCACCTATGGATGTAAAAGAGCATTTACAGAAACAATTAGACGCATTAGTAGCTCAAAAAGATGCTGAAAAGAA
AGTGGCGTAA

N192A

ATGAGAGGATCGCATCACCATCACCATCACGGATCCGAACGTCAAAATATTGAAAATGCGGATAAAGCAATTAAAG
ATTTCCAAGATAACAAAGCACCACACGATAAATCAGCAGCATATGAAGCTAACTCAAAATTACCTAAAGATTTACG
CGATAAAAAT**GCC**CGCTTTGTAGAAAAAGTTTCAATTGAAAAAGCAATCGTTCGTCATGATGAGCGTGTGAAATCA
GCAAATGATGCAATCTCAAAATTAAATGAAAAAGATTCAATTGAAAACAGACGTTTAGCACAACGTGAAGTTAACA
AAGCACCTATGGATGTAAAAGAGCATTTACAGAAACAATTAGACGCATTAGTAGCTCAAAAAGATGCTGAAAAGAA
AGTGGCGTAA

S199A

ATGAGAGGATCGCATCACCATCACCATCACGGATCCGAACGTCAAAATATTGAAAATGCGGATAAAGCAATTAAAG
ATTTCCAAGATAACAAAGCACCACACGATAAATCAGCAGCATATGAAGCTAACTCAAAATTACCTAAAGATTTACG
CGATAAAAATAACCGCTTTGTAGAAAAAGTT**GCA**ATTGAAAAAGCAATCGTTCGTCATGATGAGCGTGTGAAATCA
GCAAATGATGCAATCTCAAAATTAAATGAAAAAGATTCAATTGAAAACAGACGTTTAGCACAACGTGAAGTTAACA
AAGCACCTATGGATGTAAAAGAGCATTTACAGAAACAATTAGACGCATTAGTAGCTCAAAAAGATGCTGAAAAGAA
AGTGGCGTAA

D208N

ATGAGAGGATCGCATCACCATCACCATCACGGATCCGAACGTCAAAATATTGAAAATGCGGATAAAGCAATTAAAG
ATTTCCAAGATAACAAAGCACCACACGATAAATCAGCAGCATATGAAGCTAACTCAAAATTACCTAAAGATTTACG
CGATAAAAATAACCGCTTTGTAGAAAAAGTTTCAATTGAAAAAGCAATCGTTCGTCAT**AAT**GAGCGTGTGAAATCA
GCAAATGATGCAATCTCAAAATTAAATGAAAAAGATTCAATTGAAAACAGACGTTTAGCACAACGTGAAGTTAACA

AAGCACCTATGGATGTAAAAGAGCATTTACAGAAACAATTAGACGCATTAGTAGCTCAAAAAGATGCTGAAAAGAA
AGTGGCGTAA

K212A

ATGAGAGGATCGCATCACCATCACCATCACGGATCCGAACGTCAAAATATTGAAAATGCGGATAAAGCAATTAAAG
ATTTCCAAGATAACAAAGCACCACACGATAAATCAGCAGCATATGAAGCTAACTCAAAATTACCTAAAGATTTACG
CGATAAAAATAACCGCTTTGTAGAAAAAGTTTCAATTGAAAAAGCAATCGTTCGTCATGATGAGCGTGTG**GCA**TCA
GCAAATGATGCAATCTCAAAATTAAATGAAAAAGATTCAATTGAAAACAGACGTTTAGCACAACGTGAAGTTAACA
AAGCACCTATGGATGTAAAAGAGCATTTACAGAAACAATTAGACGCATTAGTAGCTCAAAAAGATGCTGAAAAGAA
AGTGGCGTAA

S213A

ATGAGAGGATCGCATCACCATCACCATCACGGATCCGAACGTCAAAATATTGAAAATGCGGATAAAGCAATTAAAG
ATTTCCAAGATAACAAAGCACCACACGATAAATCAGCAGCATATGAAGCTAACTCAAAATTACCTAAAGATTTACG
CGATAAAAATAACCGCTTTGTAGAAAAAGTTTCAATTGAAAAAGCAATCGTTCGTCATGATGAGCGTGTGAAA**GCA**
GCAAATGATGCAATCTCAAAATTAAATGAAAAAGATTCAATTGAAAACAGACGTTTAGCACAACGTGAAGTTAACA
AAGCACCTATGGATGTAAAAGAGCATTTACAGAAACAATTAGACGCATTAGTAGCTCAAAAAGATGCTGAAAAGAA
AGTGGCGTAA

S226A

ATGAGAGGATCGCATCACCATCACCATCACGGATCCGAACGTCAAAATATTGAAAATGCGGATAAAGCAATTAAAG
ATTTCCAAGATAACAAAGCACCACACGATAAATCAGCAGCATATGAAGCTAACTCAAAATTACCTAAAGATTTACG
CGATAAAAATAACCGCTTTGTAGAAAAAGTTTCAATTGAAAAAGCAATCGTTCGTCATGATGAGCGTGTGAAATCA
GCAAATGATGCAATCTCAAAATTAAATGAAAAAGAT**GCA**ATTGAAAACAGACGTTTAGCACAACGTGAAGTTAAC
AAAGCACCTATGGATGTAAAAGAGCATTTACAGAAACAATTAGACGCATTAGTAGCTCAAAAAGATGCTGAAAAGA
AAGTGGCGTAA

R231A

ATGAGAGGATCGCATCACCATCACCATCACGGATCCGAACGTCAAAATATTGAAAATGCGGATAAAGCAATTAAAG
ATTTCCAAGATAACAAAGCACCACACGATAAATCAGCAGCATATGAAGCTAACTCAAAATTACCTAAAGATTTACG
CGATAAAAATAACCGCTTTGTAGAAAAAGTTTCAATTGAAAAAGCAATCGTTCGTCATGATGAGCGTGTGAAATCA
GCAAATGATGCAATCTCAAAATTAAATGAAAAAGATTCAATTGAAAACAGA**GCT**TTAGCACAACGTGAAGTTAAC
AAAGCACCTATGGATGTAAAAGAGCATTTACAGAAACAATTAGACGCATTAGTAGCTCAAAAAGATGCTGAAAAGA
AAGTGGCGTAA

8.1.2.2 pQE30$^{Sbi\text{-}III\text{-}IV}$ accumulative mutants

Alanine mutations are highlighted in red, phenylalanine mutation is highlighted in green

D172A K168A

ATGAGAGGATCGCATCACCATCACCATCACGGATCCGAACGTCAAAATATTGAAAATGCGGATAAAGCAATTAAAG
ATTTCCAAGATAAC**GCA**GCACCACAC**GCC**AAATCAGCAGCATATGAAGCTAACTCAAAATTACCTAAAGATTTACG
CGATAAAAATAACCGCTTTGTAGAAAAAGTTTCAATTGAAAAAGCAATCGTTCGTCATGATGAGCGTGTGAAATCA

GCAAATGATGCAATCTCAAAATTAAATGAAAAAGATTCAATTGAAAACAGACGTTTAGCACAACGTGAAGTTAACA
AAGCACCTATGGATGTAAAAGAGCATTTACAGAAACAATTAGACGCATTAGTAGCTCAAAAAGATGCTGAAAAGAA
AGTGGCGTAA

D172A K168A K162A

ATGAGAGGATCGCATCACCATCACCATCACGGATCCGAACGTCAAAATATTGAAAATGCGGATAAAGCAATTGCAG
ATTTCCAAGATAACGCAGCACCACACGCCAAATCAGCAGCATATGAAGCTAACTCAAAATTACCTAAAGATTTACG
CGATAAAAATAACCGCTTTGTAGAAAAAGTTTCAATTGAAAAAGCAATCGTTCGTCATGATGAGCGTGTGAAATCA
GCAAATGATGCAATCTCAAAATTAAATGAAAAAGATTCAATTGAAAACAGACGTTTAGCACAACGTGAAGTTAACA
AAGCACCTATGGATGTAAAAGAGCATTTACAGAAACAATTAGACGCATTAGTAGCTCAAAAAGATGCTGAAAAGAA
AGTGGCGTAA

D172A K168A K162A K159A

ATGAGAGGATCGCATCACCATCACCATCACGGATCCGAACGTCAAAATATTGAAAATGCGGATGCAGCAATTGCAG
ATTTCCAAGATAACGCAGCACCACACGCCAAATCAGCAGCATATGAAGCTAACTCAAAATTACCTAAAGATTTACG
CGATAAAAATAACCGCTTTGTAGAAAAAGTTTCAATTGAAAAAGCAATCGTTCGTCATGATGAGCGTGTGAAATCA
GCAAATGATGCAATCTCAAAATTAAATGAAAAAGATTCAATTGAAAACAGACGTTTAGCACAACGTGAAGTTAACA
AAGCACCTATGGATGTAAAAGAGCATTTACAGAAACAATTAGACGCATTAGTAGCTCAAAAAGATGCTGAAAAGAA
AGTGGCGTAA

S174A S181A

ATGAGAGGATCGCATCACCATCACCATCACGGATCCGAACGTCAAAATATTGAAAATGCGGATAAAGCAATTAAAG
ATTTCCAAGATAACAAAGCACCACACGATAAAGCAGCAGCATATGAAGCTAACGCAAAATTACCTAAAGATTTACG
CGATAAAAATAACCGCTTTGTAGAAAAAGTTTCAATTGAAAAAGCAATCGTTCGTCATGATGAGCGTGTGAAATCA
GCAAATGATGCAATCTCAAAATTAAATGAAAAAGATTCAATTGAAAACAGACGTTTAGCACAACGTGAAGTTAACA
AAGCACCTATGGATGTAAAAGAGCATTTACAGAAACAATTAGACGCATTAGTAGCTCAAAAAGATGCTGAAAAGAA
AGTGGCGTAA

S174A S181A Y177F

ATGAGAGGATCGCATCACCATCACCATCACGGATCCGAACGTCAAAATATTGAAAATGCGGATAAAGCAATTAAAG
ATTTCCAAGATAACAAAGCACCACACGATAAAGCAGCAGCATTTGAAGCTAACGCAAAATTACCTAAAGATTTACG
CGATAAAAATAACCGCTTTGTAGAAAAAGTTTCAATTGAAAAAGCAATCGTTCGTCATGATGAGCGTGTGAAATCA
GCAAATGATGCAATCTCAAAATTAAATGAAAAAGATTCAATTGAAAACAGACGTTTAGCACAACGTGAAGTTAACA
AAGCACCTATGGATGTAAAAGAGCATTTACAGAAACAATTAGACGCATTAGTAGCTCAAAAAGATGCTGAAAAGAA
AGTGGCGTAA

K212A S213A

ATGAGAGGATCGCATCACCATCACCATCACGGATCCGAACGTCAAAATATTGAAAATGCGGATAAAGCAATTAAAG
ATTTCCAAGATAACAAAGCACCACACGATAAATCAGCAGCATATGAAGCTAACTCAAAATTACCTAAAGATTTACG
CGATAAAAATAACCGCTTTGTAGAAAAAGTTTCAATTGAAAAAGCAATCGTTCGTCATGATGAGCGTGTGGCAGCA
GCAAATGATGCAATCTCAAAATTAAATGAAAAAGATTCAATTGAAAACAGACGTTTAGCACAACGTGAAGTTAACA
AAGCACCTATGGATGTAAAAGAGCATTTACAGAAACAATTAGACGCATTAGTAGCTCAAAAAGATGCTGAAAAGAA
AGTGGCGTAA

K212A S213A S219A K220A

ATGAGAGGATCGCATCACCATCACCATCACGGATCCGAACGTCAAAATATTGAAAATGCGGATAAAGCAATTAAAG
ATTTCCAAGATAACAAAGCACCACACGATAAATCAGCAGCATATGAAGCTAACTCAAAATTACCTAAAGATTTACG
CGATAAAAATAACCGCTTTGTAGAAAAAGTTTCAATTGAAAAAGCAATCGTTCGTCATGATGAGCGTGTG**GCAGCA**
GCAAATGATGCAATC**GCAGCA**TTAAATGAAAAAGATTCAATTGAAAACAGACGTTTAGCACAACGTGAAGTTAAC
AAAGCACCTATGGATGTAAAAGAGCATTTACAGAAACAATTAGACGCATTAGTAGCTCAAAAAGATGCTGAAAAGA
AAGTGGCGTAA

K212A S213A S219A K220A K259A

ATGAGAGGATCGCATCACCATCACCATCACGGATCCGAACGTCAAAATATTGAAAATGCGGATAAAGCAATTAAAG
ATTTCCAAGATAACAAAGCACCACACGATAAATCAGCAGCATATGAAGCTAACTCAAAATTACCTAAAGATTTACG
CGATAAAAATAACCGCTTTGTAGAAAAAGTTTCAATTGAAAAAGCAATCGTTCGTCATGATGAGCGTGTG**GCAGCA**
GCAAATGATGCAATC**GCAGCA**TTAAATGAAAAAGATTCAATTGAAAACAGACGTTTAGCACAACGTGAAGTTAAC
AAAGCACCTATGGATGTAAAAGAGCATTTACAGAAACAATTAGACGCATTAGTAGCTCAA**GCA**GATGCTGAAAAGA
AAGTGGCGTAA

K212A S213A S219A K220A K259A K250A

ATGAGAGGATCGCATCACCATCACCATCACGGATCCGAACGTCAAAATATTGAAAATGCGGATAAAGCAATTAAAG
ATTTCCAAGATAACAAAGCACCACACGATAAATCAGCAGCATATGAAGCTAACTCAAAATTACCTAAAGATTTACG
CGATAAAAATAACCGCTTTGTAGAAAAAGTTTCAATTGAAAAAGCAATCGTTCGTCATGATGAGCGTGTG**GCAGCA**
GCAAATGATGCAATC**GCAGCA**TTAAATGAAAAAGATTCAATTGAAAACAGACGTTTAGCACAACGTGAAGTTAAC
AAAGCACCTATGGATGTAAAAGAGCATTTACAG**GCA**CAATTAGACGCATTAGTAGCTCAA**GCA**GATGCTGAAAAGA
AAGTGGCGTAA

K212A S213A S219A K220A K259A K250A K245A

ATGAGAGGATCGCATCACCATCACCATCACGGATCCGAACGTCAAAATATTGAAAATGCGGATAAAGCAATTAAAG
ATTTCCAAGATAACAAAGCACCACACGATAAATCAGCAGCATATGAAGCTAACTCAAAATTACCTAAAGATTTACG
CGATAAAAATAACCGCTTTGTAGAAAAAGTTTCAATTGAAAAAGCAATCGTTCGTCATGATGAGCGTGTG**GCAGCA**
GCAAATGATGCAATC**GCAGCA**TTAAATGAAAAAGATTCAATTGAAAACAGACGTTTAGCACAACGTGAAGTTAAC
AAAGCACCTATGGATGTA**GCA**GAGCATTTACAG**GCA**CAATTAGACGCATTAGTAGCTCAA**GCA**GATGCTGAAAAGA
AAGTGGCGTAA

K212A S213A S219A K220A K259A K250A K245A K263A K264A

ATGAGAGGATCGCATCACCATCACCATCACGGATCCGAACGTCAAAATATTGAAAATGCGGATAAAGCAATTAAAG
ATTTCCAAGATAACAAAGCACCACACGATAAATCAGCAGCATATGAAGCTAACTCAAAATTACCTAAAGATTTACG
CGATAAAAATAACCGCTTTGTAGAAAAAGTTTCAATTGAAAAAGCAATCGTTCGTCATGATGAGCGTGTG**GCAGCA**
GCAAATGATGCAATC**GCAGCA**TTAAATGAAAAAGATTCAATTGAAAACAGACGTTTAGCACAACGTGAAGTTAAC
AAAGCACCTATGGATGTA**GCA**GAGCATTTACAG**GCA**CAATTAGACGCATTAGTAGCTCAA**GCA**GATGCTGAA**GCGG**
CAGTGGCGTAA

K259A

ATGAGAGGATCGCATCACCATCACCATCACGGATCCGAACGTCAAAATATTGAAAATGCGGATAAAGCAATTAAAG
ATTTCCAAGATAACAAAGCACCACACGATAAATCAGCAGCATATGAAGCTAACTCAAAATTACCTAAAGATTTACG
CGATAAAAATAACCGCTTTGTAGAAAAAGTTTCAATTGAAAAAGCAATCGTTCGTCATGATGAGCGTGTGAAATCA

GCAAATGATGCAATCTCAAAATTAAATGAAAAAGATTCAATTGAAAACAGACGTTTAGCACAACGTGAAGTTAACA
AAGCACCTATGGATGTAAAAGAGCATTTACAGAAACAATTAGACGCATTAGTAGCTCAA**GCA**GATGCTGAAAAGAA
AGTGGCGTAA

K259A K250
ATGAGAGGATCGCATCACCATCACCATCACGGATCCGAACGTCAAAATATTGAAAATGCGGATAAAGCAATTAAAG
ATTTCCAAGATAACAAAGCACCACACGATAAATCAGCAGCATATGAAGCTAACTCAAAATTACCTAAAGATTTACG
CGATAAAAATAACCGCTTTGTAGAAAAAGTTTCAATTGAAAAAGCAATCGTTCGTCATGATGAGCGTGTGAAATCA
GCAAATGATGCAATCTCAAAATTAAATGAAAAAGATTCAATTGAAAACAGACGTTTAGCACAACGTGAAGTTAACA
AAGCACCTATGGATGTAAAAGAGCATTTACAG**GCA**CAATTAGACGCATTAGTAGCTCAA**GCA**GATGCTGAAAAGAA
AGTGGCGTAA

K259A K250A K263A K264A
ATGAGAGGATCGCATCACCATCACCATCACGGATCCGAACGTCAAAATATTGAAAATGCGGATAAAGCAATTAAAG
ATTTCCAAGATAACAAAGCACCACACGATAAATCAGCAGCATATGAAGCTAACTCAAAATTACCTAAAGATTTACG
CGATAAAAATAACCGCTTTGTAGAAAAAGTTTCAATTGAAAAAGCAATCGTTCGTCATGATGAGCGTGTGAAATCA
GCAAATGATGCAATCTCAAAATTAAATGAAAAAGATTCAATTGAAAACAGACGTTTAGCACAACGTGAAGTTAACA
AAGCACCTATGGATGTAAAAGAGCATTTACAG**GCA**CAATTAGACGCATTAGTAGCTCAA**GCA**GATGCTGAA**GCGGC**
AGTGGCGTAA

9.1.2.3 pQE30$^{Sbi\text{-}III\text{-}IV\text{-}cys}$ single mutant

Alanine mutation highlighted in red, cysteine location is highlighted in blue.

Sbi-III-IV-cys K173A
ATGAGAGGATCGCATCACCATCACCATCACGGATCCGAACGTCAAAATATTGAAAATGCGGATAAAGCAATTAAAG
ATTTCCAAGATAACAAAGCACCACACGAT**GCA**TCAGCAGCATATGAAGCTAACTCAAAATTACCTAAAGATTTACG
CGATAAAAATAACCGCTTTGTAGAAAAAGTTTCAATTGAAAAAGCAATCGTTCGTCATGATGAGCGTGTGAAATCA
GCAAATGATGCAATCTCAAAATTAAATGAAAAAGATTCAATTGAAAACAGACGTTTAGCACAACGTGAAGTTAACA
AAGCACCTATGGATGTAAAAGAGCATTTACAGAAACAATTAGACGCATTAGTAGCTCAAAAAGATGCTGAAAAGAA
A**TGC**GCGTAA

Sbi-III-IV-cys R231A
ATGAGAGGATCGCATCACCATCACCATCACGGATCCGAACGTCAAAATATTGAAAATGCGGATAAAGCAATTAAAG
ATTTCCAAGATAACAAAGCACCACACGATAAATCAGCAGCATATGAAGCTAACTCAAAATTACCTAAAGATTTACG
CGATAAAAATAACCGCTTTGTAGAAAAAGTTTCAATTGAAAAAGCAATCGTTCGTCATGATGAGCGTGTGAAATCA
GCAAATGATGCAATCTCAAAATTAAATGAAAAAGATTCAATTGAAAACAGA**GCT**TTAGCACAACGTGAAGTTAAC
AAAGCACCTATGGATGTAAAAGAGCATTTACAGAAACAATTAGACGCATTAGTAGCTCAAAAAGATGCTGAAAAGA
AA**TGC**GCGTAA

Sbi-III-IV-cys S199A
ATGAGAGGATCGCATCACCATCACCATCACGGATCCGAACGTCAAAATATTGAAAATGCGGATAAAGCAATTAAAG
ATTTCCAAGATAACAAAGCACCACACGATAAATCAGCAGCATATGAAGCTAACTCAAAATTACCTAAAGATTTACG
CGATAAAAATAACCGCTTTGTAGAAAAAGTT**GCA**ATTGAAAAAGCAATCGTTCGTCATGATGAGCGTGTGAAATCA
GCAAATGATGCAATCTCAAAATTAAATGAAAAAGATTCAATTGAAAACAGACGTTTAGCACAACGTGAAGTTAACA

AAGCACCTATGGATGTAAAAGAGCATTTACAGAAACAATTAGACGCATTAGTAGCTCAAAAAGATGCTGAAAAGAA
A[TGC]GCGTAA

9.2: Vector maps

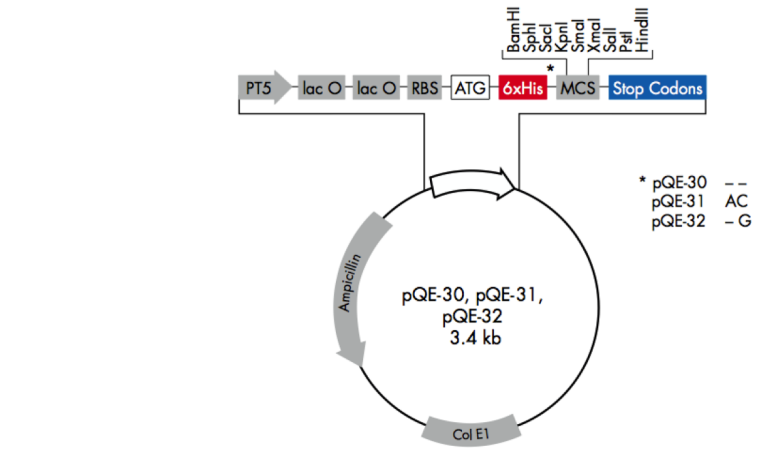

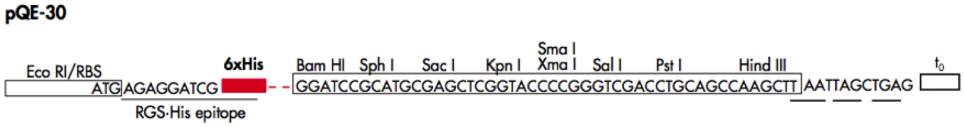

Figure 9.1: Vector map of pQE-30

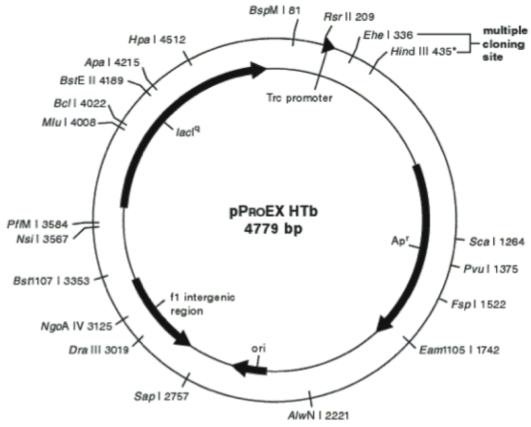

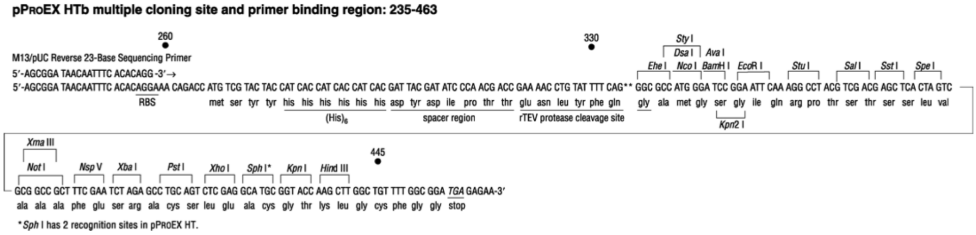

Figure 9.2: Vector map of pProEX-htb

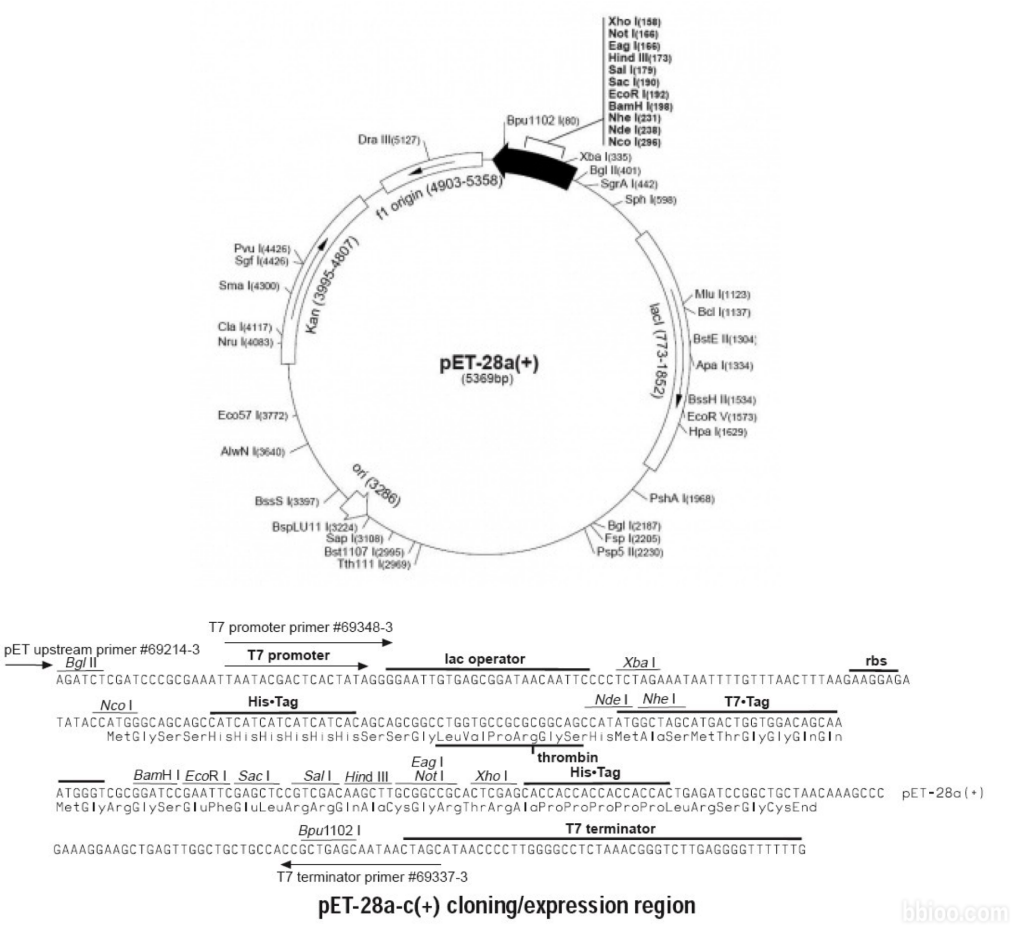

Figure 9.3: Vector map of pET28a

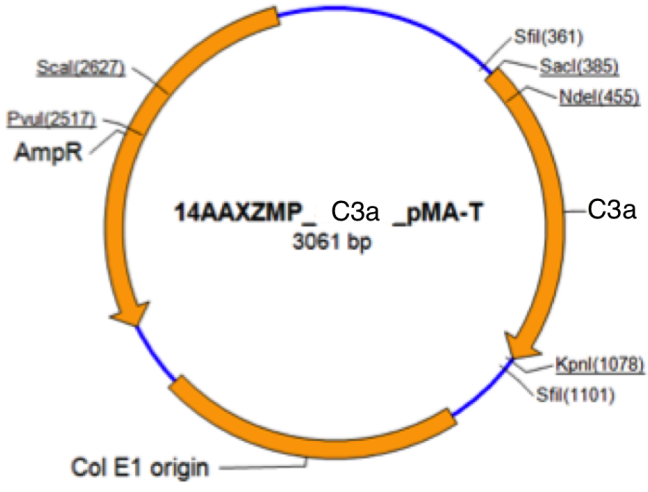

Figure 9.11: Vector map of pMA-T-C3a

9.3: Buffers and solutions

Table 9.1: Recipes for 8%, 10%, 12%, 15% acrylamide resolving gel for SDS-PAGE (4 gels).

	8% gel	10% gel	12% gel	15% gel
Tris 1.5M pH8.8 (ml)	6.25	6.25	6.25	6.25
H_20 (ml)	13.6	12.36	11.11	9.25
40% v/v 29:1 Acrylamide/bis-acrylamide (ml)	5	6.25	7.5	9.35
10% APS (µl)	125	125	125	125
TEMED (µl)	11.25	11.25	11.25	11.25

Table 9.2: Recipe for 4% acrylamide stacking gel for SDS-PAGE (4 gels)

	4% gel
Tris 0.5M pH6.8 (ml)	3.125
H_20 (ml)	8
40% v/v 29:1 Acrylamide/bis-acrylamide (ml)	1.25
10% APS (µl)	62.5
TEMED (µl)	12.5

Table 9.3: 4%, 20% acrylamide gel for gradient SDS-PAGE (3 gels)

	4% gel	20% gel
Tris 1.5M pH8.8 (ml)	3.125	3.125
H_2O (ml)	8.054	3.055
40% v/v 29:1 Acrylamide/bis-acrylamide (ml)	1.25	6.25
10% APS (µl)	114	114
TEMED (µl)	12	12

Table 9.4: 2×SDS-PAGE reducing sample buffer

	Reducing	Non-reducing
H_2O	2.25 ml	2.75 ml
0.5M Tris pH6.8	1.25 ml	1.25 ml
10% (w/v) SDS	3 ml	3 ml
50% (v/v) glycerol	2 ml	2 ml
2-mercaptoethanol	0.5 ml	0 ml
0.18% bromophenol blue	1 ml	1 ml

Table 9.5: 10×Glycine running buffer for SDS-PAGE. Make-up to 1 L with distilled H_2O. Do not need to adjust pH.

Tris Base	30.3g
Glycine	143.75g
SDS	10g

Table 9.6: Coomassie Blue stain for acrylamide gel

40% Methanol
0.1% (w/v) Brilliant blue R250
10% Acetic acid
50% H2O

Table 9.7: Destain for acrylamide gel

25% Methanol
10% Acetic acid
65% H2O

Appendix 9.4: Supporting experiments

9.4.1 Ten repetitive CD spectra of Sbi-III-IV mutant

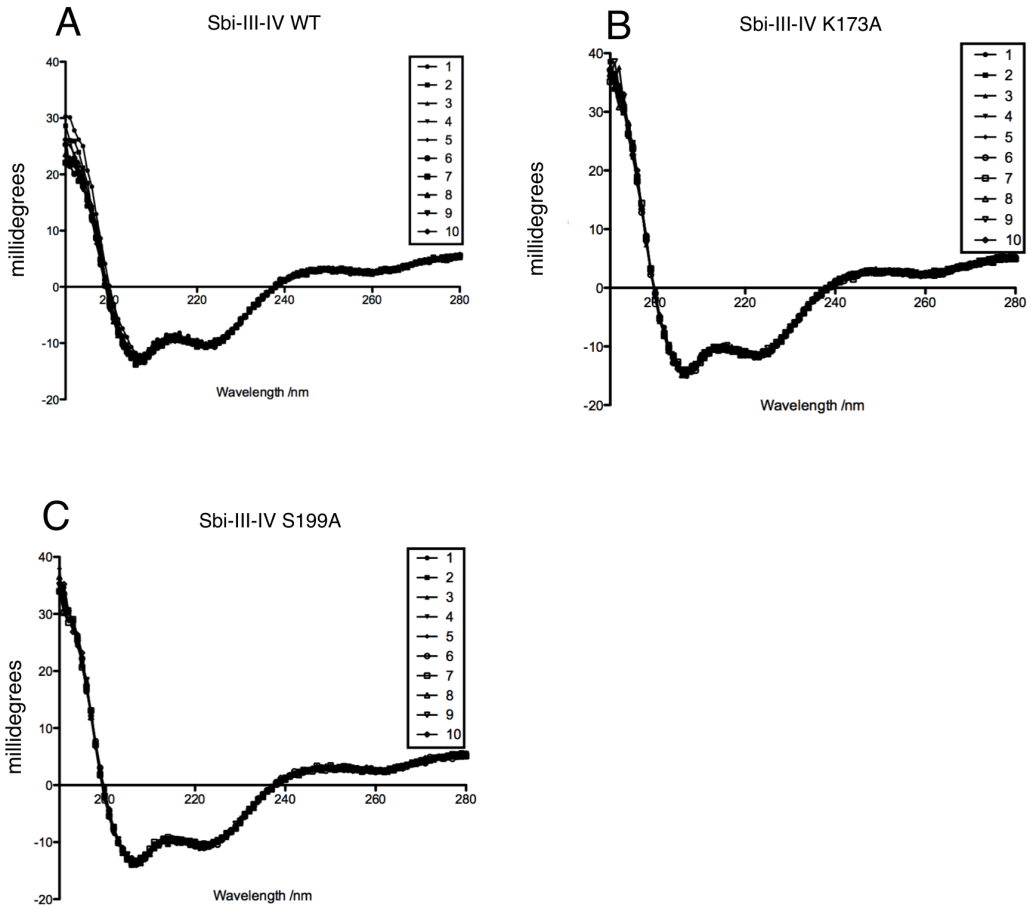

Figure 9.4: Circular dichroism (CD) spectra of Sbi-III-IV WT and mutants. (A) Ten repetitive CD spectra of Sbi-III-IV WT. **(B)** Ten repetitive CD spectra of Sbi-III-IV K173A mutant. **(C)** Ten repetitive CD spectra of Sbi-III-IV S199A mutant.

9.4.2 Sbi-III-IV-cys, mutagenesis, expression and purification

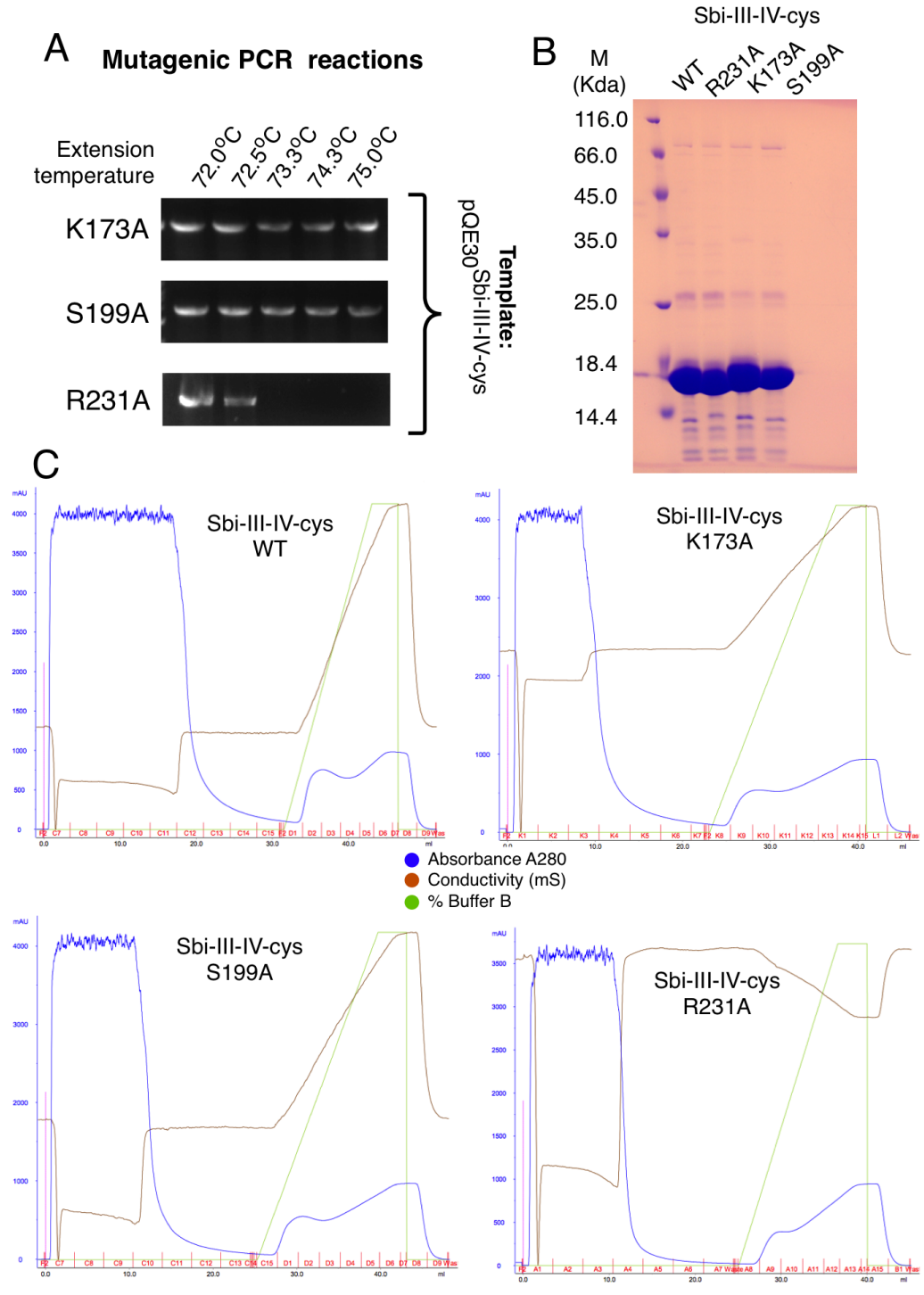

Figure 9.5: Preparation of Sbi-III-IV-cys WT and mutants. (A) Mutagenic PCR reactions of K173A, S199A and R231A mutants. **(B)** SDS-PAGE analysis of purified Sbi-III-IV-cys proteins **(C)** Chromatograms for Ni^{2+} affinity purification of WT, K173A, S199A and R231A Sbi-III-IV-cys.

9.4.3 ESI-ToF mass spectrometry protein identification

A

FHR1_HUMAN **Mass:** 38766 **Score:** 125 **Matches:** 14(5) **Sequences:** 7(3) **emPAI:** 0.51

Complement factor H-related protein 1 OS=Homo sapiens GN=CFHR1 PE=1 SV=2

Query	Observed	Mr(expt)	Mr(calc)	ppm	Miss	Score	Expect	Rank	Unique	Peptide
36	386.7026	771.3907	771.3915	-1.04	0	21	0.09	1	U	R.GWSTPPK.C 34
338	521.7482	1041.4818	1041.4879	-5.91	0	10	1	1	U	R.NGQWSEPPK.C 337
353	564.2567	1126.4988	1126.4965	2.08	0	50	7.3e-005	1	U	R.TGESAEFVCK.R 354
440	665.8377	1329.6608	1329.6564	3.27	0	5	5.6	1	U	K.INHGILYDEEK.Y
448	683.3459	1364.6772	1364.6758	1.05	0	20	0.19	1	U	R.EIMENYNIALR.W 450
453	691.3441	1380.6737	1380.6707	2.16	0	(11)	1.5	1	U	R.EIMENYNIALR.W
466	753.3504	1504.6863	1504.6868	-0.32	0	33	0.005	1	U	R.ITCTEEGWSPTPK.C 465
469	795.3685	1588.7224	1588.7263	-2.49	0	35	0.0027	1	U	R.LQNNENNISCVER.G 470

B

CO3_HUMAN **Mass:** 188569 **Score:** 19 **Matches:** 7(0) **Sequences:** 5(0) **emPAI:** 0.03

Complement C3 OS=Homo sapiens GN=C3 PE=1 SV=2

Query	Observed	Mr(expt)	Mr(calc)	ppm	Miss	Score	Expect	Rank	Unique	Peptide
116	423.2159	844.4173	844.4191	-2.13	0	2	10	1	U	R.WLNEQR.Y
129	436.2650	870.5154	870.5174	-2.40	0	8	3	2	U	R.QGALELIK.K
362	576.8048	1151.5951	1151.5975	-2.12	0	2	12	1	U	R.QPSSAFAAFVK.R
474	821.3886	1640.7627	1640.7617	0.62	0	18	0.22	1	U	K.AGDFLEANYMNLQR.S 475
484	1079.0394	2156.0643	2156.0783	-6.50	0	13	0.95	1	U	R.ILLQGTPVAQMTEDAVDAER.L 483

Figure 9.6: MS protein identification via trypic peptide mass fringerprinting. (A) Polypeptides derived from FHR-1 **(B)** Polypeptides derived from complement component C3.

9.4.4 Factor H depleted serum pull-down

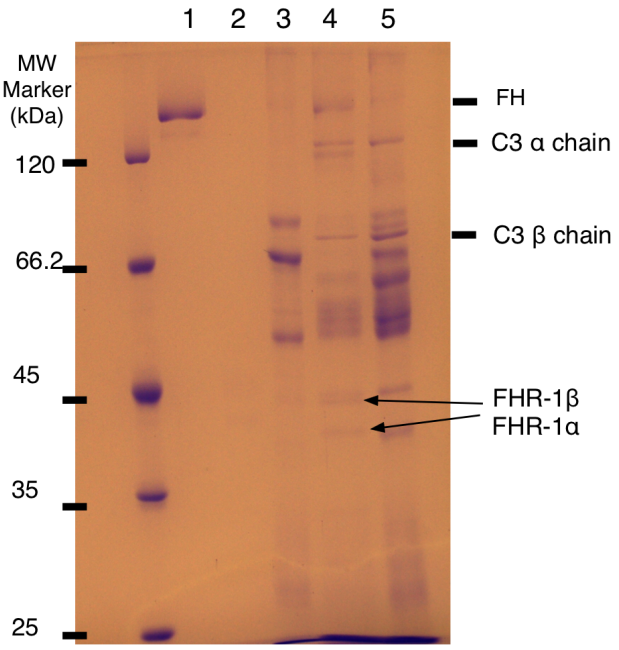

Figure 9.7: Gel of factor H depleted serum pull-down. Lane 1, purified factor H, 2 recombinant FHR-1, 3 neutravidin resin pull-down control, 4 normal serum Sbi-III-IV WT pull-down, 5 factor H depleted serum Sbi-III-IV WT pull-down.

9.4.5 Sbi-III-IV[28] trypsin digestion simulation

[Theoretical pI: 9.40 / Mw (average mass): 17966.14 / Mw (monoisotopic mass): 17955.15]

mass	position	#MC	modifications	peptide sequence
5838.7101	1-54	5		MGSSHHHHHHSSGLVPRGSH MASMTGGQQMGRGSIENADK AIKDFQDNKAPHDK
5290.4395	1-49	4		MGSSHHHHHHSSGLVPRGSH MASMTGGQQMGRGSIENADK AIKDFQDNK
4879.2580	18-63	5		GSHMASMTGGQQMGRGSIEN ADKAIKDFQDNKAPHDKSAA YEANSK
4543.1207	1-43	3		MGSSHHHHHHSSGLVPRGSH MASMTGGQQMGRGSIENADK AIK
4230.9046	1-40	2		MGSSHHHHHHSSGLVPRGSH MASMTGGQQMGRGSIENADK
3957.8388	18-54	4		GSHMASMTGGQQMGRGSIEN ADKAIKDFQDNKAPHDK
3881.0793	127-160	5		EHLQKQLDALVAQKDAEKKV AKLAAALEHHHHHH
3700.8565	33-66	5		GSIENADKAIKDFQDNKAPH DKSAAYEANSKLPK
3643.9588	113-144	5		LAQREVNKAPMDVKEHLQKQ LDALVAQKDAEK
3416.5225	1-32	1		MGSSHHHHHHSSGLVPRGSH MASMTGGQQMGR
3409.5681	18-49	3		GSHMASMTGGQQMGRGSIEN ADKAIKDFQDNK
3362.6247	33-63	4		GSIENADKAIKDFQDNKAPH DKSAAYEANSK
3356.8583	112-140	5		RLAQREVNKAPMDVKEHLQK QLDALVAQK
3303.7729	117-145	5		EVNKAPMDVKEHLQKQLDAL VAQKDAEKK
3270.6865	41-69	5		AIKDFQDNKAPHDKSAAYEA NSKLPKDLR
3245.7402	132-160	4		QLDALVAQKDAEKKVAKLAA ALEHHHHHH
3207.6828	84-111	5		AIVRHDERVKSANDAISKLN EKDSIENR
3201.5923	44-71	5		DFQDNKAPHDKSAAYEANSK LPKDLRDK
3200.7572	113-140	4		LAQREVNKAPMDVKEHLQKQ LDALVAQK
3175.6779	117-144	4		EVNKAPMDVKEHLQKQLDAL VAQKDAEK
3131.7244	121-148	5		APMDVKEHLQKQLDALVAQK DAEKKVAK
3104.6381	106-131	5		DSIENRRLAQREVNKAPMDV KEHLQK
3098.6301	94-120	5		SANDAISKLNEKDSIENRRL AQREVNK
3068.6850	75-101	5		FVEKVSIEKAIVRHDERVKS ANDAISK
3049.6752	79-105	5		VSIEKAIVRHDERVKSANDA ISKLNEK
2958.4704	44-69	4		DFQDNKAPHDKSAAYEANSK LPKDLR
2953.5636	102-126	5		LNEKDSIENRRLAQREVNKA PMDVK
2924.4932	88-112	5		HDERVKSANDAISKLNEKDS IENRR
2886.4744	41-66	4		AIKDFQDNKAPHDKSAAYEA NSKLPK
2855.5445	92-116	5		VKSANDAISKLNEKDSIENR RLAQR
2838.4605	50-74	5		APHDKSAAYEANSKLPKDLR DKNNR
2833.5240	121-145	4		APMDVKEHLQKQLDALVAQK DAEKK
2793.4642	55-78	5		SAAYEANSKLPKDLRDKNNR FVEK
2768.3921	88-111	4		HDERVKSANDAISKLNEKDS IENR
2732.4763	117-140	3		EVNKAPMDVKEHLQKQLDAL VAQK
2705.4290	121-144	3		APMDVKEHLQKQLDALVAQK DAEK
2682.4434	70-91	5		DKNNRFVEKVSIEKAIVRHD ER
2666.4848	72-93	5		NNRFVEKVSIEKAIVRHDER VK
2662.2494	18-43	2		GSHMASMTGGQQMGRGSIEN ADKAIK
2628.3812	94-116	4		SANDAISKLNEKDSIENRRL AQR
2574.2582	44-66	3		DFQDNKAPHDKSAAYEANSK LPK
2565.4107	79-101	4		VSIEKAIVRHDERVKSANDA ISK
2548.2426	41-63	3		AIKDFQDNKAPHDKSAAYEA NSK
2529.4259	67-87	5		DLRDKNNRFVEKVSIEKAIV R
2493.3531	84-105	4		AIVRHDERVKSANDAISKLN EK
2490.4038	127-148	4		EHLQKQLDALVAQKDAEKKV AK
2469.2990	106-126	4		DSIENRRLAQREVNKAPMDV K
2454.2735	50-71	4		APHDKSAAYEANSKLPKDLR DK
2441.2055	33-54	3		GSIENADKAIKDFQDNKAPH DK
2439.3215	72-91	4		NNRFVEKVSIEKAIVRHDER

2428.3670	64-83	5	LPKDLRDKNNRFVEKVSIEK	
2390.3085	112-131	4	RLAQREVNKAPMDVKEHLQK	
2387.2637	92-112	4	VKSANDAISKLNEKDSIENR R	
2350.0332	18-40	1	GSHMASMTGGQQMGRGSIEN ADK	
2312.2429	102-120	4	LNEKDSIENRRLAQREVNK	
2290.1898	55-74	4	SAAYEANSKLPKDLRDKNNR	
2282.2979	75-93	4	FVEKVSIEKAIVRHDERVK	
2279.1904	141-160	3	DAEKKVAKLAAALEHHHHHH	
→ 2262.2274	121-140	2	APMDVKEHLQKQLDALVAQK	A^{240}-K^{259}
2236.0265	44-63	2	DFQDNKAPHDKSAAYEANSK	
2234.2073	113-131	3	LAQREVNKAPMDVKEHLQK	
2231.1626	92-111	3	VKSANDAISKLNEKDSIENR	
2211.1516	50-69	3	APHDKSAAYEANSKLPKDLR	
→ 2192.2033	127-145	3	EHLQKQLDALVAQKDAEKK	E^{246}-K^{264}
2160.1003	94-112	3	SANDAISKLNEKDSIENRR	
2145.2138	70-87	4	DKNNRFVEKVSIEKAIVR	
2090.1352	67-83	4	DLRDKNNRFVEKVSIEK	
2064.1083	127-144	2	EHLQKQLDALVAQKDAEK	
2055.1345	75-91	3	FVEKVSIEKAIVRHDER	
2054.0625	88-105	3	HDERVKSANDAISKLNEK	
2009.0886	84-101	3	AIVRHDERVKSANDAISK	
2003.9992	94-111	2	SANDAISKLNEKDSIENR	
1906.0028	55-71	3	SAAYEANSKLPKDLRDK	
1902.0919	72-87	3	NNRFVEKVSIEKAIVR	
1899.8892	1-17	0	MGSSHHHHHHSSGLVPR	
1892.9348	33-49	2	GSIENADKAIKDFQDNK	
1872.0450	64-78	4	LPKDLRDKNNRFVEK	
1855.0647	132-148	3	QLDALVAQKDAEKKVAK	
1841.9940	102-116	3	LNEKDSIENRRLAQR	
1835.9888	145-160	2	KVAKLAAALEHHHHHH	
1827.9783	106-120	3	DSIENRRLAQREVNK	
1826.9395	50-66	2	APHDKSAAYEANSKLPK	
1779.0235	79-93	3	VSIEKAIVRHDERVK	
1765.9265	117-131	2	EVNKAPMDVKEHLQK	
1754.9694	112-126	3	RLAQREVNKAPMDVK	
1707.8938	146-160	1	VAKLAAALEHHHHHH	
1705.9231	70-83	3	DKNNRFVEKVSIEK	
1662.8809	55-69	2	SAAYEANSKLPKDLR	
1626.8234	41-54	2	AIKDFQDNKAPHDK	
1620.9067	127-140	1	EHLQKQLDALVAQK	
1598.8682	113-126	2	LAQREVNKAPMDVK	
1569.7979	88-101	2	HDERVKSANDAISK	
1556.8642	132-145	2	QLDALVAQKDAEKK	
1551.8601	79-91	2	VSIEKAIVRHDER	
1535.6512	18-32	0	GSHMASMTGGQQMGR	
1533.8132	67-78	3	DLRDKNNRFVEK	
1517.9049	75-87	2	FVEKVSIEKAIVR	
1516.8329	92-105	2	VKSANDAISKLNEK	
1488.7077	50-63	1	APHDKSAAYEANSK	
1462.8012	72-83	2	NNRFVEKVSIEK	
1428.7692	132-144	1	QLDALVAQKDAEK	
1409.6933	149-160	0	LAAALEHHHHHH	
1373.7131	102-112	2	LNEKDSIENRR	
1368.7706	64-74	3	LPKDLRDKNNR	

1357.7295	106-116	2	DSIENRRLAQR	
1314.6073	44-54	1	DFQDNKAPHDK	
1295.6776	121-131	1	APMDVKEHLQK	
1289.6695	94-105	1	SANDAISKLNEK	
1278.6688	55-66	1	SAAYEANSKLPK	
1222.7014	84-93	2	AIVRHDERVK	
1217.6120	102-111	1	LNEKDSIENR	
1149.6011	70-78	2	DKNNRFVEK	
1145.6160	33-43	1	GSIENADKAIK	
1130.5874	117-126	1	EVNKAPMDVK	
1113.6487	112-120	2	RLAQREVNK	
1078.6142	75-83	1	FVEKVSIEK	
1078.5527	41-49	1	AIKDFQDNK	
1032.5684	92-101	1	VKSANDAISK	
1030.5388	67-74	2	DLRDKNNR	
1014.6306	79-87	1	VSIEKAIVR	
995.5381	84-91	1	AIVRHDER	
→ 985.5676	132-140	0	QLDALVAQK	Q^{251}-K^{259}
984.5836	64-71	2	LPKDLRDK	
957.5476	113-120	1	LAQREVNK	
940.4370	55-63	0	SAAYEANSK	
906.4792	72-78	1	NNRFVEK	
889.4486	106-112	1	DSIENRR	
888.5149	141-148	2	DAEKKVAK	
833.3999	33-40	0	GSIENADK	
805.4050	94-101	0	SANDAISK	
783.4107	88-93	1	HDERVK	
766.3366	44-49	0	DFQDNK	
741.4617	64-69	1	LPKDLR	
733.3475	106-111	0	DSIENR	
660.3385	121-126	0	APMDVK	
654.3569	127-131	0	EHLQK	
646.3518	67-71	1	DLRDK	
646.3267	70-74	1	DKNNR	
643.3998	112-116	1	RLAQR	
590.3144	141-145	1	DAEKK	
575.3399	79-83	0	VSIEK	
567.2885	50-54	0	APHDK	
556.2474	88-91	0	HDER	
522.2922	75-78	0	FVEK	
503.2824	102-105	0	LNEK	
489.2667	117-120	0	EVNK	
487.2987	113-116	0	LAQR	
462.2194	141-144	0	DAEK	
458.3085	84-87	0	AIVR	
445.3133	145-148	1	KVAK	
403.2299	67-69	0	DLR	
403.2048	72-74	0	NNR	
357.2496	64-66	0	LPK	
331.2340	41-43	0	AIK	
317.2183	146-148	0	VAK	
262.1397	70-71	0	DK	
246.1812	92-93	0	VK	
175.1189	112-112	0	R	
147.1128	145-145	0	K	

Figure 9.8: Sbi-III-IV[28] trypsin digestion simulation. The peptides utilized in mass spectra interpretation are indicated by black arrows. Their residue numbers are also indicated.

9.4.6 Ramachandran analyses of Sbi-III and Sbi-III-IV predicted models

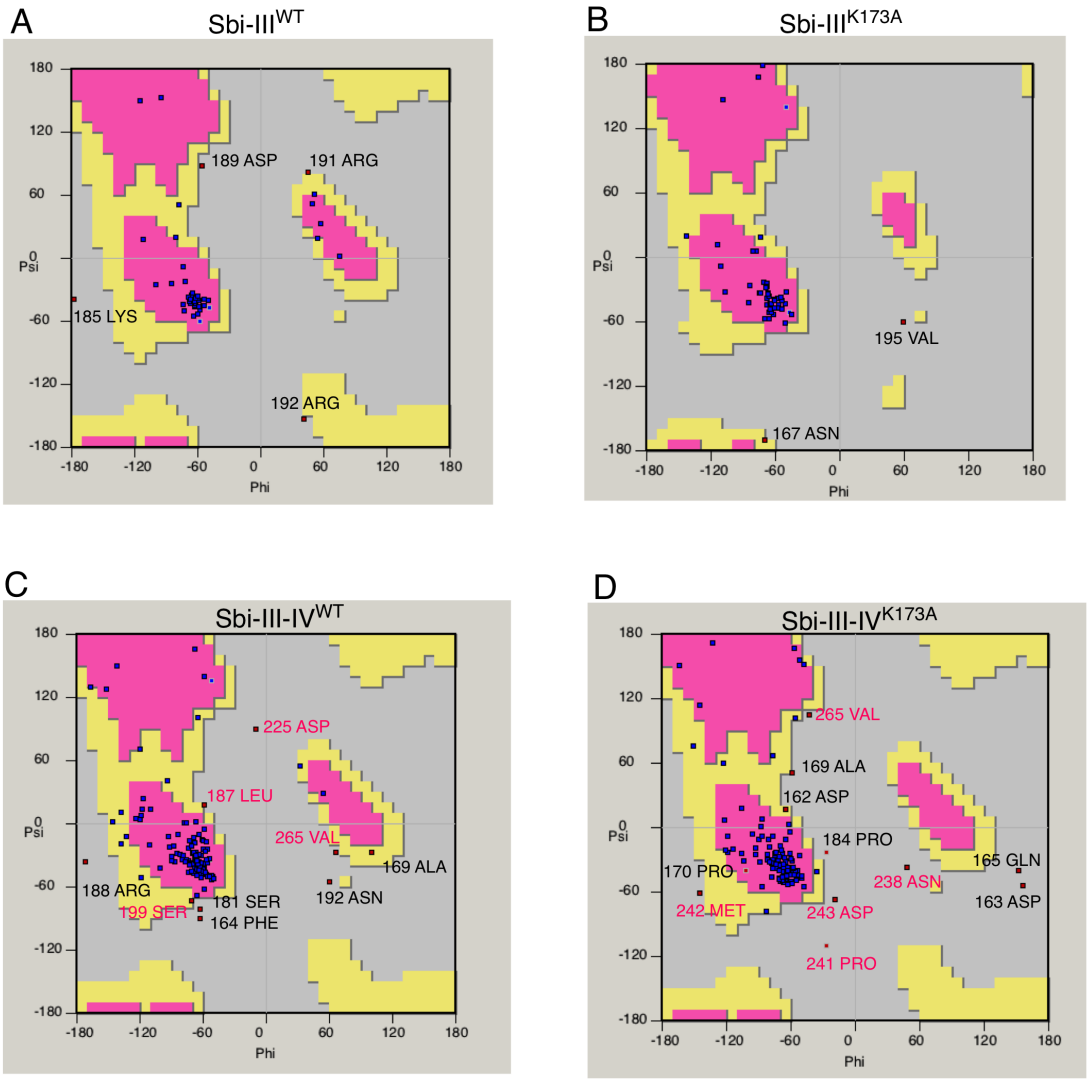

Figure 9.9: Ramachandran analysis of Sbi-III and Sbi-III-IV predicted models. (A) Predicted model of Sbi-III^{WT}. **(B)** Predicted model of Sbi-III^{K173A}. **(C)** Predicted model of Sbi-III-IV^{WT}. **(D)** Predicted model of Sbi-III-IV^{K173A}. The residues with unfavorable Psi and Phi angles were labeled in black (domain III residue) and red (domain IV residues). Ramachandran plots were generated by COOT.

9.4.7 Ligand concentrations used in ALEX smFRET

Table 9.8: Ligand concentrations used in ALEX smFRET experiments

Ligand	Concentration
Sbi-III-IV	100 pM
C3a	28 µM
C3d	24 µM
C3	20 µM
$C3_{(H20)}$	10 µM
C3b	2.8 µM
FH	3.3 µM
FHR-1	4 µM

9.4.8 SAXS sample preparation and raw scattering curves

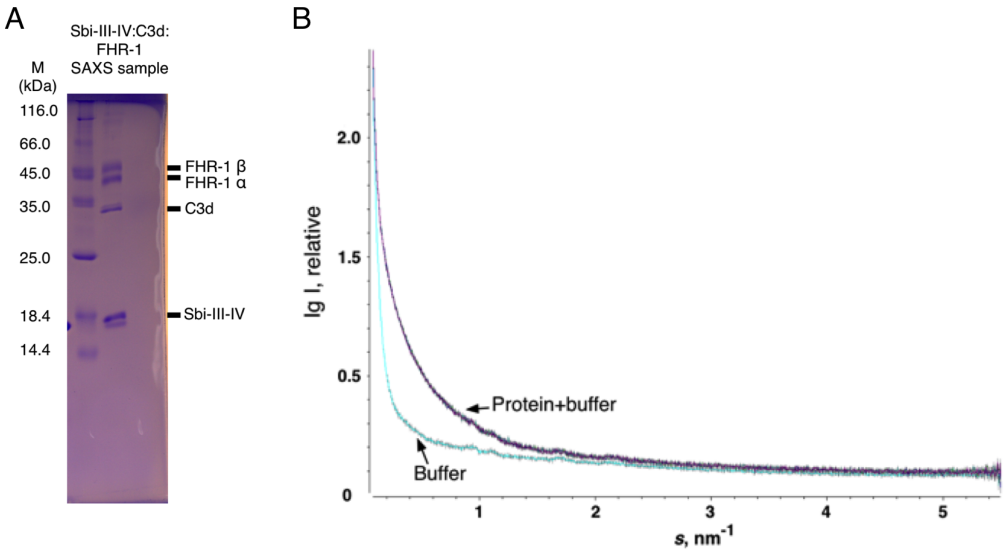

Figure 9.10: SAXS sample preparation and raw scattering profiles (A) SDS-PAGE profile of Sbi-III-IV:C3d:FHR-1 complex. Molar ratio: 1:1:1. (B) Raw scattering curves of Sbi-III-IV:C3d:FHR-1